DEFINING REOVIRUS STRAIN-SPECIFIC DIFFERENCES THAT TRIGGER INFLAMMATION TO DIETARY ANTIGEN IN THE DEVELOPMENT OF CELIAC DISEASE

By

Judy Janelle Brown

Dissertation

Submitted to the Faculty of the

Graduate School of Vanderbilt University

in partial fulfillment of the requirements

for the degree of

DOCTOR OF PHILOSOPHY

in

Microbiology and Immunology

May 11, 2018

Nashville, Tennessee

Approved by:

Luc Van Kaer, Ph.D.

Terence S. Dermody, M.D.

Holly M. Algood, Ph.D.

Daniel J. Moore, M.D., Ph.D.

M. Kay Washington, M.D., Ph.D.

To my family,
for teaching me to reach for the stars
and helping me through the climb

To my husband, Matthew
for always believing in me
You are my everything

To our little one,
remember that once upon
a time your mom rocked it

ACKNOWLEDGEMENTS

I am grateful for the financial support of the Viral Triggers of Celiac Disease fellowship grant (F31 DK108562) awarded to myself, the Viral Infections and Celiac Disease Pathogenesis grant (R01 DK098435) awarded to T.S. Dermody and B. Jabri, and the Mechanisms of Vascular Disease (T32 HL007751) training grant. Additionally, I am thankful for the generosity of the Lamb family and their continuous support of the Lamb Center for Pediatric Research at Vanderbilt University. The Kathryn M. Edwards Fellowship Award provided funds for development and training. Finally, I am grateful for the commitment that the Children's Hospital of Pittsburgh has provided for the continuation and completion of my studies.

I am forever indebted to Dr. Terry Dermody for the opportunity to complete my training in his laboratory and under his mentorship. Terry fosters an interactive group atmosphere that is conducive to teamwork and student-centered training. He is committed to guiding the scientific development of each of his students individually and is especially invested in helping students achieve their research and career goals. Terry is a remarkable example of effective leadership and mentoring, whom I hope to emulate in my career.

I thank all past and present members of the Dermody lab. I am grateful for the opportunity to have worked with such wonderful graduate students during my time in the Dermody laboratory. I would like to thank Dr. Alison Ashbrook, Jonathan Knowlton, Christopher Lee, Anthony Lentscher, Nicole McAllister, Dr. Jennifer Stencel-Baerenwald, Danica Sutherland, and Paula Zamora for their

feedback and friendship. We had the opportunity to overlap for differing amounts of time but I would not trade our time together for anything. I thank Alison Ashbrook for her guidance and thoughtful questions; Jonathon Knowlton, my graduate school counterpart, for facing classes, grant writing, qualifying exams, and graduate life together; Christopher Lee for always having a kind smile to greet me; Anthony Lentscher for his unwavering support and encouragement; Nicole McAllister for her hard work as my rotation student, for being my biggest cheerleader, and especially for her friendship; Jennifer Stencel-Baerenwald for teaching me about immunology, oral tolerance, and the ways of thoughtful experimentation; Danica Sutherland for her laughter, love, and helping me make it through the difficult days; and Paula Zamora for her lightheartedness and commitment to her passions.

My labmates in the Dermody lab made everyday enjoyable. I always felt surrounded by friends and sometimes more like a loving, dysfunctional family. I would like to thank Dr. Jennifer Konopka-Anstadt for her career advice and being someone I could look up to; Dr. Bernardo Mainou for always asking thought-provoking questions and encouraging me through every stage of my career; Dr. Andrea Pruijjsers for being my scientific mentor, tea and cookie-break buddy, and life-long friend; Dr. Laurie Silva, forever my baymate, for her maturity in difficult situations, friendship, and being someone I could always come to; Dr. Gwen Taylor for being my go-to person for everything in Pittsburgh; and Dr. Allen Wu for always making me laugh and feel better about my day. I am grateful for Solomiia Khomandiak for her curiosity and cheerful personality; Mine Ikizler for

her motherly love and bubbliness; Jason Iskarpatyoti for his willingness to teach me about reovirus and good restaurants; and Kelly Urbanek, my new baymate, for her loyal support and encouragement, open-mindedness, and exceptionally hardworking attitude.

I am so grateful to have worked with amazing collaborators. I thank Dr. Bana Jabri for her helpful advice, challenging questions, feedback on writing, and the collaborative environment that she fostered. I am so thankful to have worked and co-published with Drs. Romain Bouziat and Reinhard Hinterleitner. I very much enjoyed our time together and friendship in the battlefield of science. I greatly appreciate the Virgin laboratory, including Drs. Megan Baldridge, Sanghyun Lee, and Craig Wilen for their willingness to work together and continued support during our collaborations.

Members of my thesis committee have provided useful ideas and important suggestions that have greatly improved the quality of my thesis work. I thank Drs. Holly Algood, Luc Van Kaer, Dan Moore, and Kay Washington for their critical assessments of my work and for their generous support. I have appreciated our time spent together and am so grateful for your guidance during the difficult transitions of my graduate career.

Additionally, I would like to thank all members of the departments of Pathology, Microbiology, and Immunology and Pediatric Infectious Diseases at Vanderbilt University, the department of Microbiology and Molecular Genetics at the University of Pittsburgh, and the department of Pediatric Infectious Diseases at Children's Hospital of Pittsburgh. The fellow graduate students, postdocs,

residents, fellows, faculty members, and administrators have provided abundant support and friendship.

Finally, I would like to thank my family, whose love and devotion are without limit. Thank you for all that you have given me. I am eternally grateful for their encouragement and support throughout every stage in my life. I would not be who or where I am today without them. I am eternally grateful for my husband, Matthew, for always believing in and supporting me. I appreciate his ability to lift my spirits and make me feel special. Our time living apart was the greatest challenge of our marriage but I cannot thank him enough for supporting my dreams. I know that we will be forever stronger because of our commitment to each other during this difficult time. I am so lucky to have you as my best friend and husband and I look forward to our incredible future together.

TABLE OF CONTENTS

LIST OF FIGURES

LIST OF TABLES

LIST OF ABBREVIATIONS

5BP	5-(biotinamido)-pentylamine
ANOVA	One-way analysis of variance
AO	Acridine orange
APCs	Antigen-presenting cells
Bcl-2	B cell lymphoma 2
BH	Benjamini and Hochberg
BHK	Baby hamster kidney
BHK-T7	Baby hamster kidney cells expressing T7 polymerase
Caspase	Cysteine-aspartyl protease
CD	Celiac disease
cDNA	Cloned DNA
CFA	Complete Freund's adjuvant
CT-gliadin	Chymotrypsin-digested gliadin
CTLA4	Cytotoxic T-lymphocyte associated protein 4
d	Days
DAB	3’diaminobenzidine
DAPI	4’,6-diamidino-2-phenylindole
DCs	Dendritic cells
DISC	Death-inducing signaling complex
dLN	Draining lymph node
dpi	Days post-inoculation
dsRNA	Double-stranded RNA

DTH	Delayed type-hypersensitivity
ELISA	Enzyme-linked immunosorbent assay
EMA	Endomysium
FAE	Follicular associated epithelium
Foxp3	Forkhead box P3
GFD	Gluten-free diet
GWAS	Genome-wide association studies
h	Hour(s)
H&E	Hematoxylin and eosin
HDV	Hepatitus delta virus
HLA	Human leukocyte antigen
HLA-DQ8tg	HLA-DQ8 transgenic
hpi	Hours post-inoculation
HSV-1	Herpes simplex virus type 1
i.p.	Intraperitoneal
IC	Information content
IECs	Intestinal epithelial cells
IEL	Intestinal epithelial lymphocytes
IFN	Interferon
$IFNAR^{-/-}$	Type 1 interferon receptor-deficient
IgG	Immunoglobulin G
IL	Interleukin
IRF	Interferon regulatory factor

ISG	Interferon stimulated gene
ISVP	Infectious subvirion particles
JAM-A	Junction adhesion molecule-A
L cells	L929 cells
LP	Lamina propria
LPS	Lipopolysaccharide
MA104	Rhesus monkey kidney cells
Mda-5	Melanoma differentiation-associated protein-5
MDS	Multiple dimensional scaling
MEFs	Mouse embryonic fibroblasts
MHC	Major histocompatibility complex
MLN	Mesenteric lymph node
MOI	Multiplicity of infection
MST	Minimum spanning trees
MuMT	B cell- and antibody-deficient
NF-κB	Nuclear factor kappa-light-chain-enhancer of activated B cells
OD	Odds ratio
OVA	Ovalbumin
PBS	Phosphate-buffered saline
PFU	Plaque forming unit
PO	Peroral
poly(I:C)	Polyinosinic:polycytidylic acid
PP	Peyer's patches

PRNT60	Plaque-reduction neutralization assay
pT_{reg}	Peripheral T_{reg}
Reovirus	Mammalian orthoreovirus
RIG-I	Retinoic acid inducible gene-I
s.c.	Subcutaneous
SCID	B cell- and T cell-deficient
SED	Subepithelial dome
Sham	PBS treated
T1	Type 1
T1L	Type 1 Lang
T2	Type 2
T2J	Type 2 Jones
T3	Type 3
T3D	Type 3 Dearing
T3D-RV	T3D reassortant virus
TG2	Transglutaminase 2
TGFβ	Transforming growth factor β
T_H1	T helper 1
TNF	Tumor necrosis factor
T_{regs}	Regulatory T cells
WT	C57BL/6 wildtype

CHAPTER I

INTRODUCTION

Thesis Overview

Celiac Disease

Background

Celiac disease (CD) is a gluten-specific enteropathy triggered in genetically susceptible individuals exposed to gluten. CD occurs in approximately 1 in 133 persons in the United States (1) and affects more than 3 million people, although most are undiagnosed. Young children with CD present with diarrhea and severe malabsorption, including the inability to absorb vitamins and minerals. CD also is associated with chronic sequelae such as extra-intestinal autoimmune disorders, infertility, miscarriages, and cancer (2). The most important environmental factor that correlates with CD is the ingestion of gluten (3, 4). Accordingly, current treatment strategies are centered on maintaining a strict gluten-free diet (GFD). While such diets improve the quality of life for many CD patients, they are not always successful and can be difficult to follow (5). Due to the increasing prevalence of CD (6, 7) and the consequences of misdiagnosis, it is essential to better understand CD pathogenesis.

Clinical presentation, diagnosis, and treatment of celiac disease

Classically, CD was thought to be a pediatric illness, presenting early in childhood with diarrhea, steatorrhea, weight loss, and failure to thrive (5). However, recent recognition of the disease in older children and adults has added to the broad clinical manifestations of CD (8, 9). The spectrum of CD now encompasses four different types including typical, atypical, latent, and silent (5) (Figure I-1).

The typical form of CD occurs in children beginning between the ages of 6 and 18 months and is characterized by watery stool, malabsorption, and villous atrophy. Patients with atypical CD display structural abnormalities in the intestinal mucosa and experience minor intestinal symptoms; however, extraintestinal presentations are much more common. Such symptoms include anemia, infertility, neuropathy, and osteoporosis. Latent CD is diagnosed in genetically susceptible individuals who have normal intestinal architecture and possibly positive celiac-associated serology. These persons may or may not have extraintestinal symptoms and usually present later in life (5). Silent CD is defined by positive serology and typical intestinal pathology in the absence of clinical symptoms (10).

The broad spectrum of disease manifestations occurring in CD has made clinical diagnosis challenging. Currently, the revised European Society for Paediatric Gastroenterology Hepatology and Nutrition algorithm (11) identifies typical intestinal pathology (hyperplastic villous atrophy) and remission following a GFD as positive indicators of CD. Observation of villous atrophy, using

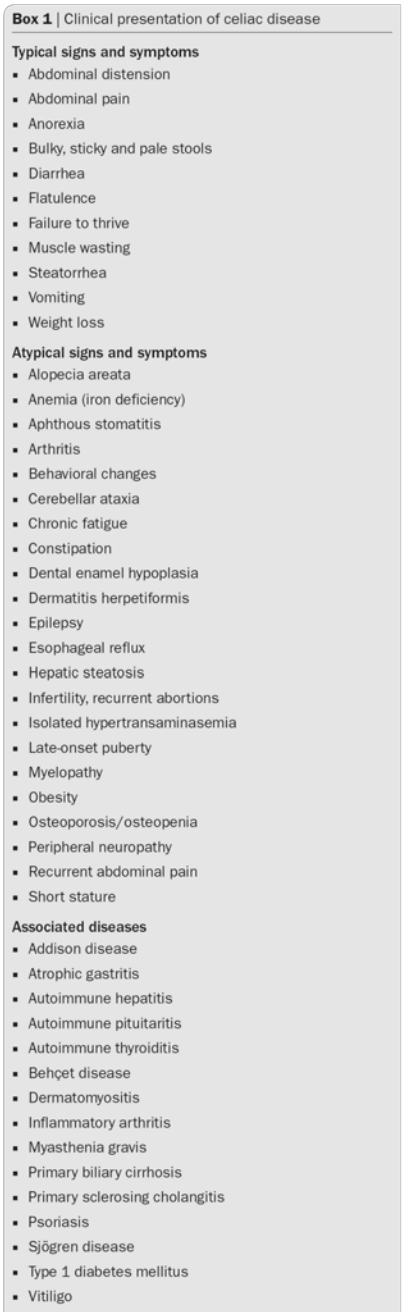

Box 1 | Clinical presentation of celiac disease

Typical signs and symptoms

- Abdominal distension
- Abdominal pain
- Anorexia
- Bulky, sticky and pale stools
- Diarrhea
- Flatulence
- Failure to thrive
- Muscle wasting
- Steatorrhea
- Vomiting
- Weight loss

Atypical signs and symptoms

- Alopecia areata
- Anemia (iron deficiency)
- Aphthous stomatitis
- Arthritis
- Behavioral changes
- Cerebellar ataxia
- Chronic fatigue
- Constipation
- Dental enamel hypoplasia
- Dermatitis herpetiformis
- Epilepsy
- Esophageal reflux
- Hepatic steatosis
- Infertility, recurrent abortions
- Isolated hypertransaminasemia
- Late-onset puberty
- Myelopathy
- Obesity
- Osteoporosis/osteopenia
- Peripheral neuropathy
- Recurrent abdominal pain
- Short stature

Associated diseases

- Addison disease
- Atrophic gastritis
- Autoimmune hepatitis
- Autoimmune pituitaritis
- Autoimmune thyroiditis
- Behçet disease
- Dermatomyositis
- Inflammatory arthritis
- Myasthenia gravis
- Primary biliary cirrhosis
- Primary sclerosing cholangitis
- Psoriasis
- Sjögren disease
- Type 1 diabetes mellitus
- Vitiligo

Figure I-1. Broad spectrum of clinical manifestations. (Figure adapted from Tack *et. al.* 2010 (5)).

histopathological analysis of small intestinal biopsies, has been the gold standard (5). The modified Marsh scale is used to classify the histopathology according to the degree of intraepithelial lymphocytosis, crypt hyperplasia, and villous atrophy (12, 13). However, technical limitations, patchy mucosal damage, and observer-bias all hinder the efficacy of using histopathology as the sole indicator of CD (5, 14).

At present, serological analysis of autoantibodies and anti-gluten antibodies are being used to supplement histopathologic analysis. CD patients maintain higher levels of IgA autoantibodies against the endomysium (EMA) of connective tissue and transglutaminase 2 (TG2) (15). Quantification of anti-gliadin (a byproduct of gluten) antibodies is less sensitive and specific than analysis of anti-EMA or anti-TG2 autoantibodies, except in very young children (5, 16).

In addition to serological testing, genetic analysis of human leukocyte antigen (HLA)-type provides a method for screening individuals, especially those with limited clinical manifestations or atypical CD (17, 18). The presence of HLA-DQ2, HLA-DQ8, or both alleles does not necessarily indicate CD, as 30 - 40% of healthy individuals have these risk alleles (19). However, the presence of these alleles is required for disease onset (20-22). Taken together, the diagnosis of CD requires a multifaceted testing platform (Figure I-2) where conclusions based on individual test results may be incorrect.

The only treatment for CD is a strict GFD and supportive care through supplementation of vitamins and minerals (23, 24). Life-long adherence to a GFD

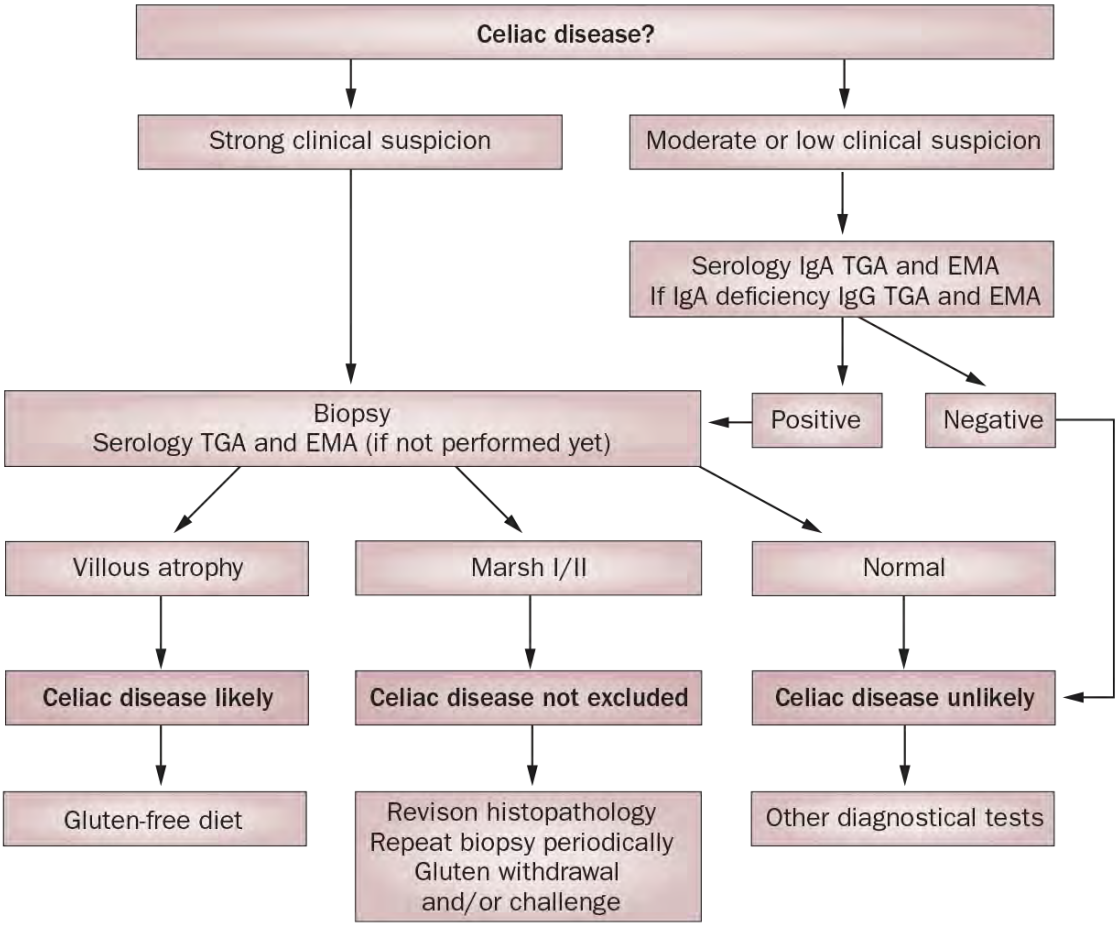

Figure I-2. Algorithm for diagnosis of celiac disease. (Figure from Tack *et. al.* 2010 (5)).

alleviates symptoms in most patients (25); nevertheless, many CD patients struggle with gluten contamination in food products, high costs and availability of gluten-free products, and the social anxiety associated with dietary restrictions (5, 26, 27). Subsequently, there have been substantial efforts to find an alternative treatment course for those with CD (5). Some treatment strategies include the hydrolysis of toxic gliadin peptide, prevention of gliadin absorption, blockade of gliadin deamidation by TG2, vaccination to restore immune tolerance, restoration of intestinal architecture, and immune modulators (28). With clinical trials ongoing, the safest and most effective treatment for CD remains a GFD (5).

Celiac disease epidemiology: genetic and environmental factors

Until recently, CD was thought to be a rare genetic disease occurring in 0.03% of the population (6). However, the prevalence of CD in Europe and the United States is approximately 1% (1, 29) and has been on the rise for many years, regardless of underdiagnosis (30). The incidence of CD varies globally, which can be only partially explained by the prevalence of risk alleles and consumption of gluten in a given region (Figure I-3). In the United States, studies of serum antibodies and biopsy screens confirmed that CD occurs in approximately 1:133 of the total population (1). As with other autoimmune diseases, CD occurs more frequently in woman than men, with a male to female ratio ranging between 1:2 and 1:3 (31, 32). While CD can develop at any age, the peak age of diagnosis occurs early in childhood during the introduction of grains

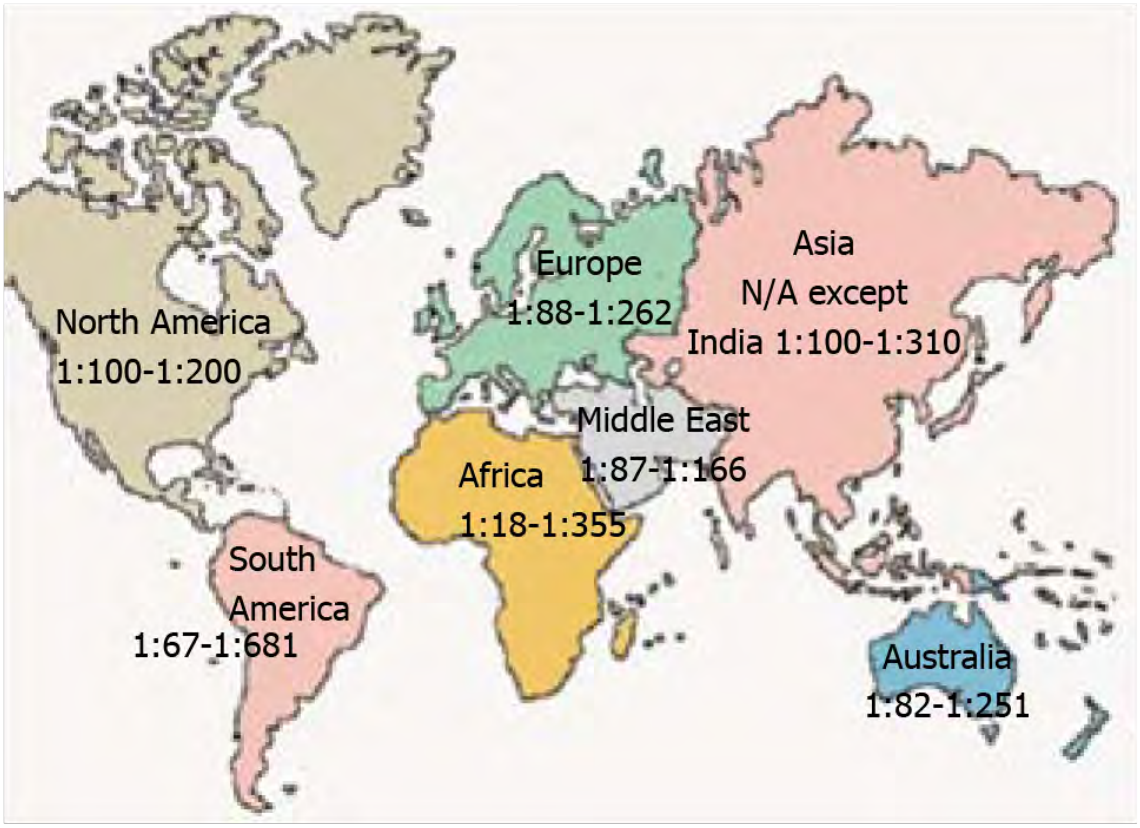

Figure I-3. Prevalence of celiac disease worldwide. (Figure from Gujral *et. al*. 2012 (28)).

(6 - 24 months of age) and later in life (third and fourth decades for women and men, respectively) (5, 28).

The significant role of genetics in CD development is indicated by a high concordance rate in monozygotic twins (33). Individuals with first- or second-degree relations to CD patients are at a higher risk with a prevalence of 1:22 and 1:39, respectively (1). CD is a polygenic disorder with linkage to more than 250 major histocompatibility complex (MHC) or non-MHC genes (28). The main genetic factors associated with CD are the MHC class II genes that encode HLA-DQ2 and DQ8. Approximately, 80-95% of those with CD possess a variant of HLA-DQ2 (encoded by *DQA1*05* and *DQB1*02* alleles), while the remaining 5% express HLA-DQ8 (encoded by *DQA1*03* and *DQB1*0302* alleles) (20-22, 34). Expression of HLA-DQ2 and DQ8 increase the likelihood of developing CD from 1 in 2518 subjects lacking all predisposing factors to 1 in 7 individuals (35).

HLA genotypes contribute to 30 - 50% of the genetic risk for CD (28, 35-38). HLA-DQ2 is frequently found in Caucasian populations in Western Europe (20 – 30%), Northern and Western Africa, the Middle East and central Asia, whereas HLA-DQ8 is more prevalent in Latin America and Northern Europe (3, 5, 39) (Table I-1, Figure I-4). In the United States, HLA-DQ2 and DQ8 occurs in approximately 20% and 5 - 20% of individuals, respectively, with a greater occurrence in Caucasian populations (28, 40, 41).

Given the frequency of genetic risk alleles in the US (37%) and prevalence of CD (~ 1%), other genetic and environment factors must prompt disease development (1). The large discrepancy in concordance rates between

Frequency of human leukocyte antigen-DQ2, encoded by human leukocyte antigen-DQB1*02 and human leukocyte antigen-DQ8, encoded by human leukocyte antigen-DQA1*0301-DQB1*0302		
< 5%	**5%-20%**	**20%**
HLA-DQ2		
Albania	Belarus Algeria	Algeria
Canada BC	Cameroon	Australia
Cook Islands	Congo	Belgium
Indonesia	Costa Rica	Central African Republic
Japan	China	Croatia
Jordan	Cuba	England
Papua New Guinea	Ecuador Africans	Equatorial Guinea Bioko Island
Philippines	France	Ethiopia
Samoa	India	Germany
	Malaysia	Greece
	Mexico	Iran
	Poland	Ireland South
	Russia	Isreal
	Singapore	Italy
	South Korea	Mongolia
	Spain	New Zealand
	Sri Lanka	Pakistan
	Sweden	Saudi Arabia
	Taiwan, China	Slovenia
	Thailand	Tunesia
	Turkey	United States
	Uganda	
	Ukraine	
	Vietnam	
HLA-DQ8		
Australia	Algeria	Argentina
China	Belgium	Ecuador
Georgia	Brazil	Ethiopia
Greece	Canada BC	Mexico
North India	Croatia	Venezuela
Spain	England Caucasoid	
Uganda	France	
	South India	
	Isreal	
	Italy	
	Japan	
	Russia	
	South Korea	
	Tunisia	
	Turkey	
	Ukraine	
	United States European American	

Table I-1. Global prevalence of HLA-DQ2 and HLA-DQ8. Estimates are based on Allele Frequency Net Database (40, 41). (Figure adapted from Gujral *et. al.* 2012 (28)).

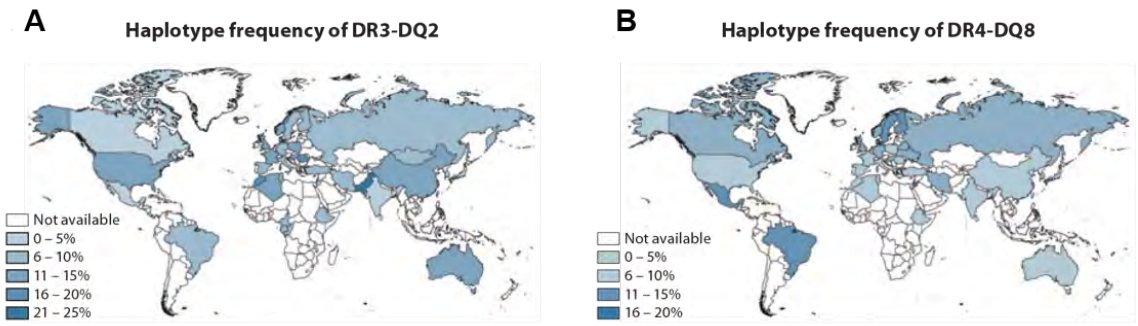

Figure I-4. Map of global prevalence of HLA-DQ2 and HLA-DQ8. (A) Frequency of the DR3-DQ2 haplotype (DRB1*0301-DQA1*0501-DQB1*0201). (B) Frequency of the DR4-DQ8 haplotype (DRB1*04-DQA1*03-DQB1*0302). (Figure from Abadie *et. al.* 2011 (3)).

monozygotic twins (approximately 75%) (33) and HLA-identical siblings (approximately 25%) (42) leads to the conclusion that non-MHC genes compose greater than 60% of inherited risk (43-45). Genome-wide association studies (GWAS) have identified 40 genomic regions and 64 candidate genes outside of the HLA as potential risk factors (3, 46). Although these regions explain only 5% of disease susceptibility (46), their functions fit well with our knowledge of disease pathogenesis.

The 64 non-HLA genes identified thus far (Table I-2) are enriched in immune pathways including chemokine receptor activity, T cell activation, lymphocyte differentiation, and cytokine binding. Genes involved in stress pathways and innate immunity also associate with CD (3). One risk locus, *IL12A*, encodes the cytokine interleukin (IL)-12 and is produced by antigen-presenting cells (APCs) to promote T cell differentiation and interferon (IFN)γ production, both of which are involved in CD pathogenesis (3, 38, 47-49). IL-2 and IL-21, which are required for proliferation and function of T cells, natural killer (NK) cell activation, and differentiation of B cells, are also associated with CD (37). Several GWAS studies identified cytotoxic T-lymphocyte associated protein 4 (CTLA4), a receptor expressed by T cells that suppresses T cell activation, as a genetic variant that increases susceptibility to CD (50, 51). Although much work remains to develop causative mechanisms for these genetic polymorphisms, several connections between risk alleles and CD pathogenesis are evident.

Human studies suggest that IL-15 (10, 52-54) and IFNα (55) are upregulated in the intestinal mucosa of patients with CD. Although GWAS studies

Loci associated with CD		
Locus	Candidate gene(s) in the region	Odds ratio
1p31.3	*NFIA*	1.11
1p36.11	*RUNX3*	1.12
1p36.23	*PARK7*, *TNFRSF9*	1.14
1p36.32	*TNFRSF14*, *MMEL1*	1.12
1q24.2	*CD247*	1.1
1q24.3	*FASLG*, *TNFSF18*, *TNFSF4*	1.1
1q31.2	*RGS1*	1.25–1.39
2p14	*PLEK*	1.14
2p16.1	*REL*, *AHSA2*	1.15
2q12.1	*IL18RAP*, *IL18R1*, *IL1RL1*, *IL1RL2*	1.19–1.28
2q31.3	*ITGA4*, *UBE2E3*	1.13
2q33.2	*CTLA4*, *ICOS*, *CD28*	1.14
3p14.1	*FRMD4B*	1.19
3p21.31	*CCR1*, *CCR2*, *CCRL2*, *CCR3*, *CCR5*, *CCR9*	1.21–1.3
3p22.3	*CCR4*	1.13
3q13.33	*CD80*, *KTELC1*	1.13
3q25.33	*IL12A*, *SCHIP1*	1.35–1.36
3q28	*LPP*	1.23–1.29
4q27	*KIAA1109*, *ADAD1*, *IL2*, *IL21*	1.44–1.59
6p21.32	*HLA-DQA1*, *HLA-DQB1*	6.23–7.04
6p25.3	*IRF4*	1.21
6q15	*BACH2*, *MAP3K7*	1.13
6q22.33	*PTPRK*, *THEMIS*	1.17
6q23.3	*TNFAIP3*	1.23
6q25.3	*TAGAP*	1.16–1.21
7p14.1	*ELMO1*	1.14
10q22.3	*ZMIZ1*	1.12
11q24.3	*ETS1*	1.21
12q24.12	*SH2B3*, *ATXN2*	1.2
14q24.1	*ZFP36L1*	1.12
16p13.13	*CIITA*, *SOCS1*, *CLEC16A*	1.16
18p11.21	*PTPN2*	1.17
21q22.3	*ICOSLG*	1.14
22q11.21	*UBE2L3*, *YDJC*	1.13
Xp22.2	*TLR7*, *TLR8*	1.14

Table I-2. Celiac disease susceptibility loci. Associations found through GWAS, in which loci replicated in at least two independent cohorts. (Figure adapted from Abadie *et. al.* (3)).

have not specifically identified polymorphisms in the genes encoding IL-15 and IFNα, several genes identified are associated with CD (Figure I-5). Preliminary analysis of intestinal biopsies from CD patients prompts a theory in which patients can be segregated into IL-15 high-expressers, IFNα high-expressers, and IL-15/IFNα high-expressers (B. Jabri unpublished data). These results may explain the heterogeneity of CD and the difficulty that ensues with identification of single genes associated with disease.

The primary environmental factor associated with the onset of CD is consumption of gluten (3, 4). Early studies identified gluten feeding as a CD trigger, and removal of gluten from the diet was found to alleviate symptoms for most individuals (2-4, 56). Compliance with a GFD diminishes anti-gliadin antibodies, autoantibodies against TG2, and histopathological findings including villous atrophy and intraepithelial lymphocytosis (57-61). Although the expression of HLA-DQ2 and DQ8 and consumption of gluten are required for the development of CD they are not sufficient (3). Furthermore, the frequency of HLA-DQ2 and DQ8 and consumption of gluten are not predictors of CD etiology (3) (Figure I-6). A remarkable example supporting a role for environmental factors is the high frequency of CD in Finnish Karelia (>2%), which contrasts with the low incidence of CD in the adjacent Russian republic of Karelia (0.2%), two neighboring regions harboring genetically similar populations and gluten consumption levels (3). Together, these observations suggest that additional environmental or genetic factors mediating CD onset have yet to be determined.

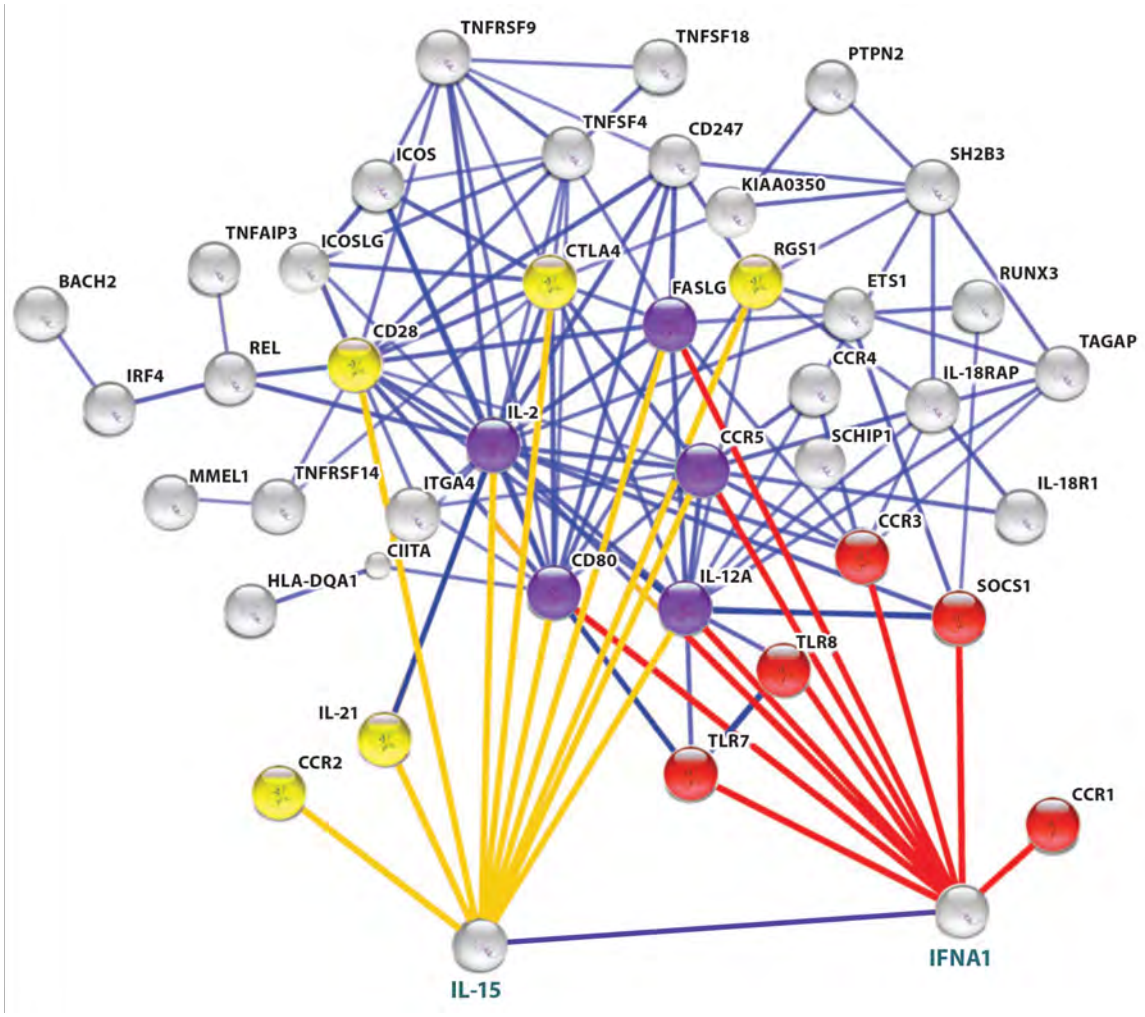

Figure I-5. Network of known functional interactions between celiac disease–associated genes and key immunological markers of disease. STRING database analysis determines functional interactions among CD susceptibility genes, as well as interactions between CD susceptibility genes and IL-15 or IFNα. Several CD susceptibility genes functionally interact with IL-15 (yellow), IFNα (red), or both (purple). (Figure from Abadie *et. al.* 2011 (3)).

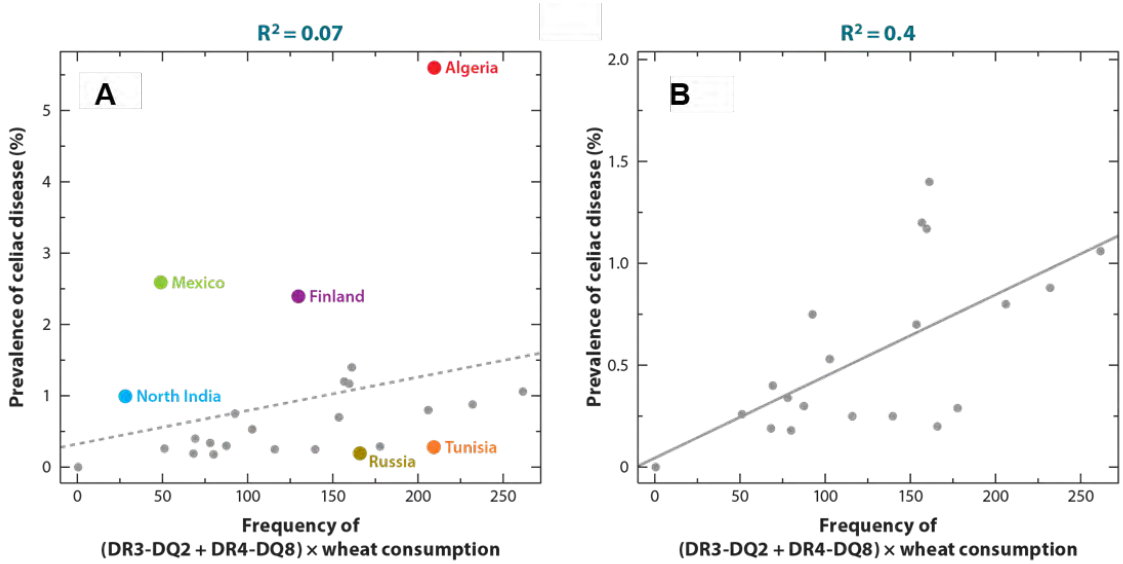

Figure I-6. Correlations between the prevalence of celiac disease, wheat consumption, and the frequencies of the DR3-DQ2 and DR4-DQ8 haplotypes. (A) Correlation between the prevalence of CD (y axis) and the product of the frequencies of DR3-DQ2 + DR4-DQ8 and the amounts of wheat consumption (x axis). (B) Correlation between the prevalence of CD (y axis) and the product of the frequencies of DR3-DQ2 + DR4-DQ8 and the amounts of wheat consumption (x axis) after excluding the following outlier populations: Algeria, Finland, Mexico, North India, and Tunisia. (Figure from Abadie *et. al.* 2011 (3)).

Important factors contributing to the development of celiac disease

Factors contributing to the onset of celiac disease	Mechanism
Gluten	Elicit T cell responses Induces cytokine production and intestinal lesion
Age of introduction of gluten	Weak gut immune during early childhood
HLA-DQ2 or HLA-DQ8	Gluten presentation
MYO9Bo	Increased permeability of the intestine
Pro-autoimmune genetic background	Shift in Th1/Th2 balance towards Th1
Viral infections	Defect in generation of active tolerance (e.g., regulatory T cells) IFN production
Tissue damage	Tissue damage Increased level of tTG Danger signals
Early termination of breastfeeding	Decreased protection against infections
Gender	Hormone-related pro-autoimmune status

Table I-3. Factors that contribute to the development of celiac disease.
(Figure adapted from Stepniak *et. al.* 2006 and Gujral *et. al.* 2012 (28)).

Since the Swedish epidemic of CD (1984 - 1996), infant feeding has been suspected in CD development (62). In this birth cohort, infant breast-feeding was abruptly stopped, and gluten feeding begun at 6 months of age. Additionally, changes to infant formula took place during this time. Although the prevalence of CD increased 3-fold during this epidemic (62), there is still much debate about the role of infant feeding in CD onset.

Epidemiological surveys suggest that socioeconomic status may also predict CD development and outcomes. One study completed in neighboring regions of Finland and Russia, where genetics and gluten intake are comparable, found that children living in worse socioeconomic conditions were slightly protected from developing CD. The authors site variations in microbiome composition, susceptibility to infections, and diet as factors that may precipitate CD (5, 63).

Finally, several studies have implicated infectious agents in the development of CD (64). This topic will be discussed further in the section on *Viral infections associated with CD*. Taken together, CD is an epidemiologically complex and multifactorial disease (Table I-3). Further study is required to identify the drivers of disease pathogenesis.

Oral tolerance

During lymphocyte development, repertoire diversity of B and T cell receptors is required to mount a successful response against microbial pathogens. Central tolerance, occurring in the thymus for T cells and bone

marrow for B cells, selects against cells that express receptors that target self-antigen and thus could be harmful to the host. Peripheral tolerance must occur outside these developmental regions to prevent excessive immune responses against nonpathogenic intruders. For example, humans ingest over 100 g of food protein per day and have approximately 10^{12} bacteria per gram of gut content colonizing the intestine, all of which could serve as targets of unnecessary immune responses (65). However, in the intestine, a unique type of peripheral tolerance, known as oral tolerance, induces local and systemic unresponsiveness following oral administration of antigens. Oral tolerance has been demonstrated in rodents using purified food proteins, cellular antigens, and haptens (66) and also occurs in humans (67-69). Following antigen feeding, oral tolerance can prevent a delayed-type hypersensitivity (DTH) response by inhibiting T cell proliferation, cytokine production, and serum antibodies against the food protein (70, 71).

Normally, food proteins absorbed by the intestine are taken up by APCs in the lamina propria (LP) underlying the villus epithelium (72, 73). Oral tolerance is dependent on LP dendritic cells (DCs) expressing integrin chain α_E (CD103) that transport oral antigen to the draining mesenteric lymph nodes (MLNs) (74). The LP $CD103^+$ DCs that travel to the MLN promote gut-homing T cell responses (75) and the proliferation of regulatory T cells (T_{regs}) (76, 77). T cells with suppressive functions, forkhead box P3 $(Foxp3)^+$ T_{regs}, inhibit inflammatory T cell responses to food antigens during oral tolerance (78), a property that can be adoptively transferred to naïve animals and abrogated by the removal of these cells (79).

Celiac disease immunopathogenesis

Disruption of oral tolerance to food proteins is thought to mediate food allergies and CD, the most prevalent food-induced pathology (65). The loss of oral tolerance to gluten produces a proinflammatory immune response in persons with CD. Following ingestion of gluten, inflammatory, gluten-specific $CD4^+$ T cells license B cells to secrete anti-gluten and autoimmune antibodies and produce cytokines that mediate cytotoxic killing of intestinal epithelial cells (IECs) (3, 47). In turn, enterocyte destruction results in blunted intestinal villi and a failure to properly absorb food nutrients.

Although gluten remains nonpathogenic in the majority of individuals, the molecular structure of the protein offers insight into its conceivably inflammatory nature. First, gluten has a high proline concentration, making it resistant to cleavage by proteases in the gut lumen (80). Second, uncleaved fragments of gluten are highly susceptible to the catalytic activity of TG2, which converts glutamine to glutamate. Deaminated, undigested, negatively charged gluten peptides preferentially bind to the positively charged HLA-DQ2 and HLA-DQ8 molecules (80-82), leading to expansion of anti-gluten $CD4^+$ T cells (83, 84). Gluten-specific, HLA-restricted $CD4^+$ T cells are found in the intestinal mucosa of CD patients (85), further solidifying their importance in disease pathogenesis.

TG2 is abundantly expressed in many tissues and localizes to extra- and intracellular regions. The enzyme functions to alter glutamines in polypeptide chains to either cross-link amines (transamidation reaction) or convert glutamine to glutamate (deamidation). Transamidation by TG2 aids in tissue repair (86),

while deamidation functions in CD pathogenesis (83, 84, 87). Specific peptide sequences, such as Gln-X-Pro, are preferentially bound by TG2, a common motif in gluten proteins, and functions as positive predictors of cereal protein “toxicity” in the CD gut (88). Experiments using mice provide evidence that TG2 is inactive in the intestinal mucosa (89), but it can be activated following treatment with polyinosinic:polycytidylic acid (poly(I:C)), a double-stranded RNA (dsRNA) analog (90). Additionally, tissue destruction and inflammation triggered by native gluten-specific T cells may lead to the activation of TG2. It is unclear whether T cell responses can occur in the absence of TG2 (47); but immunization of HLA-DQ8 transgenic (HLA-DQ8tg) mice with deamidated gluten peptides results in a greater T cell response and broader T cell repertoire (91).

Oral tolerance to food antigens is dependent on intestinal DCs that express tolerogenic factors such as retinoic acid and transforming growth factor β (TGFβ) to promote antigen-specific T_{reg} responses (92, 93). However, unlike healthy individuals, intestinal DCs stimulate inflammatory $CD4^+$ T cell responses against gluten in the intestinal mucosa of CD patients (94). The switch in DC state may result from changes in the intestinal environment. Such disruptions could be explained by high levels of inflammatory cytokines including IL-15 (52, 53, 95) and IFNα (55, 96, 97), both of which are elevated in the intestinal mucosa of those with CD (Figure I-7) Experiments using HLA-DQ8tg mice illustrate that overexpression of IL-15 alters intestinal DC homeostasis, inhibits T_{reg} conversion, and breaks tolerance to orally fed gluten (98). Additionally, type I IFN treatment also can abrogate oral tolerance in mice (99, 100). Further study is required to

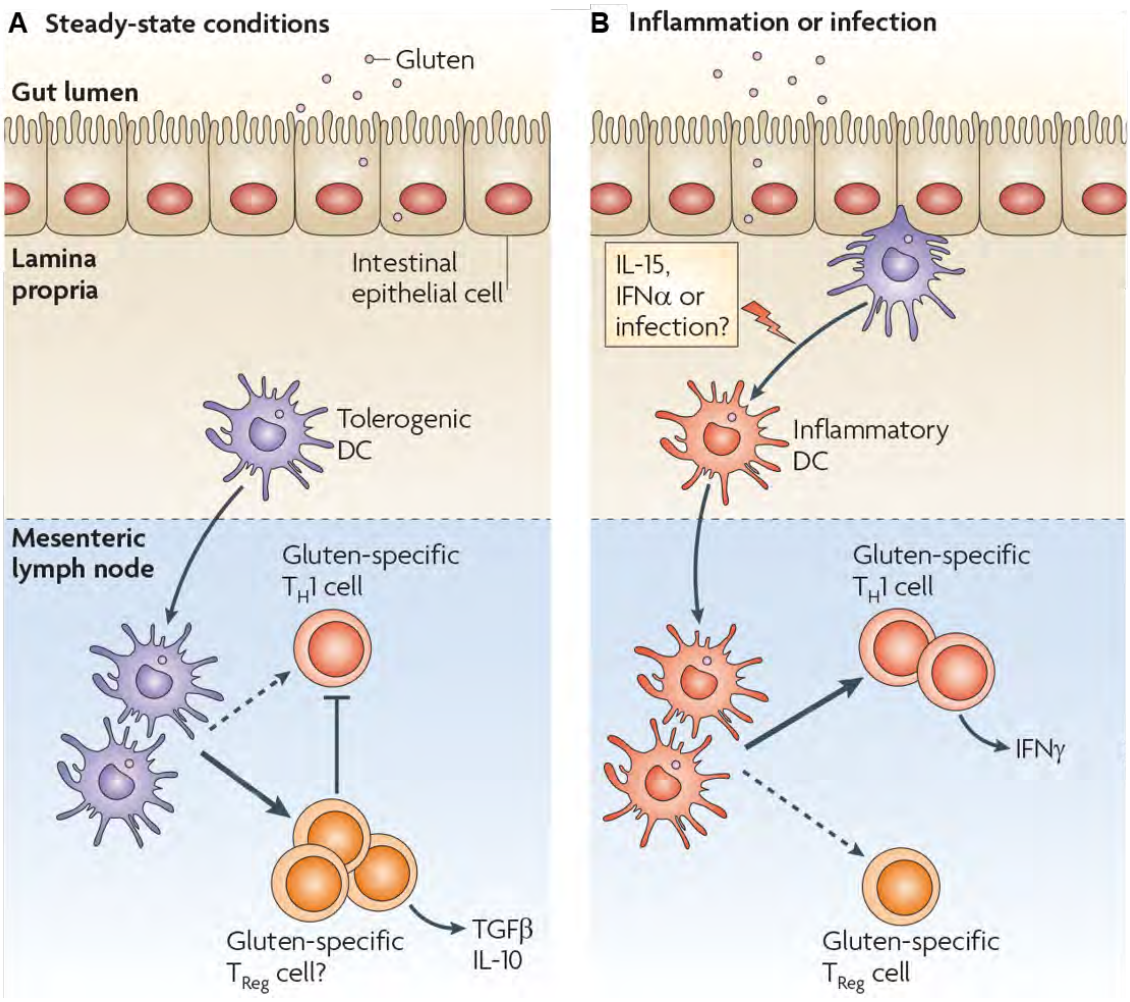

Figure I-7. Induction of inflammatory anti-gluten immune responses following gluten ingestion. (A) The default response to oral antigens is the induction of T_{reg} cells that produce TGFβ and IL-10. (B) Under inflammatory conditions, the expression of pro-inflammatory mediators, such as IL-15 and IFNα, are upregulated in the intestinal environment. DCs may acquire the ability to promote the differentiation of T cells that produce pro-inflammatory cytokines such as IFNγ. (Figure adapted from Jabri *et. al.* 2009 (47)).

determine the environmental and genetic triggers that cause higher expression of IL-15 and type 1 IFNs in the CD gut.

Several lines of evidence suggest that $CD4^+$ T cells mediate CD pathogenesis, including the identification of HLA-DQ2 and DQ8 as the most significant genetic risk determinants, the presence of gluten-specific $CD4^+$ T cells in the intestinal mucosa of persons with CD, and the decline of $CD4^+$ T cells during a GFD (47). However, gluten-specific $CD4^+$ and $CD8^+$ T cells found in the LP of CD patients do not appear to induce enterocyte cell death (85, 101). Instead, proinflammatory cytokines such as IFNγ (102) and IL-21 (103), which are secreted by these cells, provoke disease by activating intestinal epithelial lymphocytes (IELs). IELs are cytotoxic effector cells that cause enterocyte destruction in CD and are activated via stress signals instead of classical antigen recognition. The source of these stress signals is not well understood. However, gluten or other environmental factors, such as infection, may provoke their production (34).

Gluten-specific $CD4^+$ T cells also exacerbate CD immunopathogenesis by promoting B cell conversion to plasma cells that produce gluten- and TG2-specific IgA and IgG antibodies. Anti-gluten and anti-TG2 antibodies are classic hallmarks of CD that are lost during remission with a GFD (104, 105). Up to 10% of IgA produced in the LP of untreated CD patients is specific for TG2 (106), despite the lack of TG2-specific $CD4^+$ T cells. One model suggests that gluten-specific $CD4^+$ T cells aid in the formation of TG2-autoantibodies by reacting to the TG2-gluten composites analogous to hapten-carrier complexes (107).

Intestinal IgA antibodies may contribute to enterocyte death by increasing transcellular transport of gluten across the epithelial barrier and thus amplify the $CD4^+$ T cell response in the LP (108). Nevertheless, more work is required to fully understand the role of the B cell response in CD pathogenesis.

Viral infections associated with celiac disease.

Although 30-45% of the United States population has the HLA haplotypes required for CD onset, only 1% of the population develops the disease (1). Additionally, the prevalence of HLA haplotypes DQ2 and DQ8 and the amount of wheat consumption, although required, do not completely correlate with the incidence of CD (3), and HLA-DQ8 humanized mice fed gluten do not develop CD-like disease (109). Although gluten binds the MHC pocket with high affinity, there is no evidence that the peptide alone produces inflammatory T cell responses. Therefore, unidentified triggers of CD must exist to cause the initial insult that breaks oral tolerance to gluten and establishes lasting pathogenic immune memory.

There are several clues that implicate infectious agents, specifically viruses, as drivers of CD. Viral infections often induce type 1 IFNs (110), which precipitate development of CD and break oral tolerance in mice (99, 100, 111). In humans, recurrent observations of CD development have been made in patients undergoing IFNα treatment (111, 112). Type 1 IFNs also form critical nodes in the network of known CD susceptibility genes (3). Finally, viral infections are associated with an increased incidence of CD (64, 113, 114).

Epidemiological studies of children during the Swedish CD epidemic found that repeated neonatal infections were linked to CD onset (odds ratio (OD) = 1.52) (115). A prospective study of at-risk children also found that children infected with rotavirus had a higher prevalence of CD and that repeated infections intensified this effect (OD = 1.94 for one infection and OD = 3.76 for two or more infections) (114). Despite anecdotal and clinical implications that microbial pathogens act as triggers of CD, little is known about the mechanisms by which infectious agents evoke disease.

Reoviruses

Background

Viruses in the family *Reoviridae* are nonenveloped, dsRNA viruses that infect humans frequently throughout their lifetime (116). Mammalian *orthoreovirus* (reovirus) strains isolated from humans can infect mice via the oral route and activate innate immune pathways similar to the related rotavirus (117, 118). Reovirus also stimulates production of type 1 IFNs (119, 120), which are implicated in many autoimmune disorders including CD (110, 111). In concert with the availability of mouse models of infection, reovirus is ideal for studies of how infectious agents alter the host response to food antigens, as in CD.

The reovirus genome contains ten segments of dsRNA. The three large gene segments (L1, L2, and L3) encode for the λ3, λ2, and λ1 proteins, respectively. The three medium gene segments (M1, M2, and M3) encode for the μ2, μ1, and μNS proteins, respectively. The four small gene segments (S1, S2, S3, and S4) encode for the σ1 and σ1s, σ2, σNS, and σ3 proteins, respectively. The ten gene segments are packaged in an inner icosahedral core that is surrounded by an outer icosahedral capsid. The outer capsid is composed of 200 μ1-σ3 heterohexamers. The λ2 protein forms a pentameric turret-like structure at each icosahedral five-fold axis from which the trimeric σ1 attachment protein is anchored. The inner core is formed by a shell of λ1 decamers that are stabilized by σ2. Within the core lies the μ2 and λ3 proteins, the later functioning as the viral RNA-dependent RNA polymerase. Three nonstructural proteins, μNS, σNS,

and σ1s, are expressed following infection to aid in the formation of replication complexes or viral factories (117) (Figure I-8 and Table I-4). Reovirus virions are stable in the environment (121, 122) and maintain infectivity for years when refrigerated. Large quantities of infectious virions can be purified from infected mouse L929 (L) cells and used for cell culture or animal infections (123).

Reovirus infection begins with the attachment of the S1-encoded σ1 protein to cell-surface carbohydrates and the proteinaceous receptor junction adhesions molecule-A (JAM-A) (124-126). Following attachment, virions enter cells via receptor-mediated endocytosis (127-132) whereupon the particles uncoat by acid-dependent proteases to form infectious subvirion particles (ISVPs) (128, 130-133). ISVPs lack σ3 but retain σ1 and a proteolytically cleaved form of μ1 (134, 135). The μ1 cleavage fragments mediate penetration of endocytic vesicles and release of the transcriptionally active core into the cytoplasm (136-138). Primary synthesis of viral transcripts produces 11 viral proteins, including the nonstructural protein μNS, which initiates formation of viral factories (139). New virions are assembled when the 10 primary transcripts assort with the viral structural proteins that form the core particle (λ1, λ2, λ3, μ2, and σ2). Following assortment, this complex replicates each viral mRNA to form the 10 dsRNA genome segments, which can serve as templates for additional rounds of transcription. Transcriptase activity is inhibited, by a mechanism that is not well understood, by the addition of μ1, σ3, and σ1 to form progeny virions. Mature progeny virions are released from infected cells to complete the viral lifecycle.

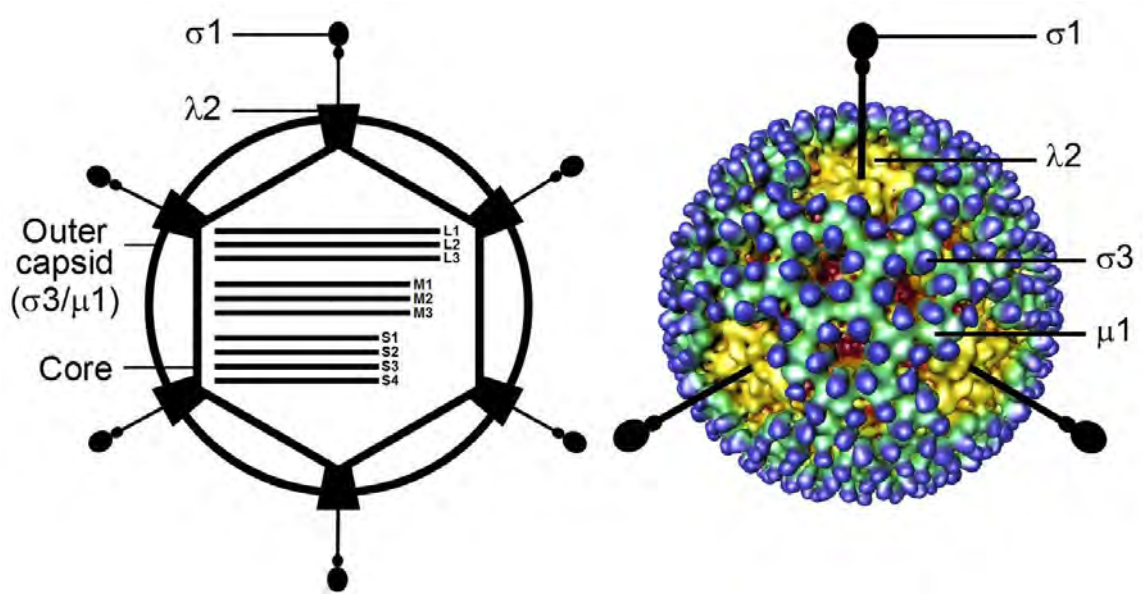

Figure I-8. The reovirus virion. Schematic of a reovirus virion (left). Cryo-electron micrograph image reconstruction of a reovirus virion (right). Outer capsid composed of σ3 (blue) and μ1 (green). Pentameric λ2 protein (yellow) forms the base for the trimeric σ1 attachment protein (added in black). (Figure adapted from Nason *et. al.* 2001 (140)).

Gene segment	Protein products
L1	λ3
L2	λ2
L3	λ1
M1	μ2
M2	μ1
M3	μNS
S1	σ1 and σ1s
S2	σ2
S3	σNS
S4	σ3

Table I-4. Reovirus gene segments and protein products. (Figure from The Molecular Basis of Serotype 1 Reovirus Glycan Interactions and the Function of Glycan-Binding in Pathogenesis, Dissertation, Jennifer Stencel-Baerenwald 2014).

History of common laboratory strains

There are three reovirus serotypes, type 1 (T1), type 2 (T2), and type 3 (T3). The prototypic strains, type 1 Lang (T1L), type 2 Jones (T2J), and type 3 Dearing (T3D), were isolated from children in the early 1950s (141, 142). Strains T1L and T3D are classically studied due to important differences in viral infection (e.g., replication biology, apoptosis induction, innate immune response activation, tissue tropism, and pathogenesis) some of which will be discussed in later sections.

Reovirus reverse genetics

The reverse genetics system for reovirus allows for the manipulation of reovirus genomes and the introduction of mutations that alter specific viral properties (143, 144). This plasmid-based system enables recovery of infectious particles from cloned DNA (cDNA) corresponding to single reovirus genes. T1L and T3D gene segment cDNAs are placed into plasmids flanked by promotor sequences for T7 RNA polymerase and hepatitis delta virus (HDV) ribozyme sequences. Transfection of plasmids into baby hamster kidney (BHK) cells that constitutively express the T7 polymerase (BHK-T7 cells) leads to transcription of reovirus genes, protein translation, and production of infectious virus. Reovirus recovered from BHK-T7 cells can be used to generate high-titer stocks in L cells (143, 145).

Reovirus tropism and pathogenesis in the intestine

Following peroral (PO) inoculation, reovirus T1L transcytoses across M cells in the ileum and disseminates to the underlying intestinal tissue (146, 147). The virus is then detected in Peyer's patches (PP), MLNs, and spleen, indicative of hematogenous dissemination (148). Reovirus can be detected in the duodenum, jejunum, ileum, and colon following PO inoculation. Early work suggested that reovirus preferentially infects intestinal IECs at the villus crypts proximal to the PP (146). However, more recent studies using neonatal mice suggest that IECs at the tip of the villus also are infected (149, 150). Differences in reovirus tropism may be linked to the age and strain of mice, housing conditions, microflora, as well as other factors yet to be determined.

Adherence of reovirus and transcellular transport into the gut occurs independently of viral serotype, viral surface proteins, and the strain and age of mice (151). Nevertheless, reovirus strains T1L and T3D differ in the capacity to infect the intestine of neonatal mice, a property that segregates with the S1 and L2 genes (152). Proteolytic processing of reovirus virions in the intestinal lumen results in generation of ISVPs (153, 154) and is required for infection of the intestine (153, 155). However, sequence polymorphisms in T3D S1 allow aberrant cleavage of the attachment protein, σ1, which decreases viral infectivity (156, 157). For my studies, I used strain T1L and engineered a T3D reassortant virus, T3D-RV, by introducing the T1L S1 and L2 gene segments into a T3D genetic background, allowing the virus to infect the intestine (152).

Reovirus has been used to study viral pathogenesis in the central nervous

system, heart, lungs, and hepatobiliary system in neonatal mice (117). Although reovirus replicates to high titers in neonatal mice, replication in adults is modest and requires large inocula (146, 158). Adult A/J mice inoculated perorally with reovirus display dose-dependent pathological changes including ileitis. However, no diarrhea occurs in these mice (146). Current dogma suggests that PO inoculation of adult mice prompts rapid viral clearance and nonpathogenic infection (89, 158).

Reovirus innate immune responses

During viral infection, cells activate antiviral immune responses to contain and inhibit viral replication. Several pattern recognition receptors recognize viral-associated molecular patterns. Recognition of reovirus requires retinoic acid inducible gene I (RIG-I) and melanoma differentiation-associated protein-5 (Mda-5) (159-161). Following ligand engagement, these intracellular sensors trigger a signaling cascade that leads to the activation of nuclear factor kappa-light-chain-enhancer of activated B cells (NF-κB) and IFN regulatory factor (IRF)-3. Activated NF-κB and IRF-3 translocate to the nucleus to induce expression of type I IFNs (IFNα and IFNβ). Secreted type 1 IFNs bind to the type 1 IFN receptor on the surface of adjacent cells. This binding triggers JAK/STAT pathway signaling, the association of phosphorylated STAT1 and STAT2 with IRF-9, translocation to the nucleus, and upregulation of type 1 IFN stimulated genes (ISGs). One ISG, IRF-7, forms homodimers or heterodimers with IRF-3 to induce a positive amplification loop (Figure I-9).

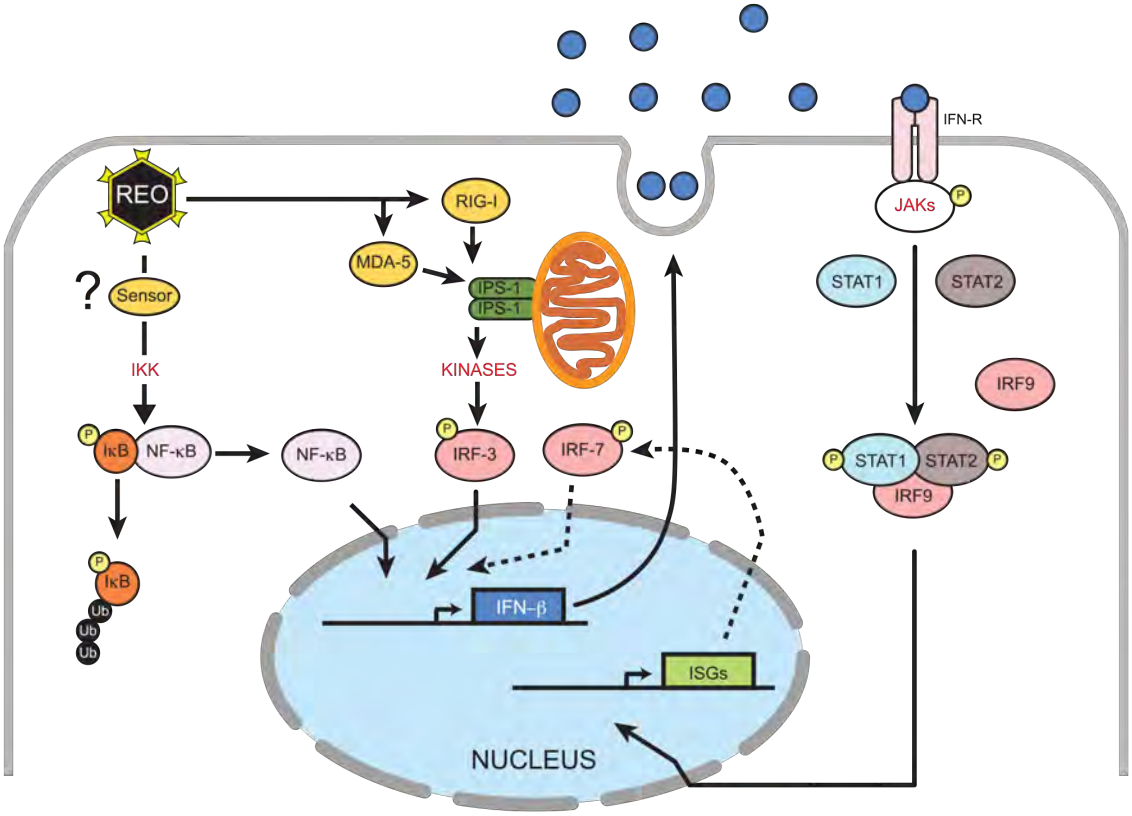

Figure I-9. Reovirus induces IFN expression. Reovirus activates RIG-I or Mda-5, which then stimulate IPS-1 to induce phosphorylation and activation of transcription factor IRF-3. Reovirus activation of NF-κB does not require RIG-I or IPS-1. Reovirus activation of NF-κB and IRF-3 leads to the production of type I IFN, which binds to the IFN-receptor (IFN-R) on adjacent cells. IFN-R binding mediates JAK-STAT signaling to elicit the production of ISGs and a positive amplification loop through IRF-7. Question mark indicates unknown protein. (Figure adapted from Fields Virology (117)).

Reovirus strain-specific differences in IFN induction have been well characterized. Reovirus T3D promotes greater expression of IFN in cultured cells and in cardiac myocytes than does T1L (89, 162), which segregates with the M1, S2, and L2 gene segments. The M1-encoded μ2 protein of T1L but not T3D functions as an IFN antagonist by sequestering IRF-9 in the nucleus and prohibiting induction of ISG expression and feedback by IRF-7 (163). Additionally, reovirus T3D is more sensitive to the effects of IFN than T1L (162, 164), which also segregates with the M1, S2, and L2 gene segments.

The type I IFN response is required for protection against reovirus infection (158, 165). Following PO inoculation, type I IFN and ISGs are upregulated in the PPs of infected mice (89). C57BL/6 (WT) mice perorally inoculated with reovirus T1L clear intestinal infection by 6 to 10 days post-inoculation (dpi) (89, 158). However, mice lacking the type 1 IFN receptor (IFNAR1-/-) have intestinal necrosis and succumb following infection with T1L. Type I IFN recognition by hematopoietic cells is required to restrict reovirus infection because irradiated IFNAR-/- mice repopulated with bone marrow from WT mice survive lethal infection (158).

Reovirus adaptive immune responses

Just as loss of innate immune pathways is detrimental during reovirus infection, mice lacking adaptive immune responses also succumb to lethal disease. PO inoculation of SCID (B cell- and T cell-deficient) mice leads to high viral titers, persistent infection, and lethal outcomes (166, 167). Transfer of

splenic lymphocytes from reovirus-immune mice protects SCID mice from reovirus infection, although, protection is lost with the removal of B cells (167). Thus, adaptive immunity is required for control of intestinal reovirus infection.

Following transcytosis via M cells (which overlay PPs), reovirus encounters DCs in the follicular associated epithelium (FAE) and subepithelial dome (SED). Actively replicating virus is found in the FAE but not the SED. Although DCs do not support viral replication, viral structural proteins are found on the surface of DCs, most likely following phagocytosis (168). Loading of viral antigen on MHC molecules of DCs and expression of inflammatory cytokines leads to the activation of T cells and NK cells for cytolysis (169). DCs from the PPs of infected mice also activate virus-specific $CD4^+$ T cells *in vitro,* an act of cross presentation (168). Activated reovirus-specific T cells migrate to the LP and intraepithelial sites. Following infection, PP, intraepithelial, and LP lymphocytes use perforin, Fas-FasL, and TRAIL pathways for cytotoxic activity against reovirus-infected cells (170). Therefore, PO inoculation of reovirus promotes a rapid and specific antiviral immune response.

Humoral immune responses to reovirus are important for protection of the intestine, clearance during primary infection, and prevention of secondary infection. Reovirus is cleared from the intestines of adult immunocompetent and β2 microglobulin-deficient ($CD8^+$ T cell-deficient) mice but not from SCID (B cell- and T cell-deficient) and MuMT (B cell- and antibody-deficient) mice (166, 167, 171). PO inoculation of adult mice with reovirus T1L results in the production of intestinal IgA and serum IgG antibodies. IgA-null mice infected with T1L are more

susceptible to secondary reovirus infection compared to WT mice, indicating that intestinal IgA is protective during mucosal reovirus infection (172). Oral administration of σ1-specific IgA or IgG protect PPs from infection with reovirus T1L (173).

Epidemiology, clinical features, and diagnosis of reovirus infections

Reovirus infections are common in humans and usually occur before adulthood. Reovirus seropositivity declines between 6 and 9 months of age, concordant with the decline in maternal antibodies (116, 174). After initial infection, reovirus antibodies increase in frequency through childhood and into adulthood (116, 174, 175). Seroprevalence of anti-reovirus IgG antibodies detected by enzyme-linked immunosorbent assay (ELISA) reaches approximately 75% to 85% in individuals 20 years and older with no decline after 60 years of age (175). Therefore, reovirus infections are common during early childhood and may occur numerous times throughout the lifespan.

Despite its near ubiquity, reovirus infections in humans are rarely symptomatic (117). When reovirus does produce symptoms, the most common manifestations occur in the respiratory tract as cough and pharyngitis (176) or in the gastrointestinal tract as gastroenteritis (177). A large outbreak of type 1 reovirus occurred in institutionalized children in Washington, D.C. in 1957. Shedding in the stool occurred for at least a week in most children. During the outbreak several symptoms were observed including rhinorrhea, pharyngitis, diarrhea, and otitis media. However, the frequency of symptoms mimicked that

prior to the preoutbreak (178). Consequently, it is unclear that reovirus infections are symptomatic.

Reovirus infections can be diagnosed by isolating virus from tissues or body fluids, detecting viral protein or RNA, or demonstrating an increase in reovirus-specific antibody titer (117). Reovirus-specific antibodies from serum can be detected by ELISA (116, 175, 179) and immunoblotting (175, 180) and confirmed using plaque-reduction neutralization or hemagluttination-inhibition assays (117). Currently, there are no commercially available, reovirus-specific ELISA kits for clinical use. However, research-based protocols remain relatively convenient and easy to use.

Apoptosis

Background

Programmed cell death, or apoptosis, is essential for life. With over 10 billion cells being produced daily in the adult human body, apoptosis must be well orchestrated and efficient to maintain homeostasis (181). Apoptosis is required for aging, embryogenesis, immune function, pathogen clearance, and wound healing. Improper regulation of apoptosis, either too much or too little, can lead to autoimmune disease, developmental defects, ischemic damage, neurodegeneration, and cancer (182). Due to its importance, apoptosis has been well characterized and most of the proteins involved in the pathway are defined. Current research seeks to understand the inducers and inhibitors of apoptosis for therapeutic use.

Apoptosis is characterized by distinct morphological changes that result from a tightly regulated proteolytic pathway. Cells undergoing this type of cell death are smaller in size, with compacted cytoplasm and organelles, and condensed chromatin (183). Although extensive membrane rearrangements occur, including membrane-blebbing and externalization of phosphatidylserine, the cell membrane remains intact, encapsulating the cellular contents (184). Apoptotic cells are rapidly phagocytosed to prevent inflammatory reactions, which is a unique process to this type of programmed cell death (185, 186).

Prior to apoptosis, cysteine-aspartyl proteases, or caspases, are sequestered in the cell as proenzymes. Following caspase cleavage, proteolytic

cascades result in the positive amplification of death signals to rapidly and irrevocably stimulate apoptosis. Ten major caspases have been identified and are categorized as initiators (caspase-2, -8, -9, and -10), effectors or executors (caspase-3, -6, and -7), and inflammatory mediators (caspase-1, -4, and -5) (182, 187, 188). There are two distinct but overlapping apoptotic pathways that initiate the caspase cascade: the extrinsic or death receptor pathway and the intrinsic or mitochondrial pathway. Both the intrinsic and extrinsic pathways converge at the execution phase to mediate the biochemical changes characteristic of apoptosis. These include cytoskeletal and nuclear protein cleavage, protein cross-linking, DNA fragmentation, formation of apoptotic bodies, and expression of ligands for recognition by phagocytic cells (182, 189).

The extrinsic pathway of apoptosis is triggered by ligand binding to death receptors in the tumor necrosis factor (TNF) receptor gene family (190). This family is defined by a cysteine-rich extracellular domain and an 80 amino acid cytoplasmic “death domain” (191). Several known ligand/receptor pairs include Apo2L/DR4, Apo2L/DR5, Apo3L/DR3, FasL/FasR, and TNF-α/TNFR1 (191-195). Stimulation of death receptors by ligand binding leads to recruitment of death domain-specific adapter proteins such as FADD, TRADD, and RIP (196-198). Activated adapter proteins associate with procaspase-8 to form the death-inducing signaling complex (DISC), which functions to auto-catalytically activate caspase-8 and trigger the execution phase of apoptosis (199).

The intrinsic pathway of apoptosis requires intracellular stimuli rather than external signaling. Such stimuli may result from cellular starvation of growth

factors, hormones, and cytokines or during stress as with hypoxia, hyperthermia, radiation, toxins, and viral infection (182). Such pro-apoptotic signals trigger changes in mitochondrial membranes, resulting in permeabilization, loss of transmembrane potential, and release of cytochrome *c* and Smac/DIABLO (200-202). Mitochondrial events are regulated by members of the B cell lymphoma 2 (Bcl-2) family of proteins (203), which function as pro- or anti-apoptotic regulators of mitochondrial membrane permeability. Following release, cytochrome *c* binds Apaf-1 to create the "apoptosome," leading to the binding, cleavage, and activation of procaspase-9 to promote the apoptosis execution phase (204, 205).

Both the extrinsic and intrinsic apoptotic pathways converge at the execution phase with the activation of caspase-3, -6, and -7. These final steps produce the morphological features of apoptosis by activating endonucleases to degrade nuclear contents and proteases to breakdown cytoskeletal proteins. The endonuclease CAD, when activated by caspase-3, cleaves chromosomal DNA leading to chromatin condensation. Caspase-3 also promotes cytoskeletal reorganization, formation of apoptotic bodies, and phosphatidylserine externalization to allow phagocytosis of dying cells (182, 206).

Several other key components of the apoptotic pathway have been described but are not fully understood. Caspase-8-mediated cleavage of Bid, a pro-apoptotic Bcl-2 family member, to its truncated form tBid provides a mechanism to connect the extrinsic and intrinsic pathways. Activated tBid promotes oligermization of other pro-apoptotic Bcl-2 family members to disturb mitochondrial membrane permeability (207, 208). Bcl-2 family members Noxa

and Puma also stimulate pro-apoptotic outcomes. Over-expression of Noxa leads to mitochondrial localization, cytochrome *c* release, and activation of caspase-9 to promote apoptosis (209). Although Noxa can be activated by *p53*, other tissue-specific factors mediate its activation (209-211). Puma, when activated in a *p53*-dependent manner, increases expression of Bcl-2 member BAX, causing its conformational change and translocation to the mitochondria to promote cytochrome *c* release (212).

Apoptosis induction during reovirus infection

Aside from an essential function in maintaining cell homeostasis, apoptotic cell death also contributes to tissue injury during disease. Several human viruses trigger apoptosis in the central nervous system (herpes simplex virus and HIV (213-215)), heart (adenovirus, cytomegalovirus, and enterovirus (216)), and liver (hepatitis B and C viruses (217-221)). Apoptosis contributes to the pathology observed in the central nervous system and heart of newborn mice infected with reovirus (117). However, prior to my thesis, the function of apoptosis in intestinal reovirus infections was not well studied.

Reovirus infection triggers cell death in many types of cell lines (222-225) and primary cell cultures (226, 227). Infection with reovirus can activate both intrinsic and extrinsic pathways of apoptosis (228) (Figure I-10). Following reovirus infection, cytochrome *c* and Smac/DIABLO are released from the mitochondria, prompting activation of the intrinsic apoptosis pathway (229). Additionally, reovirus infection is associated with elaboration of TRAIL, which

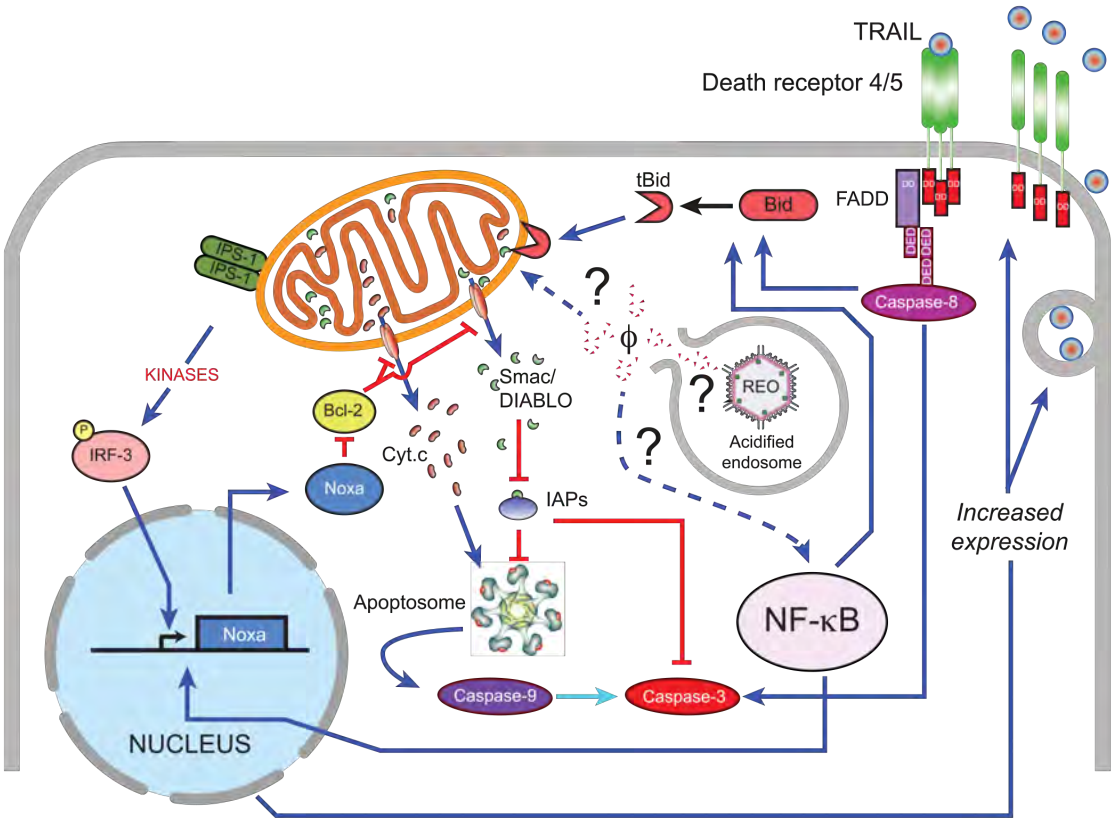

Figure I-10. Reovirus activates both intrinsic and extrinsic apoptotic pathways. Reovirus-induced apoptosis requires disassembly of virions. Reovirus stimulates mitochondrial release of cytochrome c and Smac/DIABLO, which together activate caspase-9 as part of the intrinsic apoptotic pathway. Smac/DIABLO represses IAP, which inhibits caspase-3. Reovirus activates IRF-3 and NF-κB, resulting in induction of the proapoptotic protein, NOXA. Reovirus also induces TRAIL binding to DR5, which together activate caspase-8 as part of the extrinsic apoptotic pathway. Reovirus activates Bid cleavage to tbid to promote “cross-talk” between the extrinsic and intrinsic apoptotic pathways. Known stimulatory pathways are indicated by dark blue arrows (light blue arrows if not required); known inhibitory pathways are indicated by red bars. Possible stimulatory pathways are indicated by dashed blue arrows or question marks. (Figure adapted from Fields Virology (117)).

binds the death receptor DR5 (222), and leads to recruitment of FADD, activation of DISC, and cleavage of caspase-8 to stimulate the extrinsic pathway (222, 228). However, activation of the extrinsic pathway alone is insufficient for reovirus-mediated apoptosis, and intrinsic pathway activation must occur for maximum cell death (228, 230).

Reovirus-induced apoptosis requires induction of NF-κB and IRF-3 in most cell types and is triggered during recognition of the virus during viral entry by cellular pattern recognition receptors (159, 231). NF-κB signaling is required for both intrinsic and extrinsic pathway activation (232). For example, NF-κB is required for cleavage of Bid and sensitization of cells to TRAIL (230, 233). Additionally, reovirus mutants with diminished NF-κB activation also display limited apoptosis potential, but the mechanism is unknown (234). Along with activation of NF-κB, IRF-3 activation is required for maximal levels of apoptosis (159). NF-κB and IRF-3, independent of IFN, can stimulate expression of Noxa, which markedly enhances reovirus-induced apoptosis (165).

Replication of reovirus is not required for programmed cell death (225). Therefore, steps in the reovirus replication cycle that occur prior to synthesis of viral proteins and RNA, such as attachment, membrane penetration, or particle disassembly, likely mediate apoptosis. Strain-specific differences in cell death suggest the existence of viral determinants of apoptosis. Cells infected with T3 strains produce apoptosis significantly more efficiently than T1L, a property that segregates with the S1 and M2 gene segments (224, 225, 235). A variant virus incapable of expressing σ1s retains the capacity to induce apoptosis, suggesting

that σ1 is the S1 gene product required for programmed cell death (236). However, the requirement for σ1 may be tissue-specific and has only been studied using neonatal mouse models of encephalitis and myocarditis (237). The reovirus M2-encoded μ1 protein is delivered to the cytoplasm during viral membrane penetration, a step that is required for apoptosis (238). The ϕ domain of μ1 is necessary and sufficient to promote apoptosis in cell culture (234, 239). Prior to my thesis work, reovirus-induced apoptosis in the intestine had not been studied, therefore little was known about the viral determinants required to induce cell death in this tissue.

Physiological and pathogenic apoptosis induction in the gut

The intestinal epithelium uniquely functions to passively transport nutrients and water while remaining impermeable to the external environment. Any insult, whether microbial, toxic, or traumatic, can lead to cell death, loss of epithelial contiguity, breakdown in gut barrier function, and disease. The intestinal epithelium of most mammals is capable of regenerating to alleviate disruptions in barrier function and maintain homeostasis. Newly generated IECs or enterocytes migrate from the villus crypt towards the villus tip, before being extruded into the gut lumen. The rapid renewal of the villus epithelium by stem cells occurs every 2 to 6 days in adult mammals, with approximately 10^{11} cells extruded per day in humans (240). Mathematical models of the mouse intestine suggest that 1400 mature enterocytes are shed from a single villus in a 24-hour period, equating to 2×10^8 cells extruded per day (241).

In a healthy gut, extruded IECs are replenished from stem cells undergoing mitosis in the villus crypts, maintaining a predefined crypt:villus ratio and a homeostatic villus length. With the surface area of the small intestine estimated to be about 250 square meters, maintenance of the epithelial barrier requires the largest turnover rate of any fixed cell in the body (242). Circadian rhythms (243), luminal nutrients (244), hormones (244, 245), the microbiota (246), and expression of TGFβ (245) influence the physiological growth rate of intestinal villi. Enterocyte shedding at the villus tip is difficult to observe in fixed tissue, with only 6% of hematoxylin and eosin (H&E) stained sections of human intestines containing evidence of IEC extrusion (247) (Figure I-11). Therefore, many studies rely on quantification of crypt:villus ratios, crypt proliferation, and cell death as surrogates to understand the effects of various factors in gut homeostasis.

The physiological loss of enterocytes from the villus tip is thought to be a passive process by which cells or clusters of cells are sloughed into the intestinal lumen (240). Although the process is energy efficient, it requires a complex orchestration of cellular events (248). From the small percentage of shedding events observed in humans, it appears that whole cells are expelled from the intestinal villus without the association of lymphocytes or macrophages. Similar processes occur in mice, rats, and hamsters, making these animals useful models for studies of enterocyte sloughing (247). The “zipper model” of epithelial cell shedding is used to explain the extrusion of IECs (249). Basolateral movement of tight junctions down the plasma membrane of neighboring

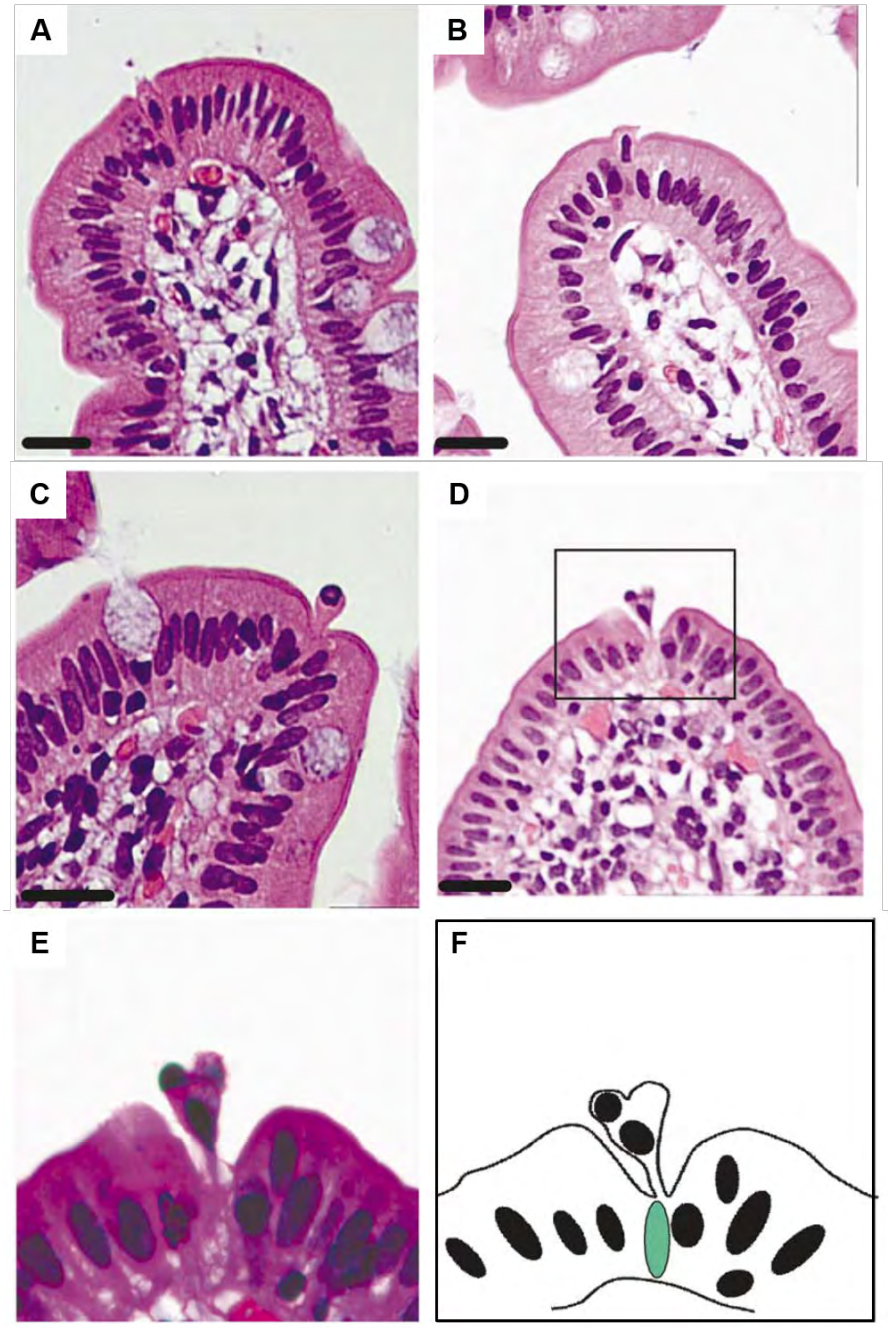

Figure I-11. Morphology of enterocytes during shedding. Small intestinal sections were stained with H&E. Representative sections of sloughing cells are shown (A-D). The nuclei become condensed and fragmented during shedding. Eosin staining is reduced beneath the shedding cell in (D) and highlighted green in the line drawing (F). This is extending from the level of neighboring nuclei to the basement membrane. A magnification of image (D) is shown in (E). (Figure from Bullen *et. al.* 2006 (247)).

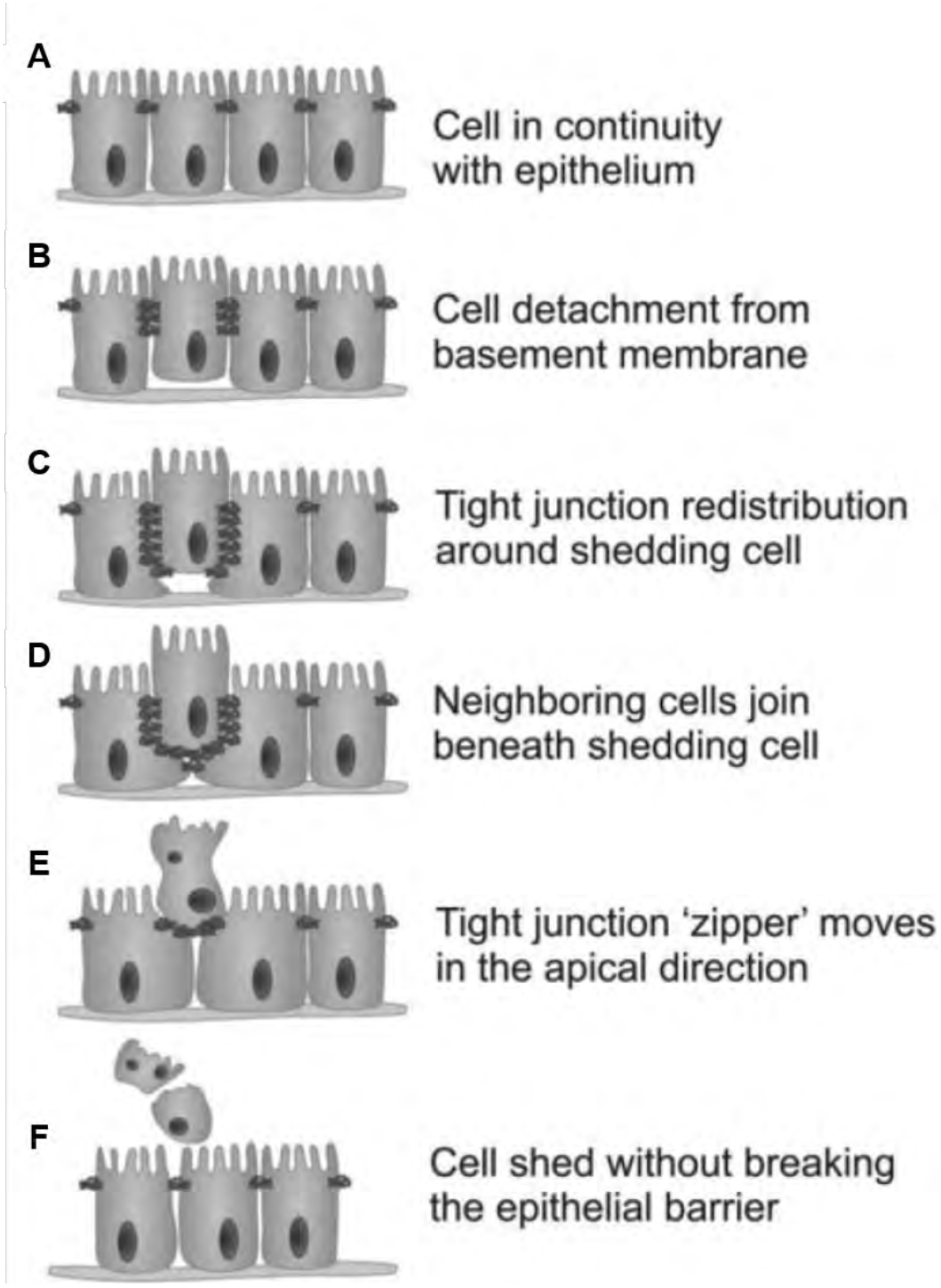

Figure I-12. Zipper model of epithelial shedding. Neighboring cells maneuver tight junctions to extrude the cell without breaking the epithelial barrier. (Figure from Williams *et. al.* 2015 (248)).

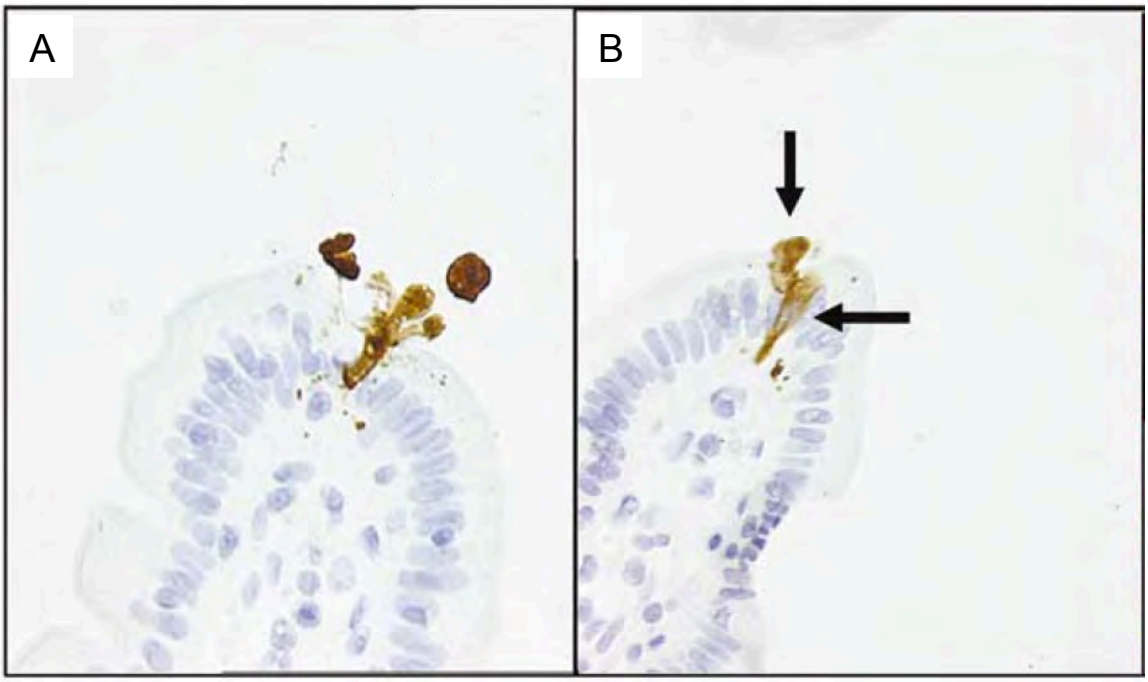

Figure I-13. Apoptosis and cell shedding of enterocytes. Small intestinal sections were stained with an antibody against cleaved caspase-3. (A) An apoptotic cell, expressing activated caspase-3 sloughs from the epithelial membrane. (B) A cell in the process of being shed from a villus tip (vertical arrow) and a second cell (horizontal arrow) with activated caspase-3 that does not actively shedding and remains attached to the basement membrane. (Figure from Bullen *et. al.* 2006 (247)).

enterocytes leads to a joining of the neighbor cells beneath the extruding cell. The neighboring cells “zipper” up their tight junctions forcing the extruding cell out of the epithelium and enabling the entire cell to be expelled without barrier breakdown (Figure I-12) (249).

Although the exact signals that trigger enterocyte extrusion are unknown, shedding of neighboring cells can occur within 5 to 10 minutes of the initial event, suggesting that intercellular communication coordinates enterocyte shedding (250). IECs undergoing cell death can be identified using biochemical markers of apoptosis, such as activated caspase-3 (247) (Figure I-13). However, it is unknown whether apoptosis precedes cellular extrusion or whether apoptosis occurs rapidly after loss of survival signals due to extrusion (248). Studies of *ex-vivo* models of the murine small intestine indicate that loss of tight junction proteins, such as E-cadherin, results in intrinsic apoptosis pathway stimulation, including the activation of caspase-9 (251). Analysis of cleaved caspase-3 immunostaining of fixed tissue suggests that apoptotic pathways can be triggered prior to cell shedding, although this relationship is temporal and not causal (252-254).

Spontaneous apoptosis rarely occurs in healthy intestinal tissue, with only 0.4% of villus cells expressing activated caspase-3 in mice ((255), Brown unpublished). However, pathogenic insults can cause enterocytes to die and slough into the intestinal lumen. If crypt cells do not proliferate efficiently, villi become blunted and, if unresolved, such insults can cause a breakdown in the gut barrier and disease. Pathogenic stimuli of enterocyte sloughing include

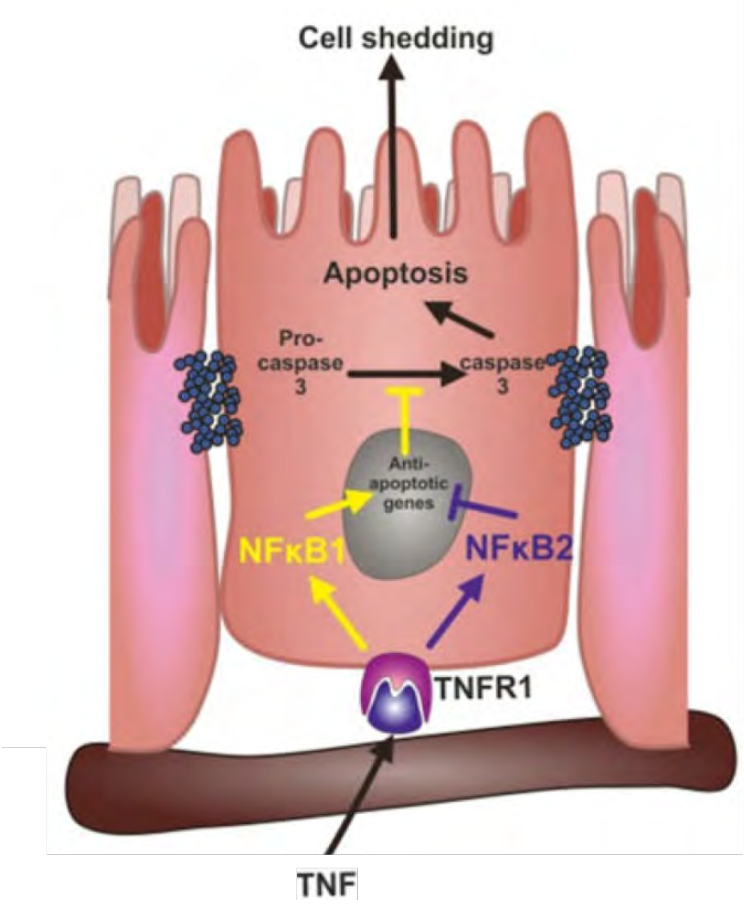

Figure I-14. Proposed diagram of TNF treatment inducing enterocyte apoptosis and cell shedding. TNF binds the TNF receptor (TNFR1) on intestinal epithelial cells, triggering NF-κB and pro-apoptotic genes. The execution phase of apoptosis is activated by caspase-3 cleavage, which leads to cell death and possibly mediates cell sloughing. (Figure adapted from Williams *et. al.* 2015 (248)).

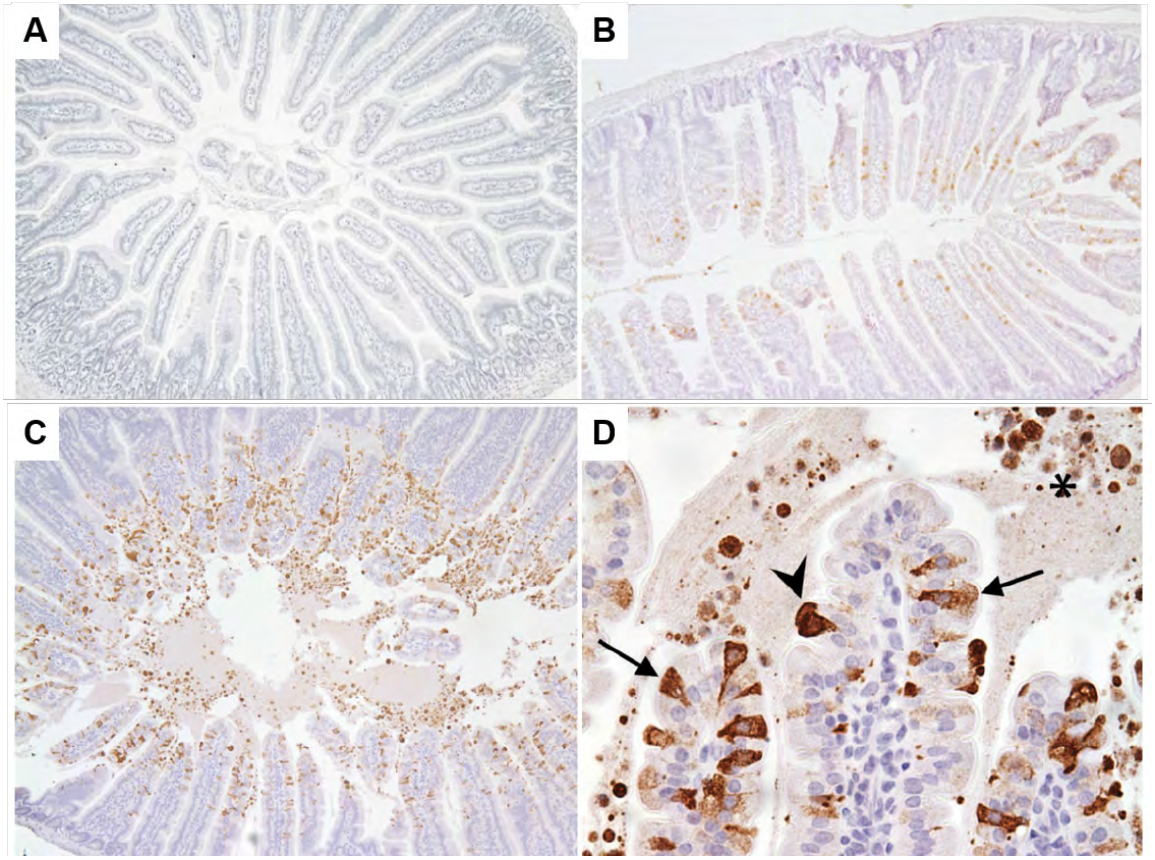

Figure I-15. Pathological enterocyte apoptosis and cell shedding following lipopolysaccharide (LPS) injection. Small intestinal sections were stained with an antibody against cleaved caspase-3. (A) Untreated control. (B) Representative image of intestinal epithelium 1 hour after LPS administration. (C) Representative image of intestinal epithelium 1.5 h after LPS administration. A magnification of image (C) is shown in (D). Activated caspase-3 labeled apoptotic cells in the epithelium (arrows) or undergoing extrusion/cell shedding (arrowhead) into the intestinal lumen are shown. (Figure from Williams *et. al.* 2015 (248)).

bacterial lipopolysaccharide (LPS) (254, 256) and other bacterial toxins (257), burn injury (258), ischemia (245), poly(I:C) (253), trauma (259), and TNF (260) (261, 262). Treatment with TNF potently stimulates IEC apoptosis and shedding in mice (261, 262), which appears to be NF-κB dependent (254) (Figure I-14). Administration of bacterial LPS also exacerbates enterocyte apoptosis and cell sloughing, causing increased gut permeability and diarrhea (254) (Figure I-15). Intraperitoneal (i.p.) injections of mice with poly(I:C) or rotavirus genomic dsRNA are sufficient to stimulate enterocyte cell death as observed by activated caspase-3 immunostaining, villus shortening, and diarrhea (253, 263). Intestinal epithelial pathology caused by dsRNA analogs is dependent on TLR3 recognition and caspase-8 signaling. However, more remains to be elucidated about pathways used by viruses to promote cell death and sloughing in the gut and whether these mechanisms alter viral capacity to induce CD.

Hypothesis

Viral infections of the intestine alter the immune response to oral antigens such as gluten and lead to development of celiac disease

Significance

CD occurs in approximately 1 in 133 persons in the United States and is a significant cause of morbidity. Cumulatively, my thesis work has enhanced understanding of virus-mediated disruption of immune tolerance to orally fed antigen and defined viral determinants required for CD development. Understanding the viral factors and mechanisms by which loss of oral tolerance is provoked will contribute to the development of improved prevention strategies, screening approaches, and treatment for CD patients.

CHAPTER II

REOVIRUS INFECTION TRIGGERS INFLAMMATORY RESPONSES TO DIETARY ANTIGENS AND DEVELOPMENT OF CELIAC DISEASE

Introduction

CD is a complex immune disorder with an autoimmune component in which genetically susceptible individuals display an inflammatory T-helper 1 (T_H1) immune response against dietary gluten present in wheat (3, 56, 264). The HLA-DQ2 or -DQ8 restricted T_H1 response against gluten is central to CD pathogenesis and thought to precede development of villous atrophy (48). However, epidemiological and immunological observations support a role for additional genetic and environmental factors in CD pathogenesis. Previous studies have implicated adenovirus, enterovirus, hepatitis C virus, and rotavirus as triggers of CD (64). Working with the laboratory of Dr. Bana Jabri at the University of Chicago, we proposed that viral infections significantly contribute to CD development and immunopathogenesis. However, little was known about the mechanisms by which viruses evoke the disease. Therefore, we established a virus-induced model of oral tolerance abrogation to define the specific viral characteristics involved in disease etiology.

Results

Viral infection experimental model using genetically engineered reoviruses.

Viruses in the family *Reoviridae* commonly infect humans during early childhood (116), and seroprevalence remains intact throughout life (175). Reovirus T1L infects the intestine of mice and perturbs intestinal immune homeostasis (168, 265), whereas T3D is incapable of infecting the intestine (265). Based on pathobiological differences that occur during infection with T1L and T3D, we hypothesized that engineering a T3D reassortant virus capable of intestinal infection would yield two viruses with potentially different effects on tolerance to dietary antigen. Therefore, we engineered T3D-RV by introducing the S1 and L2 gene segments of T1L into a T3D genetic background, thus allowing the virus to infect the intestine (152) (Figure II-1A). Such reassortants arise naturally (117, 118) and can be readily recovered in the laboratory using reverse genetics (168). T1L and T3D-RV replicate comparably in intestinal Caco-2 cells (Figure II-1B) and display a similar capacity to infect the small intestine at early time points (Figure II-1, C and D). As in humans, these viruses are cleared (Figure II-1E) without inducing intestinal damage (Figure II-1F) (116) and elicit neutralizing anti-reovirus antibodies (Figure II-1G). Of note, although both viruses induced high anti-reovirus antibody titers, antibody levels observed following T1L infection were significantly higher than those following T3D-RV infection (Figure II-1G). However, comparison of the host T cell response in phosphate-buffered saline (PBS) (sham) and virus-inoculated mice revealed that T1L and T3D-RV

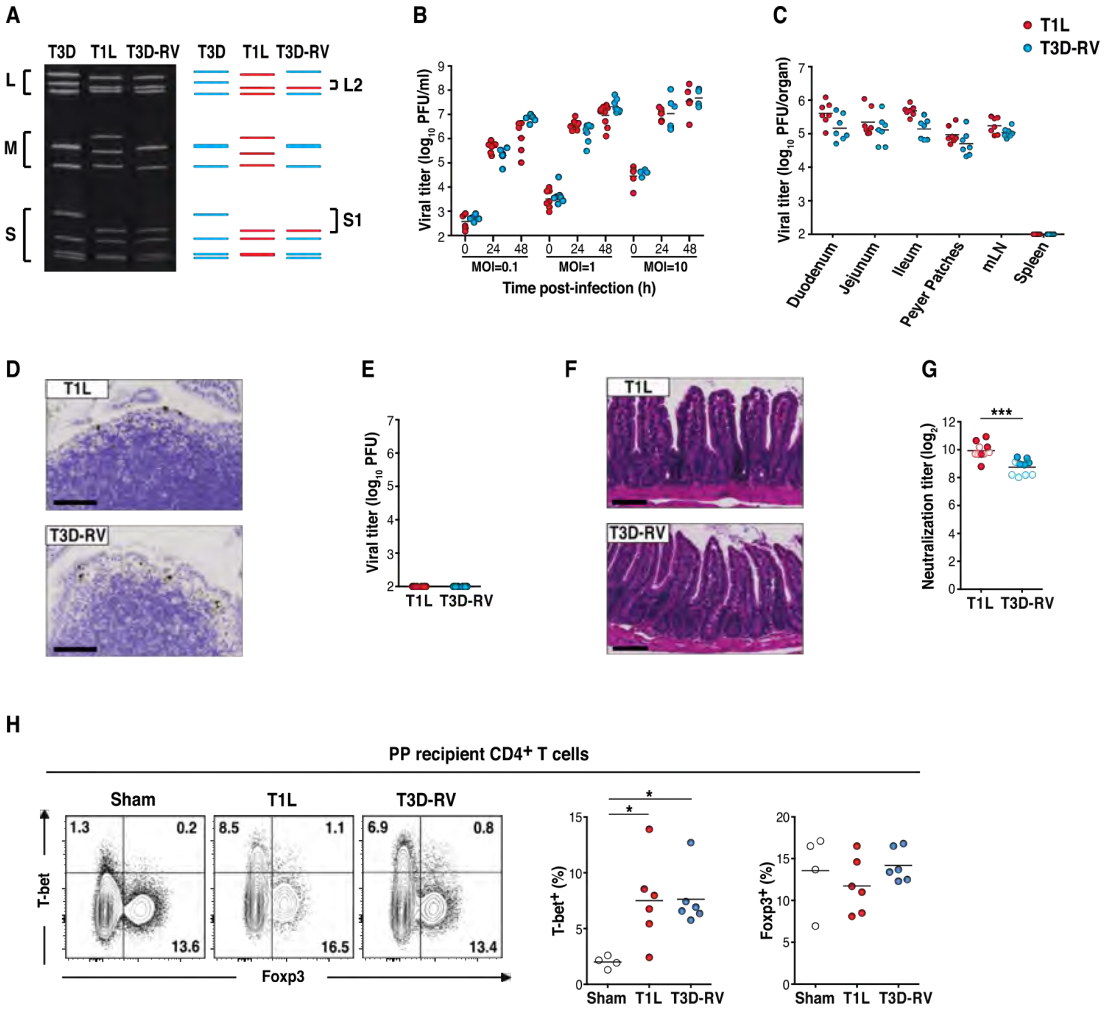
A
T3D T1L T3D-RV T3D T1L T3D-RV
L
M
S
L2
S1
B
Viral titer (log10 PFU/ml)
MOI=0.1
MOI=1
MOI=10
Time post-infection (h)
C
T1L
T3D-RV
Viral titer (log10 PFU/organ)
Duodenum
Jejunum
Ileum
Peyer Patches
mLN
Spleen
D
T1L
T3D-RV
E
Viral titer (log10 PFU)
T1L T3D-RV
F
T1L
T3D-RV
G
***
Neutralization titer (log2)
T1L T3D-RV
H
PP recipient CD4+ T cells
Sham
T1L
T3D-RV
T-bet
Foxp3
1.3
0.2
13.6
8.5
1.1
16.5
6.9
0.8
13.4
T-bet+ (%)
Foxp3+ (%)
Sham T1L T3D-RV

Figure II-1. Experimental model of viral infection using genetically engineered reoviruses. (A) Electropherotypes and schematic of T1L, T3D, and T3D-RV gene segments. Purified viral particles were electrophoresed in an SDS-polyacrylamide gel, which was stained with ethidium bromide to visualize viral gene segments. Size classes of gene segments, large (L), medium (M), and small (S) are indicated. (B) Titers of T1L (red circles) and T3D-RV (blue circles) in Caco-2 cells were determined at the indicated times and multiplicity of infection (MOIs) by plaque assay. (C to H) WT mice were inoculated perorally with 10^{10} plaque forming units (PFU) of T1L or T3D-RV. (C) Titers of T1L (n = 7) and T3D-RV (n = 7) in the indicated small intestinal compartments, PP, MLN, and spleen were determined at 24 hours post-inoculation (hpi) by plaque assay. The small intestine was resected from the pylorus to the cecum and sectioned into three equal parts comprising the duodenum, jejunum and ileum. (D) At 24 hpi, small intestines of infected mice were resected and processed for histology. Sections were stained with polyclonal reovirus antiserum (brown). Representative sections of PP are shown (scale bar: 100 μm). (E) At 6 dpi, the ileum was resected, and titers of T1L and T3D-RV were determined by plaque assay (n = 6 mice per virus strain). (F) At 8 dpi, small intestines of infected mice were resected and processed for histology. Sections were stained with H&E. Representative sections of ileum are shown (scale bar: 100 μm). (G) At 18 (open circles) or 21 (filled circles) dpi, sera were collected, heat-inactivated, and used for a plaque-reduction neutralization assay (PRNT60) (n = 10 mice per virus strain). (H) The intracellular expression of Foxp3 and T-bet in PP $CD4^+$ T cells at 6 dpi was evaluated by flow cytometry. Representative dot plots and percentages of Foxp3- and T-bet-expressing $CD4^+$ T cells are shown. (B) Data represent two independent experiments performed in triplicate. (C, E, G, and H) Graphs depict two independent experiments. (B, C and H) *, $P < 0.05$; one-way analysis of variation (ANOVA)/Tukey's multiple comparison. (E and G) ***, $P < 0.001$; unpaired t-test.

induced similar antiviral T_H1 responses in PP (Figure II-1H), the site at which protective immunity to reovirus is induced (168).

Reovirus T1L infection promotes inflammatory immunity to dietary antigen.

Having established that the two strains infect and induce protective immunity in PPs, we next investigated whether they affect immune responses to dietary antigens at inductive and effector sites of oral tolerance, MLN and LP (65, 266), respectively. In collaboration with the Jabri laboratory, we transcriptionally profiled the virus-host interaction at multiple sites of the gut. Minimum spanning trees (MST) (267, 268) and multidimensional scaling ordination (Figure II-2A), performed by the laboratory of Dr. Aylwin Ng at Harvard University, revealed transcriptional profile clusters that were strongly driven by differences in location (epithelium, LP, PP, and MLN) and were influenced by reovirus infection in a location- and time-dependent manner. This strong location effect was evident and predominantly captured along Dimension 1, which together with Dimension 2, also captured virus-dependent differences. At the early time point (6 h), the transcriptional profile of both viruses segregated from sham in PP and the epithelial compartment (primary sites of infection (168)) and had no effect on MLN (Figure II-2A). In contrast, at 48 h, the viruses altered the transcriptional profile of the LP and MLN (sites of induction of immune responses to dietary antigens) (65, 266), and transcriptional differences between the two viruses emerged (Figure II-2A). The Ng lab performed an in-depth factorial design analyses (Figure II-3) to identify host genes that were differentially expressed in

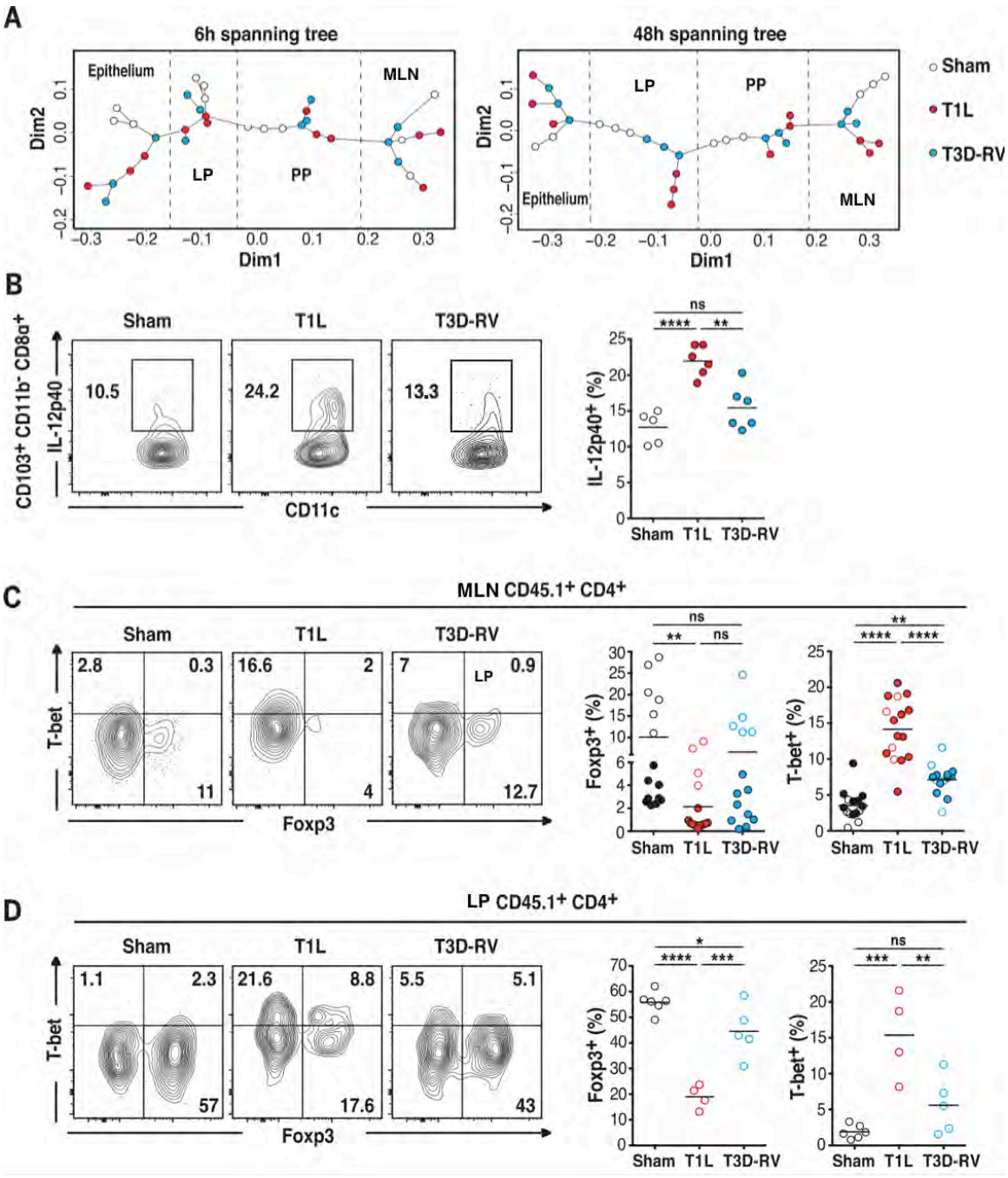
A
6h spanning tree
48h spanning tree
Epithelium
LP
PP
MLN
Dim1
Dim2
Sham
T1L
T3D-RV
B
Sham
T1L
T3D-RV
10.5
24.2
13.3
CD103+ CD11b- CD8α+
IL-12p40
CD11c
IL-12p40+ (%)
ns
****
**
C
MLN CD45.1+ CD4+
2.8
0.3
11
16.6
2
4
7
0.9
12.7
T-bet
Foxp3
Foxp3+ (%)
T-bet+ (%)
D
LP CD45.1+ CD4+
1.1
2.3
57
21.6
8.8
17.6
5.5
5.1
43
*
***

Figure II-2. T1L blocks the differentiation of peripheral T_{reg} (pT_{regs}) and promotes T_H1 immunity to dietary antigen at inductive and effector sites of the gut. (A) For each time point, WT mice were inoculated perorally with 10^{10} PFU of T1L (n = 3 mice; red circles), 10^{10} PFU of T3D-RV (n = 3 mice; blue circles), or PBS (sham, n = 3 mice; open circles) and euthanized 6 or 48 hpi. RNA of MLN, PP, epithelium, and LP were isolated and analyzed by means of microarray. MST is represented on multidimensional scaling ordination. The MST traces a path of minimum weight through each vertex or node that represents the profile of differentially expressed genes for each sample state shown. The lengths of edges (or connecting paths) indicate the level of dissimilarity between samples. Each sample state and the distances between them are represented in two-dimensional space. The coordinates of each sample along each dimension are indicated by the two axes. (B) Mice were inoculated perorally with 10^8 PFU of T1L (n = 6 mice), 10^8 PFU of T3D-RV (n = 6 mice), or PBS (sham, n = 5 mice) for 2 d. The expression of IL-12p40 on gated MHC-II$^+$ CD11c$^+$ CD103$^+$ CD11b$^-$ CD8α$^+$ MLN DCs was evaluated by means of flow cytometry. Representative dot plots and percentages of IL-12p40 in the MLN are shown in the CD103$^+$ CD11b$^-$ CD8α$^+$ DC subset. (C and D) OT-II$^+$ CD45.1$^+$ CD4$^+$ T cells were transferred into WT CD45.2$^+$ mice. One day after transfer, mice were inoculated perorally with 10^{10} PFU of T1L (n = 4 to 16 mice), 10^{10} PFU of T3D-RV (n = 5 to 14 mice), or PBS (sham, n = 6 to 15 mice) and fed 1.5% ovalbumin (OVA) in the drinking water (filled circles) or an OVA-containing diet (open circles) for 6 d. The intracellular expression of Foxp3 and T_{bet} in transferred OT-II$^+$ CD45.1$^+$ CD4$^+$ T cells in the MLN and in the LP was evaluated by means of flow cytometry. Representative dot plots and percentages of Foxp3$^+$ T-bet$^-$ and T-bet$^+$ Foxp3$^-$ cells are shown in the MLN (C) and in LP (D), respectively. (B to D) Graphs depict at least two independent experiments. *, $P < 0.05$; **, $P < 0.01$; ***, $P < 0.001$; ****, $P < 0.0001$; one-way ANOVA/Tukey's multiple comparison.

Early (6h) impact by T1L and T3D-RV

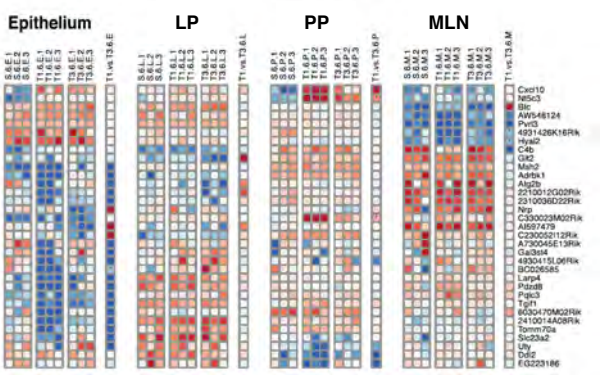

Late (48h) impact by T1L and T3D-RV

Late (48h) impact by T1L and T3D-RV (cont'd)

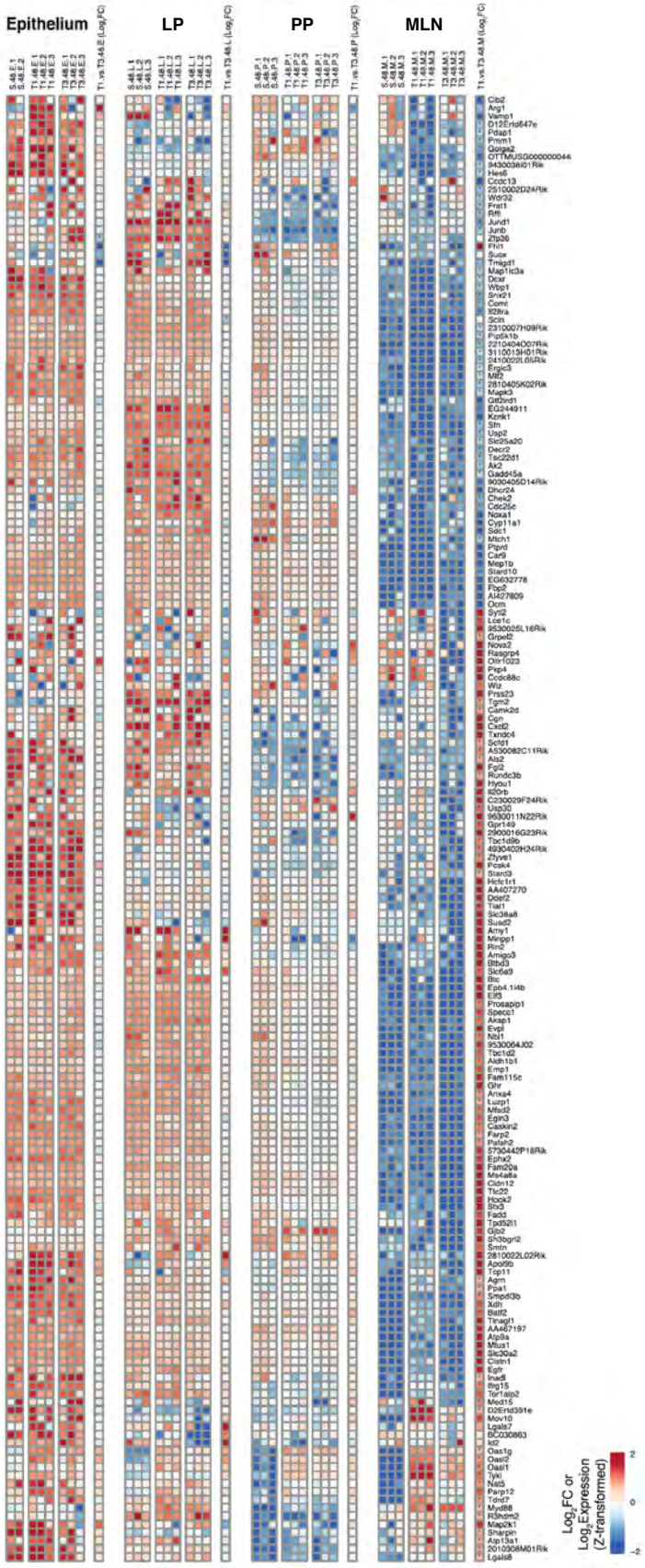

Figure II-3. Temporal and spatial gene expression in response to reovirus infection. Heatmap shows the subset of the 2307 gene features used for generation of the spanning trees (Fig. II-2 A). These key genes were found to be significantly expressed in the virus response with respect to sham and exhibited significant expression differences between T1L (T1) and T3D-RV (T3) in the indicated tissue types.

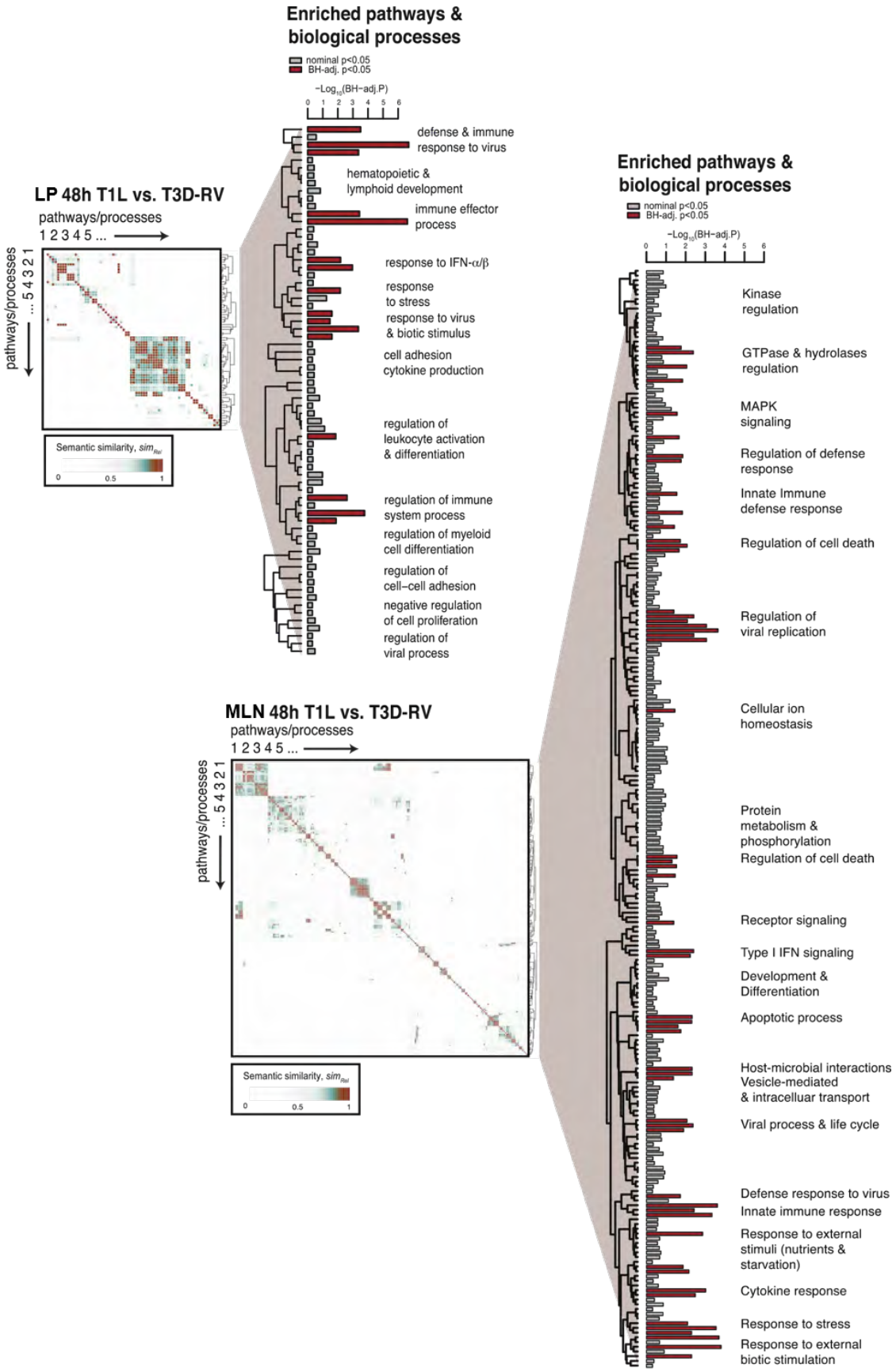
Enriched pathways & biological processes
nominal p<0.05
BH-adj. p<0.05
−Log10(BH−adj.P)
0 1 2 3 4 5 6
defense & immune response to virus
hematopoietic & lymphoid development
immune effector process
response to IFN-α/β
response to stress
response to virus
& biotic stimulus
cell adhesion
cytokine production
regulation of leukocyte activation & differentiation
regulation of immune system process
regulation of myeloid cell differentiation
regulation of cell−cell adhesion
negative regulation of cell proliferation
regulation of viral process
LP 48h T1L vs. T3D-RV
pathways/processes
1 2 3 4 5 ...
... 5 4 3 2 1
Semantic similarity, sim_Rel
0 0.5 1
MLN 48h T1L vs. T3D-RV
pathways/processes
1 2 3 4 5 ...
... 5 4 3 2 1
Semantic similarity, sim_Rel
0 0.5 1
Enriched pathways & biological processes
nominal p<0.05
BH-adj. p<0.05
−Log10(BH−adj.P)
0 1 2 3 4 5 6
Kinase regulation
GTPase & hydrolases regulation
MAPK signaling
Regulation of defense response
Innate Immune defense response
Regulation of cell death
Regulation of viral replication
Cellular ion homeostasis
Protein metabolism & phosphorylation
Regulation of cell death
Receptor signaling
Type I IFN signaling
Development & Differentiation
Apoptotic process
Host-microbial interactions
Vesicle-mediated & intracelluar transport
Viral process & life cycle
Defense response to virus
Innate immune response
Response to external stimuli (nutrients & starvation)
Cytokine response
Response to stress
Response to external biotic stimulation

Figure II-4. Enrichment analysis of pathway and biological processes enriched among differentially expressed genes between T1L- and T3D-RV-infected mice. Pathways or biological processes found enriched among genes that were differentially expressed between T1L and T3D-RV in LP or MLN were grouped on the basis of their relatedness by performing semantic similarity analysis using the relevance similarity measure, sim_{Rel} (scale ranging from 0 to 1, with 0 being distinct and 1 being identical). The analysis examines each pair of enriched pathway or process in turn and a semantic similarity matrix of sim_{Rel} values was constructed. From this analysis, a semantic cluster heatmap was generated and hierarchical clustering was applied to group similar pathways and processes together. The extent of similarity between pathways and processes scales with color intensity on the heatmap. Bar graphs showing enrichment scores ($-Log_{10}$(BH-adj.P)) associated with each pathway and process are shown. All meet the nominal (unadjusted) enrichment significance threshold of $P < 0.05$ as denoted by the grey bars. Red bars denote those achieving enrichment significance after Benjamini-Hochberg adjustment (BH-adj.$P < 0.05$) to control for the false discovery rate. Clusters of similar pathways and processes are grouped as indicated by dendrograms, and annotated by shared concepts.

response to the two viruses, characterizing their expression in a time- and location-dependent manner. In both LP and MLN at 48 h, we observed a strong enrichment of immune, defense, and antiviral response pathways, including type 1 IFN signaling, among genes that were differentially expressed following T1L or T3D-RV infection (Figure II-4).

To determine whether the changes in gene expression alter host responses to food antigen, the Jabri lab infected MLN DCs *in-vivo*. The $CD103^+$ $CD11b^-$ DC subset has the highest tolerogenic potential (269, 270) but also drives T_H1 responses to intestinal infections (271-273). Relative to T3D-RV, T1L more substantially upregulated the costimulatory molecule CD86 (Figure II-5A) and IL-12p40 in $CD103^+$ $CD11b^-$ $CD8\alpha^+$ DCs (Figure II-2B), the DC subset that also exhibited the highest level of ovalbumin (OVA) uptake after oral administration (Figure II-5B), which occurs independently of T1L or T3D-RV infection (Figure II-5C). However, both viruses induced similar levels of IL-12p40 in resident $CD103^-$ $CD11b^-$ $CD8\alpha^+$ DCs (Figure II-5D), while no upregulation of IL-12p40 was detectable in the other MLN DC subsets (Figure II-5E). Concordantly, using a T-cell conversion assay (Figure II-6A) in conjunction with the Jabri lab, we found that T1L significantly inhibited the conversion of OVA-specific OT-II $CD4^+$ T cells into pT_{regs} (Figure II-2, C and D and Figure II-6B) and instead promoted their differentiation into T-bet^+ (Figure II-2, C and D and Figure II-6B) and $IFN\gamma^+$ (Figure II-6, B to D) $CD4^+$ T cells in MLN and LP, respectively. Conversely, T3D-RV neither markedly blocked the induction of pT_{regs} nor induced T_H1 immune responses against dietary OVA (Figure II-2, C to D and Figure II-6,

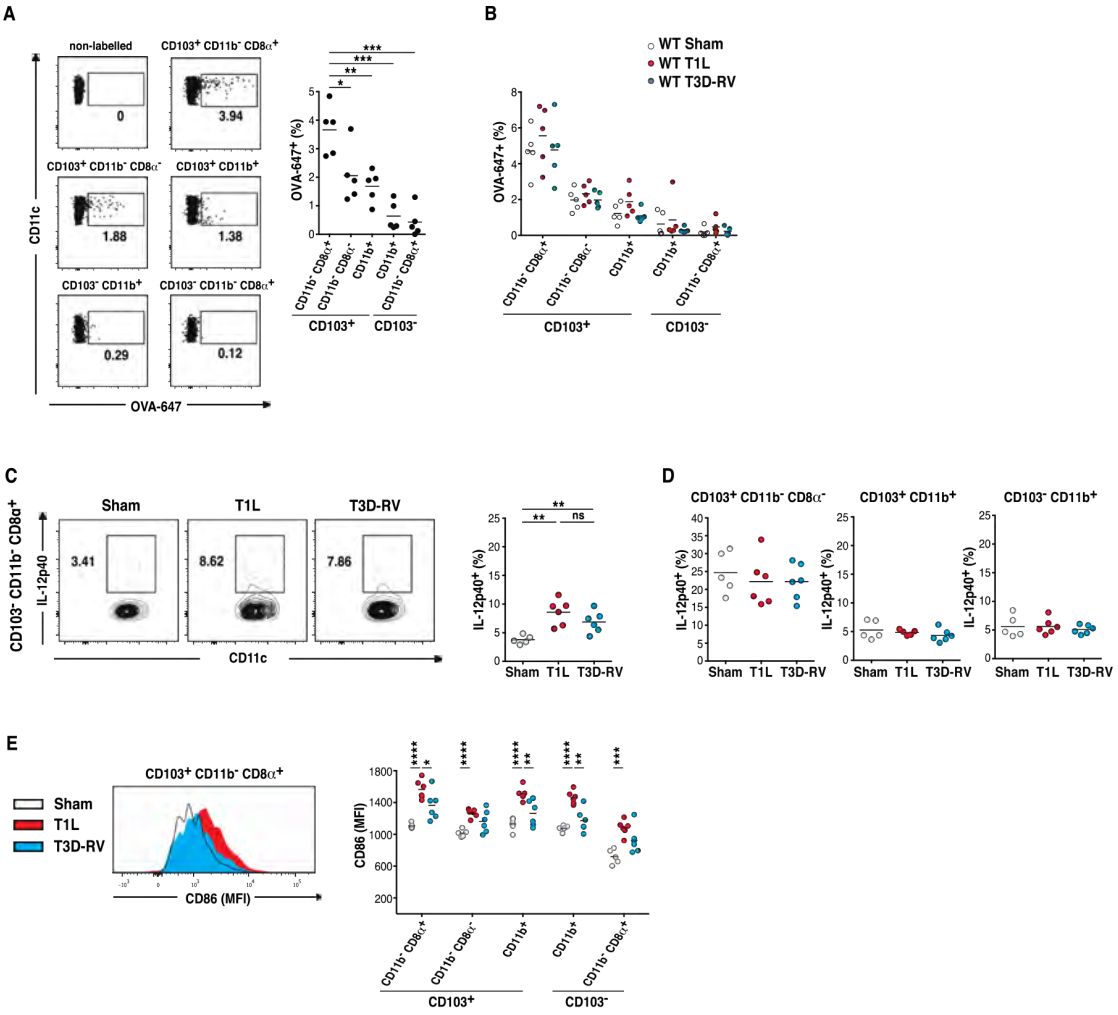

Figure II-5. Dendritic cell activation and ovalbumin uptake upon reovirus infection. (A) WT mice (n = 5) were gavaged with OVA-Alexa Fluor-647 18 h before euthanasia and OVA-Alexa Fluor-647 uptake by DCs in the MLN was analyzed by flow cytometry. Representative dot plots and percentages of OVA-Alexa Fluor-647 uptake are shown in the indicated DC subsets. (B) Similar to (A) but mice were inoculated with 10^8 PFU of T1L (n = 5), 10^8 PFU of T3D-RV (n = 5), or PBS (sham, n = 5) at the time of gavaging with OVA-Alexa Fluor-647. (C to E) WT mice were inoculated perorally with 10^8 PFU of T1L (n = 6), 10^8 PFU of T3D-RV (n = 6), or PBS (sham, n = 5) for 2 d. (C and D) The expression of IL-12p40 in MLN DC subsets was evaluated by flow cytometry. Representative dot plots (C) and percentages (C and D) of IL-12p40$^+$ cells in indicated MLN DC subsets are shown. (E) The expression of CD86 in MLN DC subsets was evaluated by flow cytometry. Representative histogram and MFI for CD86 expression in the indicated DC subsets in the MLN of WT mice is shown. Graphs depict two independent experiments. (A to E) *, $P < 0.05$; **, $P < 0.01$; ***, $P < 0.001$; ****, $P < 0.0001$; one-way ANOVA/Tukey's multiple comparison.

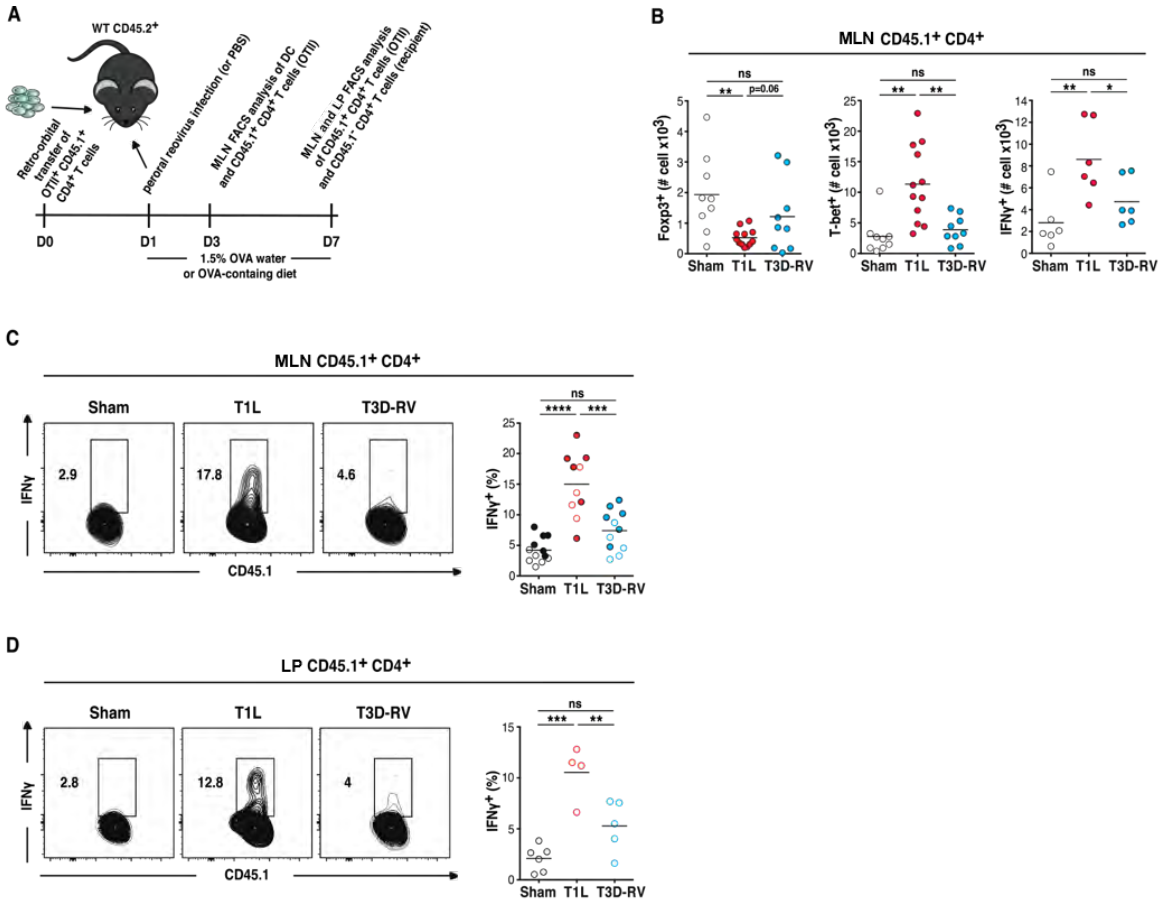

Figure II-6. T1L promotes T_H1 immunity to dietary antigen at inductive and effector sites of the gut. (A) *In-vivo* T cell conversion assay model. (B) OT-II$^+$ CD45.1$^+$ CD4$^+$ T cells were transferred into WT CD45.2$^+$ mice. One day after transfer, mice were inoculated perorally with 10^{10} PFU of T1L (n = 6-12), 10^{10} PFU of T3D-RV (n = 6 - 9), or PBS (sham, n = 6 - 9) and fed 1.5% OVA in the drinking water for 6 d. The intracellular expression of Foxp3, T-bet, and IFNγ in MLN OT-II$^+$ CD45.1$^+$ CD4$^+$ T cells was evaluated by flow cytometry. Absolute numbers of Foxp3-, T-bet- and IFNγ-expressing CD45.1$^+$ CD4$^+$ T cells are shown. (C and D) OT-II$^+$ CD45.1$^+$ CD4$^+$T cells isolated by MACS beads separation (filled circles) or FACS sorting (open circles) were transferred into WT CD45.2$^+$ mice. One day after transfer, mice were inoculated perorally with 10^{10} PFU of T1L (n = 4-16), 10^{10} PFU of T3D-RV (n = 5-14), or PBS (sham, n = 6-15) and fed 1.5% OVA in the drinking water (filled circles) or an OVA-containing diet (open circles) for 6 d. The intracellular expression of IFNγ in transferred OT-II$^+$ CD45.1$^+$ CD4$^+$ T cells in the MLN and in the was evaluated by flow cytometry. Representative dot plots and percentages of IFNγ-producing CD45.1$^+$ CD4$^+$ T cells are shown in MLN (C) and in LP (D) respectively. (B to D) Graphs depict at least two independent experiments. *, $P < 0.05$; **, $P < 0.01$; ***, $P < 0.001$; ****, $P < 0.0001$; one-way ANOVA/Tukey's multiple comparison.

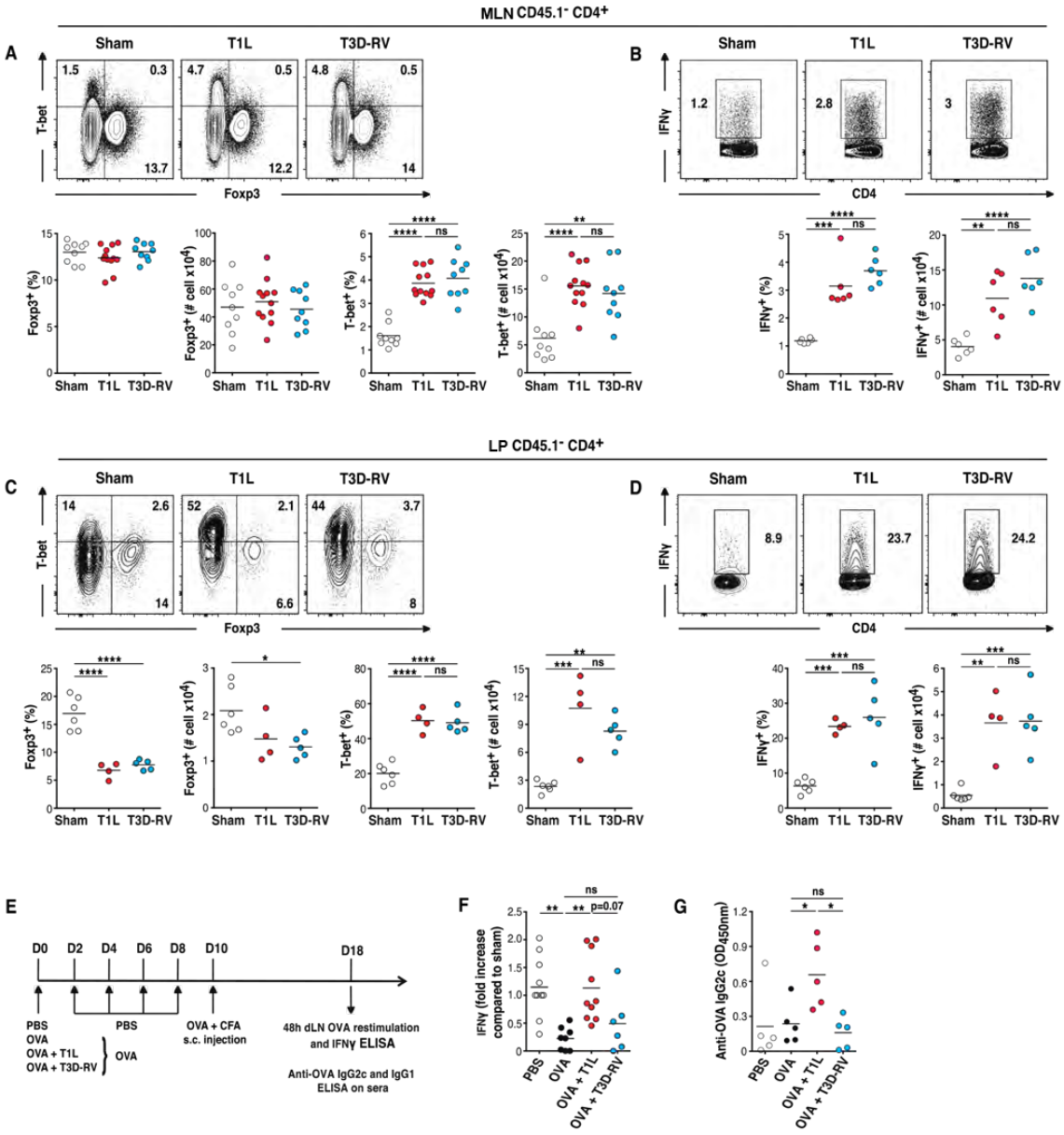
MLN CD45.1⁻ CD4⁺
A
Sham
T1L
T3D-RV
T-bet
Foxp3
1.5
0.3
13.7
4.7
0.5
12.2
4.8
0.5
14
Foxp3⁺ (%)
Foxp3⁺ (# cell x10⁴)
T-bet⁺ (%)
T-bet⁺ (# cell x10⁴)
B
IFNγ
CD4
1.2
2.8
3
IFNγ⁺ (%)
IFNγ⁺ (# cell x10⁴)
LP CD45.1⁻ CD4⁺
C
14
2.6
14
52
2.1
6.6
44
3.7
8
D
8.9
23.7
24.2
E
D0
D2
D4
D6
D8
D10
D18
PBS
OVA
OVA + T1L
OVA + T3D-RV
PBS
OVA
OVA + CFA
s.c. injection
48h dLN OVA restimulation
and IFNγ ELISA
Anti-OVA IgG2c and IgG1
ELISA on sera
F
IFNγ (fold increase
compared to sham)
p=0.07
G
Anti-OVA IgG2c (OD450nm)

Figure II-7. T cell responses to dietary antigen and viral infection. (A and B) OT-II$^+$ CD45.1$^+$ CD4$^+$ T cells were transferred into WT CD45.2$^+$ mice. One day after transfer, mice were inoculated perorally with 10^{10} PFU of T1L (n = 6 - 12), 10^{10} PFU of T3D-RV (n = 6 - 9), or PBS (sham, n = 6 - 9) and fed 1.5% OVA in the drinking water for 6 d. The intracellular expression of Foxp3, T-bet, and IFNγ in MLN CD4$^+$ T cells was evaluated by flow cytometry. Representative dot plots, percentages and absolute numbers of Foxp3-, T-bet- (A) and IFNγ-expressing CD45.1$^-$ recipient CD4$^+$ T cells (B) are shown. (C and D) OT-II$^+$ CD45.1$^+$ CD4$^+$ T cells were transferred into WT CD45.2$^+$ mice. One day after transfer, mice were inoculated perorally with 10^{10} PFU of T1L (n = 4), 10^{10} PFU of T3D-RV (n = 5), or PBS (sham, n = 6) and fed with an OVA-containing diet for 6 d. The intracellular expression of Foxp3, T-bet and IFNγ in LP CD4$^+$ T cells was evaluated by flow cytometry. Representative dot plots, percentages and absolute numbers of Foxp3-, T-bet- (C) and IFNγ-expressing CD45.1$^-$ recipient CD4$^+$ T cells (D) are shown. (E and F) WT mice were inoculated perorally with 10^{10} PFU of T1L, or 10^{10} PFU of T3D-RV, or PBS at the initiation of an oral tolerance protocol. Mice were gavaged every other day with OVA or PBS for 8 d and all mice were immunized subcutaneously (s.c.) with OVA-complete Freund's adjuvant (CFA) at 10 dpi. On day 18, draining lymph node (dLN) cells were harvested and analyzed for production of IFNγ by ELISA following OVA *in-vitro* restimulation. Sham (n = 11), OVA (n = 11), OVA + T1L (n = 10), and OVA + T3D-RV (n = 6). (G) WT mice were inoculated perorally with 10^{10} PFU of T1L, 10^{10} PFU of T3D-RV, or PBS at the initiation of an oral tolerance protocol. Mice were fed with an OVA-containing diet or a control diet (sham) for 8 d and then immunized subcutaneously with OVA-CFA at 10 dpi. The levels of OVA-specific IgG2c antibodies were evaluated in the serum at day 18 by ELISA. Sham (n = 5), OVA (n = 5), OVA + T1L (n = 5), and OVA + T3D-RV (n = 5). (A to D and F and G) Graphs depict at least two independent experiments. *, $P < 0.05$; **, $P < 0.01$; ***, $P < 0.001$; ****, $P < 0.0001$; one-way ANOVA/Tukey's multiple comparison.

B to D). In contrast to differences observed between T1L and T3D-RV in the response to dietary antigens, both viruses induced similar antiviral T_H1 $CD45.1^-$ $CD4^+$ T cell responses in MLN (Figure II-7, A and B) and LP (Figure II-7, C and D).

Oral tolerance is defined as the establishment of peripheral immune tolerance by oral administration of antigen and thought to be dependent on the induction of pT_{regs} (274). As expected, T1L but not T3D-RV prevented induction of peripheral tolerance upon oral administration of OVA (Figure II-7, E to G). Collectively, these results suggest that as a consequence of T1L infection, the tolerogenic response to dietary antigens is abrogated and, instead, T_H1 immunity to dietary antigens is induced.

Distinct host pathways block induction of pT_{regs} and induce T_H1 immunity to dietary antigen.

We next sought to determine the mechanistic basis for the differential effect of T1L and T3D-RV infection on the response to dietary antigen. Type 1 IFNs are upregulated in CD and have been suggested to explain development of T_H1 immunity against dietary gluten (275). Further analysis from MLN confirmed that T1L induced higher levels of canonical ISGs such as *Mx1* and *Isg15* (Figure II-8A and II-9A) than T3D-RV. This result was contrary to studies performed *in-vitro* (Figure II-9, B to D) and previously reported describing the capacity of T1L, but not T3D, to inhibit type 1 IFN signaling (276). Therefore, these findings suggest that differences in virus-host interactions displayed by T1L and T3D-RV

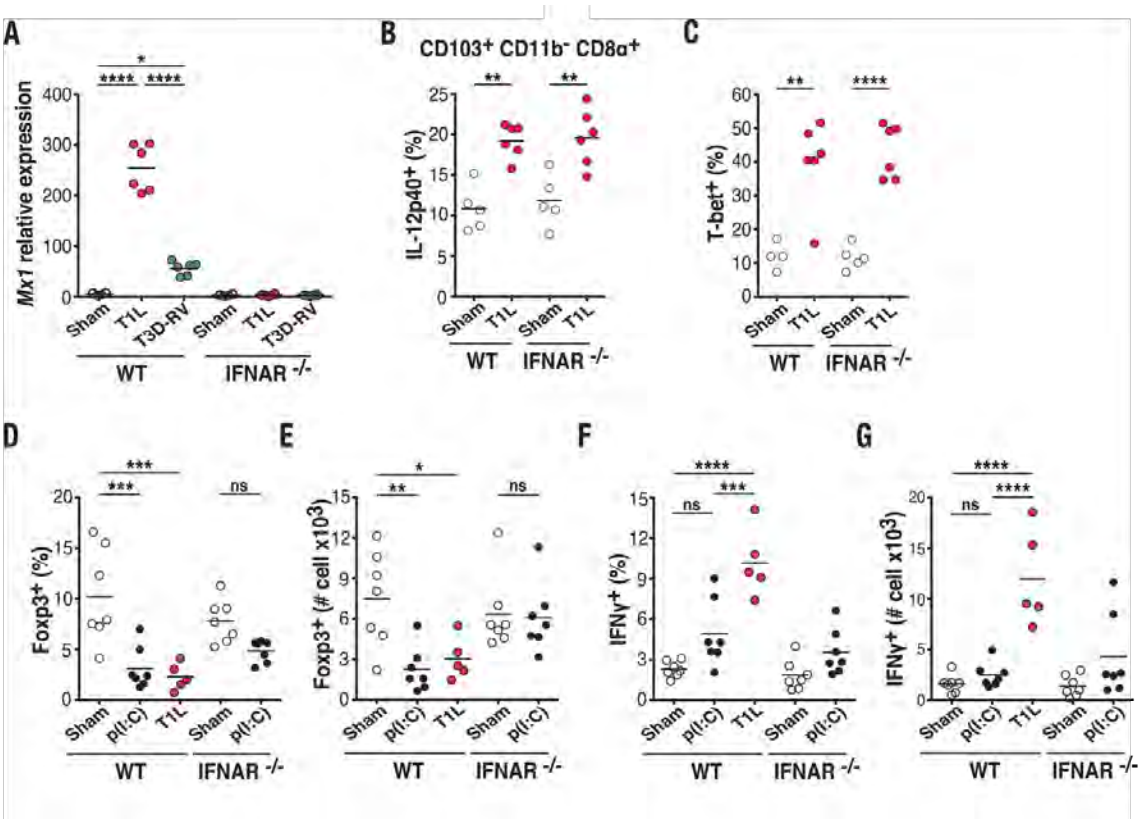

Figure II-8. Type-1 IFN is required for blockade of pT_{reg} conversion but not for induction of T_H1 immunity to dietary antigen. (A) WT and IFNAR$^{-/-}$ mice were inoculated perorally with 10^8 PFU of T1L (n = 6 mice), 10^8 PFU of T3D-RV (n = 6 mice), or PBS (sham, n = 6 mice) for 2 d. Mx1 expression in the MLN was analyzed by means of RT-PCR. (B and C) OT-II$^+$ CD45.1$^+$ CD4$^+$ T cells were transferred into WT CD45.2$^+$ or IFNAR$^{-/-}$ CD45.2$^+$ mice. One day after transfer, mice were inoculated perorally with 10^8 PFU of T1L (n = 6 mice) or PBS (sham, n = 4 or 5 mice) and fed 1.5% OVA in the drinking water for 2 d. The expression of IL-12p40 on gated MHC-II$^+$ CD11c$^+$ CD103$^+$ CD11b$^-$ CD8α$^+$ MLN DCs (B) and T-bet in OT-II$^+$ CD45.1$^+$ CD4$^+$ T cells (C) in the MLN was evaluated by means of flow cytometry. (D to G) OT-II$^+$ CD45.1$^+$ CD4$^+$ T cells were transferred into WT CD45.2$^+$ or IFNAR$^{-/-}$ CD45.2$^+$ mice. One day after transfer, mice were inoculated with PBS (n = 7 mice) or 50 mg of poly(I:C) (n = 7 mice) intraperitoneally or 10^{10} PFU of T1L (n = 5 mice) perorally and fed an OVA-containing diet for 6 d. The intracellular expression of Foxp3 and IFNγ in OT II$^+$ CD45.1$^+$ CD4$^+$ T cells in the MLN was evaluated by means of flow cytometry. Percentages and absolute numbers of Foxp3 (D and E) and IFNγ (F and G) are shown. (A to G) Graphs depict at least two independent experiments. *, $P < 0.05$; **, $P < 0.01$; ***, $P < 0.001$; ****, $P < 0.0001$; one-way ANOVA/Tukey's multiple comparison.

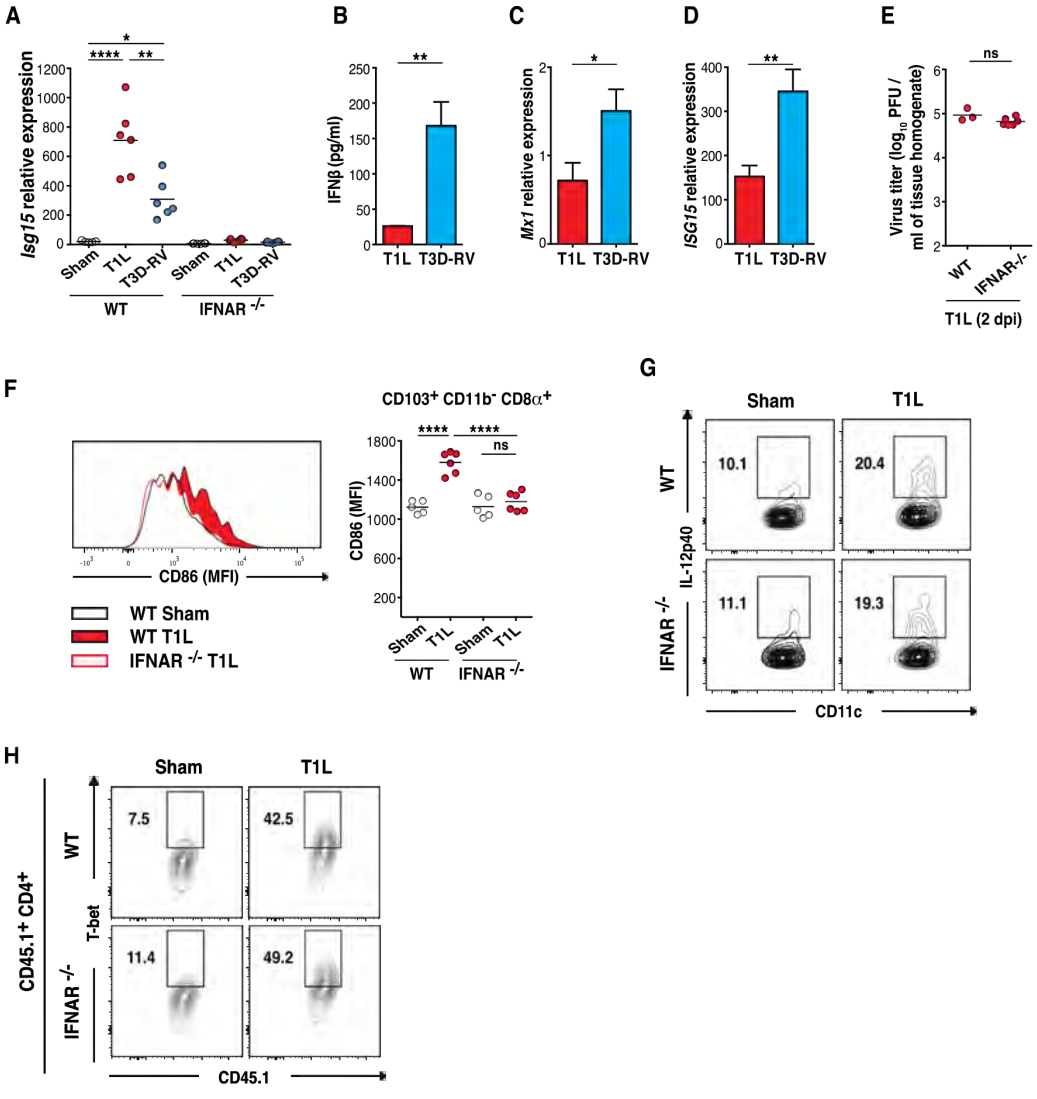
A
Isg15 relative expression
Sham
T1L
T3D-RV
WT
IFNAR -/-
B
IFNβ (pg/ml)
T1L T3D-RV
C
Mx1 relative expression
D
ISG15 relative expression
E
Virus titer (log10 PFU / ml of tissue homogenate)
ns
WT
IFNAR-/-
T1L (2 dpi)
F
CD103+ CD11b- CD8α+
CD86 (MFI)
WT Sham
WT T1L
IFNAR -/- T1L
G
Sham
T1L
WT
IFNAR -/-
IL-12p40
10.1
20.4
11.1
19.3
CD11c
H
CD45.1+ CD4+
T-bet
7.5
42.5
11.4
49.2
CD45.1

Figure II-9. Impact of type-1 IFN signaling on the response to dietary antigen. (A) WT and IFNAR$^{-/-}$ mice were inoculated perorally with 10^8 PFU of T1L (n = 6), 10^8 PFU of T3D-RV (n = 6) or PBS (sham, n = 6) and euthanized at 2 dpi. *ISG15* expression in the MLN was analyzed by RT-PCR. (B) IFNβ protein expression was analyzed by ELISA in WT mouse embryonic fibroblasts (MEFs) 16 hpi with T1L or T3D-RV at an MOI of 500 PFU/cell. (C and D) *Mx1* and *Isg15* mRNA levels were quantified by RT-PCR in Caco-2 cells 24 hpi with T1L or T3D-RV at an MOI of 100 PFU/cell. (E) OT-II$^+$ CD45.1$^+$ CD4$^+$ T cells were transferred into WT CD45.2$^+$ or IFNAR$^{-/-}$ CD45.2$^+$ mice. One day after transfer, mice were inoculated perorally with 10^8 PFU of T1L and fed 1.5% OVA in the drinking water for 2 d. At 2 dpi, a 1 cm section of ileum was resected, and viral titers in WT (n = 3) and IFNAR$^{-/-}$ (n = 6) tissue were determined by plaque assay and expressed as PFU per ml of tissue homogenate. (F, G and H) OT-II$^+$ CD45.1$^+$ CD4$^+$ T cells were transferred into WT CD45.2$^+$ or IFNAR$^{-/-}$ CD45.2$^+$ mice. One day after transfer, mice were inoculated perorally with 10^8 PFU of T1L or PBS (sham) and fed 1.5% OVA in the drinking water for 2 d. The expression of CD86 (F) IL-12p40 (G) and T-bet (H) in the MLN was evaluated by flow cytometry. (F) Representative histogram and MFI of the expression of CD86 is shown in CD103$^+$ CD11b$^-$ CD8α$^+$ DCs in the MLN. (G) Representative dot plots of MLN IL-12p40-producing CD103$^+$ CD11b$^-$ CD8α$^+$ DCs are shown. (H) Representative dot plots of MLN T-bet-expressing OT-II$^+$ CD45.1$^+$ CD4$^+$ T cells are shown. (A and F) *, $P < 0.05$; **, $P < 0.01$; ***, $P < 0.001$; ****, $P < 0.0001$; one-way ANOVA/Tukey's multiple comparison. (B to E) *, $P < 0.05$; **, $P < 0.01$; unpaired t-test.

can lead to alternative outcomes *in-vivo* and that type 1 IFN may be responsible for initiating T_H1 immunity against dietary antigen in T1L-infected mice. To assess this possibility, but avoid confounding factors associated with uncontrolled viral replication in the absence of type 1 IFN signaling (158), the Jabri laboratory analyzed DCs and OVA-specific T cell conversion at 48 h, a time point at which viral titers in the ileum during T1L infection are similar in WT and $IFNAR^{-/-}$ mice (Figure II-9E). Surprisingly, while CD86 was not induced in $IFNAR^{-/-}$ $CD103^+$ $CD11b^-$ $CD8\alpha^+$ DCs (Figure II-9F), IL-12p40 (Figure II-8B and II-9G) was upregulated following T1L infection, suggesting that type 1 IFNs are not required for acquisition of an inflammatory phenotype by MLN APCs. Consistent with these findings, T1L infection induced comparable T-bet expression in OVA-specific $CD4^+$ T cells in WT and $IFNAR^{-/-}$ mice (Figure II-8C and II-9H). Of note, at this early time point, neither Foxp3 nor IFNγ can be detected in OVA-specific T cells in the MLN. To assess the role of type 1 IFN in pT_{reg} conversion, an *in-vivo* OT-II T cell conversion assay was conducted using WT and $IFNAR^{-/-}$ mice inoculated intraperitoneally with the dsRNA analog poly(I:C) (executed by the Jabri lab). As shown in Figures II-8, D to E, and II-10, A to B, dsRNA was sufficient to block pT_{reg} conversion in a type 1 IFN-dependent manner. Furthermore, treatment with type 1 IFNs blocked pT_{reg} conversion (Figure II-10C) comparable to infection with T1L. However, poly(I:C) (Figure II-8, F and G; and II-10D) and type 1 IFN (Figure II-10C) did not promote T_H1 immunity as indicated by levels of IFNγ.

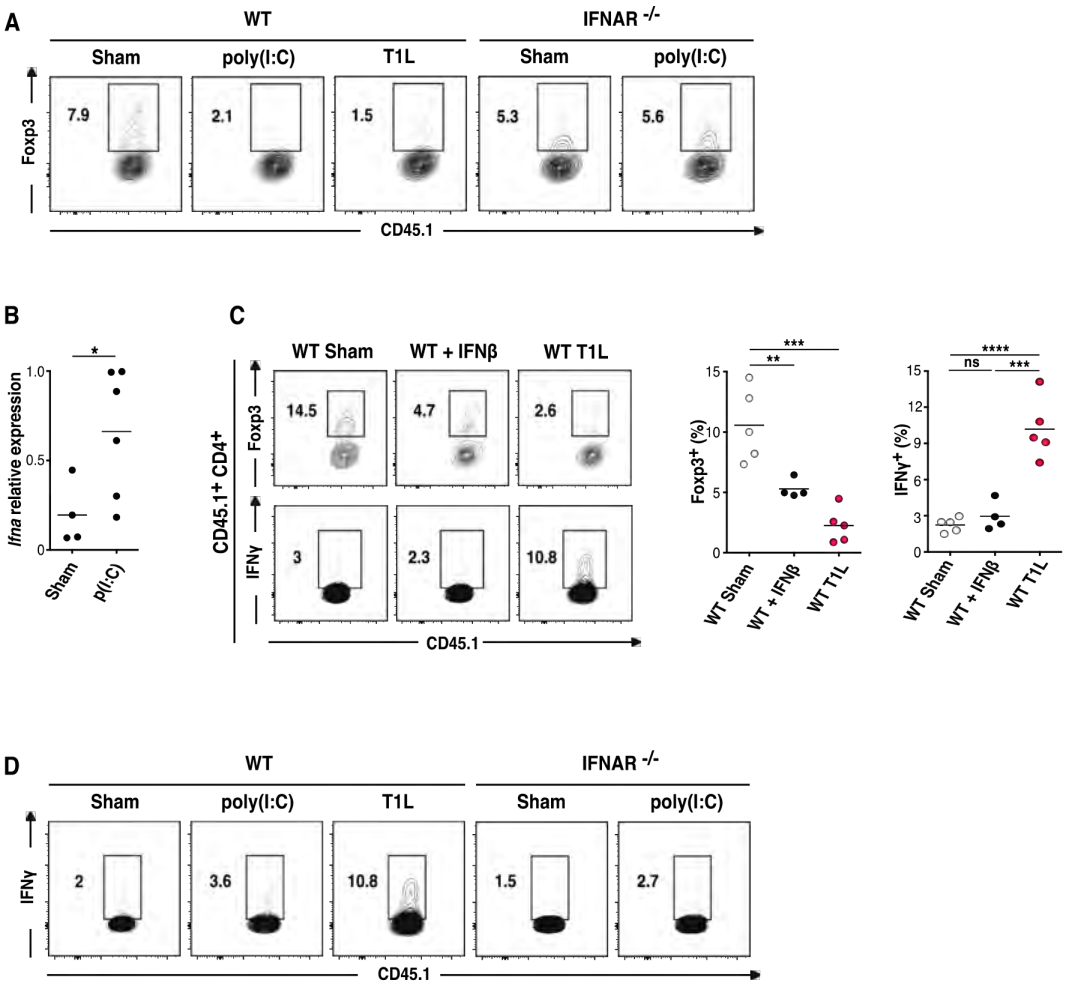

Figure II-10. dsRNA is sufficient to block pT_{reg} conversion in a type-1 IFN-dependent manner. (A and D) OT-II$^+$ CD45.1$^+$ CD4$^+$ T cells were transferred into WT CD45.2$^+$ or IFNAR$^{-/-}$ CD45.2$^+$ mice. One day after transfer, mice were inoculated with PBS (n = 7) or 50 mg of poly(I:C) (n = 7) i.p. or 10^{10} PFU of T1L (n = 5) perorally, and fed an OVA-containing diet for 6 d. The intracellular expression of Foxp3 and IFNγ in OT-II$^+$ CD45.1$^+$ CD4$^+$ T cells in the MLN was evaluated by flow cytometry. Representative dot plots of Foxp3- (A) and IFNγ-expressing CD45.1$^+$ CD4$^+$ T cells (D) are shown. (B) WT mice were inoculated with PBS (sham, n = 4) or 50 mg of poly(I:C) (n = 6) i.p. and euthanized 2 d post injection. *Ifn*α expression in the MLN was evaluated by RT-PCR. (C) OTII$^+$ CD45.1$^+$ CD4$^+$ T cells were transferred into WT CD45.2$^+$ mice. One day after transfer, mice received PBS (sham, n = 5) or IFNβ (n = 4) i.p. or were inoculated perorally with 10^{10} PFU of T1L (n = 5), and fed an OVA-containing diet for 6 d. The intracellular expression of Foxp3 and IFNγ in OT-II$^+$ CD45.1$^+$ CD4$^+$ T cells in the MLN was evaluated by flow cytometry. Representative dot plots and percentages of Foxp3$^-$ and IFNγ-expressing CD45.1$^+$ CD4$^+$ T cells are shown. (B and C) Graphs depict two independent experiments. (B) *, $P < 0.05$; unpaired t-test. (C) **, $P < 0.01$; ***, $P < 0.001$; ****, $P < 0.0001$; (one-way ANOVA / Tukey's multiple comparison).

To define the mechanism underlying T1L-induced T_H1 immunity to dietary antigen, we probed transcriptional differences occurring in T1L- and T3D-RV-infected WT and IFNAR$^{-/-}$ mice using RNA-seq data from MLN and defined genes that were differently expressed in a type 1 IFN-independent manner (Figure II-11A). IL-15, which prevents pT_{reg} conversion and induces T_H1 immunity to dietary antigens (98), was eliminated because *IL15* was not upregulated following T1L infection in MLN of IFNAR$^{-/-}$ mice (Figure II-11B). In contrast, IRF-1, a transcription factor regulated at the transcriptional level (277) and implicated in multistage regulation of T_H1 immune responses (278), was significantly upregulated following T1L infection in both WT and IFNAR$^{-/-}$ mice (Figure II-12 and II-11A). IRF-1 was a particularly intriguing candidate, as it is upregulated in the mucosa of children with CD (279). To determine whether IRF-1 is required in T1L-mediated immunopathology, we analyzed DCs and OT-II T cell conversion in IRF-1$^{-/-}$ mice (conducted by the Jabri laboratory). Importantly, viral titers were similar at 48 hpi and 6 dpi in WT and IRF-1$^{-/-}$ mice (Figure II-11, C and D), enabling us to analyze the response to dietary antigen after oral OVA administration at these two time points. We found that IL-12p40 (Figure II-12B and II-11E) showed significantly less induction in IRF-1$^{-/-}$ mice relative to WT mice. Additionally, mRNA expression levels of *Il12b*, cytokines that function in T_H1 immunity (278, 280, 281), were significantly impaired in IRF-1$^{-/-}$ mice (Figure II-11F). Consistent with preserved type 1 IFN upregulation following T1L infection in IRF-1$^{-/-}$ mice (Figure II-11, G and H), absence of IRF-1 failed to restore pT_{reg} conversion (Figure II-3, C and D; and II-11I). However, while type 1 IFN signaling

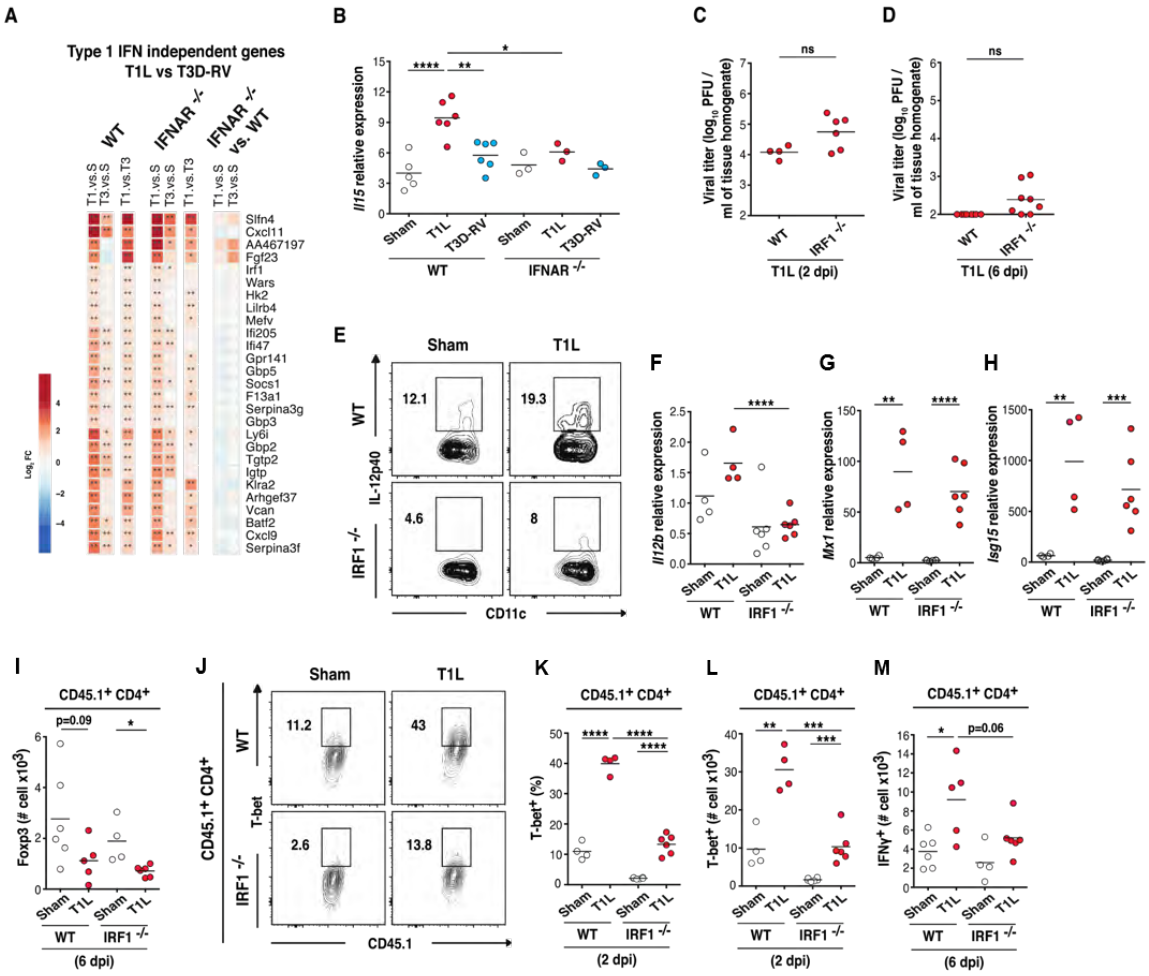
A
Type 1 IFN independent genes
T1L vs T3D-RV
WT
IFNAR -/-
IFNAR -/- vs. WT
T1.vs.S
T3.vs.S
T1.vs.T3
Log2 FC
Slfn4
Cxcl11
AA467197
Fgf23
Irf1
Wars
Hk2
Lilrb4
Mefv
Ifi205
Ifi47
Gpr141
Gbp5
Socs1
F13a1
Serpina3g
Gbp3
Ly6i
Gbp2
Tgtp2
Igtp
Kira2
Arhgef37
Vcan
Batf2
Cxcl9
Serpina3f
B
Il15 relative expression
Sham
T1L
T3D-RV
WT
IFNAR -/-
C
Viral titer (log10 PFU / ml of tissue homogenate)
ns
WT
IRF1 -/-
T1L (2 dpi)
D
Viral titer (log10 PFU / ml of tissue homogenate)
ns
WT
IRF1 -/-
T1L (6 dpi)
E
Sham
T1L
WT
IRF1 -/-
IL-12p40
CD11c
12.1
19.3
4.6
8
F
Il12b relative expression
G
Mx1 relative expression
H
Isg15 relative expression
I
CD45.1+ CD4+
p=0.09
Foxp3 (# cell x10^3)
WT
IRF1 -/-
(6 dpi)
J
Sham
T1L
CD45.1+ CD4+
WT
IRF1 -/-
T-bet
CD45.1
11.2
43
2.6
13.8
K
CD45.1+ CD4+
T-bet+ (%)
(2 dpi)
L
CD45.1+ CD4+
T-bet+ (# cell x10^3)
(2 dpi)
M
CD45.1+ CD4+
p=0.06
IFNγ+ (# cell x10^3)
(6 dpi)

Figure II-11. Role of IRF-1 signaling in the response to dietary antigens upon reovirus infection. (A) WT and IFNAR$^{-/-}$ mice were inoculated perorally with 10^8 PFU of T1L (n = 3), 10^8 PFU of T3D-RV (n = 3), or PBS (sham, n = 3) and euthanized at 2 dpi. RNA of LP was isolated for RNA-seq analysis. Heatmap showing genes differentially expressed between T1L and T3D-RV in a type-1 IFN-independent manner. Differential transcriptional responses for T1L versus sham (T1. vs. S), T3D-RV versus sham (T3. vs. S), and T1L (with respect to sham) versus T3D-RV (with respect to sham) (T1. vs. T3) are shown in sub-sections labeled "WT" or "IFNAR$^{-/-}$". Factorial design analysis indicates no statistical difference between IFNAR$^{-/-}$ and WT MLN (third sub-section labeled "IFNAR$^{-/-}$ vs. WT") for these genes. **denotes Benjamini-Hochberg-adjusted P <0.05, *denotes nominal $P < 0.05$. (B) WT and IFNAR$^{-/-}$ mice were inoculated perorally with 10^8 PFU of T1L, 10^8 PFU of T3D-RV or PBS (sham) and euthanized at 2 dpi. *Il15* expression in the MLN was analyzed by RT-PCR. WT sham (n = 5), WT T1L (n = 6), WT T3D-RV (n = 6), IFNAR$^{-/-}$ sham (n = 3), IFNAR$^{-/-}$ T1L (n = 3), and IFNAR$^{-/-}$ T3D-RV (n = 3). (C, E, J to L) OT-II$^+$ CD45.1$^+$ CD4$^+$ T cells were transferred into WT CD45.2$^+$ or IRF-1$^{-/-}$ CD45.2$^+$ mice. One day after transfer, mice were inoculated perorally with 10^8 PFU of T1L or PBS (sham) and fed 1.5% OVA in the drinking water for 2 d. (C) At 2 dpi, a 1 cm section of ileum was resected, and viral titers in this tissue were determined by plaque assay. (E, J to L) The expression of IL-12p40 and T-bet in the MLN was evaluated by flow cytometry. (E) Representative dot plots of MLN IL-12p40-producing CD103$^+$ CD11b$^-$ CD8α$^+$ DC are shown. (J) Representative dot plots, (K) percentages and, (L) absolute numbers of T-bet-expressing CD45.1$^+$ CD4$^+$ T cells are shown. (D, I, and M) OT-II$^+$ CD45.1$^+$ CD4$^+$ T cells were transferred into WT CD45.2$^+$ or IRF-1$^{-/-}$ CD45.2$^+$ mice. One day after transfer, mice were inoculated perorally with 10^{10} PFU of T1L or PBS (sham) and fed 1.5% OVA in the drinking water for 6 d. (D) At 6 dpi, a 1 cm section of ileum was resected, and viral titers in this tissue were determined by plaque assay. (I and M) Intracellular expressions of Foxp3 and IFNγ were evaluated by flow cytometry. Absolute numbers of Foxp3- (I) and IFNγ-expressing CD45.1$^+$ CD4$^+$ T cells (M) in the MLN are shown. WT sham (n = 6), WT T1L (n = 5), IRF-1$^{-/-}$ sham (n = 4), and IRF-1$^{-/-}$ T1L (n = 6). (G to J) WT and IRF-1$^{-/-}$ mice were inoculated perorally with 10^8 PFU of T1L or PBS (sham) and euthanized at 2 dpi. (F) *Il12b,* (G) *Mx1,* and (H) *Isg15* expression in the MLN was analyzed by RT-PCR, WT sham (n = 4), WT T1L (n = 4), IRF-1$^{-/-}$ sham (n = 6), IRF-1$^{-/-}$ T1L (n = 6). (B to M) Graphs depict two independent experiments. (B, F to I, K to M) *, $P < 0.05$; **, $P < 0.01$; ***, $P < 0.001$; ****, $P < 0.0001$; one-way ANOVA/Tukey's multiple comparison. (C and D) unpaired t-test.

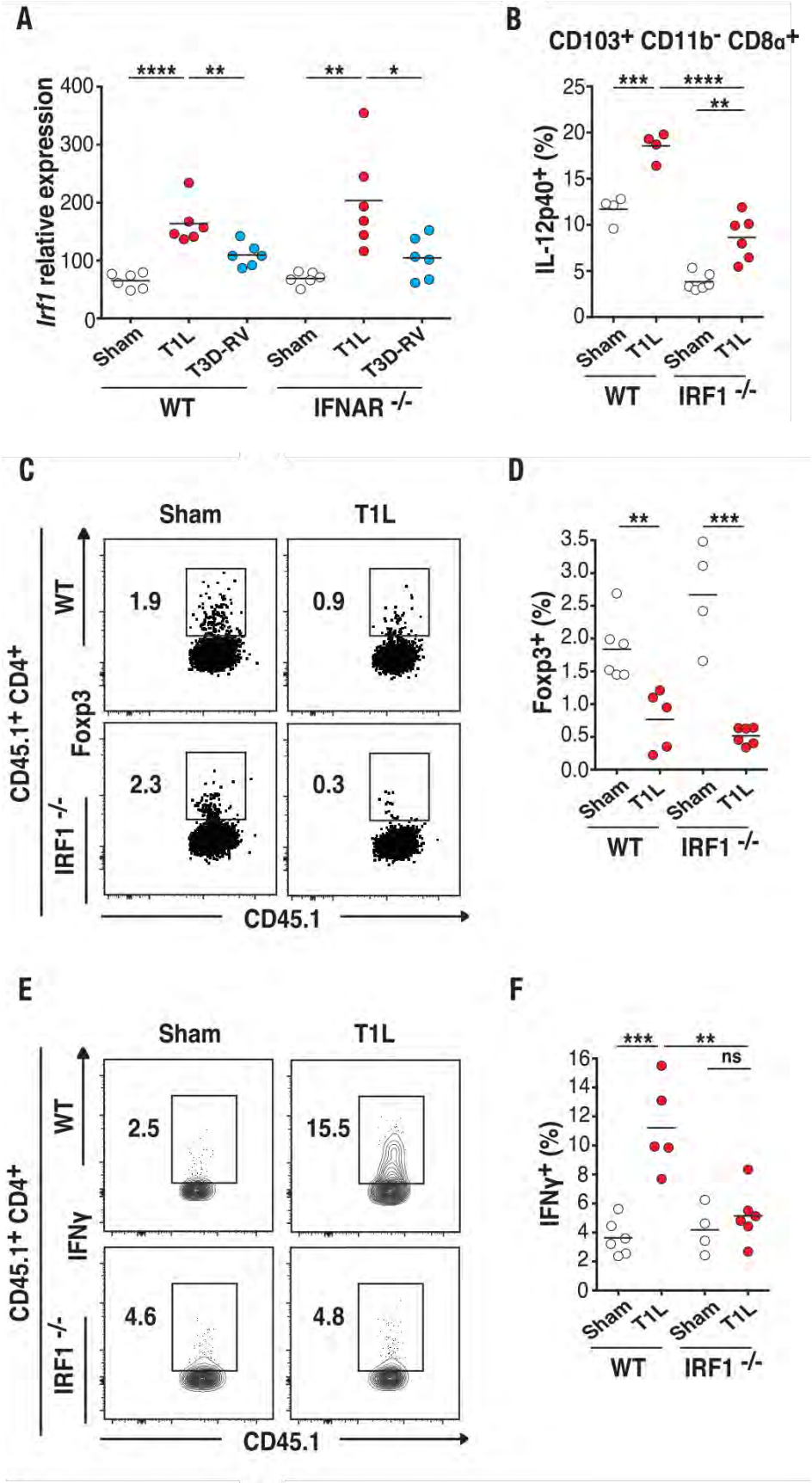
A
Irf1 relative expression
400
300
200
100
0
****
**
**
*
Sham
T1L
T3D-RV
Sham
T1L
T3D-RV
WT
IFNAR -/-
B
CD103+ CD11b- CD8α+
IL-12p40+ (%)
25
20
15
10
5
0
***
****
**
Sham
T1L
Sham
T1L
WT
IRF1 -/-
C
Sham
T1L
CD45.1+ CD4+
WT
Foxp3
IRF1 -/-
1.9
0.9
2.3
0.3
CD45.1
D
Foxp3+ (%)
3.5
3.0
2.5
2.0
1.5
1.0
0.5
0.0
**
***
Sham
T1L
Sham
T1L
WT
IRF1 -/-
E
Sham
T1L
CD45.1+ CD4+
WT
IFNγ
IRF1 -/-
2.5
15.5
4.6
4.8
CD45.1
F
IFNγ+ (%)
16
14
12
10
8
6
4
2
0
***
**
ns
Sham
T1L
Sham
T1L
WT
IRF1 -/-

Figure II-12. A central role for IRF-1 in reovirus-mediated T_H1 immunity to dietary antigen. (A) WT and IFNAR$^{-/-}$ mice were inoculated perorally with 10^8 PFU of T1L (n = 6 mice), 10^8 PFU of T3D-RV (n = 6 mice), or PBS (sham, n = 6 mice) for 2 d. IRF-1 expression in the MLN was analyzed by means of RT-PCR. (B) OT-II$^+$ CD45.1$^+$ CD4$^+$ T cells were transferred into WT CD45.2$^+$ or IRF-1$^{-/-}$ CD45.2$^+$ mice. One day after transfer, mice were inoculated perorally with 10^8 PFU of T1L (n = 4 to 6 mice) or PBS (sham, n = 4 to 6 mice) and fed 1.5% OVA in the drinking water for 2 d. The expression of IL-12p40 on gated MHC-II$^+$ CD11c$^+$ CD103$^+$ CD11b$^-$ CD8α$^+$ MLN DCs was evaluated by means of flow cytometry. (C to F) OT-II$^+$ CD45.1$^+$ CD4$^+$ T cells were transferred into WT CD45.2$^+$ or IRF-1$^{-/-}$ CD45.2$^+$ mice. One day after transfer, mice were inoculated perorally with 10^{10} PFU of T1L (n = 5 or 6 mice) or PBS (sham, n = 4 to 6 mice) and fed 1.5% OVA in the drinking water for 6 d. Intracellular expression of Foxp3 and IFNγ was evaluated by means of flow cytometry. Representative dot plots (C), percentages of Foxp3 (D), representative dot plots (E), and percentages of IFNγ (F) are shown in transferred OT-II$^+$ CD4$^+$ T cells in the MLN. (A to F) Graphs depict two independent experiments. *, $P < 0.05$; **, $P < 0.01$; ***, $P < 0.001$; ****, $P < 0.0001$; one-way ANOVA/Tukey's multiple comparison.

was dispensable at 48 h (Figure II-8C), IRF-1 was required for T1L-mediated T_H1 immunity to oral antigen 48 hours- (Figure II-11, J to L) and 6 days- (Figure II-12, E and F; and II-11M) post OVA feeding.

Taken together our studies analyzing the effect of T1L on the response to dietary antigen using OVA as a model antigen (Figure II-13), suggest that two reovirus strains can induce similar antiviral T_H1 responses in PPs and yet display distinct immunopathological properties. T1L, but not T3D-RV, promotes an inflammatory phenotype in DCs taking up dietary antigen. In addition, our results indicate that type 1 IFN signaling and IRF-1 upregulation are differentially implicated in blocking pT_{reg} conversion and promoting T_H1 immunity to dietary antigen following T1L infection. IRF-1 functions in T1L-induced T_H1 immunity to dietary antigen by promoting IL-12 in DCs. Of note, while type 1 IFNs are not required (Figure II-12A) for T_H1 immunity, they likely contribute to IRF-1 upregulation (282) following reovirus infection in WT mice.

T1L infection breaks oral tolerance to gluten and TG2 activation in DQ8tg mice.

To determine the relevance of these findings to CD, we analyzed the effect of T1L infection in transgenic mice expressing CD-predisposing HLA molecule DQ8 (HLA-DQ8tg mice) (98). First, the Jabri lab confirmed that *IRF-1* was upregulated in HLA-DQ8tg mice following T1L infection (Figure II-15A). Next, they verified that like OVA-fed WT mice (Figure II-2B and II-5B), gluten peptides were preferentially found in $CD103^+$ $CD11b^-$ $CD8\alpha^+$ DCs of HLA-DQ8tg mice orally inoculated with either PBS (sham) or T1L (Figure II-14, A to

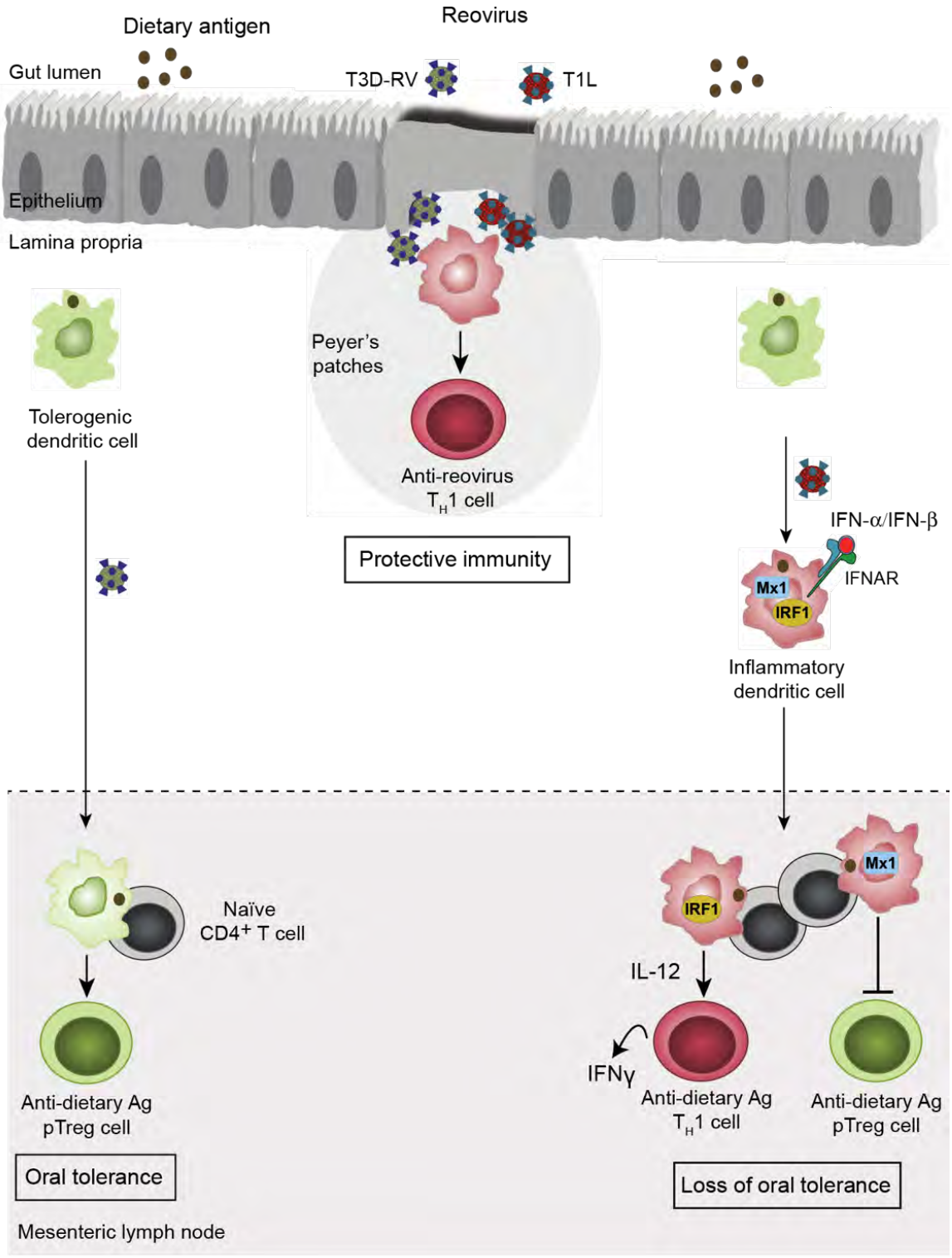
Dietary antigen
Reovirus
Gut lumen
T3D-RV
T1L
Epithelium
Lamina propria
Peyer's patches
Tolerogenic dendritic cell
Anti-reovirus T_H1 cell
Protective immunity
IFN-α/IFN-β
IFNAR
Mx1
IRF1
Inflammatory dendritic cell
Naïve CD4+ T cell
Anti-dietary Ag pTreg cell
Oral tolerance
IL-12
IFNγ
Anti-dietary Ag T_H1 cell
Anti-dietary Ag pTreg cell
Loss of oral tolerance
Mesenteric lymph node

Figure II-13. Two reoviruses similarly infect the intestine and induce protective immunity, but differ in their immunopathological outcomes. Under homeostatic conditions, regulatory T cell responses to dietary antigen are induced in the small intestine (Oral tolerance). T1L and T3D-RV reoviruses induce immune responses in PPs, the site where protective immunity to reovirus is induced. In contrast, in MLN, the site of oral tolerance induction, T1L but not T3D-RV upregulates type-1 IFN signaling (Mx1; type-1 IFN induced gene; proxy for type-1 IFN) as well as IL-12 production by DCs. Consequently, T1L but not T3D-RV infection inhibits the conversion of pT_{regs} and promotes development of T_H1 immunity to dietary antigen (Loss of oral tolerance). While type-1 IFN signaling (Mx1) in APCs plays a role in blocking pT_{reg} conversion, IRF-1 is required for the induction of IL-12, and the subsequent development of T_H1 immunity to dietary antigen.

C). This DC subset upregulated IL-12p40 (Figure II-15B and II-14D) and CD86 (Figure II-14E). The pattern of IL-12p40 expression in the other MLN DC subsets of HLA-DQ8tg mice also was similar to that in WT mice (Figure II-14F). In agreement with MLN DCs acquiring a proinflammatory phenotype, T1L infection induced loss of oral tolerance to gluten in HLA-DQ8tg mice as assessed by the presence of anti-gluten IgG2c antibodies (Figure II-15C) and the development of a T_H1 DTH reaction (Figure II-15D, II-14H) (executed by the Jabri lab). In addition to intestinal environmental conditions favoring T_H1 immunity against dietary antigens, TG2 activation is thought to promote CD pathogenesis by increasing the affinity of gluten peptides for HLA-DQ2 and HLA-DQ8 molecules (3, 264) through post-translational modifications. Importantly, T1L infection induced TG2 activation, as quantified by incorporation of 5-(biotinamido)-pentylamine (5BP), a small-molecule TG2 activity probe, in more than 60% of infected HLA-DQ8tg mice (Figure II-15E) without inducing detectable intestinal damage. Thus, in a CD relevant mouse model, T1L infection breaks oral tolerance to gluten and promotes TG2 activation, supporting the hypothesis that reovirus infection, despite being clinically silent, can initiate critical events that set the stage for development of CD.

Evidence for a role of reovirus infection in celiac disease.

To directly investigate a role for reovirus in human CD, we compared anti-reovirus antibody titers in control individuals to those with active CD and CD patients on a GFD. Interestingly, CD patients tended to have higher anti-reovirus

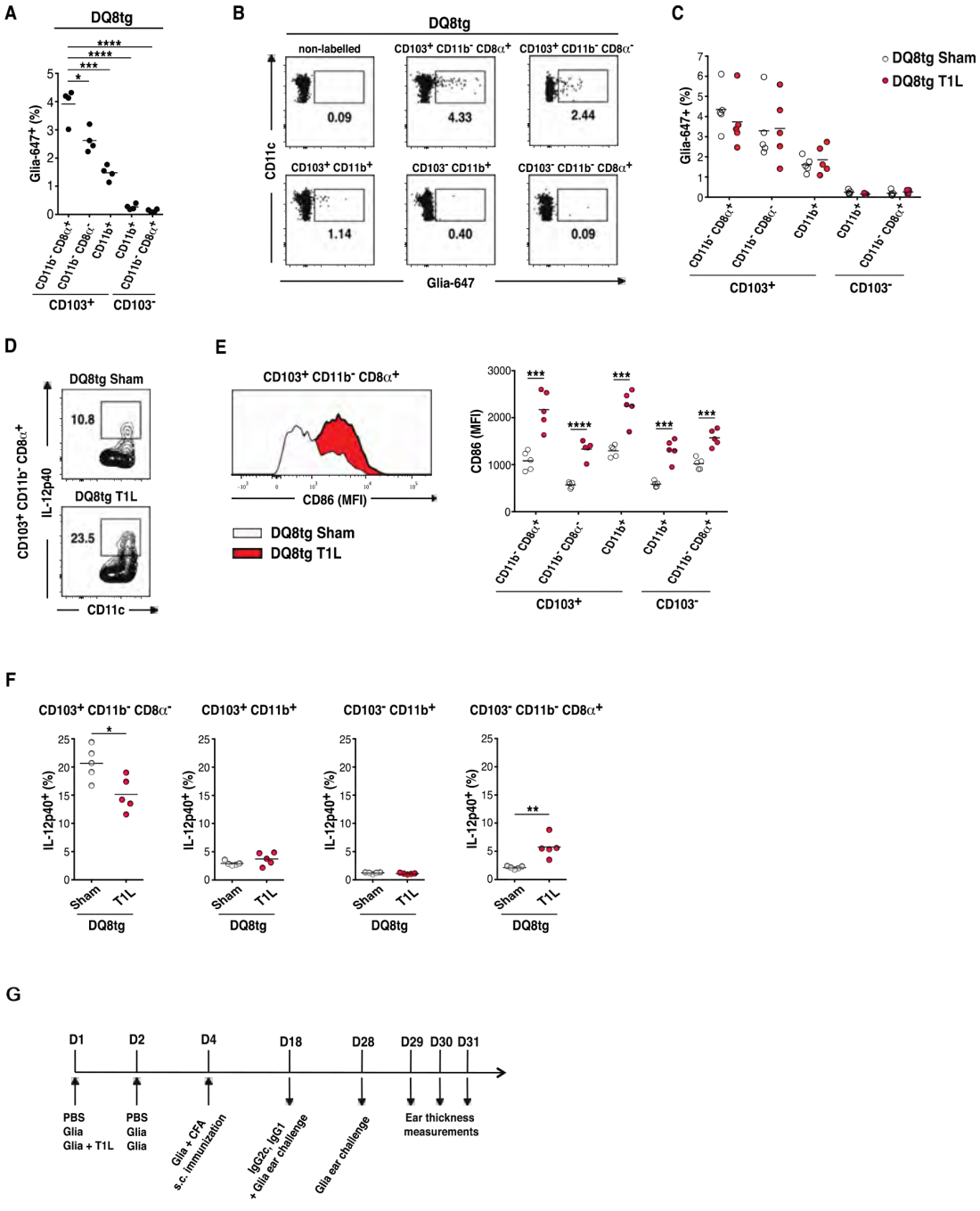
A
DQ8tg
Glia-647+ (%)
CD11b- CD8α+
CD11b- CD8α-
CD11b+
CD11b+
CD11b- CD8α+
CD103+
CD103-
B
DQ8tg
non-labelled
CD103+ CD11b- CD8α+
CD103+ CD11b- CD8α-
0.09
4.33
2.44
CD103+ CD11b+
CD103- CD11b+
CD103- CD11b- CD8α+
1.14
0.40
0.09
CD11c
Glia-647
C
DQ8tg Sham
DQ8tg T1L
Glia-647+ (%)
CD103+
CD103-
D
DQ8tg Sham
10.8
DQ8tg T1L
23.5
CD103+ CD11b- CD8α+ IL-12p40
CD11c
E
CD103+ CD11b- CD8α+
CD86 (MFI)
DQ8tg Sham
DQ8tg T1L
CD86 (MFI)
CD103+
CD103-
F
CD103+ CD11b- CD8α-
CD103+ CD11b+
CD103- CD11b+
CD103- CD11b- CD8α+
IL-12p40+ (%)
Sham
T1L
DQ8tg
G
D1
D2
D4
D18
D28
D29
D30
D31
PBS
Glia
Glia + T1L
PBS
Glia
Glia + CFA
s.c. immunization
IgG2c, IgG1
+ Glia ear challenge
Glia ear challenge
Ear thickness
measurements

Figure II-14. Dendritic cell activation and gliadin uptake upon reovirus infection of HLA-DQ8tg mice. (A and B) HLA-DQ8tg mice (n = 4) were gavaged with Alexa Fluor-647-labelled gliadin (Glia-Alexa 32 Fluor-647) 18 h before euthanasia, and Glia-Alexa Fluor-647 uptake by DCs was analyzed by flow cytometry. (A) Percentages and (B) dot plots depicting Glia-Alexa Fluor-647 uptake by the indicated DC subsets are shown. (C) HLA-DQ8tg mice were gavaged with OVA-Alexa Fluor-647 and inoculated with 10^8 PFU of T1L (n = 5) or PBS (sham, n= 5). At 18 hpi, mice were euthanized, and Glia-Alexa Fluor-647 uptake by DCs in the MLN was analyzed by flow cytometry. Percentages of Glia-Alexa Fluor-647 uptake by the indicated DC subsets are shown. (D to F) HLA-DQ8tg mice were inoculated perorally with 10^8 PFU of T1L (n = 5) or PBS (sham, n = 5) and euthanized at 2 dpi. (D to F) The expression of IL-12p40 and CD86 in MLN DCs was evaluated by flow cytometry. (D) Representative dot plots of IL-12p40-producing $CD103^+$ $CD11b^-$ $CD8\alpha^+$ DCs are shown.(E) Representative histogram and MFI for CD86 expression and (F) percentage of MLN IL-12p40-producing DCs are shown. (G) Delayed type hypersensitivity (DTH) experimental design. (A to F) Graphs depict two independent experiments. (A) *, $P < 0.05$; ***, $P < 0.001$; ****, $P < 0.0001$; one-way ANOVA/Tukey's multiple comparison. (C and E to G) *, $P < 0.05$; **, $P < 0.01$; ***, $P < 0.001$; ****, $P < 0.0001$; unpaired t-test.

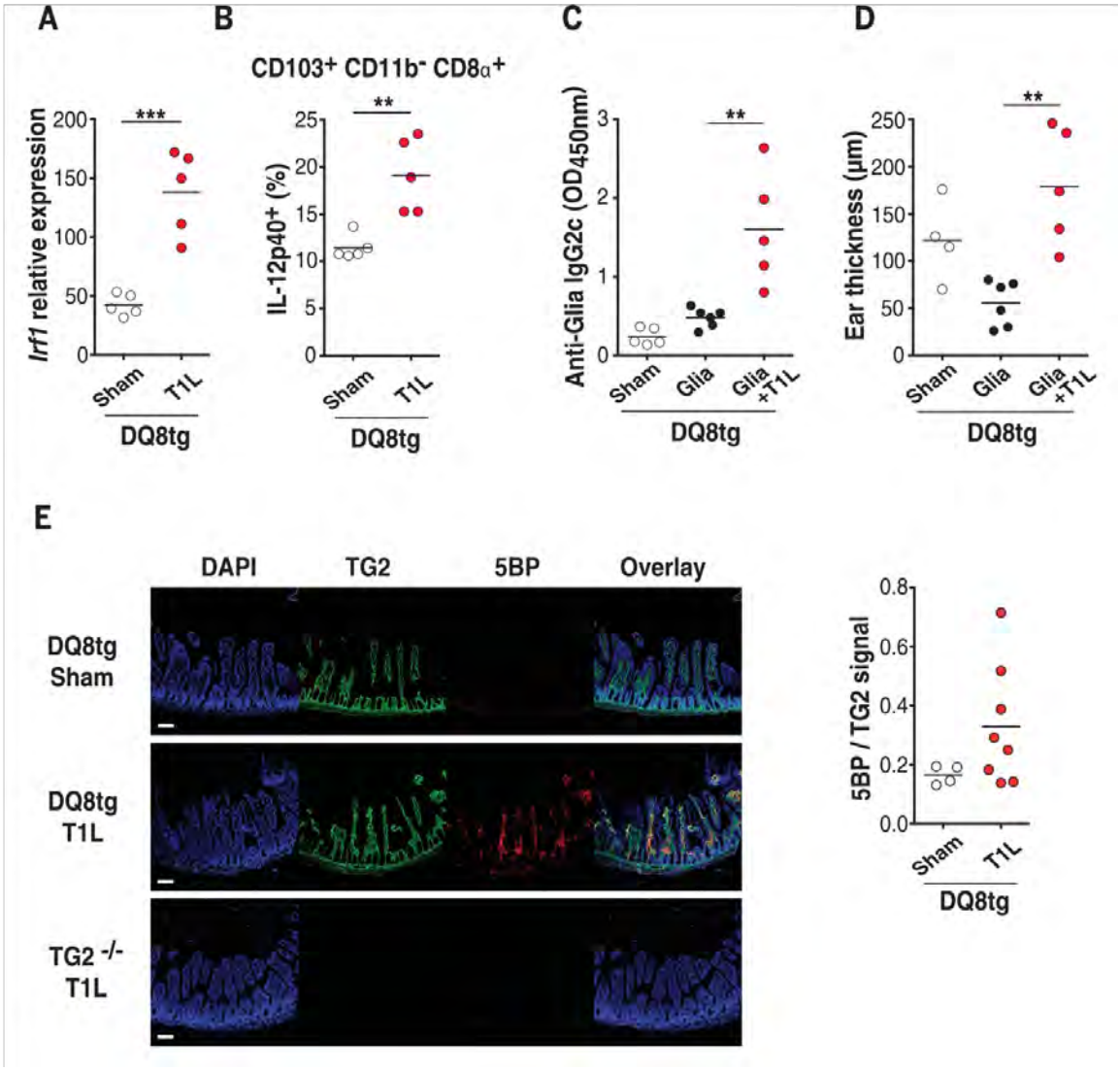
A
B
C
D
CD103+ CD11b- CD8α+
Irf1 relative expression
IL-12p40+ (%)
Anti-Glia IgG2c (OD450nm)
Ear thickness (μm)
***
**
Sham
T1L
Glia
Glia +T1L
DQ8tg
E
DAPI
TG2
5BP
Overlay
DQ8tg Sham
DQ8tg T1L
TG2 -/- T1L
5BP / TG2 signal

Figure II-15. Role of reovirus infection in loss of oral tolerance to gluten and transglutaminase 2 activation. (A and B) HLA-DQ8tg mice were inoculated perorally with 10^8 PFU of T1L (n = 5 mice) or PBS (sham, n = 5 mice) for 2 d. (A) Levels of IRF-1 expression in the MLN were analyzed by means of RT-PCR. (B) The expression of IL-12p40 on gated $CD11c^+$ $CD103^+$ $CD11b^-$ $CD8\alpha^+$ MLN DCs was evaluated by means of flow cytometry. (C and D) HLA-DQ8tg mice were inoculated perorally with 10^{10} PFU of T1L at the initiation of an oral tolerance/delayed type hypersensitivity protocol. Mice were fed orally with gliadin (Glia) for 2 d and then immunized subcutaneously with a CFA-Glia emulsion. (C) Levels of Glia-specific IgG2c antibodies in the serum were quantified at day 18 by means of ELISA. (D) On day 28, mice were challenged subcutaneously with Glia, and the degree of ear swelling was determined 24 h after challenge. Sham, n = 4 or 5 mice; Glia, n = 6 mice; and Glia + T1L, n = 5 mice. (E) HLA-DQ8tg mice were inoculated perorally with 10^{10} PFU of T1L (n = 8 mice) or PBS (sham, n = 4 mice). $TG2^{-/-}$ mice were inoculated perorally with 10^{10} PFU of T1L (n = 2 mice) and used as a negative control. Mice were euthanized at 18 hpi, and small intestines were collected and frozen in optimal cutting temperature compound. Representative images from stained frozen sections of the proximal small intestines are shown. Scale bars, 100 mm. Staining with 4′,6-diamidino-2-phenylindole (DAPI) is shown in blue, TG2 protein is shown in green, and TG2 enzymatic activity as assessed by means of 5BP cross-linking is shown in red. TG2 enzymatic activity normalized to TG2 protein levels was quantified for each villus. The mean enzymatic activity in the proximal small intestine per mouse is shown. (A to E) Graph depicts two independent experiments. (A, B, and E), **, $P < 0.01$; ***, $P < 0.001$; unpaired *t* test, (C and D), **, $P < 0.01$; one-way ANOVA/Tukey's multiple comparison.

antibody titers ($p = 0.06$) (Figure II-16A) and were significantly overrepresented among patients with very high titers (Figure II-16B). Furthermore, individuals with high anti-reovirus titers (above the median of our samples) have significantly higher *IRF-1* levels compared with individuals with low anti-reovirus titers (below the median of our samples) (Figure II-16C). However, there was no direct correlation between the anti-reovirus antibody titers and the level of *IRF-1* expression, indicating that there is not a linear relationship between antibody titers and *IRF-1* levels. Together, these results suggest that the presence of anti-reovirus antibody titers above a certain threshold indicates an antecedent virus-host interaction that caused long-lasting changes in immune homeostasis associated with high IRF-1 expression. This hypothesis is in agreement with the concept that viruses may leave a permanent mark on the transcriptional program of the host (283). A link between rotavirus infection and development of CD was suggested in a longitudinal study in children (114). However, our study failed to show such an association (Figure II-16, D to F). Our results do not exclude a role for rotavirus in CD pathogenesis and could be explained by rotavirus-host immune interactions that differ from those observed with reovirus. Finally, high anti-reovirus antibody titers in CD patients did not correlate with either high anti-rotavirus (Figure II-16G) or high anti-herpes simplex virus type 1 (HSV-1) antibody titers (Figure II-16H), indicating that CD patients displaying high anti-reovirus antibody titers do not mount generally high antibody responses against viruses. Taken together these results suggest that reovirus infection can trigger the onset of CD in a subset of CD patients.

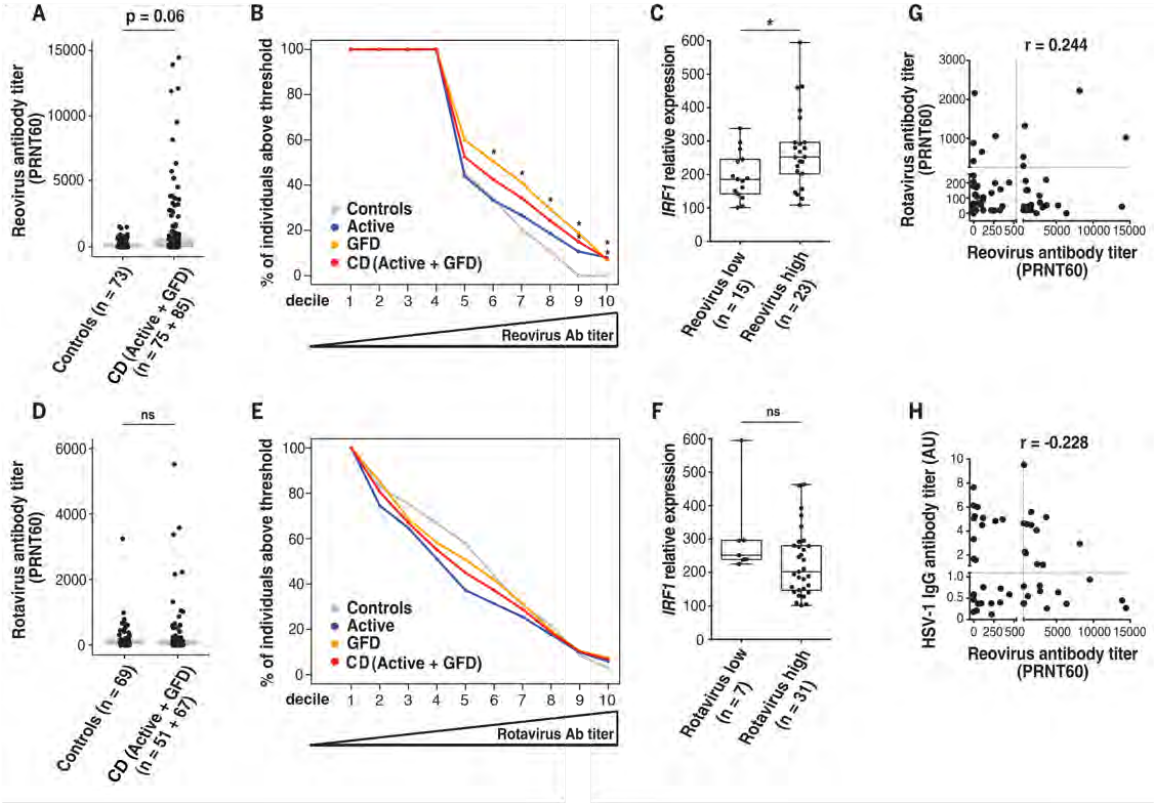

Figure II-16. Role of human reovirus infections in celiac disease pathogenesis. (A and D) Boxplots showing levels of reovirus antibody titers (A) and rotavirus antibody titers (D) in control (n = 73) and CD patients (n = 160). (B and E) Percentage of control patients (gray), active CD patients (blue), CD patients on a gluten-free diet (GFD) (orange), and active CD and GFD patients combined (red) that have reovirus (B) or rotavirus (E) antibody titers above an increasingly higher cutoff (left to right). Cutoffs were determined by defining the deciles of the distribution of reovirus (B) or rotavirus (E) antibody titers observed in the patient samples analyzed. GFD and CD (Active + GFD) patient groups are significantly overrepresented among individuals with reovirus titers above a PRNT60 = 156 (6th decile) and PRNT60 = 1597 (9^{th} decile), respectively. (C and F) *IRF-1* expression in small intestinal biopsies of GFD patients (n = 38) was analyzed by means of RT-PCR. Relative expression level of IRF-1 in GFD patients with low (left) and high (right) levels of reovirus (C) or rotavirus (F) antibody titers is shown. (C) Reovirus low and reovirus high were respectively defined as individuals with antibody titers below and above the median PRNT60 = 47 (B, 5th decile). (F) Rotavirus low and rotavirus high were respectively defined as individuals with antibody titers below and above the median PRNT60 = 53 (E, 5th decile). (G and H) Reovirus and rotavirus antibody titers in serum of patients were determined by means of plaque-reduction neutralization assay. Levels of HSV-1 antibody titers were determined by means of ELISA. Correlations between the levels of reovirus antibody titers and rotavirus antibody titers (G) or HSV-1 antibody titers (H) in GFD patients are shown. r, Pearson correlation. (A to F), *, $P < 0.05$; mann-whitney U test.

Discussion

This study provides support for the concept that viruses can disrupt intestinal immune homeostasis and initiate loss of oral tolerance and T_H1 immunity to dietary antigen. Furthermore, our findings suggest that an avirulent pathogen, such as reovirus, which is successfully cleared from the infected host, can nonetheless promote immunopathology. In support of this idea, clinically silent norovirus infections increase susceptibility to development of colitis (284). Importantly, our data also indicate that two reovirus strains can have substantially different immunopathological effects. Analysis of the transcriptional profiles induced in response to T1L and T3D-RV suggests that the capacity of a virus to trigger the loss of oral tolerance is associated with its capacity to disrupt immune homeostasis at sites where responses to oral antigens are initiated (Figure II-13).

In addition to reoviruses, it is probable that other enteric viruses, detected by different immune sensors and involved in different signaling pathways, also trigger loss of tolerance to dietary antigen. Expanding the concept of virotypes (283), we propose that the common feature of viruses eliciting pro-inflammatory immune responses to dietary antigen is the capacity to alter immune homeostasis and in particular endow DCs with proinflammatory properties at sites where oral tolerance is induced (Figure II-13). Identification of other viruses and defining key aspects of virus-host interactions leading to the abrogation of oral tolerance will help to design vaccine strategies to prevent CD and possibly other autoimmune disorders in at-risk populations. Based on our findings, even

viruses that do not lead to overt clinical pathology could be candidates for such prophylactic intervention.

CD is a complex disorder that likely requires several environmental perturbations to permanently disrupt tolerance to gluten. Indeed, epidemiological studies longitudinally monitoring genetically at-risk children report transient anti-gluten immune responses before development of fully developed CD (285, 286) and suggest that anti-gluten antibodies precede anti-TG2 antibodies (287). Furthermore, induction of T_H1 immunity to gluten, while required, is insufficient to cause villous atrophy, both in humans and mouse models of CD (288-290). This study indicates that while reovirus infections may trigger development of T_H1 immunity to gluten as well as activation of TG2, additional events likely will be required for induction of anti-TG2 antibodies and villous atrophy. Furthermore, non-viral triggers such as pathogenic members of the microbiota (291, 292), may have disease-causing properties similar to reovirus, and it is possible that the combination of different types of environmental factors will eventually lead to formation of a memory pool of T_H1 anti-gluten T cells of sufficient magnitude to cause enduring CD with villous atrophy.

CHAPTER III

VIRUS-INDUCED APOPTOSIS IN THE INTESTINE LIMITS ESTABLISHMENT OF ENTERIC INFECTION

Introduction

PO inoculation with reovirus strain T1L abrogates tolerance to food antigen, whereas inoculation with strain T3D-RV does not. Although T1L intestinal infection is well characterized, little is known about T3D-RV infection in the intestine or how these viruses differ in interactions with intestinal tissue to induce tolerance blockade. T1L and T3D differ in the capacity to induce apoptosis in cultured cells (224). In mice, this property is associated with viral injury in the heart and brain of newborn animals (117). However, the function of apoptosis during reovirus intestinal infection and whether it dictates pathogenesis in this tissue is not understood.

Several viruses, including human norovirus (293), rotavirus (294), and simian immunodeficiency virus (295), cause enterocyte cell death in animal models of viral gastroenteritis. Following PO inoculation with T1L, apoptotic cellular debris from infected enterocytes is observed in phagocytic vesicles of DCs found in PPs (168). Additionally, newborn mice inoculated perorally with an

apoptosis-deficient strain of reovirus develop higher viral titers in the intestine compared with those produced by an apoptosis-proficient strain (296). Therefore, I hypothesized that T1L and T3D-RV vary in induction of apoptosis during intestinal infection and that this difference associates with viral pathogenesis in this tissue, including the capacity to replicate and break oral tolerance.

To test this hypothesis, I quantified levels of apoptosis induced by T1L and T3D-RV during infection of cultured cells, intestinal organoids, and mice. I found that T3D-RV induces higher levels of apoptosis relative to T1L in all three assay systems. Additionally, T3D-RV intestinal infection was cleared more rapidly than T1L. To examine the relationship between apoptosis and infection in the intestine, I recovered a panel of T1L x T3D-RV reassortant viruses and found that reassortant viruses capable of producing high levels of apoptosis in the intestine also displayed diminished infection capacity, similar to T3D-RV. Expression of the T1L M1 and M2 genes in a T3D-RV background was sufficient to limit epithelial cell apoptosis and enhance viral infection to levels displayed by T1L. These results define an important antiviral role for apoptosis during enteric viral infection and illuminate strain-specific determinants that may be required for reovirus-induced tolerance blockade.

Results

T1L-infected mice maintain higher titers in the intestine during acute infection.

To determine whether T1L and T3D-RV produce comparable viral loads in intestinal tissue, I infected mice perorally with each virus strain and determined viral titers at 24, 48, and 72 hours post-inoculation (hpi). T1L produced higher titers in mice than did T3D-RV at 48 and 72 hpi (Figure III-1), a pathobiological phenotype I decided to study further. Therefore, although both virus strains produced comparable titers in the intestine, PP, MLN, and spleen 24 h after PO inoculation, T1L titers remain elevated throughout infection compared to T3D-RV.

T3D-RV infection induces caspase-3 activation and villus shedding in the gut.

To determine whether T1L and T3D-RV induce cell death and cause tissue damage *in-vivo,* WT mice were inoculated perorally and euthanized 1 and 8 dpi. Sections of intestinal tissue were stained for activated caspase-3 to identify cells undergoing apoptosis. Overall, viral infection led to an increase in caspase-3 activation relative to PBS-inoculated controls (Figure III-2A). Although activated caspase-3 levels increased during viral infection, no pathology was observed at either 1 or 8 dpi (Figure III-2A and Figure II-1F), and both strains were cleared by 8 dpi (data not shown). At 1 dpi, substantial caspase-3-positive cellular debris was present in the gut lumen of infected mice. These results suggest that reovirus infection leads to cell death and sloughing of enterocytes, perhaps as an antiviral response.

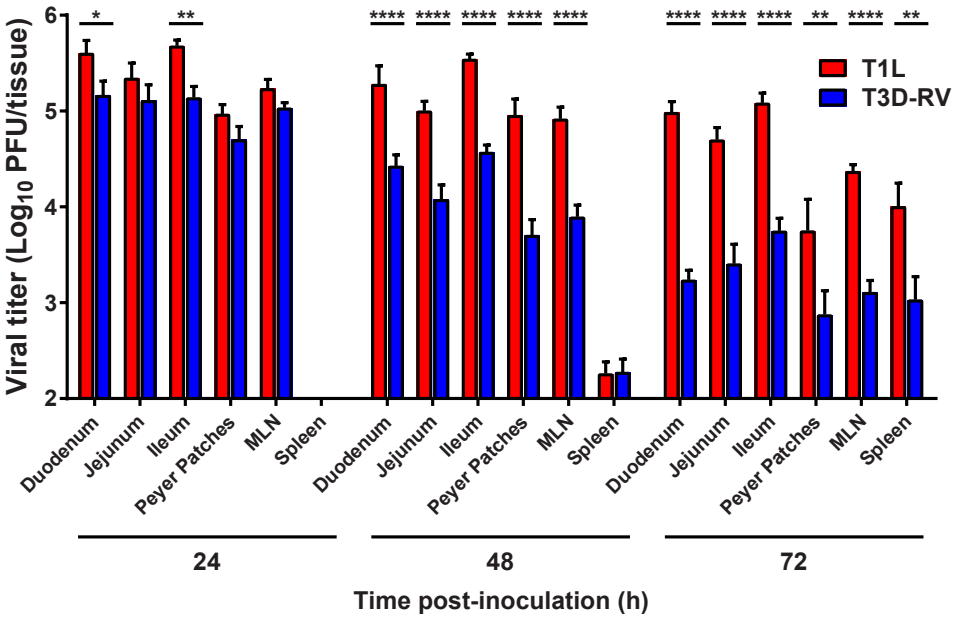

Figure III-1. Viral titers in murine tissues following reovirus T1L and T3D-RV infection. WT mice were inoculated perorally with 10^{10} PFU of T1L or T3D-RV (n = 7-10 mice per virus strain). Titers of T1L and T3D-RV in different regions of the intestine and secondary lymphoid organs were determined at 24, 48, and 72 hpi by plaque assay. The small intestine was sectioned into thirds, approximately the duodenum, jejunum, and ileum. Viral titers are expressed as PFU per tissue. *, $P < 0.05$; **, $P < 0.01$; ****, $P < 0.0001$; one-way ANOVA/Sidak's multiple comparison test.

Since T1L and T3D differ in the capacity to induce apoptosis, I hypothesized that T3D-RV induces more apoptosis in the gut, which could stimulate sloughing of infected enterocytes to mediate rapid viral clearance. To determine whether T1L and T3D-RV differ in the capacity to trigger apoptosis, cleaved caspase-3-positive epithelial cells were enumerated and normalized to the total number of villi examined. T3D-RV-infected mice had significantly more cleaved caspase-3-positive epithelial cells per villus than did those infected with T1L (Figure III-2B). To test whether T1L and T3D-RV differ in the shedding of apoptotic enterocytes into the intestinal lumen, I outlined the luminal region using Ariol Review software, demarcated the cleaved caspase-3-positive area, and quantified the percentage of positive staining in the lumen relative to the positive staining in the entire tissue section. Compared with mice infected with T1L, cleaved caspase-3 staining was increased in the lumen of mice infected with T3D-RV (Figure III-2C). The distribution of detectable reovirus antigen and apoptotic cells did not overlap, suggesting that viral infection is not required for activation of caspase-3 in a given cell (Figure III-2A). Therefore, T1L and T3D-RV infect the intestine comparably at 24 hpi, but T3D-RV promotes rapid enterocyte cell death and sloughing of apoptotic cells into the intestinal lumen.

T3D-RV replicates comparably to T1L in cultured cells but stimulates enhanced levels of apoptosis.

Viral reassortants occur naturally and are useful tools for identifying genes required for strain-specific polymorphisms. Before testing T1L x T3D-RV

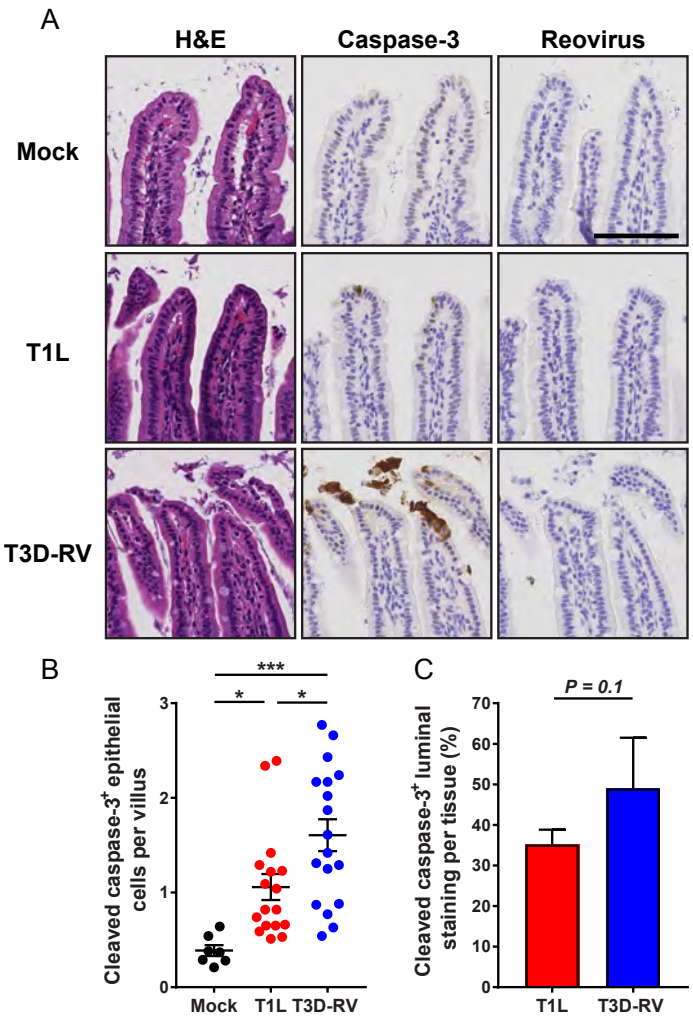

Figure III-2. Cleaved caspase-3 in the intestine of mice following infection with reovirus T1L or T3D-RV. WT mice were inoculated perorally with 10^8 PFU of T1L or T3D-RV or PBS (mock). One day after inoculation, intestines were resected. The proximal half was prepared for viral titer determination by plaque assay, and the distal half was flushed, Swiss-rolled, and processed for histology. (A) Sections were stained with H&E, reovirus polyclonal antiserum, or antibody against cleaved caspase-3. Representative sections of jejunum are shown (scale bar, 100 μM). (B) Cleaved caspase-3-positive-cells were enumerated manually and normalized per villus. Each symbol represents an individual mouse (n = 5-18 mice per group). (C) Cleaved caspase-3 staining in the lumen was quantified by outlining the luminal region using the Digital Histology Shared Resource tool (n = 3 mice per virus). The luminal staining (%) refers to the ([positive cleaved caspase-3 staining area in the lumen divided by positive cleaved caspase-3 staining area in the whole tissue] multiplied by 100). (B) Error bars denote the standard error of the mean. (C) Error bars denote standard deviation. *, $P < 0.05$; ***, $P < 0.001$; (B) one-way ANOVA/Tukey's multiple comparison test and (C) Mann-Whitney test.

reassortants in mice, I assessed whether differences in apoptosis displayed by T1L and T3D-RV could be studied using cultured cells. By first testing the reassortants in cultured cells, I could define a subset of viral genes required for cellular apoptosis and select viruses that express these genes to test using mice, thus limiting the number of mice studied. For these experiments, I decided to use L cells, a mouse fibroblast cell line highly susceptible to reovirus infection. To define the replication efficiency of T1L and T3D-RV, L cells were adsorbed with each virus strain, incubated for 0, 24, or 48 hpi, and lysed by freeze-thaw. Viral titers in cell lysates were determined by plaque assay (Figure III-3A). T1L and T3D-RV replicate comparably in these cells, producing nearly identical yields at all time points. To determine whether T1L and T3D-RV differ in the capacity to induce apoptosis in cultured cells, L cells were adsorbed with each strain, and apoptosis was quantified at 38 hpi using an acridine orange (AO)/ethidium bromide stain assay. T3D-RV infection led to a significantly higher percentage of apoptotic cells than did T1L. To complement the AO staining assay, L cells were adsorbed with T1L and T3D-RV, and caspase-3/7 activity in cell lysates was quantified at 24 hpi using a fluorogenic substrate (Figure III-3C). T3D-RV-infected samples expressed higher levels of activated caspase 3/7 relative to T1L- or mock-infected cells. Thus, T1L and T3D-RV replicate comparably in cultured cells, but T3D-RV induces the morphological and biochemical hallmarks of apoptosis more efficiently.

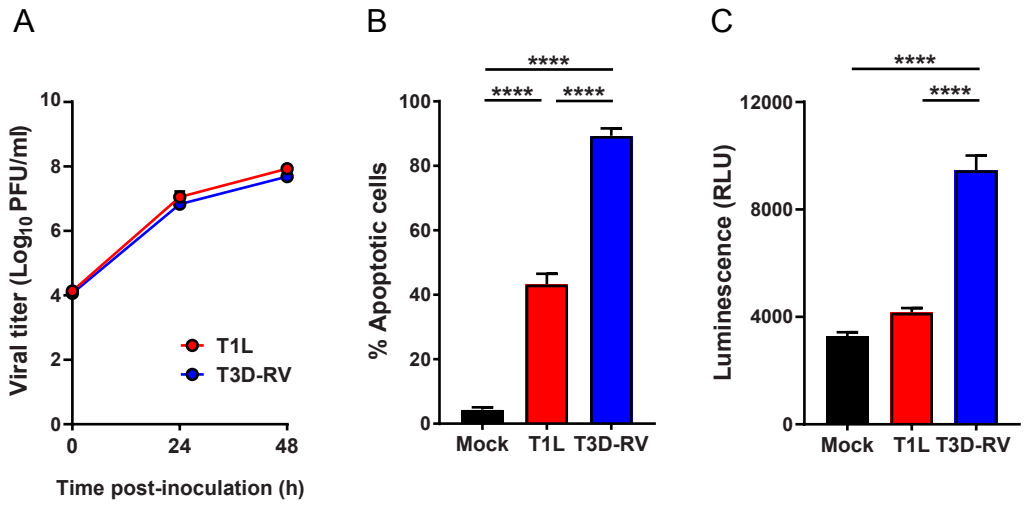

Figure III-3. Viral titers and apoptosis in L cells following reovirus T1L and T3D-RV infection. (A) L cells were adsorbed with T1L or T3D-RV at an MOI of 1 PFU/cell, and viral titers were determined at intervals shown by plaque assay. Viral titers are expressed as PFU/mL of cell homogenate. (B and C) L cells were adsorbed with T1L or T3D-RV at an MOI of 100 PFU/cell. (B) Cells were evaluated by AO assay at 38 hpi. The results are expressed as percentage of apoptotic cells per field of view. (C) Cell lysates were subjected to a Caspase Glo 3/7 assay at 24 hpi. Caspase-3 activity is expressed in relative luminescence units. Data represent three independent experiments performed in triplicate. ****; $P < 0.0001$; one-way ANOVA/Tukey's multiple comparison test.

T3D-RV provokes apoptosis and cell shedding in infected enteroids.

Recent development of techniques to cultivate intestinal organoids or "enteroids" in culture has advanced opportunities to study virus-host interactions at intestinal sites (297-299). To determine whether reovirus infects tissue-derived organoids from mice and promotes apoptotic cell death in these cultures, I collaborated with Sarah Short from the laboratory of Dr. Chris Williams at Vanderbilt University. Sarah dissected intestines from adult mice and isolated intestinal crypts to be grown in 3-D spheroids in Matrigel. These cultures contain crypt- and villus-like structures. Based on previous studies, I predicted that IECs are exposed to reovirus in the mouse intestine from the apical or luminal side of the epithelium (149, 150). To examine the susceptibility of polarized murine enteroids to reovirus infection and subsequent virus-induced apoptosis, crypts were seeded onto transwell plates, adsorbed with T1L or T3D-RV, and scored for reovirus infection and apoptosis. At 24 hpi, infectivity was comparable between the strains, as visualized by immunofluorescence using reovirus polyclonal antiserum (Figure III-4, A and B). Murine enteroids infected with T3D-RV displayed a greater percentage of apoptotic cells, as judged by staining with an antibody specific for cleaved caspase-3 (Figure III-4, D and E). At 24 hpi, the apical medium was collected, and cells in the medium were enumerated using an automated cell counter. T3D-RV-infected enteroids had a larger number of cells in the apical medium, as an indicator of cell sloughing (Figure III-4F). T1L titers in enteroids were significantly higher than those produced by T3D-RV (Figure III-4C), which correlates with increased apoptosis and decreased cell number in

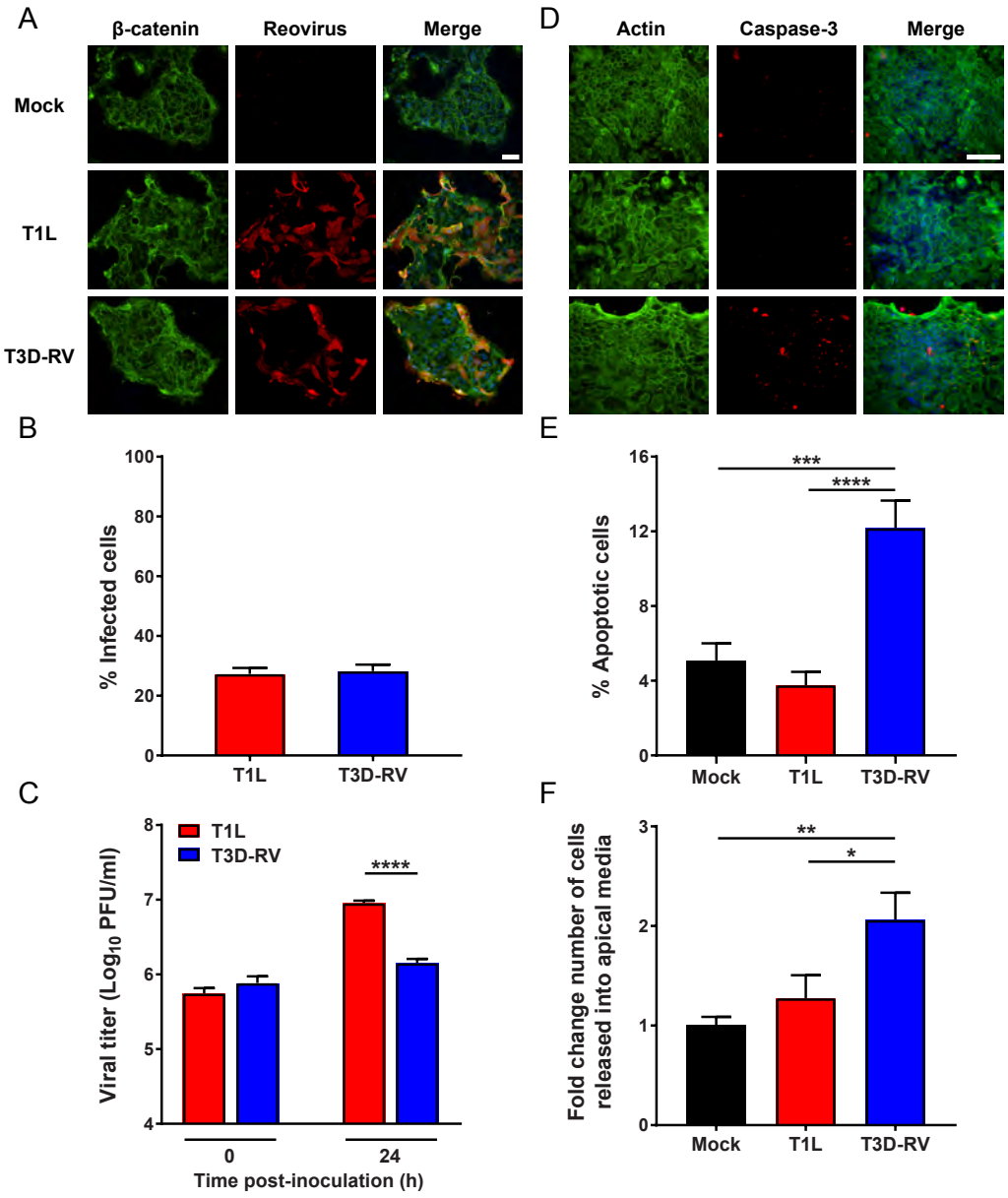
A
β-catenin
Reovirus
Merge
Mock
T1L
T3D-RV
D
Actin
Caspase-3
Merge
B
% Infected cells
100
80
60
40
20
0
T1L
T3D-RV
E
% Apoptotic cells
16
12
8
4
0
***
****
Mock
T1L
T3D-RV
C
Viral titer (Log10 PFU/ml)
8
7
6
5
4
T1L
T3D-RV
****
0
24
Time post-inoculation (h)
F
Fold change number of cells released into apical media
3
2
1
0
**
*
Mock
T1L
T3D-RV

Figure III-4. Viral infectivity and apoptosis in murine-derived enteroids following reovirus T1L and T3D-RV infection. Intestinal crypts were harvested from WT mice and established as enteroids in Matrigel. The enteroids were dissociated, seeded onto transwell plates, and incubated at 37° for 4 d. Enteroids were adsorbed with T1L or T3D-RV at an MOI of 100 PFU/cell or PBS as a mock control. At 24 hpi, cells were fixed and stained with antibodies specific for β-catenin and reovirus (A) or actin and cleaved caspase-3 (D). Nuclei were labeled with ProLong Gold antifade mountant containing DAPI (scale bar, 50 μM). (B) The percentage of infected cells was determined by enumeration of reovirus-positive cells from immunofluorescence images. (C) Viral titers were determined at the intervals shown by plaque assay and expressed as PFU/mL of cell homogenate. (E) The percentage of apoptotic cells was determined using the Nikon Elements Basic Research analysis software and represents the number of cleaved caspase-3-positive cells per total number of cells in the selected field. (F) The number of cells released into the apical medium was quantified using an automated cell counter. Data represent two to four independent experiments performed in triplicate. Error bars denote the standard error of the mean. *, $P < 0.05$; **, $P < 0.01$; ***, $P < 0.001$; ****, $P < 0.0001$; (C) Mann-Whitney test and (E and F) one-way ANOVA/Tukey's multiple comparison test.

T3D-RV-infected cultures (data not shown). Therefore, T1L and T3D-RV infect enteroids comparably but differ in the capacity to promote apoptosis and cell sloughing.

Viral gene segments M1 and M2 dictate reovirus apoptosis induction in cultured cells.

To identify viral genes that segregate with differences in apoptosis efficiency displayed by T1L and T3D-RV, eight T1L x T3D-RV reovirus reassortants (Figure III-5A) were recovered using reverse genetics (143). All reassortants contain the T1L S1 and L2 gene segments, which allows these strains to infect the intestine (154). To quantify viral replication efficiency of the newly engineered reassortants, L cells were adsorbed with each virus strain, incubated for 24 h, and lysed by freeze-thaw. Viral titers in cell lysates were determined by plaque assay. All reassortant viruses replicated comparably (Figure III-5B). To identify viral gene segments that segregate with apoptosis, L cells were adsorbed with T1L, T3D-RV, or one of eight T1L x T3D-RV reassortants and scored for apoptosis following AO staining. Reassortant viruses containing a T3D M2 gene induced more apoptosis by AO assay than those containing a T1L M2 gene (Figure III-5, C and D). Additionally, the T3D M1 gene appeared to enhance apoptosis efficiency, albeit not as clearly as the T3D M2 gene (Figure III-5D). Therefore, the T3D M2 gene segment is required for increased levels of apoptosis in cultured cells. However, the M1 gene also may influence apoptosis efficiency in this context.

A

Virus	Source of gene segment									
	S1	S2	S3	S4	M1	M2	M3	L1	L2	L3
Parental viruses										
T1L	1	1	1	1	1	1	1	1	1	1
T3D-RV	1	3	3	3	3	3	3	3	1	3
Reassortant viruses										
A	1	1	3	1	1	3	1	3	1	3
B	1	1	1	3	3	3	1	1	1	3
C	1	1	1	3	3	3	3	1	1	1
D	1	1	1	1	3	3	3	3	1	1
E	1	3	1	1	3	1	3	3	1	1
F	1	3	3	1	1	1	3	1	1	3
G	1	3	3	3	1	1	1	1	1	3
H	1	3	3	3	1	1	1	3	1	1

C

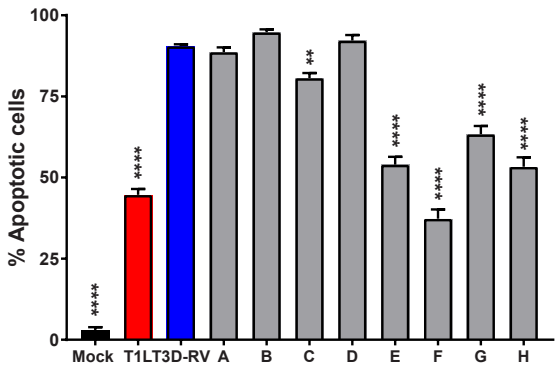

B

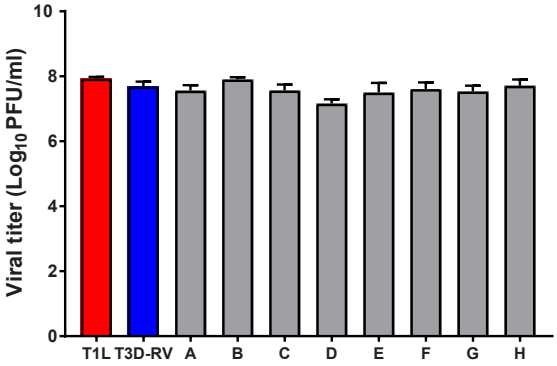

D

Virus	Source of gene segment										Rank
	S1	S2	S3	S4	M1	M2	M3	L1	L2	L3	
B	1	1	1	3	3	3	1	1	1	3	10
D	1	1	1	1	3	3	3	3	1	1	9
T3D-RV	1	3	3	3	3	3	3	3	1	3	8
A	1	1	3	1	1	3	1	3	1	3	7
C	1	1	1	3	3	3	3	1	1	1	6
G	1	3	3	3	1	1	1	1	1	3	5
E	1	3	1	1	3	1	3	3	1	1	4
H	1	3	3	3	1	1	1	3	1	1	3
T1L	1	1	1	1	1	1	1	1	1	1	2
F	1	3	3	1	1	1	3	1	1	3	1
Rank Sum	ns	ns	ns	#	**	ns	ns		ns		

Figure III-5. Viral replication and apoptosis in L cells following infection with reovirus reassortant viruses. (A) T1L x T3D-RV reassortant viruses used to identify genes that segregate with strain-specific differences in the capacity of reovirus to induce apoptosis in the intestine. Gene segments labeled “1” in red represent those derived from T1L; gene segments labeled “3” in blue represent those derived from T3D. (B) L cells were adsorbed with T1L, T3D-RV, or one of eight T1L x T3D-RV reassortants at an MOI of 1 PFU/cell, and viral titers were determined at 48 hpi by plaque assay. Viral titers are expressed as PFU/mL of cell homogenate. (C) L cells were adsorbed with T1L, T3D-RV, or one of eight T1L x T3D-RV reassortants at an MOI of 100 PFU/cell. PBS-inoculated samples (mock) were used as controls. Cells were evaluated by AO assay at 38 hpi. The results are expressed as percentage of apoptotic cells per field of view. (D) Rank sum analysis of reassortants used to identify genes that segregate with the capacity to induce apoptosis. The rank number of each reassortant and the significance levels of each gene segment are shown. Data represent two or three experiments performed in triplicate. Error bars denote the standard error of the mean. ns = non-significant; #, $P = 0.06$; **, $P < 0.01$; ****, $P < 0.0001$; (C) one-way ANOVA/Dunnett’s multiple comparison test (as compared with T3D-RV) and (D) Wilcoxon rank sum distribution test.

Viral gene segments M1 and M2 dictate reovirus pathogenesis by altering apoptosis induction in the gut.

To examine the requirement of the M1 and M2 genes for apoptosis induction in the murine intestine, I engineered six T1L x T3D-RV M gene reciprocal reassortants. The reciprocal reassortants maintain the parental strain background but were constructed to exchange the M1 and M2 genes individually or together (Figure III-6A). To examine replication capacity and subsequent virus-induced apoptosis of these reassortant viruses, L cells were adsorbed with each virus strain, incubated for various intervals, and scored for reovirus infection and apoptosis. The M gene reassortant viruses replicated comparably (Figure III-6B). At 38 hpi, the percentage of apoptotic cells was increased 3-fold following T3D-RV infection compared with T1L (Figure III-6C). The presence of a T3D M2 gene on a T1L background was sufficient to reconcile this difference, as the percentage of apoptotic cells was increased 2-3-fold following infection with these reassortant viruses compared to the parental strain T1L (Figure III-6C). Additionally, reciprocal reassortant viruses containing the T1L M2 gene on a T3D-RV background displayed a significant reduction in apoptosis efficiency relative to parental strain T3D-RV (Figure III-6C). Surprisingly, the reassortant virus that contains the T3D M1 gene in a T1L background induced a two-fold increase in the percentage of apoptotic cells compared with parental strain T1L (Figure III-6C). However, the reciprocal virus (T1L M1 gene in a T3D-RV background) produced a high percentage of apoptotic cells, likely due to the T3D M2 gene that appears to override any effects of the T1L M1 gene (Figure III-6C).

A

Virus	M Gene Reassortant Panel									
	S1	S2	S3	S4	M1	M2	M3	L1	L2	L3
Parent T1L	1	1	1	1	1	1	1	1	1	1
T1L T3 M1	1	1	1	1	3	1	1	1	1	1
T1L T3 M2	1	1	1	1	1	3	1	1	1	1
T1L T3 M1, M2	1	1	1	1	3	3	1	1	1	1
Parent T3D-RV	1	3	3	3	3	3	3	3	1	3
T3D-RV T1 M1	1	3	3	3	1	3	3	3	1	3
T3D-RV T1 M2	1	3	3	3	3	1	3	3	1	3
T3D-RV T1 M1, M2	1	3	3	3	1	1	3	3	1	3

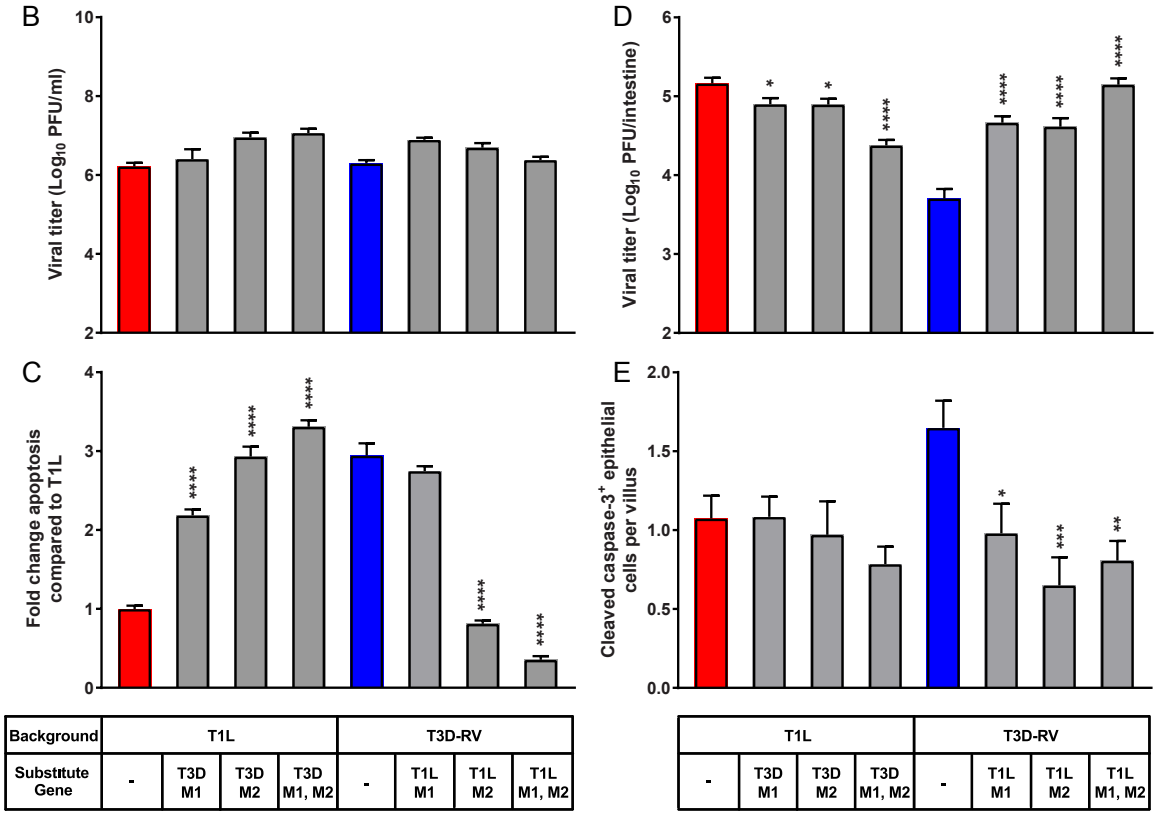

Figure III-6. Viral replication and apoptosis in cultured cells and murine intestine following infection with M gene reassortant viruses.
Viral replication and apoptosis in cultured cells and murine intestine following infection with M gene reassortant viruses. (A) T1L x T3D-RV M gene reassortant viruses used to define genes that segregate with the apoptosis-inducing capacity of reovirus. Gene segments labeled “1” in red represent those derived from T1L; gene segments labeled “3” in blue represent those derived from T3D. (B) L cells were adsorbed with T1L, T3D-RV, or one of six T1L x T3D-RV M gene reassortants at an MOI of 1 PFU/cell, and viral titers were determined at 24 hpi by plaque assay. Viral titers are expressed as PFU/mL of cell homogenate. (C) L cells were adsorbed with T1L, T3D-RV, or one of six T1L x T3D-RV M gene reassortants at an MOI of 100 PFU/cell. Cells were evaluated by AO assay at 38 hpi. The results are expressed as fold change in apoptosis compared with T1L. Data are presented from two experiments performed in triplicate. (D and E) Mice were inoculated perorally with 10^8 PFU of T1L, T3D-RV, or one of six T1L x T3D-RV M gene reassortants. The proximal half of the intestine was processed for viral titer, and the distal half was flushed, Swiss-rolled, and processed for histology. (D) Titers of reovirus in the intestine were determined at 72 hpi by plaque assay ($n \geq 10$ mice per virus). (E) At 24 hpi, histological sections were stained with an antibody against cleaved caspase-3. Cleaved caspase-3-positive cells were enumerated manually and normalized per villus ($n \geq 8$ mice per virus). Error bars denote the standard error of the mean. *, $P < 0.05$; **, $P < 0.01$; ***, $P < 0.001$; ****, $P < 0.0001$; (C-E) one-way ANOVA and Dunnett’s multiple comparison test (as compared with the parental strain).

Furthermore, the reassortant virus that contains the T3D M1 and M2 genes in the T1L background slightly enhanced apoptosis levels compared with those expressing the T3D M1 or M2 genes alone (Figure III-6C). Taken together, a T3D M2 gene in a T1L background is necessary and sufficient to stimulate apoptosis in cultured cells and, in conjunction with the T3D M1 gene, promotes maximum levels of apoptosis.

Since T3D-RV activates apoptosis and subsequent villous sloughing and is cleared from the intestine more efficiently than T1L, I hypothesized that genes associated with enhanced apoptosis of T3D-RV also are associated with diminished infection capacity in the gut. To test this hypothesis, mice were inoculated perorally with T1L, T3D-RV, or each of the six T1L x T3D-RV M gene reassortant viruses and euthanized 24 hpi for histological analysis and 72 hpi for determination of viral titer. Tissue sections were stained for activated caspase-3 to identify cells undergoing apoptosis within the intestine. At 72 hpi, viral titers in the intestine of mice infected with T1L were approximately 30-fold greater than those in animals infected with T3D-RV. Reassortant viruses that express T1L M1, M2, or M1 and M2 genes in a T3D-RV background replicate comparably to T1L, indicating that these gene segments are sufficient to increase T3D-RV titers in the intestine (Figure III-6D). Furthermore, reduced numbers of cleaved caspase-3-positive enterocytes were observed in mice infected with these viruses (Figure III-6D). These findings suggest that enterocyte apoptosis serves as an antiviral response to inhibit viral infection in the intestine. Of note, the T3D M1 and M2 genes are not sufficient to limit T1L infection to levels comparable to

T3D-RV or enhance apoptosis efficiency in the intestine of infected mice (Figure III-6, D and E), suggesting that additional viral or host factors contribute to T1L replication capacity in the intestine.

Discussion

Reovirus T1L and T3D-RV differ in the capacity to illicit immune responses to orally fed antigen. However, it is not understood how these viruses differ during intestinal infection to mediate this response. In this study, I evaluated the function of apoptosis in T1L and T3D-RV intestinal infection and found that compared to T3D-RV, T1L induces less caspase-3 activation, less sloughing of intestinal villi, and prolonged infection, providing a plausible mechanism by which T1L abrogates oral tolerance. T1L x T3D-RV reassortant viruses that stimulate greater levels of apoptosis in the intestine also display diminished replication capacity in this tissue. Therefore, the capacity to promote apoptosis in the intestine inversely correlates with replication, suggesting that enterocyte apoptosis and sloughing mediate an antiviral response to protect the host.

The finding that T1L-infected mice produce higher viral loads in the intestine could be explained by other pathobiological factors such as replication capacity, tissue tropism, and immune evasion, among others. However, T1L and T3D-RV do not differ in the capacity to replicate in cultured cells (Figure II-1B and III-3A), and there is no evidence that these strains differ in cell tropism in the intestine (Figure II-1D). Furthermore, T1L-infected mice express higher levels of type 1 IFNs and ISGs compared with T3D-RV-infected mice at 48 hpi (Figure II-

8A and II-9A). These findings suggest that T1L is recognized by the innate antiviral immune response and that subversion of the IFN response is not responsible for the differences in viral titers.

Enterocytes have the highest turnover rate of any cell population in the body (242, 248), most likely due to environmental insults and the necessity to maintain a healthy gut barrier. Despite the high rate of turnover, shedding events are rarely observed in healthy individuals and seldom visualized by biochemical markers such as cleaved caspase-3 (248, 255). However, a variety of stimuli and disease states can promote apoptosis during pathological cell shedding. For example, poly(I:C) (253), viral dsRNA (263), and some enteric viruses (293-295) can stimulate apoptotic cell death of IECs, usually in combination with gastrointestinal pathology. Infection with reovirus T3D-RV led to extensive caspase-3 activation in IECs and sloughing of caspase-3-positive cells into the intestinal lumen. Interestingly, apoptosis was not associated with shortening of intestinal villi or other pathological markers, and barrier function was maintained. Most activated caspase-3 was found at the villus tips, often with multiple cells undergoing apoptosis in a localized region of the villus. During infection with T1L and T3D-RV, cleaved caspase-3 staining was patchy but could be observed throughout the distal half of the small intestine. Virus-induced apoptosis was observed within the first 24 h following infection and declined at later time points. The distribution of reovirus- and caspase-3-postive antigen staining did not overlap, possibly because apoptosis is triggered without reovirus replication or the detection of reovirus antigen-positive cells was limited. Future studies will

determine whether empty viral particles or UV-inactivated virus can promote similar caspase-3 activation in the intestine without viral replication or genomic content. If so, follow-up studies would define viral structural proteins required to trigger apoptosis in the intestine and identify any strain-specific polymorphisms that exist.

Enteroids are useful for studying virus-host interactions *ex vivo*. There are several methods for enteroid isolation, which differ in the species types, starting material, expandability, and developmental stage. For these studies, I used murine tissue-derived organoids due to phenotypic similarities to the mouse intestine. I found that enteroids are susceptible to reovirus infection and observed strain-specific differences in apoptosis efficiency. The research described here will provide the basis for studies examining the capacity of other enteric viruses to promote apoptosis. Furthermore, enteroids harvested from mice deficient in antiviral response pathways may lead to discovery of host factors required for virus-induced apoptosis.

Differences in apoptosis induction segregate with the viral M2 gene (300), which differs between T1L and T3D-RV. It is not surprising that in our study the M2 gene segment segregated with differences in apoptosis efficiency following infection of cultured cells, as this association has been described previously (224, 225, 300). More interesting was the observation that the T1L M2 gene on a T3D-RV background was sufficient to increase viral titers in the intestine to levels comparable to T1L. The T1L M2 gene was identified in a previous study as a virulence factor required for replication in the intestine of neonatal mice (301). A

subsequent study suggested that only the S1 and L2 genes are required for intestinal replication (152). My studies resolve these discrepancies by using reassortant viruses with common S1 and L2 genes of T1L. Following PO inoculation with these strains, the M2 gene emerges as a determinant of reovirus intestinal infection. Furthermore, viruses with the T1L M2 gene promoted less apoptosis in the intestine, providing additional evidence that epithelial cell death promotes an antiviral state and suggesting a mechanism by which the M2 gene dictates intestinal pathogenesis.

The M2 gene encodes outer-capsid protein μ1, which functions to penetrate endosomal membranes during viral entry, a property required for apoptosis induction (238). Following infection of IECs, it is possible that the T3D M2-encoded μ1 protein mediates penetration of endosomal membranes exposing viral particles and dsRNA to pattern recognition receptors. Activation of these receptors stimulates proapoptotic signaling by NF-κB and IRF-3 and upregulation of IFNs and other cytokines, which may evoke cell death. Such a scenario provides a mechanism by which T3D-RV could induce enterocyte apoptosis and extrusion from the villus to protect adjacent cells from subsequent infection.

The Φ domain of μ1 is necessary and sufficient to promote apoptosis in cell culture (234, 239), and polymorphisms in this domain influence the apoptotic efficiency of T3D (234). A virus containing an M2 gene with the apoptosis-attenuating polymorphisms in a T3D-RV background would likely lose apoptotic capacity in cultured cells, enteroids, and mice. Furthermore, other evidence

suggests that reovirus strains that have diminished apoptotic capacity replicate to higher titers in the intestine (296).

Although the M2 gene is the primary driver of differences in apoptosis efficiency between T1L and T3D-RV, my findings suggest that the M1 gene exacerbates cell death when combined with the M2 gene. The reovirus M1 gene-encoded μ2 protein is a strain-specific IFN antagonist that dictates pathogenesis in neonatal mice (276). A single amino acid polymorphism in μ2 modulates cytopathic effects by regulating the host IFN response (276). However, the M1 gene has not been identified in studies of viral genes required for intestinal infection. The absence of such linkage might be attributable to the use of newborn mice, which may lack mature IFN signaling. The T1L μ2-encoded IFN antagonist may subvert host antiviral responses in the gut including the induction of apoptosis, allowing this strain to replicate more efficiently in this tissue. Compared with T3D-RV, T1L infection induces greater levels of type 1 IFNs and ISGs after 24 hpi (Figure II-8A and II-9A), which could be a byproduct of prolonged T1L infection. Studies including viruses with the single amino acid polymorphism reciprocally exchanged in parental backgrounds would determine whether IFN antagonism associates with diminished apoptosis and enhanced replication of T1L.

PO inoculation with reovirus strain T1L stimulates inflammatory responses to fed antigen, whereas inoculation with T3D-RV does not. In this study, I found that T3D-RV titers are diminished due to a capacity to promote apoptosis in IECs. I predict that prolonged viral infection by T1L during the introduction of new

food proteins stimulates inflammatory signals such as type 1 IFNs and IRF-1 to promote food-antigen-specific T_H1 cells and inhibit T_{regs} (Figure III-7). From studies of reassortant viruses, I found that the T1L M1 and M2 genes on a T3D-RV background are sufficient to increase viral titers in the intestine to levels comparable to T1L. Using these reassortant viruses, we can now determine whether decreased intestinal apoptosis and prolonged viral replication are associated with tolerance blockade. Thus, this work provides a possible mechanism by which certain enteric, nonpathogenic viruses establish prolonged replication by subverting the host cell-death response to stimulate the inflammatory signals required to break immunological tolerance to food antigens.

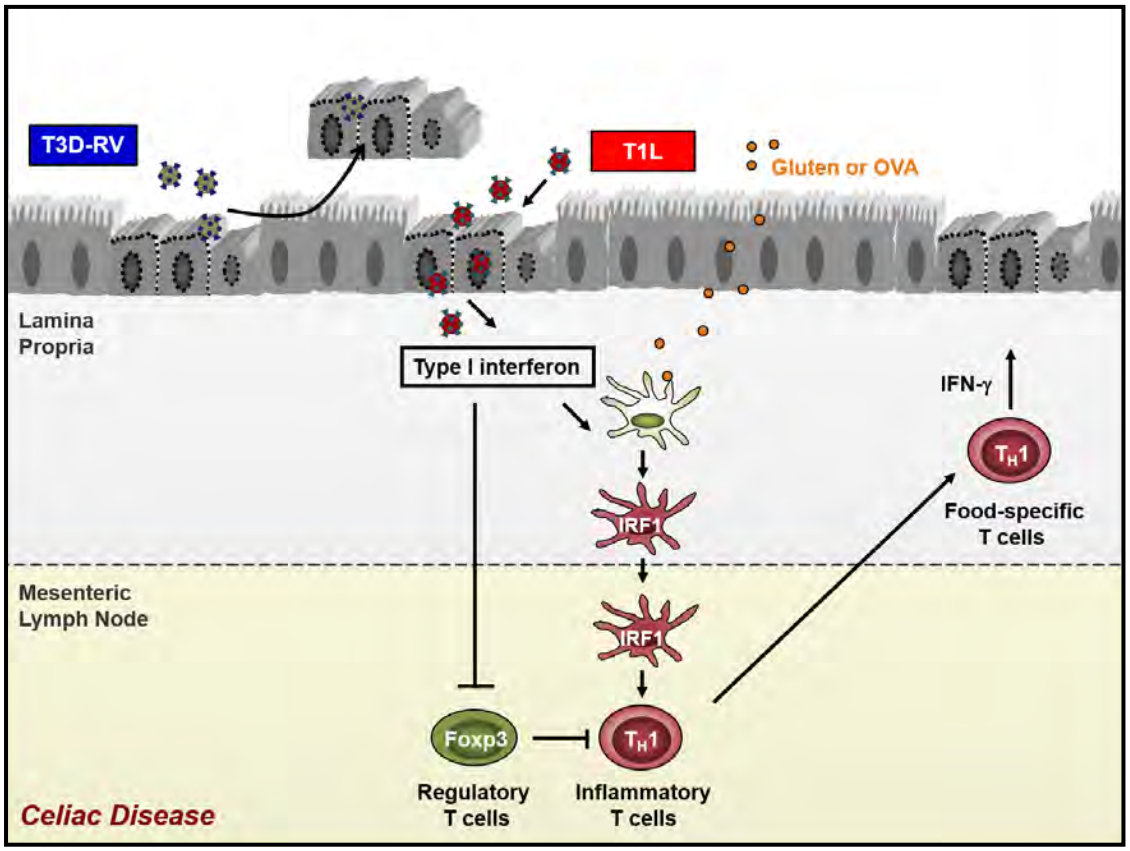

Figure III-7. Model of reovirus strain-specific abrogation of oral tolerance. Following PO inoculation, T1L and T3D-RV infect the intestine. T3D-RV induces caspase-3 activation and IEC sloughing subsequently leading to rapid viral clearance. T1L, however, subverts these antiviral responses to establish prolonged infection, triggering type 1 IFN signaling and IRF-1 expression in LP DCs. In the context of this inflammatory cytokine milleu, DCs phagocytose new food antigen (Gluten or OVA) and traffic to the MLN to activate inflammatory T cells. Type 1 IFNs upregulated during T1L infection also inhibit T_{regs} leading to subsequent development of T_H1 immunity to dietary antigen.

CHAPTER IV

SUMMARY AND FUTURE DIRECTIONS

Thesis Summary

CD is an immune-mediated intestinal disorder that occurs in genetically predisposed individuals exposed to dietary gluten. Although 30-45% of the U.S. population carries the risk alleles, only 1% of the population develops the disease (1). This finding suggests that other genetic and environmental factors are required for CD development. Viral infections are associated with the induction of many autoimmune and inflammatory diseases. Accordingly, several viruses have been implicated in CD onset, including *Reoviridae* viruses (114). However, not all viruses confer disease susceptibility, and little is known about specific viral characteristics that dictate immunopathologic outcomes.

Mammalian reovirus infects the intestine following oral inoculation. In humans, infections are common during early childhood (116) when maternal immunity is waning and solid foods, including wheat cereals, are introduced into the infant diet. Reovirus infections of the intestine are often nonpathogenic, and therefore may go undetected. To study the effects of reovirus infection on oral tolerance our lab established a collaboration with the laboratory of Dr. Bana Jabri at the University of Chicago.

Feeding mice OVA as a model antigen results in systemic tolerance to OVA following subcutaneous (s.c.) challenge, which is marked by induction of

regulatory T cells and absence of OVA-specific inflammatory B and T cells (70, 71). Early studies first performed by Drs. Jennifer Stencel-Baerenwald and Romain Bouziat illustrated that PO inoculation with reovirus strain T1L abrogated oral tolerance to OVA, as evidenced by the promotion of OVA-specific B cells and IFN-γ-producing T cells, whereas inoculation with strain T3D-RV did not. The goals of my studies presented in Chapters II and III were to define the mechanisms of reovirus-induced tolerance blockade and determine the reovirus strain-specific differences that mediate this phenomenon.

First, I tested whether T1L and T3D-RV differ in the capacity to replicate in cultured cells and infect the intestine of mice. T1L and T3D-RV produced identical viral yields in two different cell lines (Figure II-1B and III-3A). Following PO inoculation of mice, both virus strains produced similar titers in the intestine, PP, MLN, and spleen 24 h after PO inoculation (Figure II-1C). T1L and T3D-RV were cleared by 6 dpi (Figure II-1E), and no pathology was observed in infected mice (Figure II-1F). The antiviral $CD4^+$ T cell response was comparable between T1L and T3D-RV (Figure II-1H), although neutralizing antibody titers were slightly higher in T1L-infected animals (Figure II-1G). These results confirmed that T1L and T3D-RV establish intestinal infection without overt signs of intestinal pathology.

PO inoculation with T1L abrogated tolerance to OVA in experiments in which mice were fed OVA and immunized subcutaneously with OVA and complete Freund's adjuvant (CFA). However, the experiments were challenging, and the results varied within a given experiment. Therefore, the Jabri laboratory

developed a T cell conversion assay to test whether T1L alters the effector state of food-antigen-specific T cells and to determine the mechanism by which this occurs. We found that T1L significantly inhibited the conversion of OVA-specific OT-II $CD4^+$ T cells into pT_{regs} (Figure II-2C and D, Figure II-6 B) and instead promoted their differentiation into T-bet^+ T_H1 cells. Therefore, infection with T1L directly inhibited the establishment of tolerance to fed antigen.

To define the immune cell types required for the development of inflammation to dietary antigen, the Jabri laboratory profiled the DC populations required for the development of oral tolerance. They found that $CD103^+$ $CD11b^-$ DCs from the LP exhibited the highest levels of OVA uptake and upregulated costimulatory molecules during infection with T1L (Figure II-5A), indicating that this normally tolerogenic DC subset (268, 269) is likely activating OVA-specific T_H1 cells.

Relative to infection with T3D-RV, T1L infection was associated with increased levels of inflammatory cytokines including type 1 IFNs (Figure II-8A and II-9A), which also are upregulated in the intestinal mucosa of CD patients (55, 96, 97). Additionally, IFN treatment disrupts oral tolerance in mouse models (99, 100). To determine whether type I IFNs are required for virus-induced tolerance blockade, $IFNAR^{-/-}$ mice were subjected to a T cell conversion assay. Surprisingly, type 1 IFNs were not required for the proliferation of inflammatory anti-OVA T_H1 cells (Figure II-8C). However, IFN activation during poly(I:C) treatment was sufficient to inhibit $Foxp3^+$ T_{reg} conversion, suggesting that type 1 IFN, although not required for the development of inflammatory food-specific T

cells, are required to inhibit tolerogenic processes.

To identify other host factors required for virus-induced inflammation to dietary antigen, mice were infected with T1L and T3D-RV, and tissues were taken for microarray analysis. IRF-1, a transcription factor implicated in multistage regulation of T_H1 immune responses (278), was identified due to its IFN-independent upregulation during T1L infection (Figure II-11A). Using IRF-$1^{-/-}$ mice, we found that IRF-1 is required for the development of OVA-specific inflammatory T_H1 cells, likely because it stimulates IL-12 expression in $CD103^+$ $CD11b^-$ DCs.

After establishing that T1L infection breaks tolerance to OVA, we were curious whether T1L breaks tolerance to gluten, as observed in CD. HLA-DQ8tg mice inoculated perorally with T1L acquire gluten-specific antibodies and a DTH response to the fed antigen, indicating that the mice do not establish tolerance to gluten (Figure II-15 C and D). Tolerance blockade was associated with higher levels of IRF-1 and inflammatory cytokine expression by the $CD103^+$ $CD11b^-$ DCs (Figure II-15 A and B). HLA-DQ8tg mice infected with T1L expressed activated TG2 (Figure II-15E), an enzyme that enhances gluten peptide loading on the MHC of DCs during CD (80-82). Together, these findings suggest that reovirus can trigger inflammation to dietary gluten and establishes a model of virus-induced CD.

To directly investigate the role of reovirus infection in human CD, we analyzed serum from patients and found that persons with CD expressed higher levels of reovirus antibodies compared with controls (Figure II-16 A and B). The

enhanced humoral response was reovirus-specific, as illustrated by the absence of an association between rotavirus and HSV-1 titers and the prevalence of CD (Figure II-16 G and H). IRF-1 expression also was increased in patients with high reovirus antibody titers, suggesting a correlation between recent infection and immune markers that stimulate inflammation to dietary antigen (Figure II-16 C). Taken together, these studies provide evidence that reovirus infection may be linked to the development of CD in humans.

At the conclusion of Chapter II, I had two reovirus strains, which differed by only eight gene segments; T1L induced loss of tolerance, as seen in CD, while T3D-RV did not. The culmination of my thesis project was to understand the viral pathobiological properties that differ between these strains in the context of an intestinal infection and to determine whether these properties associate with tolerance blockade. The most striking difference I observed was the enhanced replication capacity of T1L (Figure III-1) and diminished levels of cleaved caspase-3 staining in the intestine compared with T3D-RV (Figure III-2 A and B).

Since T3D-RV infection induced greater numbers of caspase-3-positive cells in the intestine, I tested whether virus-induced apoptosis could be observed following inoculation of cultured cells and enteroids. Infection of L cells with T1L and T3D-RV led to an overall increase in the morphological features of apoptosis and activation of caspase-3. However, apoptotic efficiency was greater in cells infected with T3D-RV compared with those infected with T1L (Figure III-3, B and C). In mouse enteroids, which contain a diverse population of IECs, T3D-RV also

induced greater numbers of caspase-3-postive cells and cellular sloughing (Figure III-4, E and F). Interestingly, T3D-RV-infected enteroids displayed diminished viral replication compared to T1L, which mimics the replication defect observed in mice.

Since strain-specific differences in apoptosis efficiency in cultured cells tracked with observations made using mice, I decided to screen a panel of T1L x T3D-RV reassortant in cultured cells. Each reassortant virus contained the S1 and L2 genes of T1L but differed in the other eight gene segments (Figure III-5A). Following inoculation of L cells with the eight reassortant viruses, I observed a bimodal distribution in the percentage of apoptotic cells, in which four reassortants displayed levels similar to T3D-RV and four reassortants displayed levels similar to T1L (Figure III-5C). A rank sum analysis determined that the M2 gene most strongly correlated with the capacity to induce apoptosis in cultured cells, with some additional contribution from the M1 gene.

Based on these results, I engineered a panel of M gene reassortant viruses with the M1, M2, or M1 and M2 genes expressed in reciprocal parental backgrounds. As observed previously, the T3D M2 gene, and to a lesser extent the M1 gene, were associated with increased frequency of apoptosis when expressed in a T1L background. To determine whether apoptotic potential affected viral replication in the intestine, mice were infected with T1L, T3D-RV, or each of the six M gene reassortants. Analogous to T3D-RV-infected mice, reassortants that induced greater levels of caspase-3-positive cells at 24 hpi exhibited diminished viral replication in the intestine at 72 hpi (Figure III-6, D and

E). This association suggests that the host triggers cell death in IECs to illicit antiviral responses and protect against enteric infection.

Collectively, findings presented in this thesis enhance insights into the functional viral properties required for loss of tolerance to orally fed antigen and establish links between host responses to infection and tolerance abrogation.

Future Directions

Viral reassortants differ in capacity to induce IRF-1 in WT and IFNAR$^{-/-}$ mice

IRF-1 is a transcription factor that functions in the antiviral immune response. We examined mRNA levels of IRF-1 in WT and IFNAR$^{-/-}$ mice and observed higher expression in T1L-infected mice compared to T3D-RV-infected or PBS-inoculated controls. T1L tolerance abrogation was reversed in IRF-1$^{-/-}$ mice, suggesting that IRF-1 is required for virus-induced tolerance blockade

To identify the viral gene segments that segregate with increased IRF-1 expression, I inoculated WT and IFNAR$^{-/-}$ mice with T1L, T3D-RV, and one of eight T1L x T3D-RV reassortants. Although all eight viruses replicated in the intestines of these mice (Figure IV-1, B and C), differential expression of IRF-1 occurred between the reassortants (Figure IV-1, D and E). Consequently, I chose to study two reciprocal reassortants that showed the greatest difference in IRF-1 expression. When I repeated these experiments, infecting WT and IFNAR$^{-/-}$ mice with only these reassortants, IRF-1 expression was variable. However, Reassortant G, which contains the M1, M2, M3, and L1 genes from T1L, induced IRF-1 expression comparable to T1L, while Reassortant D, which contains the

A

Parent viruses										
T1L	S1	S2	S3	S4	M1	M2	M3	L1	L2	L3
T3D-RV	S1	S2	S3	S4	M1	M2	M3	L1	L2	L3
Reassortant viruses										
A	S1	S2	S3	S4	M1	M2	M3	L1	L2	L3
B	S1	S2	S3	S4	M1	M2	M3	L1	L2	L3
C	S1	S2	S3	S4	M1	M2	M3	L1	L2	L3
D	S1	S2	S3	S4	M1	M2	M3	L1	L2	L3
E	S1	S2	S3	S4	M1	M2	M3	L1	L2	L3
F	S1	S2	S3	S4	M1	M2	M3	L1	L2	L3
G	S1	S2	S3	S4	M1	M2	M3	L1	L2	L3
H	S1	S2	S3	S4	M1	M2	M3	L1	L2	L3

Key: T1L, T3D

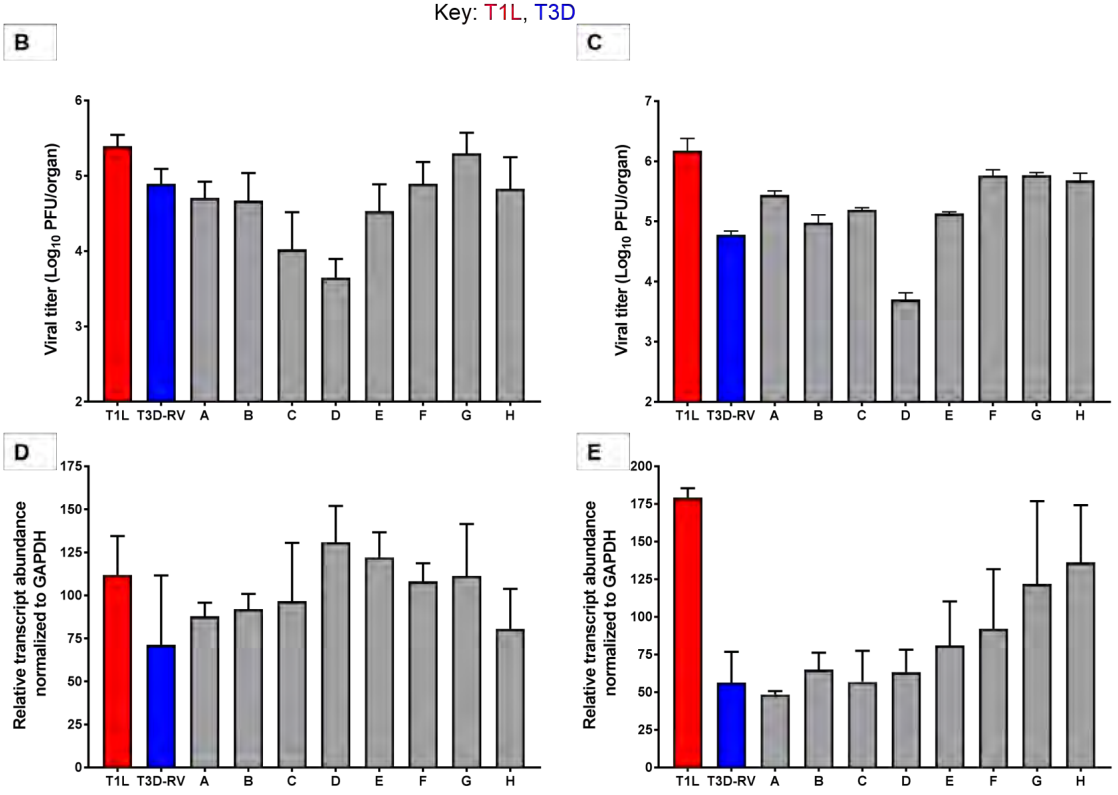

Figure IV-1. Viral replication in the intestine and IRF-1 expression in mesenteric lymph nodes of WT and IFNAR$^{-/-}$ mice infected with reassortant viruses. (A) T1L x T3D-RV reassortant viruses used to define genes that segregate with strain-specific differences in the capacity of reovirus to induce IRF-1 in the MLN. Gene segments in red represent those derived from T1L, while gene segments in blue represent those derived from T3D. (B and D) WT and (C and E) IFNAR$^{-/-}$ mice were inoculated perorally with 10^8 PFU of T1L, T3D-RV, or one of eight T1L x T3D-RV reassortant viruses. At 48 hpi, the proximal half of the intestine was prepared for viral titer and MLN harvested for RNA extraction. (B and C) Viral titers were determined by plaque assay. (D and E) RNA was extracted from the MLN, and mRNA levels were quantified by RT-PCR using primers specific for murine IRF-1. Data represent one experiment.

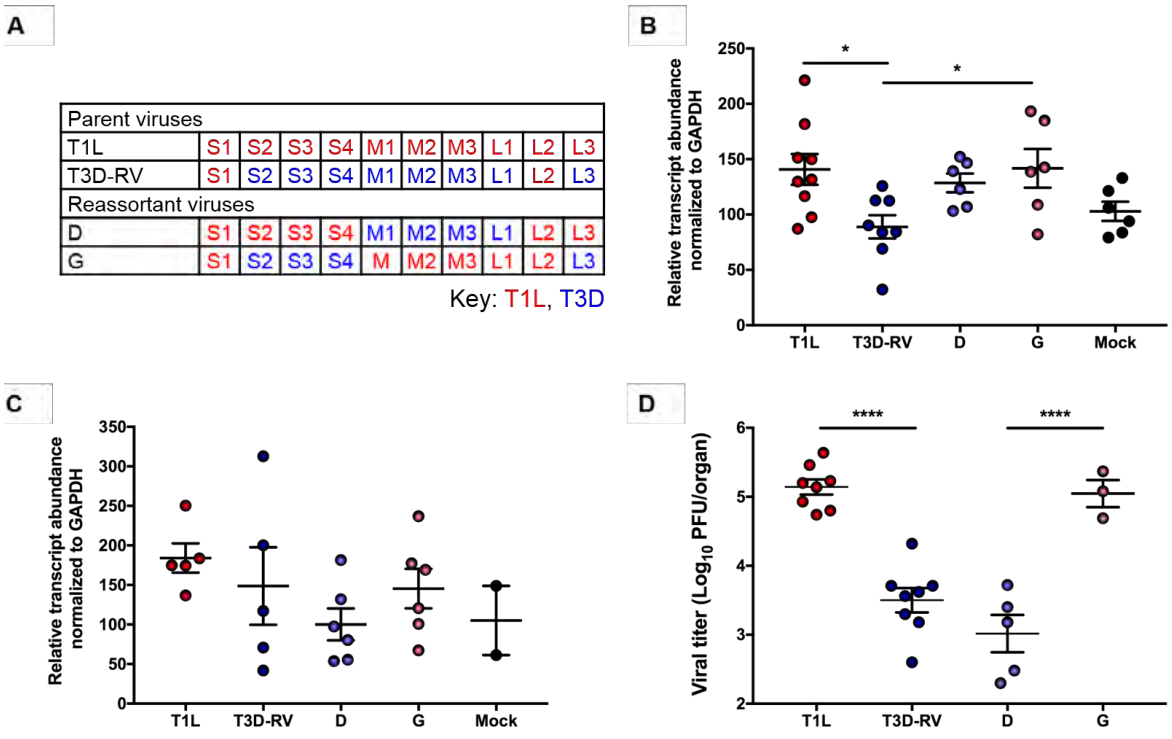

Figure IV-2. Viral replication in the intestine and IRF-1 expression in mesenteric lymph nodes of WT and IFNAR$^{-/-}$ mice infected with Reassortants D and G. (A) T1L x T3D-RV reassortant viruses used to define genes that segregate with strain-specific differences in the capacity of reovirus to induce IRF-1 in the MLN. Gene segments in red represent those derived from T1L, while gene segments in blue represent those derived from T3D. (B and D) WT and (C) IFNAR$^{-/-}$ mice were inoculated perorally with 10^8 PFU of T1L, T3D-RV, Reassortant D, or Reassortant G. (B and C) At 48 hpi, MLNs were harvested for RNA extraction. RNA was extracted from the MLN, and mRNA levels were quantified by RT-PCR using primers specific for murine IRF-1. (D) At 72 hpi, the proximal half of the intestine was prepared for viral titer as determined by plaque assay. *, $P < 0.05$; ****, $P < 0.0001$; one-way ANOVA/Tukey's multiple comparison test.

M1, M2, M3, and L1 genes from T3D, more closely resembled T3D-RV (Figure IV-2, B and C). Future studies including a larger number of mice will determine whether this difference is significant.

Interestingly, Reassortant D and G differed in replication capacity at later times post-inoculation (Figure IV-2D). Analogous to studies using the parental strains, viruses that replicated more efficiently in the intestine produced more IRF-1 expression. Future studies using the M gene reassortants will determine whether viruses that subvert antiviral cell death also upregulate IRF-1 expression. If so, I predict that viruses capable of enhanced replication subsequently induce IRF-1 and alter tolerance to orally-fed antigen, thus providing a mechanistic link between the capacity of a virus to replicate in the intestine and the promotion of inflammatory responses to dietary antigen.

Role of viral gene segments M1 and M2 during reovirus-induced tolerance blockade.

From studies in Chapter III, I concluded that the T1L M1 and M2 genes in a T3D-RV background are sufficient to inhibit caspase-3 activation in IECs and enhance replication in the intestine (Figure III-6, E and D). Although the presence of both genes contributed individually to both phenotypes, the effects of the T1L M1 and M2 genes together were synergistic. T cell conversion assays testing reassortants constructed to exchange the M1 and M2 genes together or the M1 and M2 genes individually in a T3D-RV background will determine whether these genes are sufficient to break oral tolerance. I think it likely that the T1L M1 and

M2 genes, which segregated with decreased apoptosis and prolonged viral titer, also will associate with inflammation to dietary antigen. Such findings would rationalize studies to define the minimum viral gene products required to inhibit oral tolerance during the development of CD.

Caspase inhibition promotes viral replication in the intestine.

Data presented in Chapter III demonstrated an inverse relationship between viral induction of apoptosis in epithelial cells and the capacity to replicate in the intestine. Therefore, I hypothesize that i.p. injections with a caspase inhibitor prior to infection with T3D-RV would promote replication in the intestine. Future studies will test this hypothesis by determination of viral titer at 72 hpi and confirm apoptosis inhibition using immunohistochemical staining of cleaved caspase-3 at 24 hpi.

Based on the culmination of this thesis, I hypothesize that the capacity of T1L to subvert antiviral apoptosis and replicate for prolonged intervals in the intestine are required for the abrogation of tolerance to dietary antigen. Upcoming studies will test this hypothesis by treating mice with caspase inhibitors prior to conducting a T cell conversion assay. If T3D-RV viral replication is prolonged during caspase inhibitor treatment, subsequent stimulation of inflammatory cytokines at the onset of feeding may cause a breakdown in oral tolerance, as observed in T1L-infected mice.

Function of Noxa, a pro-apoptotic host factor, in viral replication of the intestine and abrogation of oral tolerance.

From previous microarray studies, I observed that relative to T1L, T3D-RV stimulates higher expression of Noxa, a transcriptionally regulated proapoptotic gene, in the MLN at 48 hpi. Noxa is a member of the Bcl-2 protein family activated during noxious stress to promote mitochondrial perturbations by inhibiting other Bcl-2 family members (209). T3D upregulates Noxa in cultured cells independent of IFN but dependent on IRF-3 and NF-κB and exacerbates reovirus-induced apoptosis (165).

To test whether T1L and T3D-RV induce Noxa expression in cultured cells, Caco2 cells were adsorbed with each virus strain, incubated for 24 h, and harvested for RNA extraction, followed by RT-qPCR. Although both strains replicate comparably in Caco2 cells (Figure II-1B), T3D-RV-infected cells expressed higher levels of Noxa compared with T1L-infected or mock-inoculated cells (Figure IV-3A). Concordantly, T3D-RV-infected mice also upregulated Noxa expression at 24 hpi in the intestinal mucosa (Figure IV-3B). T1L displayed slightly lower levels of Noxa expression relative to mock-infected mice, although this difference was not statistically significant.

To determine whether Noxa is required for T3D-RV-induced apoptosis in the intestine, Noxa-deficient ($Noxa^{-/-}$) mice should be infected with T1L and T3D-RV and euthanized at 24, 48, and 72 hpi for determination of viral titer and histological analysis. Tissue sections stained for activated caspase-3 will identify cells undergoing apoptosis within the intestine. If Noxa is required for the antiviral

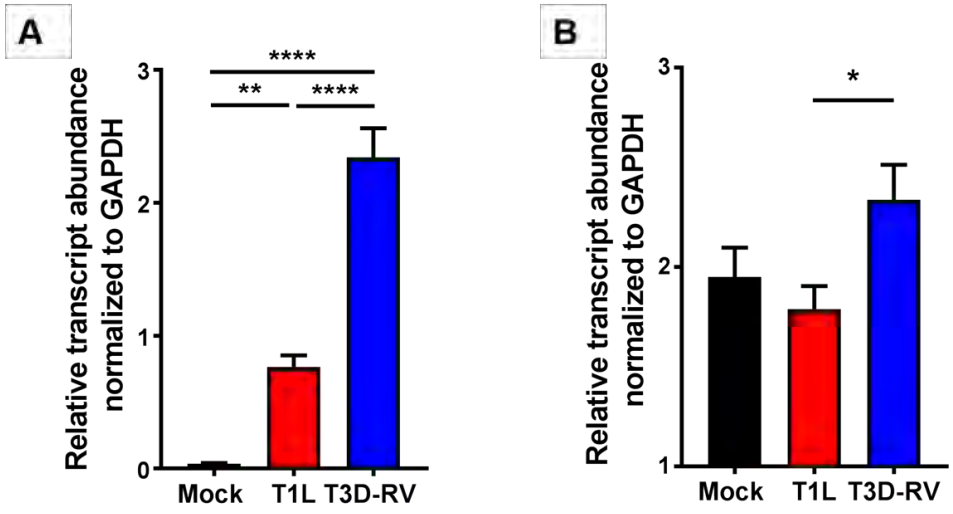

Figure IV-3. Noxa gene expression in Caco-2 cells and intestinal mucosa after reovirus T1L and T3D-RV infection. (A) Caco-2 cells were adsorbed with T1L or T3D-RV at an MOI of 100 PFU/cell. RNA was extracted from infected cultures at 24 hpi, and mRNA levels were quantified by RT-PCR using primers specific for human Noxa. Levels of Noxa mRNAs were normalized to GAPDH mRNA. Data represent two independent experiments performed in triplicate. (B) WT mice were inoculated perorally with 10^8 PFU of T1L or T3D-RV or PBS (mock) (n = 9-10 mice per inoculum). One day after inoculation, intestines were resected. The proximal half was prepared for viral titer determination by plaque assay, and the distal half was flushed and cut longitudinally, and intestinal mucosa was harvested. RNA was extracted from the intestinal mucosa, and mRNA levels were quantified by RT-PCR using primers specific for murine Noxa. *, $P < 0.05$; **, $P < 0.01$; ****, $P < 0.0001$; one-way ANOVA/Tukey's multiple comparison test.

apoptotic response, T3D-RV titers in the Noxa$^{-/-}$ mice will increase. Additionally, cleaved caspase-3 activation in the intestinal villi will be reduced in the absence of Noxa relative to WT mice, and the differences in apoptosis efficiency displayed by T1L and T3D-RV will be diminished. These studies will define Noxa as a host factor required to limit reovirus replication through the activation of apoptosis in IECs and may enhance our understanding of broad intestinal antiviral immunity.

If the removal of Noxa promotes T3D-RV viral replication in the intestine, it would be interesting to determine whether T3D-RV infection of Noxa$^{-/-}$ mice breaks tolerance to dietary antigen. To test this, T cell conversion assays could be conducted using Noxa$^{-/-}$ mice infected with T1L or T3D-RV at the onset of antigen feeding. If Noxa is required for the maintenance of oral tolerance during T3D-RV infection, we should observe an increase in inflammatory OVA-specific T cells and an inhibition of T_{regs} in Noxa$^{-/-}$ mice infected with T3D-RV. However, if Noxa is not required for viral replication or apoptosis in the intestine, other pro-apoptotic host factors could be examined using knockout mouse lines.

Conclusions

Acute viral infections are thought to be cleared by the host with few lasting consequences. However, there may be a much broader and long-lasting effect of viruses on immune homeostasis. My thesis work now provides mechanistic evidence that acute viral infections influence immune regulation and lead to development of chronic autoimmunity and inflammatory disease. I found that infection with reovirus, a common, nonpathogenic virus, triggers inflammation against innocuous food antigens, implicating this virus in the development of CD. For persons with CD, this work provides the basis for prevention strategies based on reovirus vaccination and screening approaches focused on acquisition of viral infections. This work contributes new knowledge about virus-host interactions and opens new fields to determine how viruses induce immunopathology.

CHAPTER V

MATERIALS AND METHODS

Cells and viruses

Spinner-adapted murine L cells were grown in either suspension or monolayer cultures in Joklik's modified Eagle's minimal essential medium (SMEM; Lonza) supplemented to contain 5% fetal bovine serum (FBS; Gibco), 2 mM L-glutamine, 100 U/ml penicillin, 100 µg/ml streptomycin (Gibco), and 25 ng/ml amphotericin B (Sigma). BHK-T7 cells were grown in Dulbecco's modified Eagle's minimal essential medium (DMEM; Gibco) supplemented to contain 5% FBS, 2 mM L-glutamine, 1 mg/ml geneticin (Gibco), and nonessential amino acids (Sigma). Caco-2 cells were grown in DMEM supplemented to contain 10% FBS, 100 U/ml penicillin, 100 µg/ml streptomycin, 1 mM sodium pyruvate (Gibco), nonessential amino acids, and 12.5 ng/ml amphotericin B. Caco-2 cells were plated at a density of 10^5 cells/well in 24-well plates (Costar). Rhesus monkey kidney (MA104) cells were provided by Dr. John Patton and grown in DMEM supplemented to contain 5% FBS, 2 mM L-glutamine, nonessential amino acids, and 1 mg/ml geneticin as previously described (302). Mouse embryonic fibroblasts (MEFs) from C57BL/6 mice were grown in DMEM supplemented to contain 10% FBS, 2 mM L-glutamine, 100 U/ml penicillin, 100 µg/ml streptomycin, and nonessential amino acids.

Recombinant reoviruses were generated using plasmid-based reverse

genetics (143). Recombinant strain (rs) type 1 Lang (T1L) is a stock generated by plasmid-based rescue from T1L cDNAs (144). The engineered reassortant virus strain, T3D-RV, was recovered following transfection of BHK-T7 cells with plasmid constructs encoding the S1 and L2 gene segments from strain T1L and the remaining eight gene segments from strain type 3 Dearing (T3D). T1L x T3D-RV reassortant viruses were generated using T1L or T3D cDNAs in the constellation shown. After 3 to 5 d of incubation, cells were frozen and thawed three times, and virus was isolated by plaque purification using monolayers of L cells (303). Purified reovirus virions were generated from second- or third-passage L cell lysate stocks (304). Viral particles were extracted from infected cell lysates using Vertrel XF (DuPont), layered onto 1.2- to 1.4- g/cm^3 CsCl gradients, and centrifuged at 62,000 × *g* for 16 h. Bands corresponding to virions (1.36 g/cm^3) were collected and dialyzed in virion storage buffer (150 mM NaCl, 15 mM $MgCl_2$, and 10 mM Tris-HCl [pH 7.4]) (305). Viral titer was determined by plaque assay using L cells (303). Purified viral particles were electrophoresed on SDS-polyacrylamide gel. The gel was stained with ethidium bromide to visualize viral gene segments.

Mice

All knockout and transgenic mice used in these studies are on a C57BL/6 background. C57BL/6 (WT), IFNAR$^{-/-}$ (B6.129S2-*Ifnar1tm1Agt*/Mmjax), and IRF-1$^{-/-}$ (B6.129S2-*IRF-1tm1Mak*/J) were purchased from Jackson Laboratories. RAG$^{-/-}$ OT-II$^{+/-}$ CD45.1$^{+/+}$ mice were provided by Dr. Peter Savage. HLA-DQ8

transgenic (HLA-DQ8tg) mice (98) were maintained on a GFD (AIN76A, Envigo) at the University of Chicago. $TG2^{-/-}$ mice were previously described (306). For all experiments, mice were analyzed at 6-8 weeks of age. WT and $IFNAR^{-/-}$ mice were maintained in an SPF environment at the University of Chicago, the University of Pittsburgh, and Vanderbilt University. $IRF\text{-}1^{-/-}$, $RAG^{-/-}$ $OT\text{-}II^{+/-}$ $CD45.1^{+/+}$, HLA-DQ8tg, and $TG2^{-/-}$ mice were housed exclusively at the University of Chicago. $Noxa^{-/-}$ mice were housed exclusively at the University of Pittsburgh. Animal husbandry and experimental procedures were performed in accordance with Public Health Service policy and approved by the University of Chicago, the University of Pittsburgh, and Vanderbilt University School of Medicine Institutional Animal Care and Use Committees.

Infection of mice

Mice were inoculated perorally with 10^{10} and 10^{8} plaque forming unit (PFU)/mouse of purified reovirus diluted in PBS using a 22-gauge round-tipped needle (Cadence Science) (146). Titers of virus in the inocula were determined to confirm the number of infectious particles in the administered dose. For analysis of viral titer, mice were euthanized at various intervals post-inoculation, organs were harvested into 1 ml of PBS and stored at -20 °C prior to assay. Samples were thawed (37 °C), bead beaten for 8 minutes, frozen (-20 °C), and bead beaten again for 5 minutes prior to quantitation by plaque assay. Viral titers in organ homogenates were determined as the number of PFU per ml of tissue homogenate (303).

Antibodies and flow cytometry

The following fluorophore conjugated antibodies were purchased from eBioscience: T-bet (4B10), Foxp3 (FJK-16s), MHCII (M5/114.15.2), CD11b (M1/70), IL-12p40 (C17.8), CD62L (MEL-14), CD25 (PC61.5), Rat IgG1, Rat IgG2a, Rat IgG2b and Mouse IgG1. The following antibodies were purchased from BD Biosciences: IFNγ (XMG1.2), CD103 (M290), CD45 (30-F11), and Fc BlockTM (2.4G2). The following antibodies were purchased from Biolegend: CD4 (GK1.5), TCRb (H57-597), CD45.1 (A20), CD11c (N418), CD8a (53-6.7), CD86 (GL-1), CD44 (IM7), and F4/80 (BM8). Aqua LIVE/DEAD® Fixable Aqua Dead Cell Stain Kit was purchased from Life Technologies. Cells were permeabilized with the Foxp3 fixation/permeabilization kit for transcription factor (eBioscience) or Cytofix/Cytoperm (BD Biosciences) for cytokine staining. Flow cytometry was performed with a 9-color BD FACSCanto (BD Biosciences) and data were analyzed using FlowJo software (Treestar). Sorting experiments were performed with an Aria Fusion (BD Biosciences). Immunoglobulin G (IgG) fractions of rabbit antisera raised against reovirus strains (T1L) and (T3D) (307) were purified by protein A sepharose chromatography (308). Rabbit anti-cleaved caspase-3 monoclonal antibody was purchased from Cell Signaling Technologies. Anti-β-catenin antibody was purchased from BD biosciences.

Assays of reovirus replication and gene/protein expression in cell culture

L cells (2×10^5) grown in 24-well plates (Costar) were adsorbed with reovirus at a multiplicity of infection (MOI) of 1 PFU/cell, washed with PBS, and

incubated at 37 ºC for various intervals. Caco-2 cells (1×10^5) were adsorbed with reovirus at an MOI of 0.1, 1, or 10 PFU/cell, washed with PBS, and incubated at 37 ºC for various intervals. Cells were frozen and thawed twice prior to determination of viral titer by plaque assay using L cells (303). Viral titers were expressed as PFU per mL of cellular homogenate. Caco-2 cells (1×10^5) were adsorbed with reovirus at an MOI of 100 PFU/cell, washed with PBS, and incubated at 37 ºC for 24 h, at which time cells were lysed for RNA extraction. MEFs were adsorbed with reovirus at a MOI of 500 PFU/cell, washed with PBS, and incubated at 37 ºC for 16 h. Supernatants were analyzed for IFNβ by ELISA (PBL Interferon Source).

Histology and immunohistochemistry

Mice were inoculated perorally with purified reovirus diluted in PBS. At 1 dpi, mice were euthanized, and intestines were resected. The proximal half was prepared for viral titer determination by plaque assay, and the distal half was flushed with 10% formalin and Swiss-rolled. Samples were submerged in 10% formalin at room temperature for 24 or 48 h and embedded in paraffin. Consecutive 6-μm sections were stained with H&E for evaluation of histopathologic changes or processed for immunohistochemical detection of reovirus antigen and cleaved (active) caspase-3. Images were captured at 20x magnification at a resolution of 0.5 μm/pixel using a high-throughput Leica SCN400 slide scanner automated digital imaging system.

Quantification of histology

For caspase-3-positive staining area, tissue regions were differentiated from the glass slide using Ariol Review software. Upper and lower thresholds for color, saturation, and intensity were set for both blue, hematoxylin staining of nuclei and for brown, 3'diaminobenzidine (DAB) reaction products. Thus, brown positive areas were distinguished from blue-only negative areas. The area of positive staining per whole tissue region was calculated as a percent area of brown (DAB-positive) pixels divided by the total area analyzed.

Cleaved caspase-3-stained epithelial cells were quantified by an observer blinded to the conditions of the experiment by enumerating all positive cells (brown) throughout the distal half of the small intestine and normalizing to the number of villi counted. Only epithelial cells and villi from properly oriented villus structures were included in the analysis. Proper orientation was defined in villi containing a clear exterior epithelial cell column, a crypt to villus ratio of 2:1, and an unfragmented LP. Intestinal sections with fewer than 70 properly oriented villi were excluded.

Isolation of Peyer's patches, intestinal epithelium, and lamina propria

PPs were removed, treated with collagenase VIII (Sigma) and processed by mechanical disruption through a 70-μm cell strainer. The intestinal epithelium was isolated as previously described using RPMI media containing 2 mM EDTA (Corning), 1% dialyzed FBS, and 1.5 mM MgCl2. The LP was isolated as previously described using RPMI media containing 20% FBS and collagenase

VIII (Sigma) (98).

Quantification of apoptosis by acridine orange staining

L cells (2×10^5) in 24-well plates were adsorbed with reovirus at an MOI of 100 PFU/cell, washed with PBS, and incubated at 37°C for 38 h. The percentage of apoptotic cells was determined using AO staining (225). Images were collected from three fields of view per well by epi-illumination fluorescence microscopy using a Lionheart FX Automated Microscope (Biotek). The percentage of apoptotic cells exhibiting orange nuclei with condensed and fragmented chromatin versus live cells exhibiting structurally normal green nuclei was quantified using an imaging algorithm developed in the Gen5 software (Biotek). The average nucleus size and a fluorescence threshold were established by the user. Color values from each individual-pixel RGB triplet were obtained and compared to the user-defined threshold. To exclude false-positive signals, an exclusion criterion was established based on the average pixels of false-positive cells and included in the imaging algorithm. Therefore, green nuclei with condensed chromatin (early apoptotic) and red, structurally normal nuclei were subtracted from the final count.

Detection of caspase-3/7 activity

L cells (5×10^4) in black, clear-bottom 96-well plates (Costar) were adsorbed with reovirus at an MOI of 100 PFU/cell at room temperature for 1 h.

Following incubation of cells at 37°C for 24 h, caspase-3/7 activity was quantified using the Caspase-Glo 3/7 assay (Promega).

Establishing small intestinal enteroids

Crypt enteroid cultures were established as described (309). Eight centimeters of the proximal small intestine was dissected, flushed with PBS, and minced. Following a PBS wash, tissue was transferred to 5 mL chelation buffer (2 mM EDTA in PBS) and incubated at 4 °C for 30 min. After removal of chelation buffer, tissue fragments were resuspended in 5 mL of shaking buffer (PBS with 43.3 mM sucrose and 54.9 mM sorbitol) and agitated gently for 2 min to release intestinal crypts. Crypt-containing supernatants were filtered through a 100-μM filter, enumerated, and transferred into round-bottomed polystyrene tubes. Following centrifugation, crypts were resuspended in growth-factor-reduced Matrigel (BD Bioscience) at a concentration of 300 crypts per 50 μL of Matrigel. Following polymerization, the crypt/Matrigel mixture was overlayed with 500 μL of mini-gut culture medium (Advanced Dulbecco's modified Eagle's medium/F12 (Invitrogen) supplemented to contain 1x glutaMAX (Thermo-Fisher), 100 U/mL penicillin (Invitrogen), 100 μg/mL streptomycin (Invitrogen), 1 mM HEPES (Gibco), N2 Supplement (R&D Systems), B27 Supplement (Invitrogen), 50 ng/mL EGF (R&D Systems), 500 ng/mL R-spondin (Vanderbilt Antibody and Protein Resource), 100 ng/mL Noggin (R&D Systems), and 50% Wnt3a conditioned media). The medium was replaced every 2-4 days. Enteroids were passaged as needed by collection and shearing through a 25-gauge needle prior to plating in

Matrigel.

Enteroid transwell plating

Enteroids were collected 2 d after passage and incubated with TrypLE (Thermo Fisher Scientific) solution at 37 °C for 90 min to dissociate cells into single-cell suspensions. Cells (2×10^5) were plated onto the top of a 24-well, 0.4 μm pore transwell filter coated with collagen 1 (Gibco) in medium supplemented to contain 10 μM Y27632 (Sigma). After 24 h, medium on the top and bottom of the transwell filters was replaced with differentiation medium (Advanced DMEM/F12 supplemented to contain 1x Glutamax, 100 U/mL penicillin, 100 μg/mL streptomycin, and 20% FBS).

Assays for reovirus replication, infectivity, and cell death in enteroids

On day 4 post-transwell plating, enteroids were adsorbed with virus at a MOI of 100 PFU/cell, assuming 2.5×10^5 cells/well, by adding 30 μl of virus inoculum to the apical compartment. After adsorption of virus at room temperature for 1 h, cells were washed twice with PBS, 200 μl of medium was added to the apical compartment, and 1 mL of medium was added to the basolateral compartment. Enteroids were incubated at 37 °C for 24 h. For quantification of released cells, 100 μL of apical medium was collected, and cells in the medium were enumerated using a Scepter Handheld Automated Cell Counter. For viral replication assays, transwell membrane inserts were removed from transwells with a scalpel, submerged in 500 μL of medium, and frozen and

thawed twice. Viral titers in cell lysates were determined by plaque assay using L cells (303). For enteroid staining, transwell inserts were gently washed with PBS and fixed at room temperature for 30 min in 3% paraformaldehyde before continuing with the transwell staining protocol.

Transwell insert staining and quantification

After washing and fixing, cells were permeabilized with 0.2% Triton-X (Sigma) followed by blocking in 3% milk solution. The following primary antibodies were used: reovirus polyclonal antiserum (307) at 1:1000, anti-β-catenin (BD Biosciences) at 1:500, and anti-cleaved caspase-3 (Cell Signaling Technology) at 1:400. Appropriate species-specific Alexa Fluor secondary antibodies (Thermo Fisher Scientific) were used at a dilution of 1:1000. Enteroids were stained with ActinGreen ReadyProbe (Thermo Fisher Scientific). Following antibody incubation, inserts were excised from the transwell and mounted on glass slides with 4',6-diamidino-2-phenylindole (DAPI)-containing ProLong Gold mounting medium (Thermo Fisher Scientific). Images were collected using a Nikon Eclipse E800 Microscope, and cleaved caspase-3 positive cells were enumerated using the Nikon Elements Basic Research software. For viral infectivity, the percentage of reovirus antigen-positive cells was determined. No background staining of uninfected control cells was detected.

In-vivo T cell conversion assay

To assess T cell conversion *in-vivo*, $CD4^+$ T cells were purified from the

spleen and lymph nodes of RAG$^{-/-}$ OT-II$^{+/-}$ CD45.1$^{+/+}$ mice using the CD4^{+} T cell isolation Kit (Miltenyi) or sorted on a FACS Aria Fusion (BD Biosciences). CD4^{+} T cells (4×10^5 to 7.5×10^5 cells) were transferred retro-orbitally into congenic naïve WT mice. Mice received OVA (grade V, Sigma) dissolved in the drinking water (1.5%) for 2 or 6 d, as indicated or were fed an OVA-containing diet (Harlan Envigo TD 130362 10 mg/kg) for 6 d. One day after transfer, mice were infected perorally with equal PFU of T1L or T3D-RV as indicated or injected intraperitoneally every other day with 50 ug of poly(I:C) (Invivogen) or 1000 IU of mIFNβ (PBL Interferon Source). Mice were euthanized and intranuclear levels of Foxp3, T-bet, or cytokine IFNγ were evaluated by flow cytometry in transferred CD45.1^{+} and recipient T cells from MLN incubated in the presence of 50 ng/ml phorbol 12-myristate 13-acetate (PMA), 500 ng/ml ionomycin (Sigma) and 1.3 µl/ml Golgi Stop (BD Biosciences) for 2 h at 37 ºC, 5% CO2. For IL-12 staining, cells were incubated in RPMI (Corning) for 6 h at 37 ºC, 5% CO2 in the presence of 1 µl/ml Golgi Plug (BD Biosciences)

In-vitro T cell conversion assays

MLN DC subsets (CD103^{+} CD11b^{-} CD8α^{+}, CD103^{+} CD11b^{-} CD8α^{-}, CD103^{+} CD11b^{+}, CD103^{-} CD11b^{+}) were FACS sorted (Aria Fusion BD Biosciences) 2 d after inoculation of WT or IRF-1$^{-/-}$ mice with T1L or PBS (sham). DC subsets were then mixed back at a WT ratio and 5×10^3 DC/mix were co-cultured for 5 d with 2.5×10^4 FACS sorted naïve CD4^{+} T cells (Aria Fusion BD Biosciences) from the spleen and lymph nodes of RAG$^{-/-}$ OT-II$^{+/-}$ CD45.1$^{+/+}$ mice

in presence of 100 µg/ml of OVA (Sigma) with or without 1 µg/ml of anti-mouse IL-12p40 neutralizing antibody (BD Pharmingen).

Analysis of cytokine production

IFNγ and IL-12p40 cytokine levels in culture supernatants were determined with BioPlex multianalyte technology (Biorad).

Oral tolerance assay

Mice were inoculated perorally with purified reovirus diluted in PBS or with PBS alone. 100 µg OVA (grade V, Sigma) feeding occurred every other day for 8 d. At day 10 mice were immunized with CFA-OVA (emulsion of 50 µl CFA (Sigma) and 50 µl PBS containing 100 µg OVA) subcutaneously at the back left and right flank. Draining lymph nodes (dLN) were harvested on day 18 and cells were restimulated for 48 h with OVA. Supernatants were analyzed for IFNγ by ELISA (BD Biosciences). Alternatively, when indicated, mice were fed an OVA-containing diet (10 mg/kcal, Envigo) for 8 d. At day 10, mice were immunized subcutaneously between the shoulder blades with an emulsion of 100 µl CFA and 100 µl PBS containing 300 µg OVA under isofluorane gas anesthesia. At day 18, mouse sera were obtained by submandibular bleeding for anti-OVA IgG2c ELISA quantification.

Preparation of chymotrypsin-digested gliadin

Gliadin (Sigma) was dissolved in 2 M NH4HCO3 2 M urea buffer pH 8.0, by vortexing and digested using a-chymotrypsin (Sigma) for 24 h on a roller mixer at room temperature. The reaction was stopped by incubation at 98 ºC for 10 minutes. Digested gliadin was filtered through a 0.45 µm membrane (Millipore) and dialyzed against sterile PBS using snakeskin dialysis tubing with a molecular weight cut-off of 3.5 kDa (Thermo Scientific). Concentration of chymotrypsin-digested gliadin (CT-gliadin) was determined using a BCA assay (Pierce).

Oral antigen uptake by dendritic cells

OVA or CT-gliadin was labeled with Alexa Fluor-647 succinimidyl ester according to the manufacturer's protocol (Molecular Probes). Mice received 3.2 mg OVA-Alexa Fluor-647 or Gliadin-Alexa Fluor-647 by intragastric administration, respectively. Control mice received similar amounts of unlabeled OVA or CT-gliadin (310). Mice were euthanized 18 h post-feeding and DCs in MLN were analyzed by flow cytometry.

Complete Freund's adjuvant immunization and subcutaneous ear challenge

HLA-DQ8tg mice received 50 mg CT-gliadin orally for 2 d. At the start of feeding mice were inoculated perorally with purified T1L. Two days after CT-gliadin administration, CFA-CT-gliadin was administered subcutaneously between the shoulder blades as an emulsion of 100 µl CFA and 100 µl PBS

containing 300 µg CT-gliadin under isofluorane gas anesthesia. Ear challenges were performed 14 and 24 d after immunization. A volume of 20 µl of 100 µg CT-gliadin/PBS was injected under isofluorane gas anesthesia. Ear thickness was measured on days 1, 2, and 3 after each CT-gliadin challenge using a digital precision caliper (Fisher Scientific). Swelling was determined by subtracting pre-challenge from post-challenge ear thickness.

Anti-ovalbumin and anti-gliadin IgG2c ELISA

High-binding ELISA 96-well plates (Corning) were coated with 50 µl of 10 µg/ml OVA in PBS or 50 µl of 100 µg/ml CT-gliadin in 100 mM Na2HPO4 overnight at 4 °C. Plates were washed three times with PBS 0.05% Tween 20 and blocked with 200 µl of PBS 10% FBS (Anti-OVA ELISA) or 200 µl of 2% BSA in PBS 0.05% Tween 20 (Anti-gliadin ELISA) for 2 h at room temperature. Unlabeled IgG2c (Southern Biotech) was used as positive control. Serum was assessed in duplicate and at two dilutions, typically 1/1000 and 1/5000. Sera were incubated overnight at 4 °C and plates were washed three times with PBS 0.05% Tween 20. Anti-mouse IgG2c-horseradish peroxidase (HRP) (Southern Biotech) in blocking buffer (50 µl at 1/500 dilution) was added to plates and incubated for 1 hour at room temperature. Plates were washed five times with PBS containing 0.05% Tween 20. HRP substrate TMB (50 µl) was added and the reaction stopped by the addition of 50 µl 2 N H2SO4. Absorbance was read at 450 nm. Levels of anti-OVA IgG2c or anti-gliadin IgG2c were expressed in OD values.

Visualization and quantification of transglutaminase 2 activity

HLA-DQ8tg or TG2$^{-/-}$ mice were inoculated perorally with purified T1L reovirus diluted in PBS or with PBS alone and *in-vivo* TG2 enzymatic activity was assessed 18 hpi, essentially as previously described (311). Six and three h prior to euthanasia, mice were injected i.p. (100 mg/kg) with 5-(biotinamido)-pentylamine (5BP), a substrate for TG2 transamidation activity, which was synthesized following a published protocol (311). Small intestinal pieces were collected and frozen in optimum cutting temperature compound (Tissue-Tek). Frozen sections of 5 μm thickness were cut, fixed in 1% paraformaldehyde, and TG2 protein was visualized by staining with a rabbit polyclonal anti-TG2 antibody (custom produced by Pacific Immunology), followed by AF647-conjugated goat anti-rabbit IgG (Life Technologies). TG2 enzymatic activity was measured using 5BP crosslinking, and was visualized by costaining with AF555-conjugated streptavidin (Life Technologies). Images were acquired at 10x magnification using a Leica SP8 Laser Scanning Confocal microscope. TG2 activity was quantified by systematically taking two sections of proximal small intestine from each mouse, quantifying the 5BP signal/TG2 protein signal on a per villi basis. The mean 5BP signal/TG2 signal is shown for each mouse that was assessed.

Human tissue and serum samples

Serum and duodenal biopsies were collected from consented controls or patients with CD. Diagnosis of CD was based on detection of anti-TG2 antibodies, villous atrophy, and clinical response to GFD. Gluten-free subjects

had been under strict GFD for at least 1 year and had become negative for anti-TG2 antibodies and recovered a normal or subnormal villous architecture (10). Control subjects with normal small intestinal histology, no family history of CD and no TG2 antibodies, underwent gastrointestinal endoscopy for a diagnostic work-up (e.g., for evaluation of anemia, abdominal discomfort, intestinal disorders of non-celiac origin, or failure to thrive).

Control patients: Age range 1-77 (average 24.06); 56.94% females, 43.06% males.
Active patients: Age range 2-69 (average 26.21); 66.21% females, 33.79% males.
GFD patients: Age range 2-79 (average 35.13); 70.5% females, 29.5% males.
These studies were approved by the University of Chicago Institutional Review Board.

Quantification of virus-specific antibody responses

Reovirus-specific antibody responses were determined using a 60% plaque-reduction neutralization assay (PRNT 60). Serum samples were heat-inactivated at 56 ºC for 30 minutes, serially diluted four-fold beginning with a dilution of 1:20, and incubated with an equal volume of a virus stock containing 100 PFU of T1L for 1 h. The serum-virus mixtures were inoculated in duplicate onto confluent L cell monolayers in 12-well tissue culture plates (Costar), incubated at room temperature for 1 h, and overlayed with a 1:1 mixture of 1% agar (BD Biosciences) and 2x199 medium (Caisson labs) supplemented to contain 5% FBS, 4 mM L-glutamine, 200 U/ml penicillin, 200 µg/ml streptomycin (Gibco), and 50 ng/ml amphotericin B (Sigma). Cells were stained with neutral red on day 7, and plaques were enumerated (303). Serum reciprocal geometric

mean titers capable of reducing plaque counts by 60% were calculated using regression analysis.

Rotavirus-specific antibody responses were determined using PRNT 60 assay with simian rotavirus strain SA11 and MA104 cells both provided by Dr. John Patton. Serum samples were heat-inactivated at 56 ºC for 30 minutes, serially diluted four-fold beginning with a dilution of 1:20, and incubated with an equal volume of a previously trypsin-activated rotavirus stock containing 100 PFU. After incubation for 1 h, the serum-virus mixtures were inoculated in duplicate onto confluent MA104 cell monolayers in 12-well tissue-culture plates. On day 3, cells were fixed with neutral-buffered formalin at room temperature for 1 h, stained with crystal violet, and plaques were enumerated (302). Serum reciprocal geometric mean titers capable of reducing plaque counts by 60% were calculated using regression analysis.

Qualitative detection of HSV-1 IgG antibodies were determined in serum samples using the Zeus Scientific ELISA HSV-1 IgG Test System (Alere) according to manufacturers' instructions. These studies were approved by the Vanderbilt University School of Medicine Institutional Review Board.

RT-PCR

RNA was prepared using the RNeasy Mini Kit (Qiagen) or High Pure RNA isolation kit (Roche). cDNA synthesis was performed using GoScript (Promega) or Superscript III First-Strand Synthesis System (Invitrogen) according to the manufacturer's instructions. Expression analysis was performed in duplicate via

real-time PCR on a Roche LightCycler 480 using SYBR Green (Clontech) or an Applied Biosystems 7500 Real-Time PCR system (Life Technologies) with a Power SYBR Green Master Mix (Thermo Fisher Scientific). Expression levels were quantified and normalized to *Gapdh* expression using the following primer pairs:

Species	Gene	Forward Primer	Reverse Primer
Murine	*Gapdh*	AGGTCGGTGTGAACGGATTTG	TGTAGACCATGTAGTTGAGGTCA
Murine	*IRF-1*	CAGAGGAAAGAGAGAAAGTCC	CACACGGTGACAGTGCTGG
Murine	*Isg15*	GGTGTCCGTGACTAACTCCAT	TGGAAAGGGTAAGACCGTCCT
Murine	*Mx1*	GACCATAGGGGTCTTGACCAA	AGACTTGCTCTTTCTGAAAAGCC
Murine	*Gapdh*	AGGTCGGTGTGAACGGATTTG	TGTAGACCATGTAGTTGAGGTCA
Murine	*Noxa*	CCCAGATTGGGGACCTTAG	CTGCGAACTCAGGTGGTAGC
Human	*GAPDH*	ATGGGGAAGGTGAAGGTCG	GGGGTCATTGATGGCAACAATA
Human	*NOXA*	GAGATGCCTGGGAAGAAGG	TTCTGCCGGAAGTTCAGTTT

Transcriptomics (microarray and RNA-sequencing analysis)

Gene expression was profiled using Illumina Mouse Expression BeadChip WG-6 according to manufacturer's instructions. Array data was background corrected using BeadStudio and quantile normalized. A linear model was applied and implemented in the R programming language, utilizing functions from linear models for microarray data. For each probe, a moderated t-statistic (with standard errors moderated across genes) was computed using a Bayesian model to assess differential expression (312). The associated p-values were adjusted to control the false discovery rate in multiple testing, using the

Benjamini and Hochberg's (BH) method (BH-adjusted $p<0.05$) (313). Multiple dimensional scaling (MDS) was applied to visualize profiles assembled from genes that were identified as differentially expressed in each state across the tissue types examined. MDS facilitates the representation of distances between pairs of samples in lower dimensional space and samples are assigned 'coordinates' in each dimension. By applying Prim's algorithm implemented as priority-first search for graphs (314), a minimum spanning tree (for dissimilarities) that connected all vertices or nodes (denoting the profile vector for each sample) was found by minimizing the total weighting for its edges.

For RNA-seq, RNA libraries were prepared using the TruSeq® Stranded Total RNA with Ribo-ZeroTM Gold kit (Illumina) and sequenced using 50-base pair single-end reading on a HiSeq 2500 instrument (Illumina). Reads were mapped to the mouse genome (mm10) using Tophat2 (315). To improve mapping, a GTF-file containing exon boundaries of all known RefSeq genes was supplied to Tophat. Quality control was performed using the RSEM-based quantification approach (316). HTSeq was used to count features from the alignment files. The count data was normalized by the trimmed mean of M-values normalization method, followed by variance estimation and applying generalized linear models in the R language, implementing empirical analysis of digital gene expression (317) to identify differentially expressed genes. Factorial designs were incorporated into the analysis by fitting these linear models with the coefficient for each of the factor combinations and then simultaneously extracting contrasts (317) for the respective 'differential-of-differential' analysis in the two

experimental dimensions (virus infection and genotype status: WT and IFNAR$^{-/-}$).

Enrichment analysis of pathway / biological processes and semantic similarity clustering

Pathway and biological process enrichment analysis were performed as previously described (318-320). Briefly, data were interrogated from KEGG pathways and gene ontology biological processes. Each module or category was assessed for statistical enrichment or over-representation among differentially expressed genes relative to their representation in the global set of genes in the genome. Nominal p- and Benjamini-Hochberg-adjusted p-values were computed using the hypergeometric test implemented in the R programming language. Following enrichment analysis, pathways and biological processes derived from gene ontology and identified as over-represented were further subjected to gene semantic similarity analysis to establish similarity or 'relatedness' between pathway/process categories, by applying node-based measures of information content (IC), i.e. how informative or specific each pathway/process category, *c* is. IC is defined as the negative log likelihood for the occurrence of *c* in the pathway/process knowledgebase or in the most informative common ancestor in the ontology hierarchy, *cMICA* (321). We utilized the relevance similarity measure (322), *simRel* :

$$simRel(c_1, c_2) = \frac{2IC(c_{MICA})}{IC(c_1) + IC(c_2)} \times (1 - p(c_A))$$

A semantic similarity map was generated by performing hierarchical clustering using the Minkowski distance metric on the resulting symmetric matrix

of *simRel* values for each pairwise comparison between pathway/process categories.

Statistical Analysis

Experiments were performed in triplicate and repeated at least twice. Representative results of single experiments are shown. Mean values were compared using the unpaired two-tailed Student's *t*-test, Mann-Whitney test, Wilcoxon rank sum distribution test, or one-way analysis of variance (ANOVA) for multiple comparisons. ANOVA analyses were followed by a Dunnett's post-hoc test for multiple comparisons to a control group, a Sidak's post-hoc test for multiple comparisons between sets of data, or a Tukey's post-hoc test for multiple comparisons between all groups. A Grubb's test was used for exclusion of outliers. Error bars denote the standard error of the mean. The statistical test used and *P* values are indicated in each figure legend. P values of < 0.05 were considered to be statistically significant. *$P < 0.05$, **$P < 0.01$, ***$P < 0.001$ and ****$P < 0.0001$. ns = non significant.

REFERENCES

1. Fasano A, Berti I, Gerarduzzi T, Not T, Colletti RB, Drago S, Elitsur Y, Green PH, Guandalini S, Hill ID, Pietzak M, Ventura A, Thorpe M, Kryszak D, Fornaroli F, Wasserman SS, Murray JA, Horvath K. 2003. Prevalence of celiac disease in at-risk and not-at-risk groups in the United States: a large multicenter study. Arch Intern Med 163:286-292.

2. Green PH, Jabri B. 2003. Coeliac disease. Lancet 362:383-391.

3. Abadie V, Sollid LM, Barreiro LB, Jabri B. 2011. Integration of genetic and immunological insights into a model of celiac disease pathogenesis. Annu Rev Immunol 29:493-525.

4. Dicke WK, Weijers HA, Van De Kamer JH. 1953. Coeliac disease. II. The presence in wheat of a factor having a deleterious effect in cases of coeliac disease. Acta paediatrica 42:34-42.

5. Tack GJ, Verbeek WH, Schreurs MW, Mulder CJ. 2010. The spectrum of celiac disease: epidemiology, clinical aspects and treatment. Nature reviews. Gastroenterology & hepatology 7:204-213.

6. Lohi S, Mustalahti K, Kaukinen K, Laurila K, Collin P, Rissanen H, Lohi O, Bravi E, Gasparin M, Reunanen A, Maki M. 2007. Increasing prevalence of coeliac disease over time. Alimentary pharmacology & therapeutics 26:1217-1225.

7. Ludvigsson JF, Rubio-Tapia A, van Dyke CT, Melton LJ, 3rd, Zinsmeister AR, Lahr BD, Murray JA. 2013. Increasing incidence of celiac disease in a North American population. The American journal of gastroenterology 108:818-824.

8. Kaukinen K, Maki M, Partanen J, Sievanen H, Collin P. 2001. Celiac disease without villous atrophy: Revision of criteria called for. Dig Dis Sci 46:879-887.

9. Wahab PJ, Crusius JB, Meijer JW, Mulder CJ. 2001. Gluten challenge in borderline gluten-sensitive enteropathy. The American journal of gastroenterology 96:1464-1469.

10. Meresse B, Chen Z, Ciszewski C, Tretiakova M, Bhagat G, Krausz TN, Raulet DH, Lanier LL, Groh V, Spies T, Ebert EC, Green PH, Jabri B. 2004. Coordinated induction by IL15 of a TCR-independent NKG2D signaling pathway converts CTL into lymphokine-activated killer cells in celiac disease. Immunity 21:357-366.

11. Walker-Smith JA. 1990. Management of infantile gastroenteritis. Arch Dis Child 65:917-918.

12. Marsh MN. 1992. Mucosal pathology in gluten sensitivity, p. 136-191. *In* Marsh M (ed.), Coeliac Disease. Blackwell Scientific Publications, Oxford, UK.

13. Dickson BC, Streutker CJ, Chetty R. 2006. Coeliac disease: An update for pathologists. J Clin Pathol 59:1008-1016.

14. Mohamed BM, Feighery C, Coates C, O'Shea U, Delaney D, O'Briain S, Kelly J, Abuzakouk M. 2008. The absence of a mucosal lesion on standard histological examination does not exclude diagnosis of celiac disease. Dig Dis Sci 53:52-61.

15. Rostami K, Kerckhaert J, Tiemessen R, von Blomberg BM, Meijer JW, Mulder CJ. 1999. Sensitivity of antiendomysium and antigliadin antibodies in untreated celiac disease: Disappointing in clinical practice. The American journal of gastroenterology 94:888-894.

16. Rostom A, Dube C, Cranney A, Saloojee N, Sy R, Garritty C, Sampson M, Zhang L, Yazdi F, Mamaladze V, Pan I, MacNeil J, Mack D, Patel D, Moher D. 2005. The diagnostic accuracy of serologic tests for celiac disease: A systematic review. Gastroenterology 128:S38-46.

17. Kaukinen K, Partanen J, Maki M, Collin P. 2002. HLA-DQ typing in the diagnosis of celiac disease. The American journal of gastroenterology 97:695-699.

18. Karinen H, Karkkainen P, Pihlajamaki J, Janatuinen E, Heikkinen M, Julkunen R, Kosma VM, Naukkarinen A, Laakso M. 2006. HLA genotyping is useful in the evaluation of the risk for coeliac disease in the 1st-degree relatives of patients with coeliac disease. Scandinavian journal of gastroenterology 41:1299-1304.

19. DiGiacomo D, Santonicola A, Zingone F, Troncone E, Caria MC, Borgheresi P, Parrilli G, Ciacci C. 2013. Human leukocyte antigen DQ2/8 prevalence in non-celiac patients with gastrointestinal diseases. World journal of gastroenterology 19:2507-2513.

20. Sollid LM, Thorsby E. 1993. HLA susceptibility genes in celiac disease: genetic mapping and role in pathogenesis. Gastroenterology 105:910-922.

21. Sollid LM, Markussen G, Ek J, Gjerde H, Vartdal F, Thorsby E. 1989. Evidence for a primary association of celiac disease to a particular HLA-DQ alpha/beta heterodimer. J Exp Med 169:345-350.

22. Spurkland A, Sollid LM, Polanco I, Vartdal F, Thorsby E. 1992. HLA-DR and -DQ genotypes of celiac disease patients serologically typed to be non-DR3 or non-DR5/7. Hum Immunol 35:188-192.

23. Hopman EG, le Cessie S, von Blomberg BM, Mearin ML. 2006. Nutritional management of the gluten-free diet in young people with celiac disease in the Netherlands. J Pediatr Gastroenterol Nutr 43:102-108.

24. Haines ML, Anderson RP, Gibson PR. 2008. Systematic review: The evidence base for long-term management of coeliac disease. Alimentary pharmacology & therapeutics 28:1042-1066.

25. Casellas F, Rodrigo L, Vivancos JL, Riestra S, Pantiga C, Baudet JS, Junquera F, Divi VP, Abadia C, Papo M, Gelabert J, Malagelada JR. 2008. Factors that impact health-related quality of life in adults with celiac disease: A multicenter study. World journal of gastroenterology 14:46-52.

26. Whitaker JK, West J, Holmes GK, Logan RF. 2009. Patient perceptions of the burden of coeliac disease and its treatment in the UK. Alimentary pharmacology & therapeutics 29:1131-1136.

27. Collin P, Maki M, Kaukinen K. 2004. It is the compliance, not milligrams of gluten, that is essential in the treatment of celiac disease. Nutr Rev 62:490; author reply 491.

28. Gujral N, Freeman HJ, Thomson AB. 2012. Celiac disease: Prevalence, diagnosis, pathogenesis and treatment. World journal of gastroenterology 18:6036-6059.

29. Dube C, Rostom A, Sy R, Cranney A, Saloojee N, Garritty C, Sampson M, Zhang L, Yazdi F, Mamaladze V, Pan I, Macneil J, Mack D, Patel D, Moher D. 2005. The prevalence of celiac disease in average-risk and at-risk Western European populations: A systematic review. Gastroenterology 128:S57-67.

30. Catassi C, Gatti S, Fasano A. 2014. The new epidemiology of celiac disease. J Pediatr Gastroenterol Nutr 59 Suppl 1:S7-9.

31. Thomas HJ, Ahmad T, Rajaguru C, Barnardo M, Warren BF, Jewell DP. 2009. Contribution of histological, serological, and genetic factors to the clinical heterogeneity of adult-onset coeliac disease. Scandinavian journal of gastroenterology 44:1076-1083.

32. Jacobson DL, Gange SJ, Rose NR, Graham NM. 1997. Epidemiology and estimated population burden of selected autoimmune diseases in the United States. Clin Immunol Immunopathol 84:223-243.

33. Nistico L, Fagnani C, Coto I, Percopo S, Cotichini R, Limongelli MG, Paparo F, D'Alfonso S, Giordano M, Sferlazzas C, Magazzu G, Momigliano-Richiardi P, Greco L, Stazi MA. 2006. Concordance, disease progression, and heritability of coeliac disease in Italian twins. Gut 55:803-808.

34. Jabri B, Sollid LM. 2006. Mechanisms of disease: immunopathogenesis of celiac disease. Nature clinical practice. Gastroenterology & hepatology 3:516-525.

35. Megiorni F, Mora B, Bonamico M, Barbato M, Nenna R, Maiella G, Lulli P, Mazzilli MC. 2009. HLA-DQ and risk gradient for celiac disease. Hum Immunol 70:55-59.

36. Karell K, Louka AS, Moodie SJ, Ascher H, Clot F, Greco L, Ciclitira PJ, Sollid LM, Partanen J, European Genetics Cluster on Celiac D. 2003. HLA types in celiac disease patients not carrying the DQA1*05-DQB1*02 (DQ2) heterodimer: Results from the European Genetics Cluster on Celiac Disease. Hum Immunol 64:469-477.

37. van Heel DA, Franke L, Hunt KA, Gwilliam R, Zhernakova A, Inouye M, Wapenaar MC, Barnardo MC, Bethel G, Holmes GK, Feighery C, Jewell D, Kelleher D, Kumar P, Travis S, Walters JR, Sanders DS, Howdle P, Swift J, Playford RJ, McLaren WM, Mearin ML, Mulder CJ, McManus R, McGinnis R, Cardon LR, Deloukas P, Wijmenga C. 2007. A genome-wide association study for celiac disease identifies risk variants in the region harboring IL2 and IL21. Nat Genet 39:827-829.

38. Hunt KA, Zhernakova A, Turner G, Heap GA, Franke L, Bruinenberg M, Romanos J, Dinesen LC, Ryan AW, Panesar D, Gwilliam R, Takeuchi F, McLaren WM, Holmes GK, Howdle PD, Walters JR, Sanders DS, Playford RJ, Trynka G, Mulder CJ, Mearin ML, Verbeek WH, Trimble V, Stevens FM, O'Morain C, Kennedy NP, Kelleher D, Pennington DJ, Strachan DP, McArdle WL, Mein CA, Wapenaar MC, Deloukas P, McGinnis R, McManus R, Wijmenga C, van Heel DA. 2008. Newly identified genetic risk variants for celiac disease related to the immune response. Nat Genet 40:395-402.

39. Cummins AG, Roberts-Thomson IC. 2009. Prevalence of celiac disease in the Asia-Pacific region. J Gastroenterol Hepatol 24:1347-1351.

40. Dorman JS, Bunker CH. 2000. HLA-DQ locus of the human leukocyte antigen complex and type 1 diabetes mellitus: a HuGE review. Epidemiol Rev 22:218-227.

41. Middleton D, Menchaca L, Rood H, Komerofsky R. 2003. New allele frequency database: http://www.allelefrequencies.net. Tissue Antigens 61:403-407.

42. Mearin ML, Biemond I, Pena AS, Polanco I, Vazquez C, Schreuder GT, de Vries RR, van Rood JJ. 1983. HLA-DR phenotypes in Spanish coeliac children: Their contribution to the understanding of the genetics of the disease. Gut 24:532-537.

43. van Heel DA, Hunt K, Greco L, Wijmenga C. 2005. Genetics in coeliac disease. Best practice & research. Clinical gastroenterology 19:323-339.

44. Petronzelli F, Bonamico M, Ferrante P, Grillo R, Mora B, Mariani P, Apollonio I, Gemme G, Mazzilli MC. 1997. Genetic contribution of the HLA region to the familial clustering of coeliac disease. Annals of human genetics 61:307-317.

45. Bevan S, Popat S, Braegger CP, Busch A, O'Donoghue D, Falth-Magnusson K, Ferguson A, Godkin A, Hogberg L, Holmes G, Hosie KB, Howdle PD, Jenkins H, Jewell D, Johnston S, Kennedy NP, Kerr G, Kumar P, Logan RF, Love AH, Marsh M, Mulder CJ, Sjoberg K, Stenhammer L, Walker-Smith J, Marossy AM, Houlston RS. 1999. Contribution of the MHC region to the familial risk of coeliac disease. J Med Genet 36:687-690.

46. Dubois PC, Trynka G, Franke L, Hunt KA, Romanos J, Curtotti A, Zhernakova A, Heap GA, Adany R, Aromaa A, Bardella MT, van den Berg LH, Bockett NA, de la Concha EG, Dema B, Fehrmann RS, Fernandez-Arquero M, Fiatal S, Grandone E, Green PM, Groen HJ, Gwilliam R, Houwen RH, Hunt SE, Kaukinen K, Kelleher D, Korponay-Szabo I, Kurppa K, MacMathuna P, Maki M, Mazzilli MC, McCann OT, Mearin ML, Mein CA, Mirza MM, Mistry V, Mora B, Morley KI, Mulder CJ, Murray JA, Nunez C, Oosterom E, Ophoff RA, Polanco I, Peltonen L, Platteel M, Rybak A, Salomaa V, Schweizer JJ, Sperandeo MP, Tack GJ, Turner G, Veldink JH, Verbeek WH, Weersma RK, Wolters VM, Urcelay E, Cukrowska B, Greco L, Neuhausen SL, McManus R, Barisani D, Deloukas P, Barrett JC, Saavalainen P, Wijmenga C, van Heel DA. 2010. Multiple common variants for celiac disease influencing immune gene expression. Nat Genet 42:295-302.

47. Jabri B, Sollid LM. 2009. Tissue-mediated control of immunopathology in coeliac disease. Nat Rev Immunol 9:858-870.

48. Nilsen EM, Jahnsen FL, Lundin KE, Johansen FE, Fausa O, Sollid LM, Jahnsen J, Scott H, Brandtzaeg P. 1998. Gluten induces an intestinal

cytokine response strongly dominated by interferon gamma in patients with celiac disease. Gastroenterology 115:551-563.

49. Lundin KE, Scott H, Fausa O, Thorsby E, Sollid LM. 1994. T cells from the small intestinal mucosa of a DR4, DQ7/DR4, DQ8 celiac disease patient preferentially recognize gliadin when presented by DQ8. Hum Immunol 41:285-291.

50. Hunt KA, McGovern DP, Kumar PJ, Ghosh S, Travis SP, Walters JR, Jewell DP, Playford RJ, van Heel DA. 2005. A common CTLA4 haplotype associated with coeliac disease. European journal of human genetics : EJHG 13:440-444.

51. Djilali-Saiah I, Schmitz J, Harfouch-Hammoud E, Mougenot JF, Bach JF, Caillat-Zucman S. 1998. CTLA-4 gene polymorphism is associated with predisposition to coeliac disease. Gut 43:187-189.

52. Jabri B, de Serre NP, Cellier C, Evans K, Gache C, Carvalho C, Mougenot JF, Allez M, Jian R, Desreumaux P, Colombel JF, Matuchansky C, Cugnenc H, Lopez-Botet M, Vivier E, Moretta A, Roberts AI, Ebert EC, Guy-Grand D, Brousse N, Schmitz J, Cerf-Bensussan N. 2000. Selective expansion of intraepithelial lymphocytes expressing the HLA-E-specific natural killer receptor CD94 in celiac disease. Gastroenterology 118:867-879.

53. Mention JJ, Ben Ahmed M, Begue B, Barbe U, Verkarre V, Asnafi V, Colombel JF, Cugnenc PH, Ruemmele FM, McIntyre E, Brousse N, Cellier C, Cerf-Bensussan N. 2003. Interleukin 15: a key to disrupted intraepithelial lymphocyte homeostasis and lymphomagenesis in celiac disease. Gastroenterology 125:730-745.

54. Maiuri L, Ciacci C, Ricciardelli I, Vacca L, Raia V, Auricchio S, Picard J, Osman M, Quaratino S, Londei M. 2003. Association between innate response to gliadin and activation of pathogenic T cells in coeliac disease. Lancet 362:30-37.

55. Monteleone G, Pender SL, Alstead E, Hauer AC, Lionetti P, McKenzie C, MacDonald TT. 2001. Role of interferon alpha in promoting T helper cell type 1 responses in the small intestine in coeliac disease. Gut 48:425-429.

56. Sollid LM, Jabri B. 2013. Triggers and drivers of autoimmunity: lessons from coeliac disease. Nat Rev Immunol 13:294-302.

57. Ratnaike RN, Wangel AG. 1977. Immunological abnormalities in coeliac disease and their response to dietary restriction. I. Serum immunoglobulins, antibodies and complement. Aust N Z J Med 7:349-352.

58. Signer E, Burgin-Wolff A, Berger R, Birbaumer A, Just M. 1979. Antibodies to gliadin as a screening test for coeliac disease. A prospective study. Helvetica paediatrica acta 34:41-52.

59. Bardella MT, Velio P, Cesana BM, Prampolini L, Casella G, Di Bella C, Lanzini A, Gambarotti M, Bassotti G, Villanacci V. 2007. Coeliac disease: A histological follow-up study. Histopathology 50:465-471.

60. Hogen Esch CE, Wolters VM, Gerritsen SA, Putter H, von Blomberg BM, van Hoogstraten IM, Houwen RH, van der Lely N, Mearin ML. 2011. Specific celiac disease antibodies in children on a gluten-free diet. Pediatrics 128:547-552.

61. De Leo L, Aeschlimann D, Hadjivassiliou M, Aeschlimann P, Salce N, Vatta S, Ziberna F, Cozzi G, Martelossi S, Ventura A, Not T. 2017. Anti-transglutaminase 6 antibody development in children with celiac disease correlates with duration of gluten exposure. J Pediatr Gastroenterol Nutr.

62. Myleus A, Ivarsson A, Webb C, Danielsson L, Hernell O, Hogberg L, Karlsson E, Lagerqvist C, Norstrom F, Rosen A, Sandstrom O, Stenhammar L, Stenlund H, Wall S, Carlsson A. 2009. Celiac disease revealed in 3% of Swedish 12-year-olds born during an epidemic. J Pediatr Gastroenterol Nutr 49:170-176.

63. Kondrashova A, Mustalahti K, Kaukinen K, Viskari H, Volodicheva V, Haapala AM, Ilonen J, Knip M, Maki M, Hyoty H, Epivir Study G. 2008. Lower economic status and inferior hygienic environment may protect against celiac disease. Ann Med 40:223-231.

64. Plot L, Amital H. 2009. Infectious associations of Celiac disease. Autoimmun Rev 8:316-319.

65. Pabst O, Mowat AM. 2012. Oral tolerance to food protein. Mucosal Immunol 5:232-239.

66. Faria AM, Weiner HL. 2005. Oral tolerance. Immunol Rev 206:232-259.

67. Kapp K, Maul J, Hostmann A, Mundt P, Preiss JC, Wenzel A, Thiel A, Zeitz M, Ullrich R, Duchmann R. 2010. Modulation of systemic antigen-specific immune responses by oral antigen in humans. Eur J Immunol 40:3128-3137.

68. Kraus TA, Toy L, Chan L, Childs J, Mayer L. 2004. Failure to induce oral tolerance to a soluble protein in patients with inflammatory bowel disease. Gastroenterology 126:1771-1778.

69. Husby S, Mestecky J, Moldoveanu Z, Holland S, Elson CO. 1994. Oral tolerance in humans. T cell but not B cell tolerance after antigen feeding. J Immunol 152:4663-4670.

70. Wells HG. 1911. Studies on the chemistry of anaphylaxis (III). Experiments with isolated proteins, especially those of the hen's egg. J Infect Dis 9.

71. Ngan J, Kind LS. 1978. Suppressor T cells for IgE and IgG in Peyer's patches of mice made tolerant by the oral administration of ovalbumin. J Immunol 120:861-865.

72. Murphy K, Travers P, Walport M, Janeway C. 2012. Janeway's immunobiology, 8th ed. Garland Science, New York.

73. Chirdo FG, Millington OR, Beacock-Sharp H, Mowat AM. 2005. Immunomodulatory dendritic cells in intestinal lamina propria. Eur J Immunol 35:1831-1840.

74. Pabst O, Bernhardt G, Forster R. 2007. The impact of cell-bound antigen transport on mucosal tolerance induction. J Leukoc Biol 82:795-800.

75. Jaensson E, Uronen-Hansson H, Pabst O, Eksteen B, Tian J, Coombes JL, Berg PL, Davidsson T, Powrie F, Johansson-Lindbom B, Agace WW. 2008. Small intestinal CD103+ dendritic cells display unique functional properties that are conserved between mice and humans. J Exp Med 205:2139-2149.

76. Coombes JL, Powrie F. 2008. Dendritic cells in intestinal immune regulation. Nat Rev Immunol 8:435-446.

77. Sun CM, Hall JA, Blank RB, Bouladoux N, Oukka M, Mora JR, Belkaid Y. 2007. Small intestine lamina propria dendritic cells promote de novo generation of Foxp3 T reg cells via retinoic acid. J Exp Med 204:1775-1785.

78. Mowat AM, Faria AMC, Weiner HL. 2005. Oral tolerance: Physiologic basis and clinical applications, p. 487–538. *In* Mestecky J, Lamm ME, McGhee JR, Bienenstock J, Mayer L, Strober W (ed.), Mucosal immunology, 3rd ed, vol. 1. Elsevier/Academic Press, Amsterdam.

79. Dubois B, Chapat L, Goubier A, Papiernik M, Nicolas JF, Kaiserlian D. 2003. Innate CD4+CD25+ regulatory T cells are required for oral tolerance and inhibition of CD8+ T cells mediating skin inflammation. Blood 102:3295-3301.

80. Shan L, Molberg O, Parrot I, Hausch F, Filiz F, Gray GM, Sollid LM, Khosla C. 2002. Structural basis for gluten intolerance in celiac sprue. Science 297:2275-2279.

81. Arentz-Hansen H, Korner R, Molberg O, Quarsten H, Vader W, Kooy YM, Lundin KE, Koning F, Roepstorff P, Sollid LM, McAdam SN. 2000. The intestinal T cell response to alpha-gliadin in adult celiac disease is focused on a single deamidated glutamine targeted by tissue transglutaminase. J Exp Med 191:603-612.

82. Moustakas AK, van de Wal Y, Routsias J, Kooy YM, van Veelen P, Drijfhout JW, Koning F, Papadopoulos GK. 2000. Structure of celiac disease-associated HLA-DQ8 and non-associated HLA-DQ9 alleles in complex with two disease-specific epitopes. Int Immunol 12:1157-1166.

83. Molberg O, McAdam SN, Korner R, Quarsten H, Kristiansen C, Madsen L, Fugger L, Scott H, Noren O, Roepstorff P, Lundin KE, Sjostrom H, Sollid LM. 1998. Tissue transglutaminase selectively modifies gliadin peptides that are recognized by gut-derived T cells in celiac disease. Nat. Med. 4:713-717.

84. van de Wal Y, Kooy Y, van Veelen P, Pena S, Mearin L, Papadopoulos G, Koning F. 1998. Selective deamidation by tissue transglutaminase strongly enhances gliadin-specific T cell reactivity. J Immunol 161:1585-1588.

85. Lundin KE, Scott H, Hansen T, Paulsen G, Halstensen TS, Fausa O, Thorsby E, Sollid LM. 1993. Gliadin-specific, HLA-DQ(alpha 1*0501,beta 1*0201) restricted T cells isolated from the small intestinal mucosa of celiac disease patients. J Exp Med 178:187-196.

86. Lorand L, Graham RM. 2003. Transglutaminases: crosslinking enzymes with pleiotropic functions. Nat Rev Mol Cell Biol 4:140-156.

87. Quarsten H, Molberg O, Fugger L, McAdam SN, Sollid LM. 1999. HLA binding and T cell recognition of a tissue transglutaminase-modified gliadin epitope. Eur J Immunol 29:2506-2514.

88. Vader LW, de Ru A, van der Wal Y, Kooy YM, Benckhuijsen W, Mearin ML, Drijfhout JW, van Veelen P, Koning F. 2002. Specificity of tissue transglutaminase explains cereal toxicity in celiac disease. J Exp Med 195:643-649.

89. Bouziat R, Hinterleitner R, Brown JJ, Stencel-Baerenwald JE, Ikizler M, Mayassi T, Meisel M, Kim SM, Discepolo V, Pruijssers AJ, Ernest JD, Iskarpatyoti JA, Costes LM, Lawrence I, Palanski BA, Varma M, Zurenski

MA, Khomandiak S, McAllister N, Aravamudhan P, Boehme KW, Hu F, Samsom JN, Reinecker HC, Kupfer SS, Guandalini S, Semrad CE, Abadie V, Khosla C, Barreiro LB, Xavier RJ, Ng A, Dermody TS, Jabri B. 2017. Reovirus infection triggers inflammatory responses to dietary antigens and development of celiac disease. Science 356:44-50.

90. Siegel M, Strnad P, Watts RE, Choi K, Jabri B, Omary MB, Khosla C. 2008. Extracellular transglutaminase 2 is catalytically inactive, but is transiently activated upon tissue injury. PLoS One 3:e1861.

91. Hovhannisyan Z, Weiss A, Martin A, Wiesner M, Tollefsen S, Yoshida K, Ciszewski C, Curran SA, Murray JA, David CS, Sollid LM, Koning F, Teyton L, Jabri B. 2008. The role of HLA-DQ8 beta57 polymorphism in the anti-gluten T-cell response in coeliac disease. Nature 456:534-538.
92. Mora JR, von Andrian UH. 2004. Retinoic acid: An educational "vitamin elixir" for gut-seeking T cells. Immunity 21:458-460.

93. Iliev ID, Matteoli G, Rescigno M. 2007. The yin and yang of intestinal epithelial cells in controlling dendritic cell function. J Exp Med 204:2253-2257.

94. Molberg O, Kett K, Scott H, Thorsby E, Sollid LM, Lundin KE. 1997. Gliadin specific, HLA DQ2-restricted T cells are commonly found in small intestinal biopsies from coeliac disease patients, but not from controls. Scand J Immunol 46:103-109.

95. Maiuri L, Ciacci C, Auricchio S, Brown V, Quaratino S, Londei M. 2000. Interleukin 15 mediates epithelial changes in celiac disease. Gastroenterology 119:996-1006.

96. Waldmann TA. 2006. The biology of interleukin-2 and interleukin-15: Implications for cancer therapy and vaccine design. Nat Rev Immunol 6:595-601.

97. Blanco P, Palucka AK, Pascual V, Banchereau J. 2008. Dendritic cells and cytokines in human inflammatory and autoimmune diseases. Cytokine Growth Factor Rev 19:41-52.

98. DePaolo RW, Abadie V, Tang F, Fehlner-Peach H, Hall JA, Wang W, Marietta EV, Kasarda DD, Waldmann TA, Murray JA, Semrad C, Kupfer SS, Belkaid Y, Guandalini S, Jabri B. 2011. Co-adjuvant effects of retinoic acid and IL-15 induce inflammatory immunity to dietary antigens. Nature 471:220-224.

99. Takayama S, Iwaki K, Nishida Y, Tanaka M, Fujii M, Ohashi K, Ikeda M, Kurimoto M. 1999. Effects of oral administration of interferon-alpha on

antibody production in mice with induced tolerance. J Interferon Cytokine Res 19:895-900.

100. Nelson PA, Akselband Y, Dearborn SM, Al-Sabbagh A, Tian ZJ, Gonnella PA, Zamvil SS, Chen Y, Weiner HL. 1996. Effect of oral beta interferon on subsequent immune responsiveness. Ann N Y Acad Sci 778:145-155.

101. Mazzarella G, Stefanile R, Camarca A, Giliberti P, Cosentini E, Marano C, Iaquinto G, Giardullo N, Auricchio S, Sette A, Troncone R, Gianfrani C. 2008. Gliadin activates HLA class I-restricted CD8+ T cells in celiac disease intestinal mucosa and induces the enterocyte apoptosis. Gastroenterology 134:1017-1027.

102. Perera L, Shao L, Patel A, Evans K, Meresse B, Blumberg R, Geraghty D, Groh V, Spies T, Jabri B, Mayer L. 2007. Expression of nonclassical class I molecules by intestinal epithelial cells. Inflammatory bowel diseases 13:298-307.

103. Kasaian MT, Whitters MJ, Carter LL, Lowe LD, Jussif JM, Deng B, Johnson KA, Witek JS, Senices M, Konz RF, Wurster AL, Donaldson DD, Collins M, Young DA, Grusby MJ. 2002. IL-21 limits NK cell responses and promotes antigen-specific T cell activation: A mediator of the transition from innate to adaptive immunity. Immunity 16:559-569.

104. Colombel JF, Mascart-Lemone F, Nemeth J, Vaerman JP, Dive C, Rambaud JC. 1990. Jejunal immunoglobulin and antigliadin antibody secretion in adult coeliac disease. Gut 31:1345-1349.

105. Di Niro R, Mesin L, Zheng NY, Stamnaes J, Morrissey M, Lee JH, Huang M, Iversen R, du Pre MF, Qiao SW, Lundin KE, Wilson PC, Sollid LM. 2012. High abundance of plasma cells secreting transglutaminase 2-specific IgA autoantibodies with limited somatic hypermutation in celiac disease intestinal lesions. Nat. Med. 18:441-445.

106. Meresse B, Malamut G, Cerf-Bensussan N. 2012. Celiac disease: An immunological jigsaw. Immunity 36:907-919.

107. Sollid LM, Molberg O, McAdam S, Lundin KE. 1997. Autoantibodies in coeliac disease: tissue transglutaminase--guilt by association? Gut 41:851-852.

108. Matysiak-Budnik T, Moura IC, Arcos-Fajardo M, Lebreton C, Menard S, Candalh C, Ben-Khalifa K, Dugave C, Tamouza H, van Niel G, Bouhnik Y, Lamarque D, Chaussade S, Malamut G, Cellier C, Cerf-Bensussan N, Monteiro RC, Heyman M. 2008. Secretory IgA mediates retrotranscytosis

of intact gliadin peptides via the transferrin receptor in celiac disease. J Exp Med 205:143-154.

109. Black KE, Murray JA, David CS. 2002. HLA-DQ determines the response to exogenous wheat proteins: a model of gluten sensitivity in transgenic knockout mice. J Immunol 169:5595-5600.

110. Devendra D, Eisenbarth GS. 2004. Interferon alpha--a potential link in the pathogenesis of viral-induced type 1 diabetes and autoimmunity. Clin Immunol 111:225-233.

111. Cammarota G, Cuoco L, Cianci R, Pandolfi F, Gasbarrini G. 2000. Onset of coeliac disease during treatment with interferon for chronic hepatitis C. Lancet 356:1494-1495.

112. Bourliere M, Oules V, Perrier H, Mengotti C. 2001. Onset of coeliac disease and interferon treatment. Lancet 357:803-804.

113. Smits SL, van Leeuwen M, van der Eijk AA, Fraaij PL, Escher JC, Simon JH, Osterhaus AD. 2010. Human astrovirus infection in a patient with new-onset celiac disease. J Clin Microbiol 48:3416-3418.

114. Stene LC, Honeyman MC, Hoffenberg EJ, Haas JE, Sokol RJ, Emery L, Taki I, Norris JM, Erlich HA, Eisenbarth GS, Rewers M. 2006. Rotavirus infection frequency and risk of celiac disease autoimmunity in early childhood: a longitudinal study. The American journal of gastroenterology 101:2333-2340.

115. Sandberg-Bennich S, Dahlquist G, Kallen B. 2002. Coeliac disease is associated with intrauterine growth and neonatal infections. Acta paediatrica 91:30-33.

116. Tai JH, Williams JV, Edwards KM, Wright PF, Crowe JE, Jr., Dermody TS. 2005. Prevalence of reovirus-specific antibodies in young children in Nashville, Tennessee. J Infect Dis 191:1221-1224.

117. Dermody TS, Parker JS, Sherry B. 2013. Orthoreoviruses, p. 1304-1346. *In* Knipe DM, Howley PM (ed.), Fields Virology, Sixth ed, vol. 2. Lippincott Williams & Wilkins, Philadelphia.

118. Angel J, Franco MA, Greenberg HB. 2012. Rotavirus immune responses and correlates of protection. Current opinion in virology 2:419-425.

119. Oie HK, Loh PC. 1971. Reovirus Type-2 - Induction of Viral Resistance and Interferon Production in Fathead Minnow Cells. Proc. Soc. Exp. Biol. Med. 136:369-&.

120. Lai MH, Joklik WK. 1973. The induction of interferon by temperature-sensitive mutants of reovirus, UV-irradiated reovirus, and subviral reovirus particles. Virology 51:191-204.

121. Gomatos PJ, Tamm I, Dales S, Franklin RM. 1962. Reovirus type 3: physical characteristics and interaction with L cells. Virology 17:441-454.

122. Halonen P. 1961. Growth, stability and hemagglutination of a reovirus. Ann Med Exp Biol Fenn 39:132-142.

123. Berard A, Coombs KM. 2009. Mammalian reoviruses: propagation, quantification, and storage. Curr Protoc Microbiol Chapter 15:Unit15C 11.

124. Barton ES, Forrest JC, Connolly JL, Chappell JD, Liu Y, Schnell FJ, Nusrat A, Parkos CA, Dermody TS. 2001. Junction adhesion molecule is a receptor for reovirus. Cell 104:441-451.

125. Campbell JA, Schelling P, Wetzel JD, Johnson EM, Forrest JC, Wilson GAR, Aurrand-Lions M, Imhof BA, Stehle T, Dermody TS. 2005. Junctional adhesion molecule a serves as a receptor for prototype and field-isolate strains of mammalian reovirus. J. Virol. 79:7967-7978.

126. Prota AE, Campbell JA, Schelling P, Forrest JC, Watson MJ, Peters TR, Aurrand-Lions M, Imhof BA, Dermody TS, Stehle T. 2003. Crystal structure of human junctional adhesion molecule 1: implications for reovirus binding. Proc Natl Acad Sci U S A 100:5366-5371.

127. Borsa J, Morash BD, Sargent MD, Copps TP, Lievaart PA, Szekely JG. 1979. Two modes of entry of reovirus particles into L cells. J. Gen. Virol. 45:161-170.

128. Borsa J, Sargent MD, Lievaart PA, Copps TP. 1981. Reovirus: evidence for a second step in the intracellular uncoating and transcriptase activation process. Virology 111:191-200.

129. Rubin DH, Weiner DB, Dworkin C, Greene MI, Maul GG, Williams WV. 1992. Receptor utilization by reovirus type 3: distinct binding sites on thymoma and fibroblast cell lines result in differential compartmentalization of virions. Microb Pathog 12:351-365.

130. Sturzenbecker LJ, Nibert ML, Furlong DB, Fields BN. 1987. Intracellular digestion of reovirus particles requires a low pH and is an essential step in the viral infectious cycle. J. Virol. 61:2351-2361.

131. Silverstein SC, Astell C, Levin DH, Schonberg M, Acs G. 1972. The mechanism of reovirus uncoating and gene activation in vivo. Virology 47:797-806.

132. Chang CT, Zweerink HJ. 1971. Fate of parental reovirus in infected cell. Virology 46:544-555.

133. Baer GS, Dermody TS. 1997. Mutations in reovirus outer-capsid protein σ3 selected during persistent infections of L cells confer resistance to protease inhibitor E64. J. Virol. 71:4921-4928.

134. Coombs KM. 1998. Stoichiometry of reovirus structural proteins in virus, ISVP, and core particles. Virology 243:218-228.

135. Dryden KA, Wang G, Yeager M, Nibert ML, Coombs KM, Furlong DB, Fields BN, Baker TS. 1993. Early steps in reovirus infection are associated with dramatic changes in supramolecular structure and protein conformation: analysis of virions and subviral particles by cryoelectron microscopy and image reconstruction. J Cell Biol 122:1023-1041.

136. Chandran K, Walker SB, Chen Y, Contreras CM, Schiff LA, Baker TS, Nibert ML. 1999. In vitro recoating of reovirus cores with baculovirus-expressed outer-capsid proteins μ1 and σ3. J. Virol. 73:3941-3950.

137. Chandran K, Farsetta DL, Nibert ML. 2002. Strategy for nonenveloped virus entry: a hydrophobic conformer of the reovirus membrane penetration protein micro 1 mediates membrane disruption. J. Virol. 76:9920-9933.

138. Lucia-Jandris P, Hooper JW, Fields BF. 1993. Reovirus M2 gene is associated with chromium release from mouse L cells. J. Virol. 67:5339-5345.

139. Broering TJ, Parker JS, Joyce PL, Kim J, Nibert ML. 2002. Mammalian reovirus nonstructural protein microNS forms large inclusions and colocalizes with reovirus microtubule-associated protein micro2 in transfected cells. J. Virol. 76:8285-8297.

140. Nason EL, Wetzel JD, Mukherjee SK, Barton ES, Prasad BVV, Dermody TS. 2001. A monoclonal antibody specific for reovirus outer-capsid protein σ3 inhibits σ1-mediated hemagglutination by steric hindrance. J. Virol. 75:6625-6634.

141. Ramos-Alvarez M, Sabin AB. 1954. Characteristics of poliomyelitis and other enteric viruses recovered in tissue culture from healthy American children. Proc Soc Exp Biol Med 87:655-661.

142. Ramos-Alvarez M, Sabin AB. 1958. Enteropathogenic viruses and bacteria; role in summer diarrheal diseases of infancy and early childhood. J Am Med Assoc 167:147-156.

143. Kobayashi T, Antar AA, Boehme KW, Danthi P, Eby EA, Guglielmi KM, Holm GH, Johnson EM, Maginnis MS, Naik S, Skelton WB, Wetzel JD, Wilson GJ, Chappell JD, Dermody TS. 2007. A plasmid-based reverse genetics system for animal double-stranded RNA viruses. Cell Host Microbe 1:147-157.

144. Kobayashi T, Ooms LS, Ikizler M, Chappell JD, Dermody TS. 2010. An improved reverse genetics system for mammalian orthoreoviruses. Virology 398:194-200.

145. Boehme KW, Ikizler M, Kobayashi T, Dermody TS. 2011. Reverse genetics for mammalian reovirus. Methods 55:109-113.

146. Rubin DH, Kornstein MJ, Anderson AO. 1985. Reovirus serotype 1 intestinal infection: a novel replicative cycle with ileal disease. J. Virol. 53:391-398.

147. Rubin DH. 1987. Reovirus serotype 1 binds to the basolateral membrane of intestinal epithelial cells. Microb Pathog 3:215-219.

148. Kauffman RS, Wolf JL, Finberg R, Trier JS, Fields BN. 1983. The σ1 protein determines the extent of spread of reovirus from the gastrointestinal tract of mice. Virology 124:403-410.

149. Antar AAR, Konopka JL, Campbell JA, Henry RA, Perdigoto AL, Carter BD, Pozzi A, Abel TW, Dermody TS. 2009. Junctional adhesion molecule-A is required for hematogenous dissemination of reovirus. Cell Host & Microbe 5:59-71.

150. Boehme KW, Guglielmi KM, Dermody TS. 2009. Reovirus nonstructural protein sigma1s is required for establishment of viremia and systemic dissemination. Proc Natl Acad Sci U S A 106:19986-19991.

151. Wolf JL, Kauffman RS, Finberg R, Dambrauskas R, Fields BN, Trier JS. 1983. Determinants of reovirus interaction with the intestinal M cells and absorptive cells of murine intestine. Gastroenterology 85:291-300.

152. Bodkin DK, Fields BN. 1989. Growth and survival of reovirus in intestinal tissue: role of the L2 and S1 genes. J. Virol. 63:1188-1193.

153. Bass DM, Bodkin D, Dambrauskas R, Trier JS, Fields BN, Wolf JL. 1990. Intraluminal proteolytic activation plays an important role in replication of type 1 reovirus in the intestines of neonatal mice. J. Virol. 64:1830-1833.

154. Bodkin DK, Nibert ML, Fields BN. 1989. Proteolytic digestion of reovirus in the intestinal lumens of neonatal mice. J. Virol. 63:4676-4681.

155. Amerongen HM, Wilson GAR, Fields BN, Neutra MR. 1994. Proteolytic processing of reovirus is required for adherence to intestinal M-cells. J. Virol. 68:8428-8432.

156. Nibert ML, Chappell JD, Dermody TS. 1995. Infectious subvirion particles of reovirus type 3 Dearing exhibit a loss in infectivity and contain a cleaved σ1 protein. J. Virol. 69:5057-5067.

157. Chappell JD, Barton ES, Smith TH, Baer GS, Duong DT, Nibert ML, Dermody TS. 1998. Cleavage susceptibility of reovirus attachment protein σ1 during proteolytic disassembly of virions is determined by a sequence polymorphism in the σ1 neck. J. Virol. 72:8205-8213.

158. Johansson C, Wetzel JD, He J, Mikacenic C, Dermody TS, Kelsall BL. 2007. Type I interferons produced by hematopoietic cells protect mice against lethal infection by mammalian reovirus. J Exp Med 204:1349-1358.

159. Holm GH, Zurney J, Tumilasci V, Danthi P, Hiscott J, Sherry B, Dermody TS. 2007. Retinoic acid-inducible gene-I and interferon-β promoter stimulator-1 augment proapoptotic responses following mammalian reovirus infection via interferon regulatory factor-3. J. Biol. Chem. 282:21953-21961.

160. Kato H, Takeuchi O, Mikamo-Satoh E, Hirai R, Kawai T, Matsushita K, Hiiragi A, Dermody TS, Fujita T, Akira S. 2008. Length-dependent recognition of double-stranded ribonucleic acids by retinoic acid-inducible gene-I and melanoma differentiation-associated gene 5. J Exp Med 205:1601-1610.

161. Loo YM, Fornek J, Crochet N, Bajwa G, Perwitasari O, Martinez-Sobrido L, Akira S, Gill MA, Garcia-Sastre A, Katze MG, Gale M, Jr. 2008. Distinct RIG-I and MDA5 signaling by RNA viruses in innate immunity. J. Virol. 82:335-345.

162. Sherry B, Torres J, Blum MA. 1998. Reovirus induction of and sensitivity to beta interferon in cardiac myocyte cultures correlate with induction of myocarditis and are determined by viral core proteins. J. Virol. 72:1314-1323.

163. Zurney J, Kobayashi T, Holm GH, Dermody TS, Sherry B. 2009. Reovirus mu2 protein inhibits interferon signaling through a novel mechanism

involving nuclear accumulation of interferon regulatory factor 9. J. Virol. 83:2178-2187.

164. Jacobs BL, Ferguson RE. 1991. The Lang strain of reovirus serotype 1 and the Dearing strain of reovirus serotype 3 differ in their sensitivities to β interferon. J. Virol. 65:5102-5104.

165. Knowlton JJ, Dermody TS, Holm GH. 2012. Apoptosis induced by mammalian reovirus is beta interferon (IFN) independent and enhanced by IFN regulatory factor 3- and NF-kappaB-dependent expression of Noxa. J. Virol. 86:1650-1660.

166. George A, Kost SI, Witzleben CL, Cebra JJ, Rubin DH. 1990. Reovirus-induced liver disease in severe combined immunodeficient (SCID) mice. A model for the study of viral infection, pathogenesis, and clearance. J Exp Med 171:929-934.

167. Barkon ML, Haller BL, Virgin HW. 1996. Circulating immunoglobulin G can play a critical role in clearance of intestinal reovirus infection. J. Virol. 70:1109-1116.

168. Fleeton MN, Contractor N, Leon F, Wetzel JD, Dermody TS, Kelsall BL. 2004. Peyer's patch dendritic cells process viral antigen from apoptotic epithelial cells in the intestine of reovirus-infected mice. J Exp Med 200:235-245.

169. Errington F, Steele L, Prestwich R, Harrington KJ, Pandha HS, Vidal L, de Bono J, Selby P, Coffey M, Vile R, Melcher A. 2008. Reovirus activates human dendritic cells to promote innate antitumor immunity. J Immunol 180:6018-6026.

170. Bharhani MS, Grewal JS, Pilgrim MJ, Enocksen C, Peppler R, London L, London SD. 2005. Reovirus serotype 1/strain Lang-stimulated activation of antigen-specific T lymphocytes in Peyer's patches and distal gut-mucosal sites: activation status and cytotoxic mechanisms. J Immunol 174:3580-3589.

171. Major AS, Cuff CF. 1997. Enhanced mucosal and systemic immune responses to intestinal reovirus infection in beta2-microglobulin-deficient mice. J. Virol. 71:5782-5789.

172. Silvey KJ, Hutchings AB, Vajdy M, Petzke MM, Neutra MR. 2001. Role of immunoglobulin A in protection against reovirus entry into Murine Peyer's patches. J. Virol. 75:10870-10879.

173. Hutchings AB, Helander A, Silvey KJ, Chandran K, Lucas WT, Nibert ML, Neutra MR. 2004. Secretory immunoglobulin A antibodies against the σ1 outer capsid protein of reovirus type 1 Lang prevent infection of mouse Peyer's patches. J. Virol. 78:947-957.

174. Lerner AM, Cherry JD, Klein JO, Finland M. 1962. Infections with reoviruses. N Engl J Med 267:947-952.

175. Selb B, Weber B. 1994. A study of human reovirus IgG and IgA antibodies by ELISA and western blot. J Virol Methods 47:15-25.

176. Jackson GG, Muldoon RL. 1973. Viruses causing common respiratory infection in man. IV. Reoviruses and Adenoviruses. J Infect Dis 128:811-866.

177. Giordano MO, Martinez LC, Isa MB, Ferreyra LJ, Canna F, Pavan JV, Paez M, Notario R, Nates SV. 2002. Twenty year study of the occurrence of reovirus infection in hospitalized children with acute gastroenteritis in Argentina. Pediatr. Infect. Dis. J. 21:880-882.

178. Rosen L, Hovis JF, Mastrota FM, Bell JA, Huebner RJ. 1960. An Outbreak of Infection with a Type-1 Reovirus among Children in an Institution. American Journal of Hygiene 71:266-274.

179. Richardson SC, Bishop RF, Smith AL. 1988. Enzyme-linked immunosorbent assays for measurement of reovirus immunoglobulin G, A, and M levels in serum. J Clin Microbiol 26:1871-1873.

180. Ouattara LA, Barin F, Barthez MA, Bonnaud B, Roingeard P, Goudeau A, Castelnau P, Vernet G, Paranhos-Baccala G, Komurian-Pradel F. 2011. Novel human reovirus isolated from children with acute necrotizing encephalopathy. Emerg Infect Dis 17:1436-1444.

181. Renehan AG, Booth C, Potten CS. 2001. What is apoptosis, and why is it important? Bmj 322:1536-1538.

182. Elmore S. 2007. Apoptosis: A review of programmed cell death. Toxicol Pathol 35:495-516.

183. Kerr JF, Wyllie AH, Currie AR. 1972. Apoptosis: a basic biological phenomenon with wide-ranging implications in tissue kinetics. Br J Cancer 26:239-257.

184. Bratton DL, Fadok VA, Richter DA, Kailey JM, Guthrie LA, Henson PM. 1997. Appearance of phosphatidylserine on apoptotic cells requires

calcium-mediated nonspecific flip-flop and is enhanced by loss of the aminophospholipid translocase. J Biol Chem 272:26159-26165.

185. Savill J, Fadok V. 2000. Corpse clearance defines the meaning of cell death. Nature 407:784-788.

186. Kurosaka K, Takahashi M, Watanabe N, Kobayashi Y. 2003. Silent cleanup of very early apoptotic cells by macrophages. J Immunol 171:4672-4679.

187. Cohen GM. 1997. Caspases: The executioners of apoptosis. Biochem J 326 (Pt 1):1-16.

188. Rai NK, Tripathi K, Sharma D, Shukla VK. 2005. Apoptosis: A basic physiologic process in wound healing. The international journal of lower extremity wounds 4:138-144.

189. Hengartner MO. 2000. The biochemistry of apoptosis. Nature 407:770-776.

190. Locksley RM, Killeen N, Lenardo MJ. 2001. The TNF and TNF receptor superfamilies: Integrating mammalian biology. Cell 104:487-501.

191. Ashkenazi A, Dixit VM. 1998. Death receptors: signaling and modulation. Science 281:1305-1308.

192. Chicheportiche Y, Bourdon PR, Xu H, Hsu YM, Scott H, Hession C, Garcia I, Browning JL. 1997. TWEAK, a new secreted ligand in the tumor necrosis factor family that weakly induces apoptosis. J Biol Chem 272:32401-32410.

193. Peter ME, Krammer PH. 1998. Mechanisms of CD95 (APO-1/Fas)-mediated apoptosis. Curr Opin Immunol 10:545-551.

194. Suliman A, Lam A, Datta R, Srivastava RK. 2001. Intracellular mechanisms of TRAIL: Apoptosis through mitochondrial-dependent and -independent pathways. Oncogene 20:2122-2133.

195. Rubio-Moscardo F, Blesa D, Mestre C, Siebert R, Balasas T, Benito A, Rosenwald A, Climent J, Martinez JI, Schilhabel M, Karran EL, Gesk S, Esteller M, deLeeuw R, Staudt LM, Fernandez-Luna JL, Pinkel D, Dyer MJ, Martinez-Climent JA. 2005. Characterization of 8p21.3 chromosomal deletions in B-cell lymphoma: TRAIL-R1 and TRAIL-R2 as candidate dosage-dependent tumor suppressor genes. Blood 106:3214-3222.

196. Hsu H, Xiong J, Goeddel DV. 1995. The TNF receptor 1-associated protein TRADD signals cell death and NF-κB activation. Cell 82:495-504.

197. Grimm LM, Goldberg AL, Poirier GG, Schwartz LM, Osborne BA. 1996. Proteasomes play an essential role in thymocyte apoptosis. EMBO J 15:3835-3844.

198. Wajant H. 2002. The Fas signaling pathway: More than a paradigm. Science 296:1635-1636.

199. Kischkel FC, Hellbardt S, Behrmann I, Germer M, Pawlita M, Krammer PH, Peter ME. 1995. Cytotoxicity-dependent APO-1 (Fas/CD95)-associated proteins form a death-inducing signaling complex (DISC) with the receptor. EMBO J 14:5579-5588.

200. Saelens X, Festjens N, Vande Walle L, van Gurp M, van Loo G, Vandenabeele P. 2004. Toxic proteins released from mitochondria in cell death. Oncogene 23:2861-2874.

201. Cai J, Yang J, Jones DP. 1998. Mitochondrial control of apoptosis: The role of cytochrome c. Biochim Biophys Acta 1366:139-149.

202. Du C, Fang M, Li Y, Li L, Wang X. 2000. Smac, a mitochondrial protein that promotes cytochrome c-dependent caspase activation by eliminating IAP inhibition. Cell 102:33-42.

203. Cory S, Adams JM. 2002. The Bcl2 family: Regulators of the cellular life-or-death switch. Nat Rev Cancer 2:647-656.

204. Chinnaiyan AM. 1999. The apoptosome: Heart and soul of the cell death machine. Neoplasia 1:5-15.

205. Hill MM, Adrain C, Duriez PJ, Creagh EM, Martin SJ. 2004. Analysis of the composition, assembly kinetics and activity of native Apaf-1 apoptosomes. EMBO J 23:2134-2145.

206. Mandal D, Mazumder A, Das P, Kundu M, Basu J. 2005. Fas-, caspase 8-, and caspase 3-dependent signaling regulates the activity of the aminophospholipid translocase and phosphatidylserine externalization in human erythrocytes. J Biol Chem 280:39460-39467.

207. Li H, Zhu H, Xu CJ, Yuan J. 1998. Cleavage of BID by caspase 8 mediates the mitochondrial damage in the Fas pathway of apoptosis. Cell 94:491-501.

208. Igney FH, Krammer PH. 2002. Death and anti-death: Tumour resistance to apoptosis. Nat Rev Cancer 2:277-288.

209. Oda E, Ohki R, Murasawa H, Nemoto J, Shibue T, Yamashita T, Tokino T, Taniguchi T, Tanaka N. 2000. Noxa, a BH3-only member of the Bcl-2

family and candidate mediator of p53-induced apoptosis. Science 288:1053-1058.

210. Fei P, Bernhard EJ, El-Deiry WS. 2002. Tissue-specific induction of p53 targets in vivo. Cancer Res 62:7316-7327.

211. Ploner C, Kofler R, Villunger A. 2008. Noxa: At the tip of the balance between life and death. Oncogene 27 Suppl 1:S84-92.

212. Liu FT, Newland AC, Jia L. 2003. Bax conformational change is a crucial step for PUMA-mediated apoptosis in human leukemia. Biochem Biophys Res Commun 310:956-962.

213. Perkins D, Gyure KA, Pereira EF, Aurelian L. 2003. Herpes simplex virus type 1-induced encephalitis has an apoptotic component associated with activation of c-Jun N-terminal kinase. J Neurovirol 9:101-111.

214. DeBiasi RL, Kleinschmidt-DeMasters BK, Richardson-Burns S, Tyler KL. 2002. Central nervous system apoptosis in human herpes simplex virus and cytomegalovirus encephalitis. J Infect Dis 186:1547-1557.

215. Li W, Galey D, Mattson MP, Nath A. 2005. Molecular and cellular mechanisms of neuronal cell death in HIV dementia. Neurotoxicity research 8:119-134.

216. Alter P, Jobmann M, Meyer E, Pankuweit S, Maisch B. 2001. Apoptosis in myocarditis and dilated cardiomyopathy: Does enterovirus genome persistence protect from apoptosis? An endomyocardial biopsy study. Cardiovasc Pathol 10:229-234.

217. Bantel H, Schulze-Osthoff K. 2003. Apoptosis in hepatitis C virus infection. Cell Death Differ 10 Suppl 1:S48-58.

218. Calabrese F, Pontisso P, Pettenazzo E, Benvegnu L, Vario A, Chemello L, Alberti A, Valente M. 2000. Liver cell apoptosis in chronic hepatitis C correlates with histological but not biochemical activity or serum HCV-RNA levels. Hepatology 31:1153-1159.

219. Patel T, Roberts LR, Jones BA, Gores GJ. 1998. Dysregulation of apoptosis as a mechanism of liver disease: An overview. Semin Liver Dis 18:105-114.

220. Rodrigues CM, Brites D, Serejo F, Costa A, Ramalho F, De Moura MC. 2000. Apoptotic cell death does not parallel other indicators of liver damage in chronic hepatitis C patients. J Viral Hepat 7:175-183.

221. Walsh MJ, Vanags DM, Clouston AD, Richardson MM, Purdie DM, Jonsson JR, Powell EE. 2004. Steatosis and liver cell apoptosis in chronic hepatitis C: A mechanism for increased liver injury. Hepatology 39:1230-1238.

222. Clarke P, Meintzer SM, Gibson S, Widmann C, Garrington TP, Johnson GL, Tyler KL. 2000. Reovirus-induced apoptosis is mediated by TRAIL. J. Virol. 74:8135-8139.

223. Connolly JL, Barton ES, Dermody TS. 2001. Reovirus binding to cell surface sialic acid potentiates virus-induced apoptosis. J. Virol. 75:4029-4039.

224. Rodgers SE, Barton ES, Oberhaus SM, Pike B, Gibson CA, Tyler KL, Dermody TS. 1997. Reovirus-induced apoptosis of MDCK cells is not linked to viral yield and is blocked by Bcl-2. J. Virol. 71:2540-2546.

225. Tyler KL, Squier MK, Rodgers SE, Schneider SE, Oberhaus SM, Grdina TA, Cohen JJ, Dermody TS. 1995. Differences in the capacity of reovirus strains to induce apoptosis are determined by the viral attachment protein σ1. J. Virol. 69:6972-6979.

226. DeBiasi RL, Robinson BA, Sherry B, Bouchard R, Brown RD, Rizeq M, Long C, Tyler KL. 2004. Caspase inhibition protects against reovirus-induced myocardial injury in vitro and in vivo. J. Virol. 78:11040-11050.

227. Richardson-Burns SM, Kominsky DJ, Tyler KL. 2002. Reovirus-induced neuronal apoptosis is mediated by caspase 3 and is associated with the activation of death receptors. J Neurovirol 8:365-380.

228. Kominsky DJ, Bickel RJ, Tyler KL. 2002. Reovirus-induced apoptosis requires both death receptor- and mitochondrial-mediated caspase-dependent pathways of cell death. Cell Death Differ 9:926-933.

229. Kominsky DJ, Bickel RJ, Tyler KL. 2002. Reovirus-induced apoptosis requires mitochondrial release of Smac/DIABLO and involves reduction of cellular inhibitor of apoptosis protein levels. J. Virol. 76:11414-11424.

230. Danthi P, Pruijssers AJ, Berger AK, Holm GH, Zinkel SS, Dermody TS. 2010. Bid regulates the pathogenesis of neurotropic reovirus. PLoS Pathog 6:e1000980.

231. Connolly JL, Rodgers SE, Clarke P, Ballard DW, Kerr LD, Tyler KL, Dermody TS. 2000. Reovirus-induced apoptosis requires activation of transcription factor NF-κB. J. Virol. 74:2981-2989.

232. DeBiasi RL, Clarke P, Meintzer S, Jotte R, Kleinschmidt-Demasters BK, Johnson GL, Tyler KL. 2003. Reovirus-induced alteration in expression of apoptosis and DNA repair genes with potential roles in viral pathogenesis. J. Virol. 77:8934-8947.

233. Clarke P, Meintzer SM, Moffitt LA, Tyler KL. 2003. Two distinct phases of virus-induced nuclear factor kappa B regulation enhance tumor necrosis factor-related apoptosis-inducing ligand-mediated apoptosis in virus-infected cells. J Biol Chem 278:18092-18100.

234. Danthi P, Coffey CM, Parker JS, Abel TW, Dermody TS. 2008. Independent regulation of reovirus membrane penetration and apoptosis by the mu1 phi domain. PLoS Pathog 4:e1000248.

235. Tyler KL, Fields BN. 1996. Reoviruses, p. 1597-1623. *In* Fields BN, Knipe DM, Howley PM (ed.), Fields Virology, Third ed. Lippincott-Raven, Philadelphia.

236. Rodgers SE, Connolly JL, Chappell JD, Dermody TS. 1998. Reovirus growth in cell culture does not require the full complement of viral proteins: Identification of a sigma 1s-null mutant. J. Virol. 72:8597-8604.

237. Hoyt CC, Richardson-Burns SM, Goody RJ, Robinson BA, Debiasi RL, Tyler KL. 2005. Nonstructural protein sigma1s is a determinant of reovirus virulence and influences the kinetics and severity of apoptosis induction in the heart and central nervous system. J. Virol. 79:2743-2753.

238. Danthi P, Kobayashi T, Holm GH, Hansberger MW, Abel TW, Dermody TS. 2008. Reovirus apoptosis and virulence are regulated by host cell membrane penetration efficiency. J. Virol. 82:161-172.

239. Coffey CM, Sheh A, Kim IS, Chandran K, Nibert ML, Parker JS. 2006. Reovirus outer capsid protein μ1 induces apoptosis and associates with lipid droplets, endoplasmic reticulum, and mitochondria. J. Virol. 80:8422-8438.

240. Mayhew TM, Myklebust R, Whybrow A, Jenkins R. 1999. Epithelial integrity, cell death and cell loss in mammalian small intestine. Histol Histopathol 14:257-267.

241. Potten CS. 1990. A comprehensive study of the radiobiological response of the murine (BDF1) small intestine. Int J Radiat Biol 58:925-973.

242. Gelberg HB. 2007. Alimentary system, p. 342–360. *In* McGavin MD, Zachary JF (ed.), Pathologic basis of veterinary disease, 4th ed. Elsevier Mosby, St. Louis, MO.

243. Kaur P, Potten CS. 1986. Circadian variation in migration velocity in small intestinal epithelium. Cell and tissue kinetics 19:591-599.

244. Burrin DG, Stoll B, Guan X, Cui L, Chang X, Holst JJ. 2005. Glucagon-like peptide 2 dose-dependently activates intestinal cell survival and proliferation in neonatal piglets. Endocrinology 146:22-32.

245. Brown CC, Baker DC, Barker IK. 2007. Alimentary system, p. 69–78. *In* Maxie MG (ed.), Jubb, Kennedy, and Palmer's pathology of domestic animals. Elsevier Saunders, Edinburgh, UK.

246. Shirkey TW, Siggers RH, Goldade BG, Marshall JK, Drew MD, Laarveld B, Van Kessel AG. 2006. Effects of commensal bacteria on intestinal morphology and expression of proinflammatory cytokines in the gnotobiotic pig. Exp Biol Med (Maywood) 231:1333-1345.

247. Bullen TF, Forrest S, Campbell F, Dodson AR, Hershman MJ, Pritchard DM, Turner JR, Montrose MH, Watson AJ. 2006. Characterization of epithelial cell shedding from human small intestine. Lab Invest 86:1052-1063.

248. Williams JM, Duckworth CA, Burkitt MD, Watson AJ, Campbell BJ, Pritchard DM. 2015. Epithelial cell shedding and barrier function: A matter of life and death at the small intestinal villus tip. Vet Pathol 52:445-455.

249. Madara JL. 1990. Maintenance of the macromolecular barrier at cell extrusion sites in intestinal epithelium: Physiological rearrangement of tight junctions. The Journal of membrane biology 116:177-184.

250. Guan Y, Watson AJ, Marchiando AM, Bradford E, Shen L, Turner JR, Montrose MH. 2011. Redistribution of the tight junction protein ZO-1 during physiological shedding of mouse intestinal epithelial cells. Am J Physiol Cell Physiol 300:C1404-1414.

251. Fouquet S, Lugo-Martinez VH, Faussat AM, Renaud F, Cardot P, Chambaz J, Pincon-Raymond M, Thenet S. 2004. Early loss of E-cadherin from cell-cell contacts is involved in the onset of Anoikis in enterocytes. J Biol Chem 279:43061-43069.

252. Foster DM, Stauffer SH, Stone MR, Gookin JL. 2012. Proteasome inhibition of pathologic shedding of enterocytes to defend barrier function requires X-linked inhibitor of apoptosis protein and nuclear factor kappaB. Gastroenterology 143:133-144 e134.

253. McAllister CS, Lakhdari O, Pineton de Chambrun G, Gareau MG, Broquet A, Lee GH, Shenouda S, Eckmann L, Kagnoff MF. 2013. TLR3, TRIF, and

caspase 8 determine double-stranded RNA-induced epithelial cell death and survival in vivo. J Immunol 190:418-427.

254. Williams JM, Duckworth CA, Watson AJ, Frey MR, Miguel JC, Burkitt MD, Sutton R, Hughes KR, Hall LJ, Caamano JH, Campbell BJ, Pritchard DM. 2013. A mouse model of pathological small intestinal epithelial cell apoptosis and shedding induced by systemic administration of lipopolysaccharide. Disease models & mechanisms 6:1388-1399.

255. Marshman E, Ottewell PD, Potten CS, Watson AJ. 2001. Caspase activation during spontaneous and radiation-induced apoptosis in the murine intestine. J Pathol 195:285-292.

256. Lai CW, Sun TL, Lo W, Tang ZH, Wu S, Chang YJ, Wu CC, Yu SC, Dong CY, Chen LW. 2013. Shedding-induced gap formation contributes to gut barrier dysfunction in endotoxemia. The journal of trauma and acute care surgery 74:203-213.

257. Wu S, Rhee KJ, Zhang M, Franco A, Sears CL. 2007. Bacteroides fragilis toxin stimulates intestinal epithelial cell shedding and gamma-secretase-dependent E-cadherin cleavage. J Cell Sci 120:1944-1952.

258. Song J, Wolf SE, Herndon DN, Wu XW, Jeschke MG. 2008. Second hit post burn increased proximal gut mucosa epithelial cells damage. Shock 30:184-188.

259. Sodhi C, Levy R, Gill R, Neal MD, Richardson W, Branca M, Russo A, Prindle T, Billiar TR, Hackam DJ. 2011. DNA attenuates enterocyte Toll-like receptor 4-mediated intestinal mucosal injury after remote trauma. Am J Physiol Gastrointest Liver Physiol 300:G862-873.

260. Garside P, Bunce C, Tomlinson RC, Nichols BL, Mowat AM. 1993. Analysis of enteropathy induced by tumour necrosis factor alpha. Cytokine 5:24-30.

261. Marchiando AM, Shen L, Graham WV, Edelblum KL, Duckworth CA, Guan Y, Montrose MH, Turner JR, Watson AJ. 2011. The epithelial barrier is maintained by in vivo tight junction expansion during pathologic intestinal epithelial shedding. Gastroenterology 140:1208-1218 e1201-1202.

262. Piguet PF, Vesin C, Guo J, Donati Y, Barazzone C. 1998. TNF-induced enterocyte apoptosis in mice is mediated by the TNF receptor 1 and does not require p53. Eur J Immunol 28:3499-3505.

263. Zhou R, Wei H, Sun R, Tian Z. 2007. Recognition of double-stranded RNA by TLR3 induces severe small intestinal injury in mice. J Immunol 178:4548-4556.

264. Tjon JM, van Bergen J, Koning F. 2010. Celiac disease: how complicated can it get? Immunogenetics 62:641-651.

265. Dermody TS, Parker JS, Sherry B. 2013. Orthoreoviruses, 6th ed. Lippincott Williams & Wilkins, Philadelphia, PA.

266. Macpherson AJ, Smith K. 2006. Mesenteric lymph nodes at the center of immune anatomy. J Exp Med 203:497-500.

267. Cannistraci CV, Ravasi T, Montevecchi FM, Ideker T, Alessio M. 2010. Nonlinear dimension reduction and clustering by Minimum Curvilinearity unfold neuropathic pain and tissue embryological classes. Bioinformatics 26:i531-539.

268. Xu Y, Olman V, Xu D. 2002. Clustering gene expression data using a graph-theoretic approach: an application of minimum spanning trees. Bioinformatics 18:536-545.

269. Coombes JL, Siddiqui KR, Arancibia-Carcamo CV, Hall J, Sun CM, Belkaid Y, Powrie F. 2007. A functionally specialized population of mucosal CD103+ DCs induces Foxp3+ regulatory T cells via a TGF-beta and retinoic acid-dependent mechanism. J Exp Med 204:1757-1764.

270. Esterhazy D, Loschko J, London M, Jove V, Oliveira TY, Mucida D. 2016. Classical dendritic cells are required for dietary antigen-mediated induction of peripheral T(reg) cells and tolerance. Nat Immunol 17:545-555.

271. Luda KM, Joeris T, Persson EK, Rivollier A, Demiri M, Sitnik KM, Pool L, Holm JB, Melo-Gonzalez F, Richter L, Lambrecht BN, Kristiansen K, Travis MA, Svensson-Frej M, Kotarsky K, Agace WW. 2016. IRF8 Transcription-Factor-Dependent Classical Dendritic Cells Are Essential for Intestinal T Cell Homeostasis. Immunity 44:860-874.

272. Hinterleitner R, Jabri B. 2016. A dendritic cell subset designed for oral tolerance. Nat Immunol 17:474-476.

273. Martinez-Lopez M, Iborra S, Conde-Garrosa R, Sancho D. 2015. Batf3-dependent CD103+ dendritic cells are major producers of IL-12 that drive local Th1 immunity against Leishmania major infection in mice. Eur J Immunol 45:119-129.

274. Curotto de Lafaille MA, Lafaille JJ. 2009. Natural and adaptive foxp3+ regulatory T cells: more of the same or a division of labor? Immunity 30:626-635.

275. Di Sabatino A, Pickard KM, Gordon JN, Salvati V, Mazzarella G, Beattie RM, Vossenkaemper A, Rovedatti L, Leakey NA, Croft NM, Troncone R, Corazza GR, Stagg AJ, Monteleone G, MacDonald TT. 2007. Evidence for the role of interferon-alfa production by dendritic cells in the Th1 response in celiac disease. Gastroenterology 133:1175-1187.

276. Irvin SC, Zurney J, Ooms LS, Chappell JD, Dermody TS, Sherry B. 2012. A single-amino-acid polymorphism in reovirus protein mu2 determines repression of interferon signaling and modulates myocarditis. J. Virol. 86:2302-2311.

277. Tamura T, Yanai H, Savitsky D, Taniguchi T. 2008. The IRF family transcription factors in immunity and oncogenesis. Annu Rev Immunol 26:535-584.

278. Taki S, Sato T, Ogasawara K, Fukuda T, Sato M, Hida S, Suzuki G, Mitsuyama M, Shin EH, Kojima S, Taniguchi T, Asano Y. 1997. Multistage regulation of Th1-type immune responses by the transcription factor IRF-1. Immunity 6:673-679.

279. Salvati VM, MacDonald TT, del Vecchio Blanco G, Mazzarella G, Monteleone I, Vavassori P, Auricchio S, Pallone F, Troncone R, Monteleone G. 2003. Enhanced expression of interferon regulatory factor-1 in the mucosa of children with celiac disease. Pediatr Res 54:312-318.

280. Maruyama S, Sumita K, Shen H, Kanoh M, Xu X, Sato M, Matsumoto M, Shinomiya H, Asano Y. 2003. Identification of IFN regulatory factor-1 binding site in IL-12 p40 gene promoter. J Immunol 170:997-1001.

281. Yoshida H, Hunter CA. 2015. The immunobiology of interleukin-27. Annu Rev Immunol 33:417-443.

282. Ivashkiv LB, Donlin LT. 2014. Regulation of type I interferon responses. Nat Rev Immunol 14:36-49.

283. Virgin HW. 2014. The virome in mammalian physiology and disease. Cell 157:142-150.

284. Cadwell K, Patel KK, Maloney NS, Liu TC, Ng AC, Storer CE, Head RD, Xavier R, Stappenbeck TS, Virgin HW. 2010. Virus-plus-susceptibility gene interaction determines Crohn's disease gene Atg16L1 phenotypes in intestine. Cell 141:1135-1145.

285. Lionetti E, Castellaneta S, Pulvirenti A, Tonutti E, Francavilla R, Fasano A, Catassi C, Italian Working Group of W, Celiac Disease R. 2012.

Prevalence and natural history of potential celiac disease in at-family-risk infants prospectively investigated from birth. J Pediatr 161:908-914.

286. Auricchio R, Tosco A, Piccolo E, Galatola M, Izzo V, Maglio M, Paparo F, Troncone R, Greco L. 2014. Potential celiac children: 9-year follow-up on a gluten-containing diet. Am J Gastroenterol 109:913-921.

287. Simell S, Hoppu S, Hekkala A, Simell T, Stahlberg MR, Viander M, Yrjanainen H, Gronlund J, Markula P, Simell V, Knip M, Ilonen J, Hyoty H, Simell O. 2007. Fate of five celiac disease-associated antibodies during normal diet in genetically at-risk children observed from birth in a natural history study. Am J Gastroenterol 102:2026-2035.

288. Setty M, Discepolo V, Abadie V, Kamhawi S, Mayassi T, Kent A, Ciszewski C, Maglio M, Kistner E, Bhagat G, Semrad C, Kupfer SS, Green PH, Guandalini S, Troncone R, Murray JA, Turner JR, Jabri B. 2015. Distinct and Synergistic Contributions of Epithelial Stress and Adaptive Immunity to Functions of Intraepithelial Killer Cells and Active Celiac Disease. Gastroenterology 149:681-691 e610.

289. Maki M, Mustalahti K, Kokkonen J, Kulmala P, Haapalahti M, Karttunen T, Ilonen J, Laurila K, Dahlbom I, Hansson T, Hopfl P, Knip M. 2003. Prevalence of Celiac disease among children in Finland. N Engl J Med 348:2517-2524.

290. Jabri B, Abadie V. 2015. IL-15 functions as a danger signal to regulate tissue-resident T cells and tissue destruction. Nat Rev Immunol 15:771-783.

291. Caminero A, Galipeau HJ, McCarville JL, Johnston CW, Bernier SP, Russell AK, Jury J, Herran AR, Casqueiro J, Tye-Din JA, Surette MG, Magarvey NA, Schuppan D, Verdu EF. 2016. Duodenal Bacteria From Patients With Celiac Disease and Healthy Subjects Distinctly Affect Gluten Breakdown and Immunogenicity. Gastroenterology 151:670-683.

292. D'Argenio V, Casaburi G, Precone V, Pagliuca C, Colicchio R, Sarnataro D, Discepolo V, Kim SM, Russo I, Del Vecchio Blanco G, Horner DS, Chiara M, Pesole G, Salvatore P, Monteleone G, Ciacci C, Caporaso GJ, Jabri B, Salvatore F, Sacchetti L. 2016. Metagenomics Reveals Dysbiosis and a Potentially Pathogenic N. flavescens Strain in Duodenum of Adult Celiac Patients. Am J Gastroenterol.

293. Cheetham S, Souza M, Meulia T, Grimes S, Han MG, Saif LJ. 2006. Pathogenesis of a genogroup II human norovirus in gnotobiotic pigs. J. Virol. 80:10372-10381.

294. Boshuizen JA, Reimerink JH, Korteland-van Male AM, van Ham VJ, Koopmans MP, Buller HA, Dekker J, Einerhand AW. 2003. Changes in small intestinal homeostasis, morphology, and gene expression during rotavirus infection of infant mice. J. Virol. 77:13005-13016.

295. Li Q, Estes JD, Duan L, Jessurun J, Pambuccian S, Forster C, Wietgrefe S, Zupancic M, Schacker T, Reilly C, Carlis JV, Haase AT. 2008. Simian immunodeficiency virus-induced intestinal cell apoptosis is the underlying mechanism of the regenerative enteropathy of early infection. J Infect Dis 197:420-429.

296. Pruijssers AJ, Hengel H, Abel TW, Dermody TS. 2013. Apoptosis induction influences reovirus replication and virulence in newborn mice. J. Virol. 87:12980-12989.

297. Zou WY, Blutt SE, Crawford SE, Ettayebi K, Zeng XL, Saxena K, Ramani S, Karandikar UC, Zachos NC, Estes MK. 2017. Human intestinal enteroids: New models to study gastrointestinal virus infections. Methods Mol Biol.

298. Ettayebi K, Crawford SE, Murakami K, Broughman JR, Karandikar U, Tenge VR, Neill FH, Blutt SE, Zeng XL, Qu L, Kou B, Opekun AR, Burrin D, Graham DY, Ramani S, Atmar RL, Estes MK. 2016. Replication of human noroviruses in stem cell-derived human enteroids. Science 353:1387-1393.

299. Drummond CG, Bolock AM, Ma C, Luke CJ, Good M, Coyne CB. 2017. Enteroviruses infect human enteroids and induce antiviral signaling in a cell lineage-specific manner. Proc Natl Acad Sci U S A 114:1672-1677.

300. Tyler KL, Squier MKT, Brown AL, Pike B, Willis D, Oberhaus SM, Dermody TS, Cohen JJ. 1996. Linkage between reovirus-induced apoptosis and inhibition of cellular DNA synthesis: role of the S1 and M2 genes. J. Virol. 70:7984-7991.

301. Rubin DH, Fields BN. 1980. Molecular basis of reovirus virulence. Role of the M2 gene. J Exp Med 152:853-868.

302. Arnold M, Patton JT, McDonald SM. 2009. Culturing, storage, and quantification of rotaviruses. Curr Protoc Microbiol Chapter 15:Unit 15C 13.

303. Virgin HWt, Bassel-Duby R, Fields BN, Tyler KL. 1988. Antibody protects against lethal infection with the neurally spreading reovirus type 3 (Dearing). J. Virol. 62:4594-4604.

304. Furlong DB, Nibert ML, Fields BN. 1988. Sigma 1 protein of mammalian reoviruses extends from the surfaces of viral particles. J. Virol. 62:246-256.

305. Smith RE, Zweerink HJ, Joklik WK. 1969. Polypeptide components of virions, top component and cores of reovirus type 3. Virology 39:791-810.

306. De Laurenzi V, Melino G. 2001. Gene disruption of tissue transglutaminase. Mol Cell Biol 21:148-155.

307. Wetzel JD, Chappell JD, Fogo AB, Dermody TS. 1997. Efficiency of viral entry determines the capacity of murine erythroleukemia cells to support persistent infections by mammalian reoviruses. J. Virol. 71:299-306.

308. Barton ES, Connolly JL, Forrest JC, Chappell JD, Dermody TS. 2001. Utilization of sialic acid as a coreceptor enhances reovirus attachment by multistep adhesion strengthening. J. Biol. Chem. 276:2200-2211.

309. Sato T, Vries RG, Snippert HJ, van de Wetering M, Barker N, Stange DE, van Es JH, Abo A, Kujala P, Peters PJ, Clevers H. 2009. Single Lgr5 stem cells build crypt-villus structures in vitro without a mesenchymal niche. Nature 459:262-265.

310. Broere F, du Pre MF, van Berkel LA, Garssen J, Schmidt-Weber CB, Lambrecht BN, Hendriks RW, Nieuwenhuis EE, Kraal G, Samsom JN. 2009. Cyclooxygenase-2 in mucosal DC mediates induction of regulatory T cells in the intestine through suppression of IL-4. Mucosal immunology 2:254-264.

311. DiRaimondo TR, Klock C, Warburton R, Herrera Z, Penumatsa K, Toksoz D, Hill N, Khosla C, Fanburg B. 2014. Elevated transglutaminase 2 activity is associated with hypoxia-induced experimental pulmonary hypertension in mice. ACS chemical biology 9:266-275.

312. Smyth GK. 2004. Linear models and empirical bayes methods for assessing differential expression in microarray experiments. Statistical applications in genetics and molecular biology 3:Article3.

313. Benjamini Y, Hochberg Y. 1995. Controlling the false discovery rate: A practical and powerful approach to multiple testing. J. Roy. Stat. Soc. Ser. B. (Stat. Method.) 57:289-300.

314. Sedgewick R, Wayne KD. 2011. Algorithms, 4th ed. Addison-Wesley, Upper Saddle River, NJ.

315. Kim D, Pertea G, Trapnell C, Pimentel H, Kelley R, Salzberg SL. 2013. TopHat2: Accurate alignment of transcriptomes in the presence of insertions, deletions and gene fusions. Genome Biol 14:R36.

316. Li B, Dewey CN. 2011. RSEM: Accurate transcript quantification from RNA-Seq data with or without a reference genome. BMC Bioinformatics 12:323.

317. McCarthy DJ, Chen Y, Smyth GK. 2012. Differential expression analysis of multifactor RNA-Seq experiments with respect to biological variation. Nucleic Acids Res 40:4288-4297.

318. Smeekens SP, Ng A, Kumar V, Johnson MD, Plantinga TS, van Diemen C, Arts P, Verwiel ET, Gresnigt MS, Fransen K, van Sommeren S, Oosting M, Cheng SC, Joosten LA, Hoischen A, Kullberg BJ, Scott WK, Perfect JR, van der Meer JW, Wijmenga C, Netea MG, Xavier RJ. 2013. Functional genomics identifies type I interferon pathway as central for host defense against Candida albicans. Nature communications 4:1342.

319. Hitomi J, Christofferson DE, Ng A, Yao J, Degterev A, Xavier RJ, Yuan J. 2008. Identification of a molecular signaling network that regulates a cellular necrotic cell death pathway. Cell 135:1311-1323.

320. DeJesus R, Moretti F, McAllister G, Wang Z, Bergman P, Liu S, Frias E, Alford J, Reece-Hoyes JS, Lindeman A, Kelliher J, Russ C, Knehr J, Carbone W, Beibel M, Roma G, Ng A, Tallarico JA, Porter JA, Xavier RJ, Mickanin C, Murphy LO, Hoffman GR, Nyfeler B. 2016. Functional CRISPR screening identifies the ufmylation pathway as a regulator of SQSTM1/p62. eLife 5.

321. Lord PW, Stevens RD, Brass A, Goble CA. 2003. Investigating semantic similarity measures across the Gene Ontology: The relationship between sequence and annotation. Bioinformatics 19:1275-1283.

322. Schlicker A, Domingues FS, Rahnenfuhrer J, Lengauer T. 2006. A new measure for functional similarity of gene products based on Gene Ontology. BMC Bioinformatics 7:302.

AMERICAN SOCIETY FOR MICROBIOLOGY | Journal of Virology®

Expression of *Ifnlr1* on Intestinal Epithelial Cells Is Critical to the Antiviral Effects of Interferon Lambda against Norovirus and Reovirus

Megan T. Baldridge,[a]* Sanghyun Lee,[a] Judy J. Brown,[b] Nicole McAllister,[c] Kelly Urbanek,[d] Terence S. Dermody,[c,d] Timothy J. Nice,[e] Herbert W. Virgin[a]

Department of Pathology and Immunology, Washington University School of Medicine, St. Louis, Missouri, USA[a]; Department of Pathology, Microbiology, and Immunology, Vanderbilt University Medical Center, Nashville, Tennessee, USA[b]; Department of Microbiology and Molecular Genetics, University of Pittsburgh School of Medicine, Pittsburgh, Pennsylvania, USA[c]; Department of Pediatrics, University of Pittsburgh School of Medicine, Pittsburgh, Pennsylvania, USA[d]; Department of Molecular Microbiology and Immunology, Oregon Health and Science University, Portland, Oregon, USA[e]

ABSTRACT Lambda interferon (IFN-λ) has potent antiviral effects against multiple enteric viral pathogens, including norovirus and rotavirus, in both preventing and curing infection. Because the intestine includes a diverse array of cell types, however, the cell(s) upon which IFN-λ acts to exert its antiviral effects is unclear. Here, we sought to identify IFN-λ-responsive cells by generation of mice with lineage-specific deletion of the receptor for IFN-λ, *Ifnlr1*. We found that expression of IFNLR1 on intestinal epithelial cells (IECs) in the small intestine and colon is required for enteric IFN-λ antiviral activity. IEC *Ifnlr1* expression also determines the efficacy of IFN-λ in resolving persistent murine norovirus (MNoV) infection and regulates fecal shedding and viral titers in tissue. Thus, the expression of *Ifnlr1* by IECs is necessary for the response to both endogenous and exogenous IFN-λ. We further demonstrate that IEC *Ifnlr1* expression is required for the sterilizing innate immune effects of IFN-λ by extending these findings in *Rag1*-deficient mice. Finally, we assessed whether our findings pertained to multiple viral pathogens by infecting mice specifically lacking IEC *Ifnlr1* expression with reovirus. These mice phenocopied *Ifnlr1*-null animals, exhibiting increased intestinal tissue titers and enhanced reovirus fecal shedding. Thus, IECs are the critical cell type responding to IFN-λ to control multiple enteric viruses. This is the first genetic evidence that supports an essential role for IECs in IFN-λ-mediated control of enteric viral infection, and these findings provide insight into the mechanism of IFN-λ-mediated antiviral activity.

IMPORTANCE Human noroviruses (HNoVs) are the leading cause of epidemic gastroenteritis worldwide. Type III interferons (IFN-λ) control enteric viral infections in the gut and have been shown to cure mouse norovirus, a small-animal model for HNoVs. Using a genetic approach with conditional knockout mice, we identified IECs as the dominant IFN-λ-responsive cells in control of enteric virus infection *in vivo*. Upon murine norovirus or reovirus infection, *Ifnlr1* depletion in IECs largely recapitulated the phenotype seen in *Ifnlr1*$^{-/-}$ mice of higher intestinal tissue viral titers and increased viral shedding in the stool. Moreover, IFN-λ-mediated sterilizing immunity against murine norovirus requires the capacity of IECs to respond to IFN-λ. These findings clarify the mechanism of action of this cytokine and emphasize the therapeutic potential of IFN-λ for treating mucosal viral infections.

KEYWORDS innate immunity, interferons, mucosal immunity, norovirus, reovirus

Received 27 October 2016 **Accepted** 6 January 2017

Accepted manuscript posted online 11 January 2017

Citation Baldridge MT, Lee S, Brown JJ, Mcallister N, Urbanek K, Dermody TS, Nice TJ, Virgin HW. 2017. Expression of *Ifnlr1* on intestinal epithelial cells is critical to the antiviral effects of interferon lambda against norovirus and reovirus. J Virol 91:e02079-16. https://doi.org/10.1128/JVI.02079-16.

Editor Susana López, Instituto de Biotecnologia/UNAM

Address correspondence to Timothy J. Nice, nice@ohsu.edu, or Herbert W. Virgin, virgin@wustl.edu.

* Present address: Megan T. Baldridge, Department of Medicine, Washington University School of Medicine, St. Louis, Missouri, USA.

M.T.B. and S.L. contributed equally to this work.

Norovirus and rotavirus are viral pathogens that infect at mucosal surfaces and induce gastroenteritis, characterized by vomiting, diarrhea, and malaise (1, 2). Viral gastroenteritis causes significant morbidity and mortality in children, the elderly, and immunocompromised persons, thus representing a substantial health care burden (3, 4). Treatments for these illnesses have been limited thus far to symptomatic care, including rehydration, because currently there is no specific antiviral therapy for these viral pathogens. Lambda interferon (IFN-λ; also called type III IFN) is an antiviral cytokine that regulates viral infection at mucosal surfaces and in the liver and brain (5–8). Administration of recombinant IFN-λ can prevent and resolve viral infections in the gastrointestinal tract (8, 9) and at other sites in mice (10). These effects are observed for murine norovirus (MNoV) in mice lacking adaptive immunity, thus representing sterilizing innate immunity in the intestine (8). These studies indicate the potential for IFN-λ as a therapeutic for viral infections, including those causing gastroenteritis, in humans, including immunocompromised hosts (11). Better understanding of the mechanisms by which this antiviral cytokine functions is essential to understanding basic mechanisms of intestinal control of viral infection and for potential therapeutic application in humans.

Binding of IFN-λ to its receptor, a heterodimer of interleukin-10R2 (IL-10R2) and IFNLR1 (12, 13), induces an antiviral gene expression program similar to that induced by type I IFN, with substantial overlap in gene sets *in vitro* (10, 14, 15). However, type I and III IFNs exhibit unique antiviral properties *in vivo*. *Ifnlr1*$^{-/-}$ mice exhibit elevated intestinal tissue replication and enhanced fecal shedding of a persistent strain of MNoV (8, 16), a model virus which allows for more tractable *in vitro* and *in vivo* analyses than human norovirus (reviewed in references 17 and 18). Recombinant IFN-λ treatment is sufficient to prevent and cure MNoV infection (8). In contrast, mice deficient for *Ifnar1* (the receptor for type I IFNs) show enhanced extraintestinal spread of virus, but levels of MNoV fecal shedding are comparable to those of wild-type mice (8, 16). Similarly, IFNLR1 restricts growth in the epithelium and fecal shedding of reovirus, while IFNAR1 instead regulates reovirus growth in the lamina propria (19). IFN-λ exhibits an antiviral role exclusive of type I IFNs against a murine rotavirus strain (9) but cooperates with type I IFNs to limit intestinal replication of a heterologous simian strain in neonatal but not adult mice (20). These findings indicate the likely importance of tissue compartment-, development-, and cell type-specific effects of type I and III IFNs *in vivo*. These effects may be secondary to unique virulence factors that counter specific IFNs or to differential expression of the IFN receptors (21, 22).

IFNAR1 is thought to be expressed ubiquitously and at especially high levels on cells of hematopoietic origin (reviewed in references 23 and 24), whereas expression of detectable IFNLR1 appears to be limited to mucosal epithelial cells (25), human hepatocytes (6), and neutrophils (26). Although IFNLR1 expression on peripheral leukocytes has also been reported, it does not appear to be functional (27). Upon IFN-λ treatment, IFN-stimulated genes accumulate in intestinal epithelial cells (IECs), indicating functional IFNLR1 expression (9, 19, 20). In contrast, in IECs of adult mice, IFNAR1 may be expressed at lower levels or alternately trafficked, such as only to the apical portion of the cell (9, 20). Differential receptor expression thus could account for complementary roles for different IFNs in protection against systemic infection (type I) and infection of mucosal (type III) sites. Importantly, however, it has been reported that cells that do not express detectably high levels of IFNLR1, such as the endothelial cells of the blood-brain barrier, may still respond to endogenous and exogenous IFN-λ with protective antiviral effects (10). Thus, to successfully identify the cell types required for the antiviral response to IFN-λ, analysis of receptor expression levels may be insufficient, and definitive resolution requires a genetic approach to selectively delete receptor expression in specific cell types.

To identify the cell types that respond to IFN-λ *in vivo* in the intestine, we generated mice with a conditional mutant allele for *Ifnlr1* and crossed them to mice expressing Cre recombinase via the action of different cell type-specific promoters (Table 1). *Ifnlr1* was targeted in cell types expected to express high receptor levels (intestinal epithelial cells

TABLE 1 Mouse lines, nomenclature, and cell types targeted by specific Cre lines

Ifnlr1 and Cre mouse line(s)	Line name[a]	Cell type(s) targeted (reference)
Ifnlr1^{tm1Palu}; no Cre line	*Ifnlr1*$^{-/-}$	All cells (28)
Ifnlr1$^{tm1a(EUCOMM)Wtsi}$; Villin-Cre	*Ifnlr1*$^{f/f}$*-Villincre*	Intestinal epithelial cells (29)
Ifnlr1$^{tm1a(EUCOMM)Wtsi}$; MRP8-Cre	*Ifnlr1*$^{f/f}$*-MRP8cre*	Neutrophils (30)
Ifnlr1$^{tm1a(EUCOMM)Wtsi}$; CD11c-Cre	*Ifnlr1*$^{f/f}$*-CD11ccre*	Dendritic cells and alveolar macrophages (31)
Ifnlr1$^{tm1a(EUCOMM)Wtsi}$; LysM-Cre	*Ifnlr1*$^{f/f}$*-LysMcre*	Macrophages, neutrophils, some dendritic cells (32, 33)
Ifnlr1$^{tm1a(EUCOMM)Wtsi}$; Deleter-Cre	*Ifnlr1*$^{f-/-}$	All cells (34)

[a]A conditional allele of *Ifnlr1* (*Ifnlr1*$^{f/f}$) was crossed to multiple different Cre lines for lineage-specific deletion of *Ifnlr1* in the specific cell types.

[25] and neutrophils [26]) and cells that are known to be permissive for MNoV replication in tissue culture (macrophages and dendritic cells [35]). Of all the cell types tested, only intestinal epithelial cells (IECs) required expression of *Ifnlr1* for the antiviral effects of IFN-λ against MNoV. To show the generality of our findings, we demonstrated the importance of IEC expression of this receptor for control of reovirus infection. This is the first study to genetically define IFN-λ-responsive cells *in vivo* in the context of two independent mucosal viral infections. This study also confirms that the cells required for responding to endogenous IFN-λ to attenuate MNoV infection are the same as those that respond to exogenous IFN-λ administration, including in the elicitation of sterilizing innate immunity.

RESULTS

***Ifnlr1* is expressed in the epithelial fraction along the length of the gastrointestinal tract.** Tissue from adult mice homozygous for a null mutation in *Ifnlr1* (28) or wild-type controls was collected from sites along the intestine, lung, mesenteric lymph node (MLN), or spleen (Fig. 1A). The small intestine was also dissociated into epithelial and lamina propria fractions as previously described (36), and RNA was isolated from

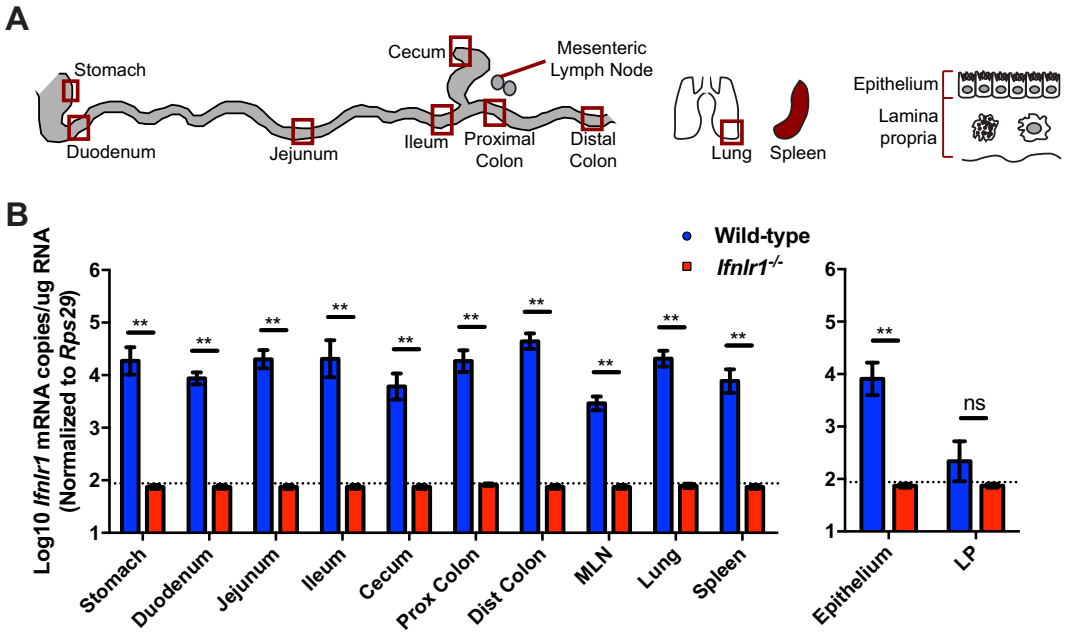

FIG 1 *Ifnlr1* is expressed in the epithelial fraction along the length of the intestine. (A) RNA was isolated from sites along the intestine and the lung, indicated by red boxes, whole mesenteric lymph node (MLN) and spleen, and epithelial and lamina propria (LP) fractions of the small intestine from *Ifnlr1*-sufficient and -deficient mice. (B) *Ifnlr1* expression was quantified by quantitative real-time PCR of RNA from sites depicted in panel A. $n = 4$ to 6 samples per group, from two independent experiments, analyzed by Mann-Whitney test. **, $P < 0.01$; ns, not significant. Prox, proximal; dist, distal.

these fractions and tissues. Expression of *Ifnlr1* was detected by quantitative real-time PCR of cDNA generated from these RNA samples. We found that *Ifnlr1* was expressed along the length of the intestine and in the lung, as well as in systemic tissues, including MLN and spleen (Fig. 1B). Intestinal *Ifnlr1* expression was substantially enriched (at least 30-fold; $P = 0.0381$) in the epithelial fraction compared to the lamina propria fraction (Fig. 1B), consistent with previous reports (9, 25). As expected, no transcript was detected in any tissue in *Ifnlr1*$^{-/-}$ mice (Fig. 1B).

***Ifnlr1* expression in the small and large intestine is significantly diminished in *Ifnlr1*$^{f/f}$*-Villincre* mice.** Embryonic stem (ES) cells targeted with a construct containing sequences homologous to *Ifnlr1*, an FLP recombinant target (FRT)-flanked *lacZ* and neomycin cassette, and loxP sites flanking exon 2 were provided by the Wellcome Trust Sanger Institute (Fig. 2A). Mice derived from these ES cells were crossed with mice expressing Flp recombinase for deletion of the FRT-flanked cassette (38), leaving a conditional allele of *Ifnlr1*, referred to as *Ifnlr1*^{f} (Fig. 2A). Following removal of the floxed region in cells expressing Cre, the resulting transcript is predicted to produce a truncated protein product (Fig. 2B). For disruption in specific cell lineages, *Ifnlr1*$^{f/f}$ mice were crossed with various Cre mouse lines (Table 1). For each line, Cre(+) *Ifnlr1*$^{f/f}$ mice were compared to Cre(−) *Ifnlr1*$^{f/f}$ littermates to assess the effects of cell type-specific deletion upon *Ifnlr1* expression along the intestine and in extraintestinal tissues (Fig. 1A). *Ifnlr1*$^{f/f}$*-Villincre* mice showed significantly diminished *Ifnlr1* expression in the small and large intestine (Fig. 2C). Fractionation of the small intestine into epithelial and lamina propria fractions revealed efficient deletion of *Ifnlr1* in the epithelium of these mice (Fig. 2C). In contrast, *Ifnlr1*$^{f/f}$*-MRP8cre*, *Ifnlr1*$^{f/f}$*-LysMcre*, and *Ifnlr1*$^{f/f}$*-CD11ccre* mice showed no alterations in intestinal *Ifnlr1* expression at the level of the whole tissues tested (Fig. 2D, E, and F). *Ifnlr1*$^{f/f}$*-MRP8cre*, *Ifnlr1*$^{f/f}$*-LysMcre*, and *Ifnlr1*$^{f/f}$*-CD11ccre* mice did exhibit substantial depletion of *Ifnlr1* in their respectively targeted cell types of neutrophils (~85%), macrophages (~91%), and dendritic cells (~85%), consistent with a previous report (39) (Fig. 2D, E, and F). Expression of *Ifnlr1* remained unchanged in lung, MLN, spleen, stomach, and duodenum in *Ifnlr1*$^{f/f}$*-Villincre* mice, indicating expression of Cre specific to distal small intestine and colon (Fig. 2C), consistent with previous reports (29, 40).

Expression of *Ifnlr1* in intestinal epithelium regulates MNoV shedding and response to recombinant IFN-λ. *Ifnlr1*$^{-/-}$ mice and wild-type controls were inoculated with CR6, a persistent strain of MNoV that replicates well in the intestine, is shed into the feces at readily detectable levels, and is sensitive to treatment with IFN-λ (8, 41). As described previously (8), *Ifnlr1*$^{-/-}$ mice allow higher levels of fecal MNoV shedding than do wild-type mice at early time points (Fig. 3A and G) and are insensitive to IFN-λ treatment, although this treatment terminates MNoV replication in wild-type mice (Fig. 3A). These results were also observed in a novel *Ifnlr1*-deficient mouse model (*Ifnlr1*$^{f-/-}$) (Table 1 and Fig. 3B). This assay was next applied to the four mouse strains with lineage-specific deletion of *Ifnlr1* (Table 1). *Ifnlr1*$^{f/f}$*-Villincre* mice phenocopied *Ifnlr1*$^{-/-}$ and *Ifnlr1*$^{f-/-}$ mice, exhibiting both elevated fecal shedding of MNoV and resistance to IFN-λ treatment (Fig. 3C). In contrast, *Ifnlr1*$^{f/f}$*-MRP8cre*, *Ifnlr1*$^{f/f}$-LysM*cre*, and *Ifnlr1*$^{f/f}$-CD11c*cre* mice exhibited viral loads and response to IFN-λ equivalent to those of *Ifnlr1*$^{f/f}$ controls (Fig. 3D, E, and F). At day 7 postinoculation, IFNLR1 regulated fecal shedding of MNoV, as seen by comparing wild-type and *Ifnlr1*$^{-/-}$ levels (Fig. 3G). *Ifnlr1*$^{f/f}$*-Villincre* mice allowed fecal shedding equivalent to *Ifnlr1*$^{-/-}$ and *Ifnlr1*$^{f-/-}$ mice, suggesting that control of MNoV fecal shedding can be fully accounted for by IFNLR1 in Villin-expressing cells (Fig. 3G). Similarly, *Ifnlr1*$^{f/f}$*-Villincre* mice exhibited no difference in comparison to *Ifnlr1*$^{-/-}$ and *Ifnlr1*$^{f-/-}$ mice along the full time course of infection (Fig. 3H).

Expression of *Ifnlr1* in intestinal epithelium is essential for induction of IFN-λ-mediated sterilizing innate immunity to MNoV infection. We previously reported that recombinant IFN-λ can cure persistently infected mice in the absence of adaptive immunity (8). To determine whether expression of *Ifnlr1* in IECs is required for IFN-λ-mediated sterilizing innate immunity to persistent MNoV infection, we established

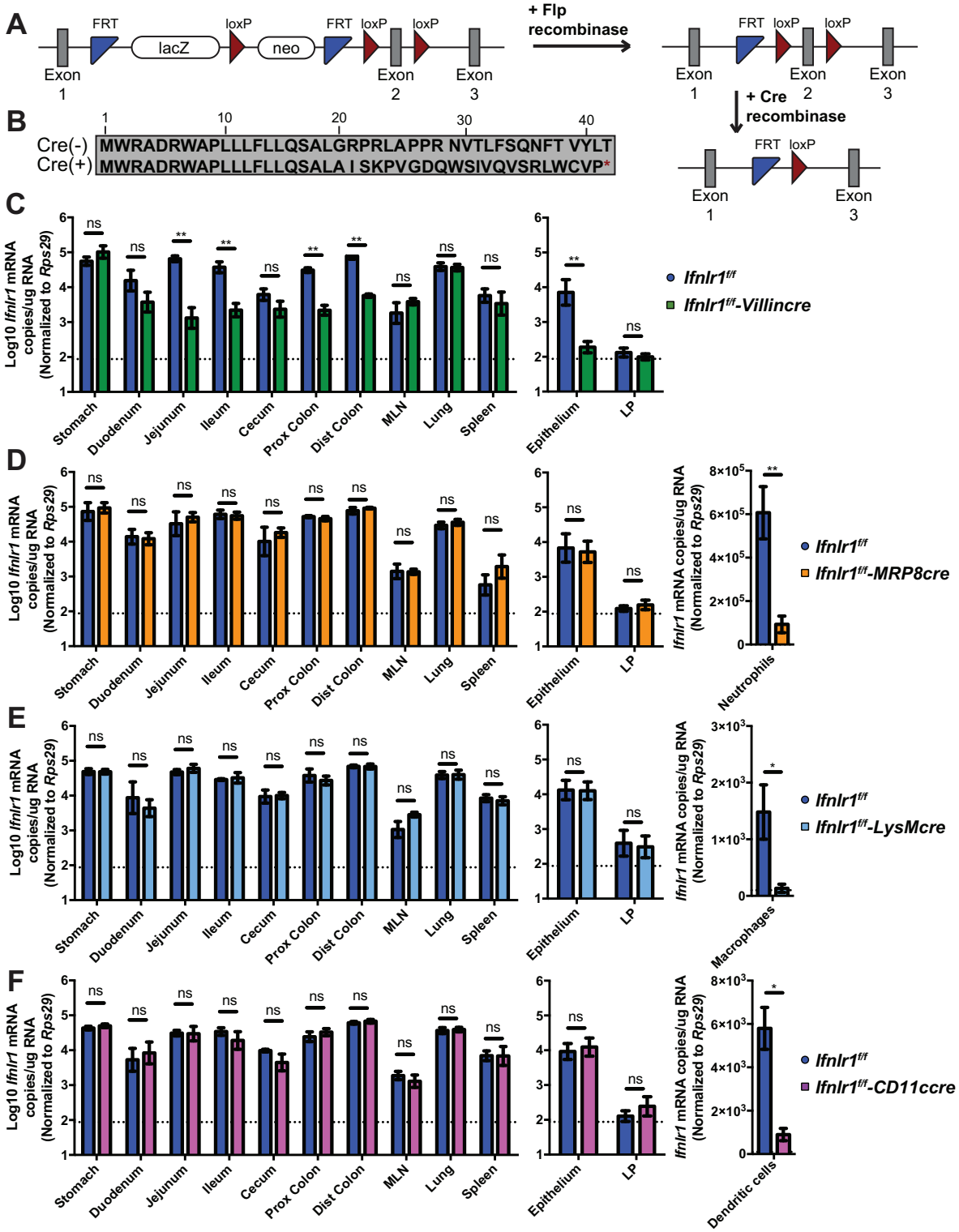

FIG 2 *Ifnlr1* expression is decreased in the small and large intestines of *Ifnlr1*$^{f/f}$*-Villincre* mice. (A) Schematic depicting the *Ifnlr1* gene locus in *Ifnlr1*$^{tm1a(EUCOMM)Wtsi}$ mice. After crossing with mice expressing Flp recombinase (+Flp recombinase), the region between the two FRT sites was deleted, leaving conditional-ready *Ifnlr1*$^{f/f}$ mice. In the absence of Cre, all exons are present. With the addition of Cre recombinase, the floxed exon 2 is deleted. (B) In the absence of Cre [Cre(−)], the IFNLR1 protein is expressed. In the presence of Cre [Cre(+)], the protein sequence is altered at amino acid 20 and a premature stop codon is introduced at amino acid 42. (C to F) *Ifnlr1* expression was assessed by quantitative real-time PCR of sites along the intestine and the lung, MLN and spleen, and epithelial and LP fractions from *Ifnlr1*$^{f/f}$*-Villincre* (C), *Ifnlr1*$^{f/f}$*-MRP8cre* (D), *Ifnlr1*$^{f/f}$*-LysMcre* (E), and *Ifnlr1*$^{f/f}$*-CD11ccre* (F) mice compared to their *Ifnlr1*$^{f/f}$ littermates. *Ifnlr1* expression was also assessed by quantitative real-time PCR of isolated bone marrow neutrophils from *Ifnlr1*$^{f/f}$*-MRP8cre* (D), splenic macrophages from *Ifnlr1*$^{f/f}$*-LysMcre* (E), and splenic dendritic cells from *Ifnlr1*$^{f/f}$*-CD11ccre* (F) mice compared to their *Ifnlr1*$^{f/f}$ littermates. $n = 4$ to 7 samples per group, from two independent experiments, analyzed by Mann-Whitney test. *, $P < 0.05$; **, $P < 0.01$; ns, not significant.

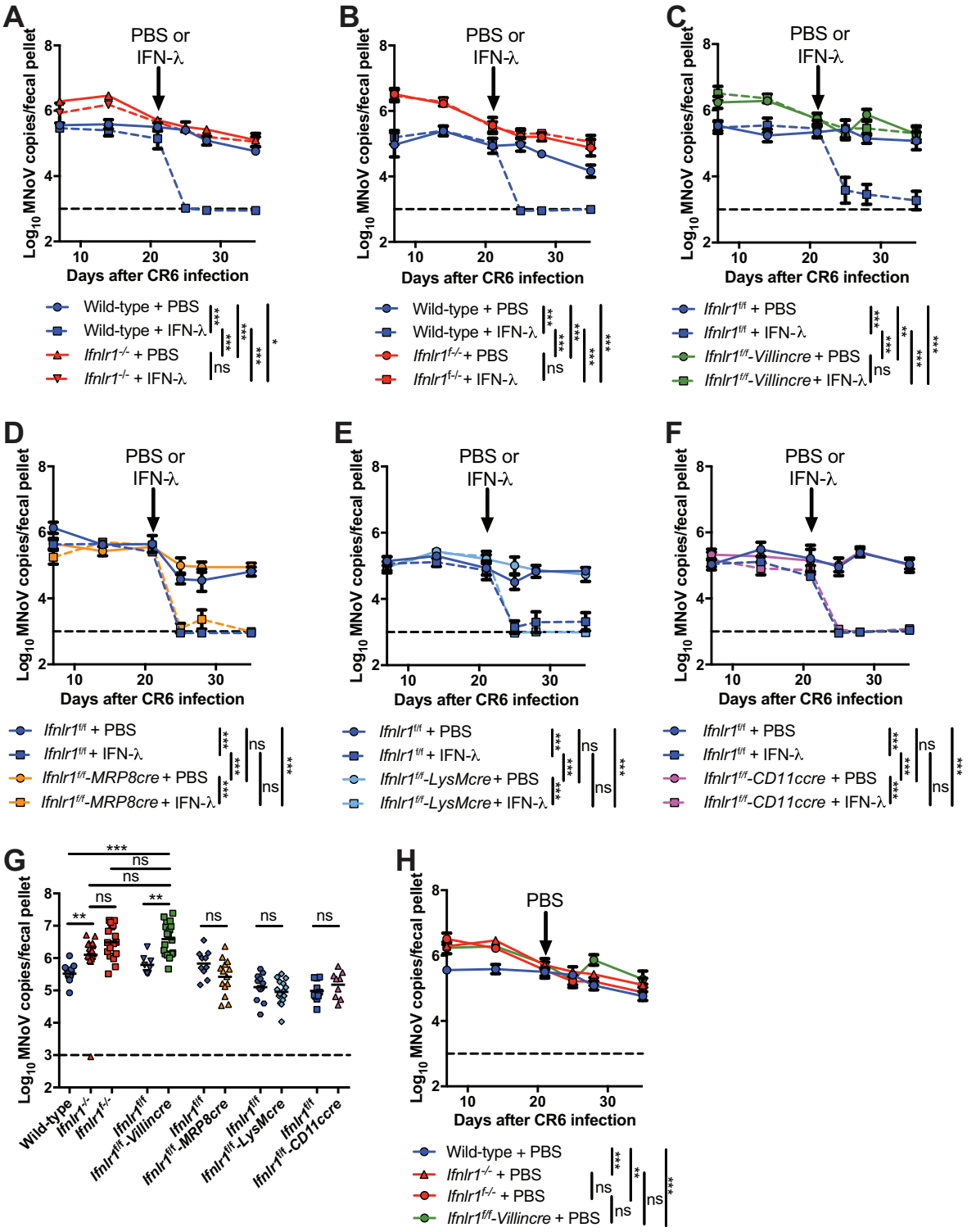

FIG 3 Expression of *Ifnlr1* on intestinal epithelial cells is required for the antiviral effects of endogenous and exogenous IFN-λ against MNoV. (A to E) Time course of MNoV genome copies shed into fecal pellets with time points at 7, 14, 21, 24, 28, and 35 days after CR6 infection. PBS or recombinant IFN-λ was injected intraperitoneally on day 21 into wild-type and $Ifnlr1^{-/-}$ (A), wild-type and $Ifnlr1^{f-/-}$ (B), $Ifnlr1^{f/f}$-*Villincre* (C), $Ifnlr1^{f/f}$-*MRP8cre* (D), $Ifnlr1^{f/f}$-*LysMcre* (E), or $Ifnlr1^{f/f}$-*CD11ccre* (F) mice and their $Ifnlr1^{f/f}$ littermates. $n = 6$ to 12 mice per group, from two to three independent experiments, analyzed by two-way ANOVA followed by Tukey's multiple-comparison test; a P value of <0.001 by ANOVA column factor was found for panels A to F. (G) Individual data points depicting MNoV genome copies shed into fecal pellets on day 7 from panels A to F. $n = 9$ to 21 mice per group, from two to three independent experiments, analyzed by one-way ANOVA followed by Tukey's multiple-comparison test; a P value of <0.001 was determined by ANOVA. (H) Fecal shedding data from PBS-treated mice in panels A to C is shown superimposed to facilitate comparison between strains. $n = 8$ to 11 mice per group, from two to three independent experiments, analyzed by two-way ANOVA followed by Tukey's multiple-comparison test; a P value of <0.001 was determined by ANOVA column factor. *, $P < 0.05$; **, $P < 0.01$; ***, $P < 0.001$; ns, not significant.

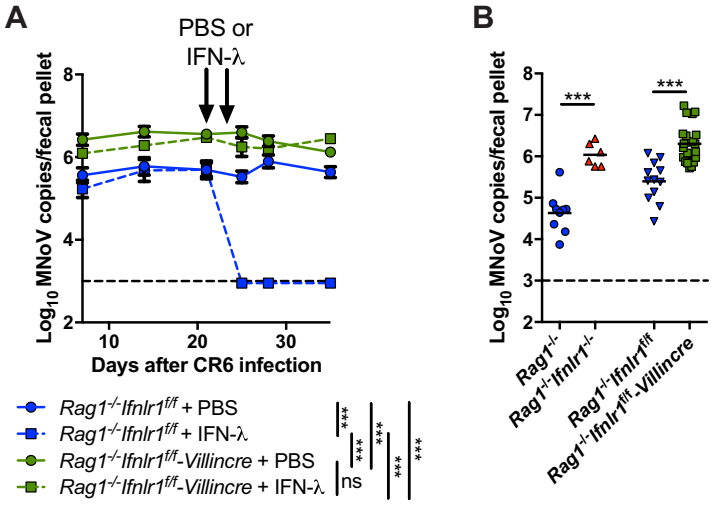

FIG 4 Expression of *Ifnlr1* on intestinal epithelial cells is required for the antiviral effects of IFN-λ against MNoV in the absence of adaptive immunity. (A) Time course of MNoV genome copies shed into fecal pellets with time points at 7, 14, 21, 24, 28, and 35 days after CR6 infection. PBS or recombinant IFN-λ was injected intraperitoneally on day 21 and day 23 into *Rag1*$^{-/-}$ *Ifnlr1*$^{f/f}$*-Villincre* or *Rag1*$^{-/-}$ *Ifnlr1*$^{f/f}$ mice. $n = 6$ to 14 mice per group, combined from three independent experiments, analyzed by two-way ANOVA followed by Tukey's multiple-comparison test; a P value of <0.001 was found by ANOVA column factor. (B) Individual data points depicting MNoV genome copies shed into fecal pellets on day 7 from *Rag1*$^{-/-}$, *Rag1*$^{-/-}$ *Ifnlr1*$^{-/-}$ double knockouts or mice depicted in panel A. $n = 6$ to 22 mice per group, combined from two to three independent experiments, analyzed by Mann-Whitney test. ***, $P < 0.001$; ns, not significant.

Rag1$^{-/-}$ *Ifnlr1*$^{f/f}$*-Villincre* conditional double knockout mice. *Rag1*$^{-/-}$ *Ifnlr1*$^{f/f}$*-Villincre* mice were orally inoculated with CR6, and viral shedding in the stool was quantified by quantitative PCR (qPCR). *Rag1*$^{-/-}$ *Ifnlr1*$^{f/f}$*-Villincre* mice showed increased viral shedding throughout the infection time course (Fig. 4A). Injection of recombinant IFN-λ terminated MNoV replication in *Rag1*$^{-/-}$ *Ifnlr1*$^{f/f}$ mice but did not affect MNoV loads in *Rag1*$^{-/-}$ *Ifnlr1*$^{f/f}$*-Villincre* mice (Fig. 4A). At 7 days postinoculation, *Rag1*$^{-/-}$ *Ifnlr1*$^{f/f}$*-Villincre* mice had significantly higher viral shedding than *Rag1*$^{-/-}$ *Ifnlr1*$^{f/f}$ mice, and the level of viral shedding in *Rag1*$^{-/-}$ *Ifnlr1*$^{f/f}$*-Villincre* mice was comparable to the level of viral shedding in *Rag1*$^{-/-}$ *Ifnlr1*$^{-/-}$ mice (Fig. 4B). Therefore, IFN-λ responses in IECs limited persistent MNoV infection in the absence of adaptive immunity, and IFN-λ signaling in IECs was essential for clearance of persistently infected MNoV by IFN-λ-mediated sterilizing innate immunity.

Control of reovirus in intestinal tissue by IFN-λ depends upon the expression of *Ifnlr1* in epithelial cells. To assess whether *Ifnlr1* expression on IECs was required for control of other enteric pathogens, *Ifnlr1*$^{-/-}$ and *Ifnlr1*$^{f/f}$*-Villincre* mice were orally inoculated with 10^8 PFU of reovirus strain type 1 Lang (T1L). At 4 days postinfection, viral titers in small intestinal tissues, including duodenum, jejunum, and ileum, as well as viral shedding in stools, were significantly higher in *Ifnlr1*$^{-/-}$ mice (Fig. 5A and B), consistent with a previous report using another strain of reovirus, type 3 Dearing (19). Control of reovirus was predominantly through the expression of IFNLR1 on IECs, as *Ifnlr1*$^{f/f}$*-Villincre* mice displayed increased titers of reovirus in small intestinal tissues as well as enhanced fecal shedding (Fig. 5A and B). These results demonstrate that expression of IFNLR1 in epithelial cells is essential for the control of reovirus infection by IFN-λ in the gut and indicate that IFN-λ signaling in IECs is an antiviral mechanism common to multiple enteric viral pathogens.

Interferon-stimulated gene expression in the intestine depends upon the expression of *Ifnlr1* in epithelial cells. Ileum and proximal colon tissues were isolated from wild-type (WT), *Ifnlr1*$^{-/-}$, *Ifnlr1*$^{f/f}$, and *Ifnlr1*$^{f/f}$*-Villincre* mice 1 day posttreatment with either PBS or IFN-λ. These tissues were then assessed for expression of canonical antiviral interferon-stimulated genes (ISGs) *Oas1a* (42), *Ifit1* (43), and *Ifi44* (44) (Fig. 6A

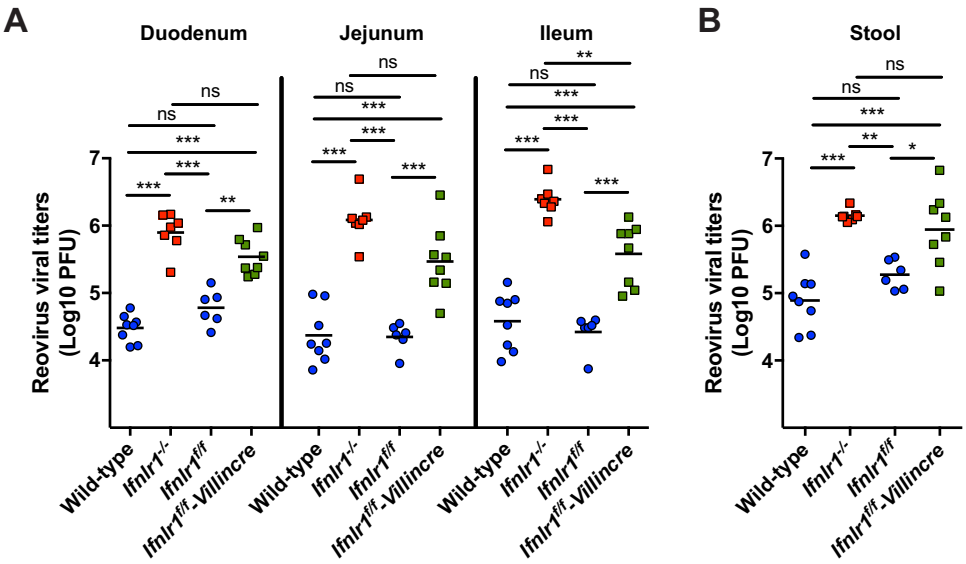

FIG 5 *Ifnlr1* expression on intestinal epithelial cells limits reovirus infection. (A and B) Titers of reovirus strain T1L were assessed at day 4 postinoculation in the different compartments of the small intestine (A) and stool (B) from wild-type, *Ifnlr1*$^{-/-}$, *Ifnlr1*$^{f/f}$*-Villincre*, and *Ifnlr1*$^{f/f}$ littermate control mice. The small intestine was resected from the pylorus to the cecum and sectioned into three equal parts, representing the duodenum, jejunum, and ileum. Titers are expressed as PFU per milliliter of tissue homogenate or gram of stool. $n = 6$ to 8 mice per group, combined from two independent experiments, analyzed by one-way ANOVA followed by Tukey's multiple-comparison test; a P value of <0.001 was determined by ANOVA column factor for all tissues and stool. *, $P < 0.05$; **, $P < 0.01$; ***, $P < 0.001$; ns, not significant.

to C). While intestinal tissues from WT and *Ifnlr1*$^{f/f}$ mice exhibited robust ISG induction in response to IFN-λ treatment, tissues from *Ifnlr1*$^{-/-}$ and *Ifnlr1*$^{f/f}$*-Villincre* mice failed to significantly upregulate these ISGs in response to IFN-λ. These data correlate with the impaired antiviral response against MNoV in *Ifnlr1*$^{-/-}$ and *Ifnlr1*$^{f/f}$*-Villincre* mice after IFN-λ treatment (Fig. 3A and C), consistent with a potentially critical role for IFNLR1 expression on epithelial cells for induction of antiviral ISGs in response to IFN-λ treatment.

DISCUSSION

In this study, we found that IECs are the predominant cell type expressing *Ifnlr1* in the small intestine and colon and that this cell type plays a major role in IFN-λ-mediated antiviral immunity in the intestine. Antiviral immunity elicited by IFN-λ to enteric reovirus and norovirus infection depends upon IFNLR1 signaling in Villin-positive IECs. Using four mouse strains with lineage-specific deletion of *Ifnlr1* to study persistent infection and IFN-λ-mediated clearance, we found that only *Ifnlr1*$^{f/f}$*-Villincre* mice exhibited a complete phenocopy of *Ifnlr1*$^{-/-}$ mice. Targeting *Ifnlr1* in other cells, including dendritic cells, macrophages, and neutrophils, had no detectable effect on basal levels of viral shedding or IFN-λ-mediated clearance of MNoV. The dominant IFN-λ-dependent antiviral contribution by IECs also was confirmed with reovirus infection. In studies using reovirus T1L, we observed viral titers in the small intestine of *Ifnlr1*$^{f/f}$*-Villincre* mice increased comparably to those detected in *Ifnlr1*$^{-/-}$ mice, although we cannot rule out a minor role for other IFN-λ-responding cells in the ileum. Therefore, IECs are the functionally dominant IFN-λ-responding cells for endogenous and exogenous IFN-λ control of viruses in the intestine. There is a clear correlation between IFN-λ-mediated induction of antiviral ISGs and IEC expression of IFNLR1, suggesting that induction of ISGs in IECs is the mechanism by which IFN-λ exerts its antiviral effects.

Expression of *Ifnlr1* mRNA throughout the gut and in other extraintestinal tissues (MLN, lung, and spleen) was quantified by qPCR analysis. In lamina propria cells, there were fewer than 500 copies of *Ifnlr1* mRNA per 1 μg total RNA. In contrast, IECs express

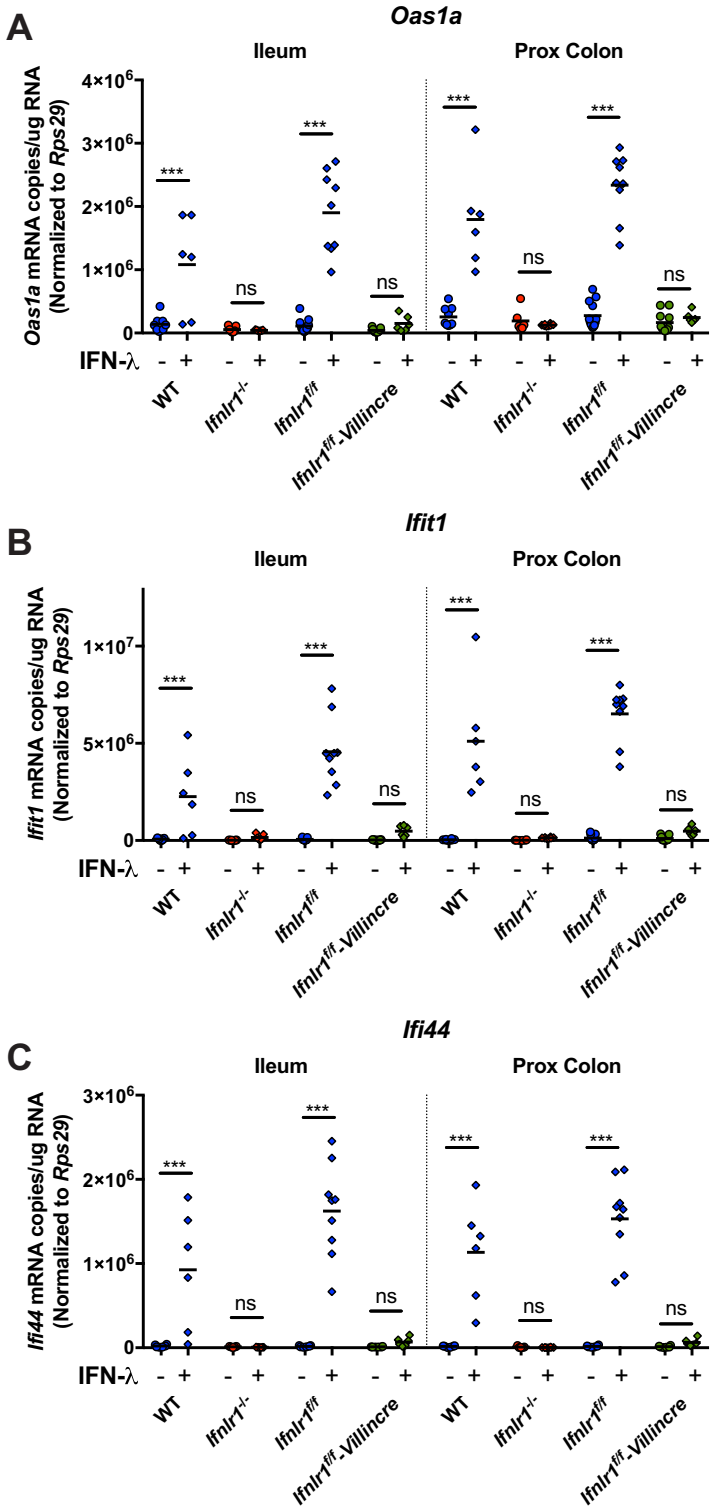

FIG 6 *Ifnlr1* expression on intestinal epithelial cells is necessary for induction of interferon-stimulated genes. *Oas1a* (A), *Ifit1* (B), and *Ifi44* (C) expression was assessed by quantitative real-time PCR of RNA from distal ileum and proximal colon tissue from wild-type (WT), *Ifnlr1*$^{-/-}$, *Ifnlr1*$^{f/f}$, and *Ifnlr1*$^{f/f}$*-Villincre* mice at 1 day posttreatment with PBS or recombinant IFN-λ. $n = 5$ to 9 mice per group, combined from two independent experiments, analyzed by one-way ANOVA followed by Tukey's multiple-comparison test; a P value of <0.001 was determined by ANOVA column factor for all tissues. ***, $P < 0.001$; ns, not significant.

more than 10,000 copies of *Ifnlr1* mRNA per 1 μg total RNA throughout the small intestine. Thus, IECs are the dominant *Ifnlr1*-expressing cells and function as the major IFN-λ-responding cells for antiviral immunity in the intestine. In MLN, spleen, and lung, we detected comparable expression of *Ifnlr1* mRNA. Villin-positive cells were not the major cell type responsible for *Ifnlr1* expression in these tissues, and neither were neutrophils, dendritic cells, or macrophages. Therefore, there may exist some other cell types that are important for IFN-λ responses in these tissues. Lung epithelial cells, which do not express Villin, likely reflect a major source of *Ifnlr1* in that tissue (29). B or T cells, which have been reported to express *Ifnlr1* even though they lack a robust response to IFN-λ, may account for *Ifnlr1* expression in the MLN and spleen (27). Another possible cellular source for this expression is endothelial cells, based on the report that blood-brain barrier endothelial cells respond to IFN-λ to restrict West Nile virus neuroinvasion (10). Thus, it would be interesting to study the role of IFN-λ in extraintestinal tissues in control of other pathogens and define the IFN-λ-responsive cell types in these contexts.

In some tissues, such as lung and vagina, there is redundancy between type I and III IFN-mediated antiviral responses. IFN-λ controls influenza virus, severe acute respiratory syndrome (SARS) coronavirus, respiratory syncytial virus infection in the lung (45–47), and herpes simplex virus 2 (HSV-2) infection in the genital tract (48), redundantly with type I IFNs. In the intestine, however, IFN-λ-mediated antiviral immunity does not redundantly overlap type I IFNs (8, 9, 19). Adult IECs have polarized apical IFNAR1 expression only at low levels (9), and although IECs in neonates exhibit robust STAT1 activation after type I IFN treatment, in adult mice they are largely unresponsive to type I IFN treatment *in vivo* (9, 19, 20). Moreover, the expression level of *Ifnlr1* mRNA is highly enriched in IECs but minimally detectable in other compartments of intestinal tissue (Fig. 1 and 2). This study, bolstering previous findings of alternate cellular expression patterns for type I and III IFN receptors, helps explain why IFN-λ-mediated immunity in the intestine is nonredundant with IFN-α/β in adult mice, even though they may stimulate transcription of highly overlapping sets of antiviral genes (7, 20). Our data support a role for IECs as sentinels for enteric virus infection via their response to compartment-specific IFN-λ signaling (19, 20).

One of the important features of IFN-λ-mediated immunity is its sterilizing activity against persistent MNoV infection in the absence of adaptive immunity (8). We observed that persistent MNoV infection of *Rag1*$^{-/-}$ *Ifnlr1*$^{f/f}$*-Villincre* mice was not resolved by IFN-λ treatment and showed increased viral titers in the stool, similar to our observations with *Rag1*$^{-/-}$ *Ifnlr1*$^{-/-}$ mice. Thus, IFN-λ-mediated sterilizing innate immunity requires IEC expression of the receptor. Since only macrophages, dendritic cells, and B cells are known to be susceptible to MNoV infection *in vitro* (35, 49), it is not clear how the IFN-λ response in IECs ablates persistent MNoV infection in the absence of adaptive immunity. One possible explanation is that there is a secondary *trans*-acting molecule induced by IFN-λ in IECs that clears MNoV in other cell types. A related study has demonstrated that rotavirus can be terminated by injecting IL-22 and IL-18 into *Rag1*$^{-/-}$ mice, but this IL-22- and IL-18-mediated viral clearance does not induce IFN-λ or Stat1 activation (50). Thus, there may be multiple innate immunological mechanisms to resolve persistent viral infection in the absence of adaptive immunity. Identifying the effectors of IFN-λ-mediated sterilizing immunity is an important area to pursue in IFN-λ immunology.

This study reveals that *Ifnlr1* expression in IECs is required for control of enteric MNoV and reovirus infections. Using a genetic approach with conditional knockout mice, we identified IECs as the dominant cell type that responds to endogenous and exogenous IFN-λ to control enteric viruses. Understanding the identity of IFN-λ-responsive cell types provides further insight into mechanisms that control enteric viruses and will enhance future development of IFN-λ-mediated antiviral therapeutics.

MATERIALS AND METHODS

Generation of MNoV stocks and determination of titers. Stocks of MNoV strain CR6 were generated from a molecular clone as previously described (51). Briefly, a plasmid encoding the CR6 genome was transfected into 293T cells to generate infectious virus, which was subsequently passaged on BV2 cells. After two passages, BV2 cultures were frozen and thawed to liberate virions. Cultures then were cleared of cellular debris and virus was concentrated by ultracentrifugation through a 30% sucrose cushion. Titers of virus stocks were determined by plaque assay on BV2 cells (51).

Generation of reovirus stocks and determination of titers. Spinner-adapted murine L929 (L) cells were grown in either suspension or monolayer cultures in Joklik's modified Eagle's minimal essential medium (SMEM; Lonza) supplemented to contain 5% fetal bovine serum (Gibco), 2 mM L-glutamine, 100 U/ml penicillin, 100 μg/ml streptomycin (Gibco), and 25 ng/ml amphotericin B (Sigma). BHK-T7 cells were grown in Dulbecco's modified Eagle's minimal essential medium (DMEM; Gibco) supplemented to contain 5% fetal bovine serum, 2 mM L-glutamine, 1 mg/ml Geneticin (Gibco), and nonessential amino acids (Sigma).

Recombinant reoviruses were generated using plasmid-based reverse genetics (52). Recombinant strain type 1 Lang (T1L) is a stock generated by plasmid-based rescue from cloned T1L cDNAs (53). After 3 to 5 days of incubation, cells were frozen and thawed three times, and virus was isolated by plaque purification using monolayers of L cells (54). Purified reovirus virions were generated from second- or third-passage L-cell lysate stocks (55). Viral particles were extracted from infected cell lysates using Vertrel XF (Dupont), layered onto 1.2- to 1.4-g/cm^3 CsCl gradients, and centrifuged at 62,000 $\times$ *g* for 16 h. Bands corresponding to virions (1.36 g/cm^3) were collected and dialyzed in virion storage buffer (150 mM NaCl, 15 mM $MgCl_2$, and 10 mM Tris-HCl [pH 7.4]) (56). The concentration of reovirus virions in purified preparations was determined from the following equivalence: one optical density (OD) unit at 260 nm equals 2.1 $\times$ 10^{12} virions (56). Viral titer was determined by plaque assay using L cells (54).

For analysis of reoviral titers in organs, mice were euthanized at various intervals postinoculation, and organs were harvested into 1 ml of PBS and homogenized by freeze-thaw and bead beating. For analysis of viral titer in stool, samples were harvested at various intervals, weighed, stored in 1 ml of PBS, and homogenized by freeze-thaw and bead beating. Viral titers in organs and stool homogenates were determined by plaque assay using L cells (54). Titers are expressed as PFU per milliliter of tissue homogenate or per gram of stool.

Mice, infections, and IFN-λ treatment. Wild-type (WT) C57BL/6J mice (stock number 000664) were purchased from Jackson Laboratories (Bar Harbor, ME) and housed at the Washington University School of Medicine under specific-pathogen-free conditions (57) according to university guidelines. *Ifnlr1*$^{-/-}$ (B6.Cg-*Ifnlr1*^{tm1Palu}) mice were obtained from Bristol-Myers Squibb (Seattle, WA) and backcrossed using speed congenics onto a C57BL/6J background (28).

To generate mice conditionally deficient for *Ifnlr1*, *Ifnlr1*$^{tm1a(EUCOMM)Wtsi}$ ES cells on a C57BL/6N background were provided by the Wellcome Trust Sanger Institute. A conditional-ready (floxed) allele in which exon 2 is flanked by loxP sites, designated *Ifnlr1*$^{f/f}$, was created (Fig. 2A) (38). *Ifnlr1*$^{f/f}$ mice were crossed to Villin-Cre (intestinal epithelial cells [29]), LysM-Cre (macrophages and neutrophils, as well as some dendritic cells [32, 33]), CD11c-Cre (dendritic cells and alveolar macrophages [31]), and MRP8-Cre (neutrophils [30]) lines for selective disruption of *Ifnlr1* in different cell types *in vivo*. *Ifnlr1*$^{f/f}$ mice were also crossed to a Deleter-Cre line (34) to generate an alternate *Ifnlr1*$^{-/-}$ line, here designated *Ifnlr1*$^{f-/-}$. *Ifnlr1*$^{f-/-}$ mice were backcrossed using speed congenics onto a C57BL/6J background. Mouse lines and naming conventions are summarized in Table 1.

For MNoV infections, mice were inoculated with a dose of 10^6 PFU of strain CR6 at 6 to 8 weeks of age by the oral route in a volume of 25 μl. For reovirus infections, mice were orally gavaged with a dose of 10^8 PFU of strain T1L virus at 6 to 8 weeks in a volume of 100 μl.

Recombinant IFN-λ was provided by Bristol-Myers Squibb (Seattle, WA) as a monomeric conjugate comprised of 20-kDa linear polyethylene glycol (PEG) attached to the amino terminus of murine IFN-λ, as previously reported (8). For treatment of mice, 25 μg of IFN-λ diluted in PBS was injected intraperitoneally.

Stool and tissues were harvested into 2-ml tubes (Sarstedt, Germany) with 1-mm-diameter zirconia/silica beads (Biospec, Bartlesville, OK). Tissues were flash frozen in a bath of ethanol and dry ice and either processed on the same day or stored at −80°C.

Isolation of epithelial and lamina propria fractions of small intestine. Epithelial and lamina propria fractions were prepared as previously described (36). In brief, after mice were euthanized, small intestines were collected. Intestinal tissues were washed with cold PBS twice and then chopped and transferred to new tubes. The tissues were incubated with stripping buffer (10% bovine calf serum, 15 mM HEPES, 5 mM EDTA, 5 mM dithiothreitol [DTT] in 1$\times$ Hanks' balanced salt solution [HBSS]) for 20 min at 37°C. The dissociated cells were collected as the epithelial fraction, consisting predominantly of IECs. The remaining tissue was used as the lamina propria fraction.

Isolation of neutrophils, macrophages, and dendritic cells. Neutrophils were isolated from *Ifnlr1*$^{f/f}$-*MRP8cre* mice and *Ifnlr1*$^{f/f}$ littermates by collecting bone marrow from femurs and tibias. Red blood cells were lysed using red blood cell lysis buffer (Sigma, St. Louis, MO), and neutrophils were isolated using the mouse neutrophil isolation kit (Miltenyi Biotec, Germany). Isolated neutrophils were confirmed to be 95 to 98% double positive for CD11b-allophycocyanin (APC) and Ly6G-fluorescein isothiocyanate (FITC) (BioLegend, San Diego, CA) (data not shown). Macrophages were isolated from *Ifnlr1*$^{f/f}$-*LysMcre* mice and *Ifnlr1*$^{f/f}$ littermates by collecting and homogenizing spleens, lysing red blood cells (RBCs), and enriching for macrophages using mouse anti-F4/80 UltraPure MicroBeads (Miltenyi Biotec). Isolated macrophages were confirmed to be 70 to 85% positive for F4/80-AF488

(Thermo Fisher Scientific) as well as CD11b-APC and CD45.2-phycoerythrin (PE) (BioLegend) (data not shown). Dendritic cells were isolated from *Ifnlr1*$^{f/f}$*-CD11ccre* mice and *Ifnlr1*$^{f/f}$ littermates by collecting and homogenizing spleens, lysing RBCs, and enriching for dendritic cells using the mouse pan-dendritic cell isolation kit (Miltenyi Biotec). Isolated dendritic cells were confirmed to be 70 to 85% CD11c-AF488 (BioLegend) single positive or CD11c-AF488 and B220-PE (BD Bioscience) double positive (data not shown).

Quantitative reverse transcription-PCR. RNA from stool was isolated using a ZR-96 viral RNA kit (Zymo Research, Irvine, CA). RNA from tissues or cells was isolated using TRI Reagent (Invitrogen) and a direct-zol-96 RNA kit (Zymo Research, Irvine, CA) according to the manufacturer's protocol. Five microliters of RNA from stool or 1 μg of RNA from tissue was used as a template for cDNA synthesis with the ImPromII reverse transcriptase system (Promega, Madison, WI). DNA contamination was removed using the DNAfree kit (Life Technologies).

MNoV TaqMan assays were performed, using a standard curve for determination of absolute viral genome copies, as described previously (58). Quantitative PCR for housekeeping gene *Rps29* was performed with forward primer 5′-GCAAATACGGGCTGAACATG-3′, reverse primer 5′-GTCCAACTTAATG AAGCCTATGTC-3′, and probe 5′-/5HEX/CCTTCGCGT/ZEN/ACTGCCGGAAGC/3IABkFQ/-3′ (where 3IABkFQ is 3′ Iowa Black fluorescence quencher; Integrated DNA Technologies), each at a concentration of 0.2 μM, using AmpliTaq gold DNA polymerase (Applied Biosystems). Quantitative PCRs for *Ifnlr1* (Mm.PT.58. 10781457), *Oas1a* (Mm.PT.58.30459792), *Ifi44* (Mm.PT.58.12162024), and *Ifit1* (Mm.PT.58.32674307) were similarly performed using PrimeTime qPCR assays (Integrated DNA Technologies). Standard curves for quantitative PCR assays were generated to facilitate absolute quantification of transcript copy numbers. For *Rps29*, the PCR product using the above-described primers was cloned into the p-ENTR/ D-TOPO vector (Thermo Fisher Scientific), and for *Ifnlr1* a full-length *Ifnlr1* cDNA clone (5036481; Open Biosystems) was used. Plasmids were Sanger sequenced to confirm the identity of the inserts. For *Oas1a*, *Ifit1*, and *Ifi44*, absolute transcripts were quantitated based on target sequence-containing gBlocks (Integrated DNA Technologies). Cycling parameters for *Rps29*, *Ifnlr1*, *Oas1a*, *Ifit1*, and *Ifi44* were identical to those for MNoV TaqMan. Absolute values of *Ifnlr1*, *Oas1a*, *Ifit1*, and *Ifi44* per microgram of RNA were normalized to the within-tissue average of housekeeping gene *Rps29*. No significant changes in absolute copy number of *Rps29* were detected between comparison groups (data not shown).

Statistical analysis. Data were analyzed with Prism 7 software (GraphPad Software, San Diego, CA). In all graphs, three asterisks indicate a P value of <0.001, two asterisks indicate a P value of <0.01, one asterisk indicates a P value of <0.05, and ns indicates not significant ($P > 0.05$) as determined by Mann-Whitney test, one-way analysis of variance (ANOVA), or two-way ANOVA with Tukey's multiple-comparison test, as specified in the relevant figure legends.

ACKNOWLEDGMENTS

We thank D. Kreamalmeyer for animal care and breeding, S. Peterson for technical assistance, members of the Virgin laboratory for manuscript review and discussion, S. Doyle and Bristol-Myers Squibb for providing *Ifnlr1*^{tm1Palu} mice, and Bill Skarnes and Wendy Bushell at the Wellcome Trust Sanger Institute for providing *Ifnlr1*$^{tm1a(EUCOMM)Wtsi}$ ES cells. Experimental support was provided by the Speed Congenics Facility of the Rheumatic Diseases Core Center.

H.W.V. was supported by National Institutes of Health (NIH) grant U19 AI109725 and the Crohn's and Colitis Foundation grant 326556. M.T.B. was supported by NIH training grant 5T32CA009547 and the W. M. Keck Fellowship from Washington University. T.J.N. was supported by NIH training grant 5T32A100716334 and postdoctoral fellowships from the Cancer Research Institute and American Cancer Society. S.L. was supported by the Basic Science Research Program through the National Research Foundation of Korea (NRF), funded by the Ministry of Education (NRF-2016R1A6A3A03012352). J.B. was supported by NIH training grant 5T32HL007751 and predoctoral fellowship F31DK108562. T.S.D. was supported by NIH grant R01 AI038296. Research reported in this publication was supported by NIH award number P30AR048335. The content is solely the responsibility of the authors and does not necessarily represent the official views of the National Institutes of Health.

REFERENCES

1. Karst SM. 2010. Pathogenesis of noroviruses, emerging RNA viruses. Viruses 2:748–781. https://doi.org/10.3390/v2030748.
2. Glass RI, Parashar UD, Estes MK. 2009. Norovirus gastroenteritis. N Engl J Med 361:1776–1785. https://doi.org/10.1056/NEJMra0804575.
3. Koo HL, Ajami N, Atmar RL, DuPont HL. 2010. Noroviruses: the leading cause of gastroenteritis worldwide. Discov Med 10:61–70.
4. Scallan E, Hoekstra RM, Angulo FJ, Tauxe RV, Widdowson MA, Roy SL, Jones JL, Griffin PM. 2011. Foodborne illness acquired in the United States–major pathogens. Emerg Infect Dis 17:7–15. https://doi.org/10.3201/eid1701.P11101.
5. Lazear HM, Nice TJ, Diamond MS. 2015. Interferon-lambda: immune functions at barrier surfaces and beyond. Immunity 43:15–28. https://doi.org/10.1016/j.immuni.2015.07.001.
6. Hermant P, Michiels T. 2014. Interferon-lambda in the context of viral infections: production, response and therapeutic implications. J Innate Immun 6:563–574. https://doi.org/10.1159/000360084.

7. Egli A, Santer DM, O'Shea D, Tyrrell DL, Houghton M. 2014. The impact of the interferon-lambda family on the innate and adaptive immune response to viral infections. Emerg Microbes Infect 3:e51. https://doi.org/10.1038/emi.2014.51.
8. Nice TJ, Baldridge MT, McCune BT, Norman JM, Lazear HM, Artyomov M, Diamond MS, Virgin HW. 2015. Interferon-lambda cures persistent murine norovirus infection in the absence of adaptive immunity. Science 347:269–273. https://doi.org/10.1126/science.1258100.
9. Pott J, Mahlakoiv T, Mordstein M, Duerr CU, Michiels T, Stockinger S, Staeheli P, Hornef MW. 2011. IFN-lambda determines the intestinal epithelial antiviral host defense. Proc Natl Acad Sci U S A 108:7944–7949. https://doi.org/10.1073/pnas.1100552108.
10. Lazear HM, Daniels BP, Pinto AK, Huang AC, Vick SC, Doyle SE, Gale M, Jr, Klein RS, Diamond MS. 2015. Interferon-lambda restricts West Nile virus neuroinvasion by tightening the blood-brain barrier. Sci Transl Med 7:284ra259.
11. Muir AJ, Arora S, Everson G, Flisiak R, George J, Ghalib R, Gordon SC, Gray T, Greenbloom S, Hassanein T, Hillson J, Horga MA, Jacobson IM, Jeffers L, Kowdley KV, Lawitz E, Lueth S, Rodriguez-Torres M, Rustgi V, Shemanski L, Shiffman ML, Srinivasan S, Vargas HE, Vierling JM, Xu D, Lopez-Talavera JC, Zeuzem S, EMERGE Study Group. 2014. A randomized phase 2b study of peginterferon lambda-1a for the treatment of chronic HCV infection. J Hepatol 61:1238–1246. https://doi.org/10.1016/j.jhep.2014.07.022.
12. Kotenko SV, Gallagher G, Baurin VV, Lewis-Antes A, Shen M, Shah NK, Langer JA, Sheikh F, Dickensheets H, Donnelly RP. 2003. IFN-lambdas mediate antiviral protection through a distinct class II cytokine receptor complex. Nat Immunol 4:69–77. https://doi.org/10.1038/ni875.
13. Sheppard P, Kindsvogel W, Xu W, Henderson K, Schlutsmeyer S, Whitmore TE, Kuestner R, Garrigues U, Birks C, Roraback J, Ostrander C, Dong D, Shin J, Presnell S, Fox B, Haldeman B, Cooper E, Taft D, Gilbert T, Grant FJ, Tackett M, Krivan W, McKnight G, Clegg C, Foster D, Klucher KM. 2003. IL-28, IL-29 and their class II cytokine receptor IL-28R. Nat Immunol 4:63–68. https://doi.org/10.1038/ni873.
14. Bolen CR, Ding S, Robek MD, Kleinstein SH. 2014. Dynamic expression profiling of type I and type III interferon-stimulated hepatocytes reveals a stable hierarchy of gene expression. Hepatology 59:1262–1272. https://doi.org/10.1002/hep.26657.
15. Kohli A, Zhang X, Yang J, Russell RS, Donnelly RP, Sheikh F, Sherman A, Young H, Imamichi T, Lempicki RA, Masur H, Kottilil S. 2012. Distinct and overlapping genomic profiles and antiviral effects of Interferon-lambda and -alpha on HCV-infected and noninfected hepatoma cells. J Viral Hepat 19:843–853. https://doi.org/10.1111/j.1365-2893.2012.01610.x.
16. Baldridge MT, Nice TJ, McCune BT, Yokoyama CC, Kambal A, Wheadon M, Diamond MS, Ivanova Y, Artyomov M, Virgin HW. 2015. Commensal microbes and interferon-lambda determine persistence of enteric murine norovirus infection. Science 347:266–269. https://doi.org/10.1126/science.1258025.
17. Karst SM, Wobus CE, Goodfellow IG, Green KY, Virgin HW. 2014. Advances in norovirus biology. Cell Host Microbe 15:668–680. https://doi.org/10.1016/j.chom.2014.05.015.
18. Wobus CE, Thackray LB, Virgin HW. 2006. Murine norovirus: a model system to study norovirus biology and pathogenesis. J Virol 80:5104–5112. https://doi.org/10.1128/JVI.02346-05.
19. Mahlakoiv T, Hernandez P, Gronke K, Diefenbach A, Staeheli P. 2015. Leukocyte-derived IFN-alpha/beta and epithelial IFN-lambda constitute a compartmentalized mucosal defense system that restricts enteric virus infections. PLoS Pathog 11:e1004782. https://doi.org/10.1371/journal.ppat.1004782.
20. Lin JD, Feng N, Sen A, Balan M, Tseng HC, McElrath C, Smirnov SV, Peng J, Yasukawa LL, Durbin RK, Durbin JE, Greenberg HB, Kotenko SV. 2016. Distinct roles of type I and type III interferons in intestinal immunity to homologous and heterologous rotavirus infections. PLoS Pathog 12:e1005600. https://doi.org/10.1371/journal.ppat.1005600.
21. Visel A, Thaller C, Eichele G. 2004. GenePaint.org: an atlas of gene expression patterns in the mouse embryo. Nucleic Acids Res 32:D552–D556. https://doi.org/10.1093/nar/gkh029.
22. Diez-Roux G, Banfi S, Sultan M, Geffers L, Anand S, Rozado D, Magen A, Canidio E, Pagani M, Peluso I, Lin-Marq N, Koch M, Bilio M, Cantiello I, Verde R, De Masi C, Bianchi SA, Cicchini J, Perroud E, Mehmeti S, Dagand E, Schrinner S, Nurnberger A, Schmidt K, Metz K, Zwingmann C, Brieske N, Springer C, Hernandez AM, Herzog S, Grabbe F, Sieverding C, Fischer B, Schrader K, Brockmeyer M, Dettmer S, Helbig C, Alunni V, Battaini MA, Mura C, Henrichsen CN, Garcia-Lopez R, Echevarria D, Puelles E, Garcia-Calero E, Kruse S, Uhr M, Kauck C, Feng G, Milyaev N, Ong CK, Kumar L, Lam M, Semple CA, Gyenesei A, Mundlos S, Radelof U, Lehrach H, Sarmientos P, Reymond A, Davidson DR, Dolle P, Antonarakis SE, Yaspo ML, Martinez S, Baldock RA, Eichele G, Ballabio A. 2011. A high-resolution anatomical atlas of the transcriptome in the mouse embryo. PLoS Biol 9:e1000582. https://doi.org/10.1371/journal.pbio.1000582.
23. Randall RE, Goodbourn S. 2008. Interferons and viruses: an interplay between induction, signalling, antiviral responses and virus countermeasures. J Gen Virol 89:1–47. https://doi.org/10.1099/vir.0.83391-0.
24. de Weerd NA, Samarajiwa SA, Hertzog PJ. 2007. Type I interferon receptors: biochemistry and biological functions. J Biol Chem 282:20053–20057. https://doi.org/10.1074/jbc.R700006200.
25. Sommereyns C, Paul S, Staeheli P, Michiels T. 2008. IFN-lambda (IFN-lambda) is expressed in a tissue-dependent fashion and primarily acts on epithelial cells in vivo. PLoS Pathog 4:e1000017. https://doi.org/10.1371/journal.ppat.1000017.
26. Blazek K, Eames HL, Weiss M, Byrne AJ, Perocheau D, Pease JE, Doyle S, McCann F, Williams RO, Udalova IA. 2015. IFN-lambda resolves inflammation via suppression of neutrophil infiltration and IL-1beta production. J Exp Med 212:845–853. https://doi.org/10.1084/jem.20140995.
27. Witte K, Gruetz G, Volk HD, Looman AC, Asadullah K, Sterry W, Sabat R, Wolk K. 2009. Despite IFN-lambda receptor expression, blood immune cells, but not keratinocytes or melanocytes, have an impaired response to type III interferons: implications for therapeutic applications of these cytokines. Genes Immun 10:702–714. https://doi.org/10.1038/gene.2009.72.
28. Ank N, Iversen MB, Bartholdy C, Staeheli P, Hartmann R, Jensen UB, Dagnaes-Hansen F, Thomsen AR, Chen Z, Haugen H, Klucher K, Paludan SR. 2008. An important role for type III interferon (IFN-lambda/IL-28) in TLR-induced antiviral activity. J Immunol 180:2474–2485. https://doi.org/10.4049/jimmunol.180.4.2474.
29. Madison BB, Dunbar L, Qiao XT, Braunstein K, Braunstein E, Gumucio DL. 2002. Cis elements of the villin gene control expression in restricted domains of the vertical (crypt) and horizontal (duodenum, cecum) axes of the intestine. J Biol Chem 277:33275–33283. https://doi.org/10.1074/jbc.M204935200.
30. Passegue E, Wagner EF, Weissman IL. 2004. JunB deficiency leads to a myeloproliferative disorder arising from hematopoietic stem cells. Cell 119:431–443. https://doi.org/10.1016/j.cell.2004.10.010.
31. Stranges PB, Watson J, Cooper CJ, Choisy-Rossi CM, Stonebraker AC, Beighton RA, Hartig H, Sundberg JP, Servick S, Kaufmann G, Fink PJ, Chervonsky AV. 2007. Elimination of antigen-presenting cells and autoreactive T cells by Fas contributes to prevention of autoimmunity. Immunity 26:629–641. https://doi.org/10.1016/j.immuni.2007.03.016.
32. Clausen BE, Burkhardt C, Reith W, Renkawitz R, Forster I. 1999. Conditional gene targeting in macrophages and granulocytes using LysMcre mice. Transgenic Res 8:265–277. https://doi.org/10.1023/A:1008942828960.
33. Jakubzick C, Bogunovic M, Bonito AJ, Kuan EL, Merad M, Randolph GJ. 2008. Lymph-migrating, tissue-derived dendritic cells are minor constituents within steady-state lymph nodes. J Exp Med 205:2839–2850. https://doi.org/10.1084/jem.20081430.
34. Schwenk F, Baron U, Rajewsky K. 1995. A cre-transgenic mouse strain for the ubiquitous deletion of loxP-flanked gene segments including deletion in germ cells. Nucleic Acids Res 23:5080–5081. https://doi.org/10.1093/nar/23.24.5080.
35. Wobus CE, Karst SM, Thackray LB, Chang KO, Sosnovtsev SV, Belliot G, Krug A, Mackenzie JM, Green KY, Virgin HW. 2004. Replication of Norovirus in cell culture reveals a tropism for dendritic cells and macrophages. PLoS Biol 2:e432. https://doi.org/10.1371/journal.pbio.0020432.
36. Lefrancois L, Lycke N. 2001. Isolation of mouse small intestinal intraepithelial lymphocytes, Peyer's patch, and lamina propria cells. Curr Protoc Immunol Chapter 3:Unit 3.19.
37. Reference deleted.
38. Kanki H, Suzuki H, Itohara S. 2006. High-efficiency CAG-FLPe deleter mice in C57BL/6J background. Exp Anim 55:137–141. https://doi.org/10.1538/expanim.55.137.
39. Abram CL, Roberge GL, Hu Y, Lowell CA. 2014. Comparative analysis of the efficiency and specificity of myeloid-Cre deleting strains using ROSA-EYFP reporter mice. J Immunol Methods 408:89–100. https://doi.org/10.1016/j.jim.2014.05.009.
40. Zhong Z, Baker JJ, Zylstra-Diegel CR, Williams BO. 2012. Lrp5 and Lrp6 play compensatory roles in mouse intestinal development. J Cell Biochem 113:31–38. https://doi.org/10.1002/jcb.23324.

41. Nice TJ, Strong DW, McCune BT, Pohl CS, Virgin HW. 2013. A single-amino-acid change in murine norovirus NS1/2 is sufficient for colonic tropism and persistence. J Virol 87:327–334. https://doi.org/10.1128/JVI.01864-12.
42. Elkhateeb E, Tag-El-Din-Hassan HT, Sasaki N, Torigoe D, Morimatsu M, Agui T. 2016. The role of mouse 2′,5′-oligoadenylate synthetase 1 paralogs. Infect Genet Evol 45:393–401. https://doi.org/10.1016/j.meegid.2016.09.018.
43. Reynaud JM, Kim DY, Atasheva S, Rasalouskaya A, White JP, Diamond MS, Weaver SC, Frolova EI, Frolov I. 2015. IFIT1 differentially interferes with translation and replication of alphavirus genomes and promotes induction of type I interferon. PLoS Pathog 11:e1004863. https://doi.org/10.1371/journal.ppat.1004863.
44. Carlton-Smith C, Elliott RM. 2012. Viperin, MTAP44, and protein kinase R contribute to the interferon-induced inhibition of Bunyamwera Orthobunyavirus replication. J Virol 86:11548–11557. https://doi.org/10.1128/JVI.01773-12.
45. Crotta S, Davidson S, Mahlakoiv T, Desmet CJ, Buckwalter MR, Albert ML, Staeheli P, Wack A. 2013. Type I and type III interferons drive redundant amplification loops to induce a transcriptional signature in influenza-infected airway epithelia. PLoS Pathog 9:e1003773. https://doi.org/10.1371/journal.ppat.1003773.
46. Mordstein M, Kochs G, Dumoutier L, Renauld JC, Paludan SR, Klucher K, Staeheli P. 2008. Interferon-lambda contributes to innate immunity of mice against influenza A virus but not against hepatotropic viruses. PLoS Pathog 4:e1000151. https://doi.org/10.1371/journal.ppat.1000151.
47. Mordstein M, Neugebauer E, Ditt V, Jessen B, Rieger T, Falcone V, Sorgeloos F, Ehl S, Mayer D, Kochs G, Schwemmle M, Gunther S, Drosten C, Michiels T, Staeheli P. 2010. Lambda interferon renders epithelial cells of the respiratory and gastrointestinal tracts resistant to viral infections. J Virol 84:5670–5677. https://doi.org/10.1128/JVI.00272-10.
48. Ank N, West H, Bartholdy C, Eriksson K, Thomsen AR, Paludan SR. 2006. Lambda interferon (IFN-lambda), a type III IFN, is induced by viruses and IFNs and displays potent antiviral activity against select virus infections in vivo. J Virol 80:4501–4509. https://doi.org/10.1128/JVI.80.9.4501-4509.2006.
49. Jones MK, Watanabe M, Zhu S, Graves CL, Keyes LR, Grau KR, Gonzalez-Hernandez MB, Iovine NM, Wobus CE, Vinje J, Tibbetts SA, Wallet SM, Karst SM. 2014. Enteric bacteria promote human and mouse norovirus infection of B cells. Science 346:755–759. https://doi.org/10.1126/science.1257147.
50. Zhang B, Chassaing B, Shi Z, Uchiyama R, Zhang Z, Denning TL, Crawford SE, Pruijssers AJ, Iskarpatyoti JA, Estes MK, Dermody TS, Ouyang W, Williams IR, Vijay-Kumar M, Gewirtz AT. 2014. Viral infection. Prevention and cure of rotavirus infection via TLR5/NLRC4-mediated production of IL-22 and IL-18. Science 346:861–865.
51. Strong DW, Thackray LB, Smith TJ, Virgin HW. 2012. Protruding domain of capsid protein is necessary and sufficient to determine murine norovirus replication and pathogenesis in vivo. J Virol 86:2950–2958. https://doi.org/10.1128/JVI.07038-11.
52. Kobayashi T, Antar AA, Boehme KW, Danthi P, Eby EA, Guglielmi KM, Holm GH, Johnson EM, Maginnis MS, Naik S, Skelton WB, Wetzel JD, Wilson GJ, Chappell JD, Dermody TS. 2007. A plasmid-based reverse genetics system for animal double-stranded RNA viruses. Cell Host Microbe 1:147–157. https://doi.org/10.1016/j.chom.2007.03.003.
53. Kobayashi T, Ooms LS, Ikizler M, Chappell JD, Dermody TS. 2010. An improved reverse genetics system for mammalian orthoreoviruses. Virology 398:194–200. https://doi.org/10.1016/j.virol.2009.11.037.
54. Virgin HWT, Bassel-Duby R, Fields BN, Tyler KL. 1988. Antibody protects against lethal infection with the neurally spreading reovirus type 3 (Dearing). J Virol 62:4594–4604.
55. Furlong DB, Nibert ML, Fields BN. 1988. Sigma 1 protein of mammalian reoviruses extends from the surfaces of viral particles. J Virol 62:246–256.
56. Smith RE, Zweerink HJ, Joklik WK. 1969. Polypeptide components of virions, top component and cores of reovirus type 3. Virology 39:791–810. https://doi.org/10.1016/0042-6822(69)90017-8.
57. Cadwell K, Patel KK, Maloney NS, Liu TC, Ng AC, Storer CE, Head RD, Xavier R, Stappenbeck TS, Virgin HW. 2010. Virus-plus-susceptibility gene interaction determines Crohn's disease gene Atg16L1 phenotypes in intestine. Cell 141:1135–1145. https://doi.org/10.1016/j.cell.2010.05.009.
58. Baert L, Wobus CE, Van Coillie E, Thackray LB, Debevere J, Uyttendaele M. 2008. Detection of murine norovirus 1 by using plaque assay, transfection assay, and real-time reverse transcription-PCR before and after heat exposure. Appl Environ Microbiol 74:543–546. https://doi.org/10.1128/AEM.01039-07.

nature publishing group

Basic Science Investigation | Articles

Age-dependent susceptibility to reovirus encephalitis in mice is influenced by maturation of the type-I interferon response

Allen G Wu[1,2,6,7], Andrea J Pruijssers[1,2,6], Judy J Brown[2,3], Jennifer E Stencel-Baerenwald[2,3,8], Danica M Sutherland[2,3], Jason A Iskarpatyoti[1,2,9] and Terence S Dermody[4,5]

BACKGROUND: Infants and young children are particularly susceptible to viral encephalitis; however, the mechanisms are unknown. We determined the age-dependent contribution of innate and adaptive immune functions to reovirus-induced encephalitis in mice.

METHODS: Newborn wild-type mice, 2–20 days of age, were inoculated with reovirus or diluent and monitored for mortality, weight gain, and viral load. Four- and fifteen-day-old IFNAR$^{-/-}$ and RAG2$^{-/-}$ mice were inoculated with reovirus and similarly monitored.

RESULTS: Weight gain was impaired in mice inoculated with reovirus at 8 days of age or less. Clinical signs of encephalitis were detected in mice inoculated at 10 days of age or less. Mortality decreased when mice were inoculated after 6 days of age. Survival was $\leq$15% in wild type (WT), RAG2$^{-/-}$, and IFNAR$^{-/-}$ mice inoculated at 4 days of age. All WT mice, 92% of RAG2$^{-/-}$ mice, and only 48% of IFNAR$^{-/-}$ mice survived following inoculation at 15 days of age.

CONCLUSIONS: Susceptibility of mice to reovirus-induced disease decreases between 6 and 8 days of age. Enhanced reovirus virulence in IFNAR$^{-/-}$ mice relative to WT and RAG2$^{-/-}$ mice inoculated at 15 days of age suggests that maturation of the type-I interferon response contributes to age-related mortality following reovirus infection.

Viral encephalitis is a major cause of morbidity and mortality worldwide. Neurotropic viruses continue to emerge and reemerge because of changes in viral virulence, expanded distribution of viral vectors, fluctuations in population immunity, and increased travel associated with globalization (1). The young are particularly susceptible to poor outcomes of viral encephalitis such as developmental delays, learning disabilities, epilepsy, and death. Neurotropic viruses replicate more efficiently and display enhanced apoptosis capacity in immature vs. mature neurons through mechanisms that are incompletely understood (2).

Reovirus serves as a highly tractable experimental system in which to study neurotropic virus–host interactions. Following peroral inoculation of newborn mice, reovirus infects the intestine and disseminates systemically to the mesenteric lymph nodes, liver, spleen, lungs, heart, and brain. Serotype 1 reovirus strains disseminate exclusively via hematogenous routes, whereas serotype 3 strains disseminate via hematogenous and neural routes (3,4). Upon entry into the brain, serotype 3 strains infect neurons located in the frontal and parietal cortex, CA1 to CA4 regions of the hippocampus, the cingulate gyrus, the thalamus, and Purkinje neurons in the cerebellum (5,6). Reovirus infection of neurons causes apoptosis and triggers inflammation, resulting in a lethal meningoencephalitis (3,7–9).

The susceptibility of mice to reovirus infection and death is age-dependent. Infection of young mice with serotype 3 reovirus leads to a lethal encephalitis and death, whereas signs of clinical disease are absent following infection of older mice (10,11). One study suggests that the age susceptibility of mice to reovirus neurovirulence is due to the inhibition of viral replication by neuronal cell intrinsic factors (12). However, the precise mechanism is unknown.

The type-I interferon (IFN) pathway is a major component of the innate immune system. Following production and secretion, IFNs act in an autocrine and paracrine manner to induce an antiviral state in infected and neighboring cells, promote a balanced natural killer cell response with controlled anti-inflammatory activities, and enhance antigen presentation to activate the adaptive immune system (13). Mice deficient in the signal transducer and activator of transcription-1, a key component of IFN signaling, display increased mortality and higher viral loads in the brain following intracranial inoculation with reovirus at 2 days of

[1]Department of Pediatrics, Vanderbilt University School of Medicine, Nashville, Tennessee; [2]Department of Elizabeth B. Lamb Center for Pediatric Research, Vanderbilt University School of Medicine, Nashville, Tennessee; [3]Department of Pathology, Microbiology, and Immunology, Vanderbilt University School of Medicine, Nashville, Tennessee; [4]Department of Pediatrics, University of Pittsburgh School of Medicine, Pittsburgh, Pennsylvania; [5]Department of Microbiology and Molecular Genetics, University of Pittsburgh School of Medicine, Pittsburgh, Pennsylvania. Correspondence: Terence S. Dermody (terence.dermody@chp.edu)
[6]These authors contributed equally to this work.
[7]Current address: Advocate Christ Medical Center Oak Lawn, Chicago, Illinois
[8]Current address: Biogen, Cambridge, Massachusetts
[9]Current address: Department of Molecular Genetics and Microbiology, Duke University School of Medicine, Durham, North Carolina

Received 5 September 2017; accepted 12 January 2018; advance online publication 21 February 2018. doi:10.1038/pr.2018.13

age, suggesting that IFN signaling reduces reovirus replication and virulence (14).

Strategies to prevent and treat viral encephalitis are limited in part because of a lack of knowledge of the cellular factors and molecular mechanisms that contribute to viral virulence. We hypothesized that the susceptibility to reovirus disease is an effect of age-dependent control of the virus by maturing components of the immune system. To test this hypothesis, we defined the age at which mice lose susceptibility to reovirus-induced disease, determined the relationship between viral replication in vital organs and disease severity, and delineated age-dependent contributions from innate and adaptive immune functions. As age restriction is a shared determinant of disease severity in many neurotropic virus infections, it is possible that mechanisms underlying reovirus age restriction will be applicable to other viral infections.

METHODS

Cell Lines and Viruses

Murine L929 cells were maintained in Eagle's minimal essential medium (Lonza; Walkersville, MD) with 5% fetal bovine serum (Gibco; Gaitersburg, MD), 2 mM L-glutamine (Invitrogen; Carlsbad, CA), 100 U/ml penicillin (Invitrogen), 100 µg/ml streptomycin (Invitrogen), and 25 ng/ml amphotericin B (Sigma-Aldrich; St. Louis, MO). Reovirus strain type 3 Dearing (T3D) is a laboratory stock recovered by plasmid-based reverse genetics (15). Reovirus was amplified in L929 cells and purified by Vertrel-XF (Dupont; Wilmington, DE) extraction, followed by CsCl-gradient centrifugation (16). Viral plaque-forming unit (PFU) titers were determined by plaque assay using L929 cells (17).

Mouse Strains

C57BL/6J (WT) mice were obtained from The Jackson Laboratory. C57BL/6 IFNAR$^{-/-}$ mice were provided by John Williams (Vanderbilt University School of Medicine; Nashville, TN), and C57BL/6 RAG2$^{-/-}$ mice were provided by Danyvid Olivares-Villagomez (Vanderbilt University School of Medicine; Nashville, TN).

Infection of Mice

Mice were weighed and inoculated intracranially (18) with purified reovirus T3D in phosphate-buffered saline (PBS) at 100 PFU/g. For analysis of virulence, mice were monitored for weight gain and symptoms of disease for 20 days post inoculation (d p.i.) and killed when moribund. For analysis of viral replication, organs were collected into 1 ml of PBS and homogenized using a TissueLyser (Qiagen; Hilden, Germany). Viral titers were determined by plaque assay. Animal husbandry and experimental procedures were performed in accordance with Public Health Service policy and approved by the Vanderbilt University School of Medicine Institutional Animal Care and Use Committee.

Histology

Mice were inoculated intracranially with reovirus T3D at 100 PFU/g. Brains were resected and divided sagittally. Left-brain hemispheres were processed for plaque assay. Right-brain hemispheres were fixed in 10% formalin and embedded in paraffin. Consecutive 6-µm sections were stained with hematoxylin and eosin or processed for immunohistochemical detection of reovirus antigen or the cleaved (active) form of caspase-3 (ref. 19).

Immunoblotting

Brain homogenates were diluted twofold in RIPA lysis buffer (Sigma-Aldrich) containing Complete Protease Inhibitor Cocktail (Roche; Basel, Switzerland). Protein extract (50 µg) was resolved by electrophoresis in 10% Tris-glycine gels (Bio-Rad; Hercules, CA) and transferred to Immun-Blot PVDF membranes (Bio-Rad). Membranes were blocked for at least 1 h in Odyssey blocking buffer (LI-COR; Lincoln, NE) and incubated with an anti-actin antibody (1:500; Santa Cruz Biotechnologies; Dallas, TX) and a cleaved (active) caspase-3 antibody (1:1,000; Cell Signaling Technologies; Danvers, MA) in Odyssey blocking buffer overnight. Membranes were washed and incubated with secondary antibodies IRDye 680CW-conjugated donkey anti-goat (1:2,000) and IRDye 800CW-conjugated goat anti-rabbit (1:5,000) in Odyssey blocking buffer for 2 h. Membranes were washed three times and scanned using an Odyssey infrared imaging system (LI-COR). Signal intensities of specific bands were quantified using ImageStudio software (LI-COR).

RESULTS

Survival of Mice from Reovirus Infection Is Age-Dependent

Following infection with a neurotropic serotype 3 strain of reovirus, neonatal mice will contract encephalitis, which is often fatal, whereas adult mice do not develop overt signs of the disease (10,11). To determine the age window during which WT mice become refractory to reovirus-induced mortality, mice were inoculated intracranially with 100 PFU/g T3D in PBS or PBS alone (mock) at 2, 4, 6, 8, 10, 15, and 20 d of age and monitored for survival for 20 d. Only 37% of 2-day-old ($n = 16$), 15% of 4-day-old ($n = 20$), and 48% of 6-day-old ($n = 27$) mice survived (**Figure 1a**). In contrast, 90% of mice inoculated with reovirus at 8 d of age ($n = 18$) and all mice inoculated at 10, 15, and 20 d of age ($n \geq 15$) survived. Mice that became ill exhibited clinical signs of encephalitis including lethargy, seizures, ataxia, and paralysis. All PBS-inoculated mice survived. These data indicate that reovirus-induced mortality is reduced in mice inoculated at or after 8 d of age.

Reovirus-Induced Disease Is Age-Dependent

We monitored the weight gain of reovirus-inoculated mice as a quantitative surrogate measure of reovirus-induced disease. Mice were inoculated intracranially with 100 PFU/g T3D in PBS at 2, 4, 6, 8, 10, 15, or 20 d of age or PBS alone at 2 d of age and weighed daily for 20 d. The mean weight gain of mice inoculated with reovirus at 2, 4, 6, and 8 d of age was significantly less than that of age-matched controls inoculated with PBS (**Figure 1b–e**). The mean weight gain of mice inoculated with reovirus at 10 d was significantly less than that of age-matched controls at early time points post inoculation (p.i.), but the differences were reduced at later time points (**Figure 1f**). Interestingly, the mean weights of mice inoculated with reovirus at 15 and 20 d of age were significantly greater than those of age-matched controls at later time points (**Figure 1g,h**). These data suggest that the capacity of reovirus to induce disease is diminished in mice inoculated at 10 d of age or older.

Viral Loads in the Brain and Peripheral Organs Do Not Strictly Correlate with Disease Severity

Disease severity is often proportional to the level of viral replication in vital organs. To determine whether the age-dependent severity in reovirus disease is a function of viral load, we quantified viral titers in organs at 4, 7, and 10 d

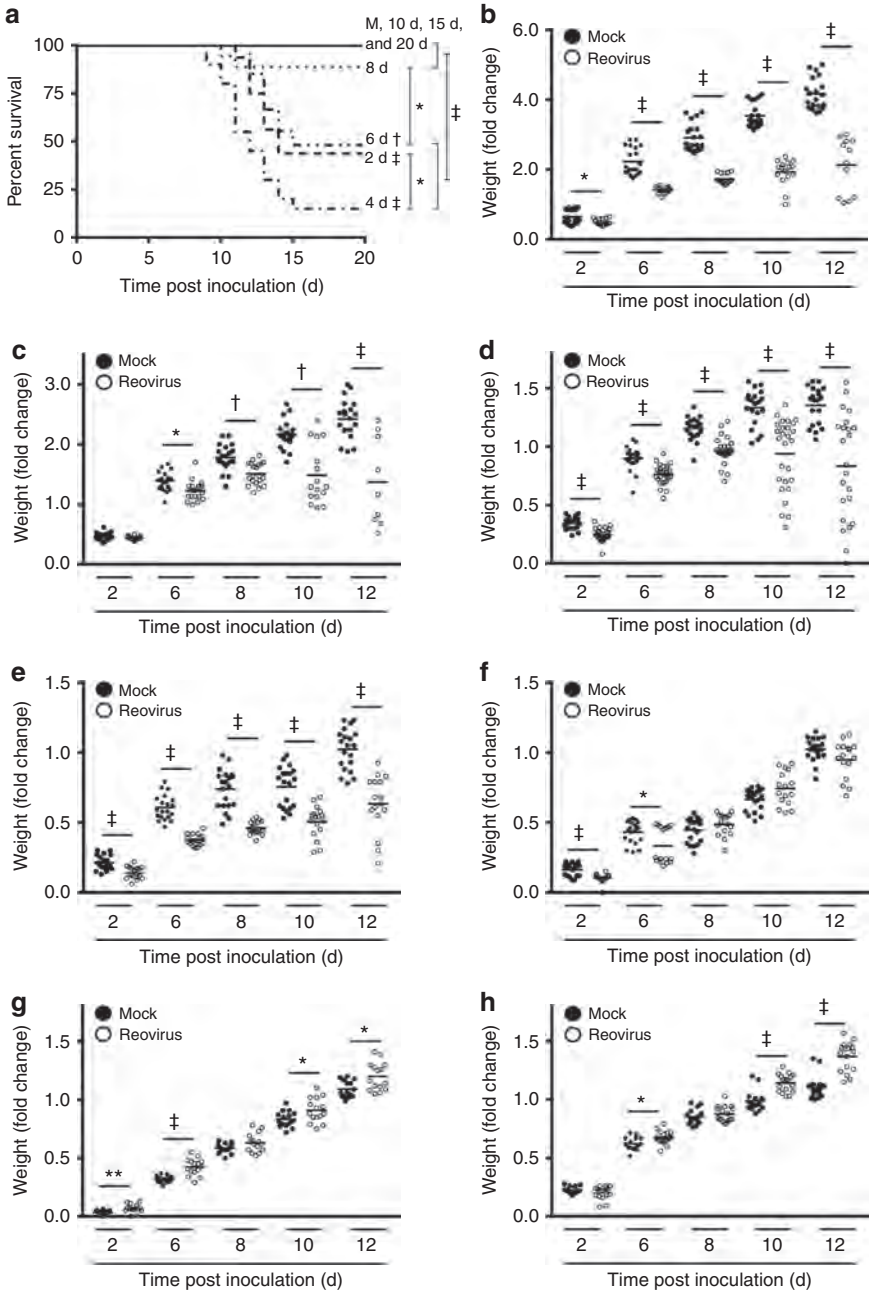

Figure 1. Survival and weight gain in mice following reovirus inoculation at various ages. WT mice were inoculated intracranially with reovirus T3D at 100 PFU/g at 2, 4, 6, 8, 10, 15, or 20 d of age or with PBS alone (mock; M) at 2 d of age. (**a**) Mice ($n \geq 15$ per experimental group) were monitored for morbidity for 20 d and killed when moribund. Statistical analyses compared each curve to mock, to the next age of inoculation (e.g., 2 vs. 4 d; 4 vs. 6 d, etc.), and between susceptible and nonsusceptible age groups (e.g., 2–6 vs. 8–20 d). $^{*}P<0.05$; $^{\dagger}P<0.005$; $^{\ddagger}P<0.0001$ as determined by log-rank test. WT mice were inoculated intracranially with reovirus T3D at 100 PFU/g at (**b**) 2, (**c**) 4, (**d**) 6, (**e**) 8, (**f**) 10, (**g**) 15, or (**h**) 20 d of age and monitored for weight gain for 20 d. Data are represented as fold change normalized to weight on the day of inoculation compared with age-matched, mock controls at 2, 6, 8, 10, and 12 d p.i. $^{*}P<0.05$; $^{**}P<0.01$; $^{\dagger}P<0.005$; $^{\ddagger}P<0.0001$ as determined by Mann–Whitney *U*-test. d p.i., day post inoculation; PBS, phosphate-buffered saline; PFU, plaque-forming unit; T3D, type 3 Dearing.

post-intracranial inoculation with T3D. The average peak viral loads in the brains of mice inoculated at 2 and 4 d of age were comparable (**Figure 2**). In contrast, the average peak viral load in the brains of mice inoculated at 6 d of age was lower compared with the average peak viral load in the brains of mice inoculated at a younger age. The average peak viral load in the brains of mice inoculated at 10 and 15 d of age was comparable to the average peak viral load in the brains of mice inoculated at 6 d of age. We calculated the area under the curve for each age of inoculation to test whether the cumulative viral loads in the brain for all three time points differed between mice inoculated at different ages. The areas

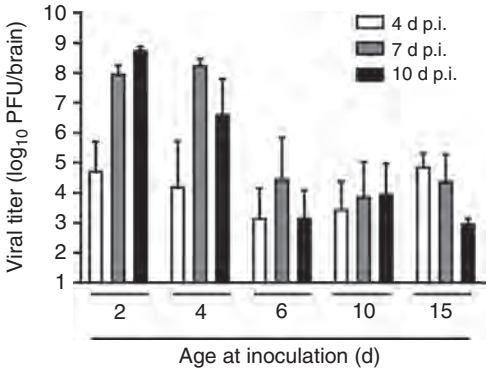

Figure 2. Viral loads in the brain following reovirus inoculation at various ages. WT mice were inoculated intracranially with reovirus T3D at 100 PFU/g at 2, 4, 6, 10, or 15 d of age. At 4, 7, and 10 d p.i., mice were killed, brains were resected, and viral loads were determined by plaque assay. $n = 5–7$ mice per bar. d p.i., day post inoculation; PFU, plaque-forming unit; T3D, type 3 Dearing.

Table 1. Viral dissemination to peripheral organs

Age of inoculation (d)	Time post inoculation (d)		
	4	7	10
2	3/6 (50%)	5/6 (83%)	6/6 (100%)
4	3/6 (50%)	5/5 (100%)	5/6 (83%)
6	1/5 (20%)	2/5 (40%)	0/7 (0%)
10	3/6 (50%)	2/6 (33%)	0/6 (0%)
15	4/6 (67%)	2/5 (40%)	0/6 (0%)

WT mice were inoculated intracranially with reovirus T3D at 100 PFU/g at 2, 4, 6, 10, or 15 d of age. Viral loads in the brain, heart, liver, spleen, and intestine were determined by plaque assay at 4, 7, and 10 d p.i. $n = 5–7$ mice per condition. Numerals represent the number of mice with detectable titer in peripheral organs divided by the total number of mice assayed, and the resulting percentage of mice with detectable titer in peripheral organs in each group.
d, day; d p.i., day post inoculation; PFU, plaque-forming unit; T3D, type 3 Dearing; WT, wild type.

under the curve of mice inoculated at 2 d of age (5.5×10^{14}) and 4 d of age (5.0×10^{13}) were markedly greater than the areas under the curve of mice inoculated at 6 d of age (4.7×10^{7}), 10 d of age (4.2×10^{7}), and 15 d of age (2.2×10^{8}). Although viral loads in the brains of mice inoculated at 6 d of age were comparable to those in mice inoculated at 10 or 15 d of age, mortality was significantly greater in mice inoculated at 6 d of age compared with mice inoculated at 10 or 15 d of age. These data suggest that viral loads in the brain do not strictly correlate with disease severity.

To determine whether the capacity to disseminate from the brain to other tissue sites in the host correlates with disease severity and, if so, whether this process is age-dependent, we quantified viral loads in the heart, spleen, liver, and intestine. We found that for each individual mouse, the virus was present either in all or none of the peripheral organs assayed. At 4 d p.i., approximately half of the mice inoculated at any age had detectable viral titers in peripheral organs with the exception of mice inoculated at 6 d of age, of which only one-fifth had detectable titers in peripheral organs (**Table 1**). At 7 d p.i., viral titers were detectable in peripheral organs of the majority of mice inoculated at 2 and 4 d of age compared with less than half the mice inoculated at 6, 10, or 15 d of age. At 10 d p.i., reovirus was detected in the majority of mice inoculated at 2 and 4 d of age, but no reovirus was detected in peripheral organs of mice inoculated at 6, 10, or 15 d of age. These data indicate that the capacity of reovirus to disseminate from the brain to peripheral organs is age-dependent. However, neither viral load in the brain nor the presence of reovirus in peripheral organs alone explain the substantial disease severity observed in mice inoculated at 6 d of age.

Reovirus Displays Enhanced Virulence in IFNAR$^{-/-}$ but Not RAG2$^{-/-}$ Mice

To test the hypothesis that maturation of innate and adaptive immune responses contributes to age-dependent susceptibility to reovirus disease, we compared reovirus virulence following inoculation of WT, IFNAR$^{-/-}$, and RAG2$^{-/-}$ mice at different ages. Mice deficient in expression of the IFN α/β receptor (IFNAR) lack an essential component of the antiviral innate immune response, whereas mice deficient in recombination-activating gene 2 (RAG2) lack functional B and T lymphocytes and are incapable of mounting adaptive immune responses. Mice were inoculated intracranially with T3D at 4 or 15 d of age and monitored for survival, weight gain, and clinical signs of neurologic diseases such as lethargy, seizures, ataxia, and paralysis (20) for 20 d. The mean survival time for IFNAR$^{-/-}$ mice inoculated with reovirus at 4 d of age was 8 d, whereas the mean survival time for WT and RAG2$^{-/-}$ mice was 12 and 11 d, respectively (**Figure 3a**). Only 48% of IFNAR$^{-/-}$ mice inoculated with reovirus at 15 d of age survived compared with 92% of RAG2$^{-/-}$ mice and 100% of WT mice inoculated at 15 d of age (**Figure 3b**). All PBS-inoculated mice survived. A majority of IFNAR$^{-/-}$ mice inoculated at either 4 or 15 d of age displayed reduced weight gain (**Figure 3c,d**) without neurological signs of illness. RAG2$^{-/-}$ mice inoculated with reovirus displayed reduced weight gain when inoculated at 4 d of age but not when inoculated at 15 d of age, a trend similar to that of WT mice inoculated with reovirus at these ages (**Figure 3e,f**). These data suggest that the absence of a functional innate but not adaptive immune response prolongs the susceptibility of mice to reovirus-induced disease and raises the possibility that maturation of the IFN response contributes to age-dependent reovirus virulence.

Viral Loads in the Brains of IFNAR$^{-/-}$ Mice Are Higher than Those In WT Mice When Inoculated at an Older Age

On the basis of the increased mortality in IFNAR$^{-/-}$ mice at older ages of inoculation, we hypothesized that reovirus produces higher titers in IFNAR$^{-/-}$ mice when inoculated at ages at which WT mice are no longer susceptible to reovirus disease. To test this hypothesis, WT, IFNAR$^{-/-}$, and RAG2$^{-/-}$ mice were inoculated intracranially with T3D at the susceptible

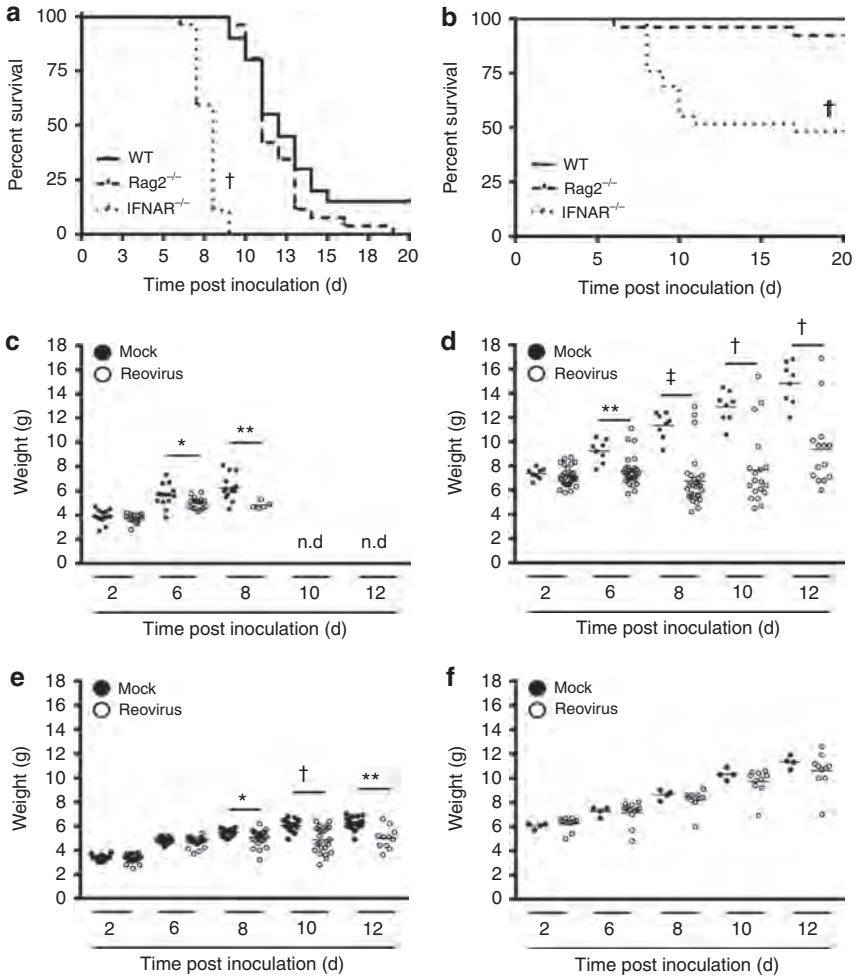

Figure 3. Survival and weight gain of reovirus-infected WT, IFNAR$^{-/-}$, and RAG2$^{-/-}$ mice. WT, IFNAR$^{-/-}$, and RAG2$^{-/-}$ mice were inoculated intracranially with reovirus T3D at 100 PFU/g at either 4 or 15 d of age and monitored for morbidity for 20 d. Mice were killed when moribund. Survival of mice inoculated at (**a**) 4 and (**b**) 15 d of age. $N \geq 23$ per experimental group. $^{\dagger}P < 0.001$ as determined by log-rank test compared with WT mice. Weights of IFNAR$^{-/-}$ mice inoculated at (**c**) 4 or (**d**) 15 d of age. Weights of RAG2$^{-/-}$ mice inoculated at (**e**) 4 or (**f**) 15 d of age. $N \geq 15$ per experimental group. $^{*}P < 0.05$; $^{**}P < 0.01$; $^{\dagger}P < 0.005$; and $^{\ddagger}P < 0.0001$ as determined by Mann–Whitney *U*-test. IFNAR, interferon α/β receptor; RAG, recombination-activating gene; T3D, type 3 Dearing.

age of 4 d and the nonsusceptible age of 15 d, and viral loads in organs were determined at 4, 7, and 10 d p.i. Viral loads in the brains of WT, IFNAR$^{-/-}$, and RAG2$^{-/-}$ mice inoculated at 4 d of age did not differ significantly on 4 and 7 d p.i (**Figure 4a**). However, viral loads in the brains of RAG2$^{-/-}$ mice were significantly higher than those in the brains of WT mice at 10 d p.i. We were unable to perform statistics comparing viral loads in the brains of IFNAR$^{-/-}$ mice at 10 d p.i. because of the lack of replicates. However, the viral load in the brain of the single surviving mouse approximated the average load of RAG$^{-/-}$ mice inoculated at that age. At all time points tested, viral loads in the brains of IFNAR$^{-/-}$ mice were significantly higher than those in the brains of WT mice inoculated at 15 d of age (**Figure 4b**). No significant differences in viral load were detected between the brains of WT and RAG2$^{-/-}$ mice inoculated at 15 d. These data suggest that adaptive immune responses function in the clearance of reovirus from the brains of younger mice, whereas IFN-mediated innate immune responses control viral replication in the brains of older mice. The lack of overwhelmingly significant immune-related differences in viral loads in the brains of mice inoculated at 4 d of age suggests that disease severity and mortality at this age of inoculation are not directly related to the modulation of viral replication by immune responses in the brain.

IFN Controls Viral Dissemination to Peripheral Organs in Both Younger and Older Mice

To determine the function of innate and adaptive immune responses in controlling viral dissemination from the site of inoculation to sites of secondary replication, viral loads were quantified in organs of WT, IFNAR$^{-/-}$, and RAG2$^{-/-}$ mice inoculated at 4 and 15 d of age (**Figure 4 c–j**). Contrary to WT mice (**Table 1**), reovirus was detected in all peripheral organs in both strains of immune-deficient mice

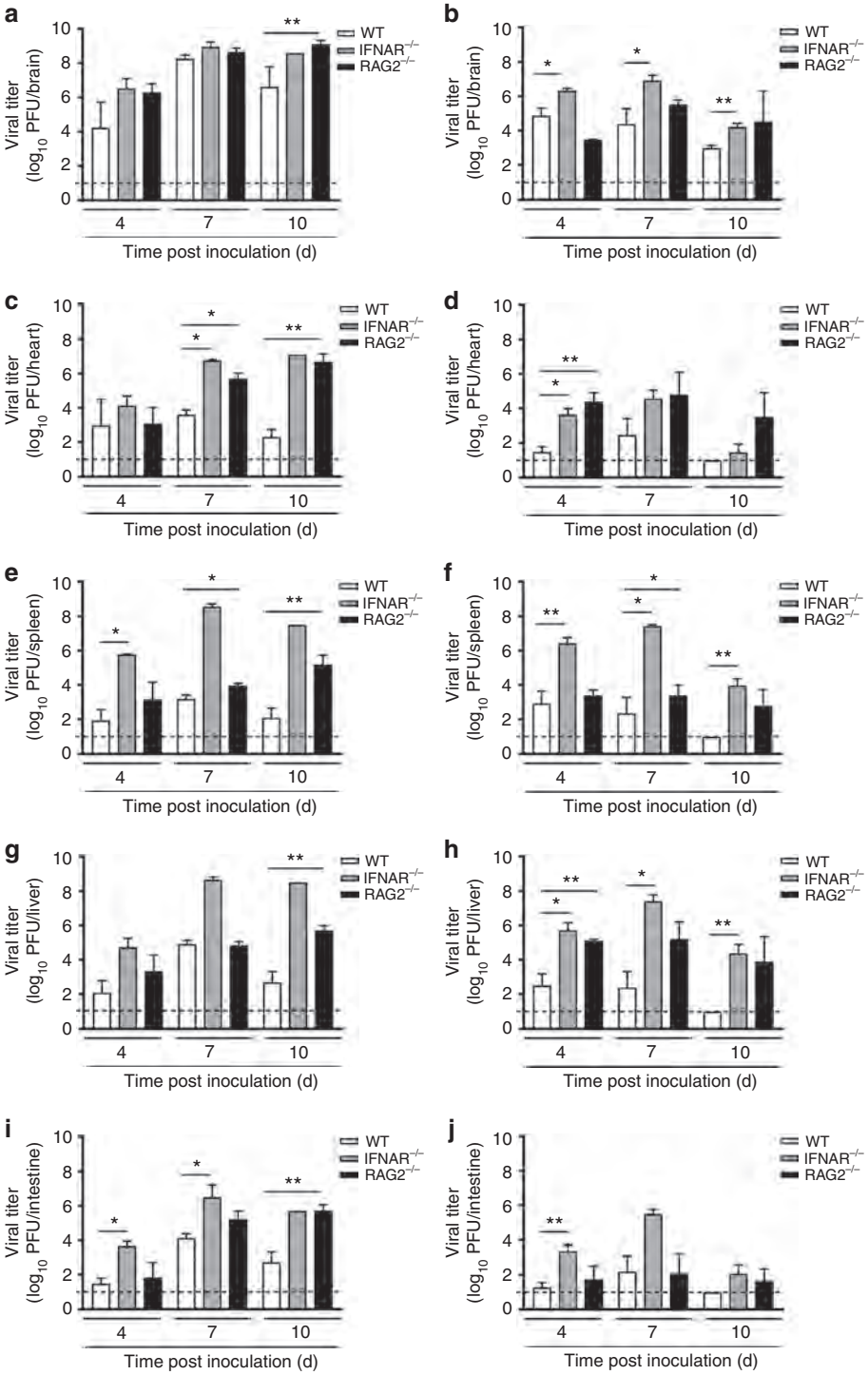

Figure 4. Viral loads in reovirus-infected WT, IFNAR$^{-/-}$, and RAG2$^{-/-}$ mice. WT, IFNAR$^{-/-}$, and RAG2$^{-/-}$ mice were inoculated intracranially with reovirus T3D at 100 PFU/g at either 4 or 15 d of age. At 4, 7, and 10 d p.i., mice were killed, organs were resected, and viral loads were determined. Viral loads in the brains of mice inoculated at (**a**) 4 or (**b**) 15 d of age, in the hearts of mice inoculated at (**c**) 4 or (**d**) 15 d of age, in the spleens of mice inoculated at (**e**) 4 or (**f**) 15 d of age, in livers of mice inoculated at (**g**) 4 or (**h**) 15 d of age, and in the intestines of mice inoculated at (**i**) 4 or (**j**) 15 d of age. $N = 2$–10 except IFNAR$^{-/-}$ mice 10 d p.i., for which $n = 1$ due to the low survival rate at that time point. Dotted lines represent the limit of detection. $^{*}P < 0.05$; $^{**}P < 0.01$ as determined by Mann–Whitney *U*-test. d p.i., day post inoculation; IFNAR, interferon α/β receptor; PFU, plaque-forming unit; RAG, recombination-activating gene; T3D, type 3 Dearing.

at all time points tested (data not shown). Overall, viral loads in peripheral organs of IFNAR$^{-/-}$ mice were increased compared with those in WT mice (Figure 4c–j). Viral loads in the heart and spleen of RAG2$^{-/-}$ mice inoculated at 4 d of age were also increased compared with those in WT mice at 7 d p.i. and in all organs at 10 d p.i. RAG2$^{-/-}$ mice

inoculated at 15 d of age displayed modestly increased viral loads in the heart and liver but not in the spleen and intestine at 4 d p.i., and the differences became smaller at later times (Figure 4d,f,h,j). Peak viral loads in all organs of IFNAR$^{-/-}$ mice inoculated at 4 d of age coincide with the sharp reduction in survival of IFNAR$^{-/-}$ mice (Figure 3a), whereas differences in weight gain and survival of WT and RAG2$^{-/-}$ mice inoculated at 4 d of age appear at later times post infection when viral loads in both the brain and peripheral organs of RAG2$^{-/-}$ mice are significantly greater than those in WT mice (Figure 4a,c,e,g,i). Interestingly, viral loads in IFNAR$^{-/-}$ mice inoculated at 4 d of age increased throughout infection until death, whereas viral loads in mice inoculated at 15 d of age peaked at 7 d p.i., followed by a decline at 10 d p.i., consistent with the enhanced survival of IFNAR$^{-/-}$ mice inoculated at this age. Together, these results suggest that IFN has an important role in controlling systemic dissemination and replication at secondary sites in mice of both susceptible and nonsusceptible ages at all time points assessed. Adaptive responses function later during infection of mice inoculated at a susceptible age and likely contribute to viral clearance.

Reovirus Tropism Is Unaltered in the Brains of Immune-Deficient Mice

To determine whether differences in brain pathology link mortality to altered immune responses, the right hemispheres of brains that matched as closely as possible for viral load were processed for histology. Consecutive sections were stained with hematoxylin and eosin, with polyclonal reovirus antiserum to detect viral antigen, or with a monoclonal antibody specific for the cleaved (activated) form of caspase-3 to detect cells undergoing apoptosis—the primary mechanism of neuronal cell death following reovirus infection (19). Reovirus antigen was detected in the hippocampus, thalamus, and cortex (Figure 5a) as well as the cerebellum and hindbrain (Figure 5b) of brains resected at 7 d p.i. from mice of all three strains inoculated with reovirus at 4 d of age. Although the overall staining intensity varied, no qualitative differences were found in viral tropism. Staining for the activated form of caspase-3 was modest in all sections analyzed and localized with reovirus staining, consistent with the pattern of reovirus-induced tissue injury (8,19,21). Histological analysis of brains resected from mice inoculated with reovirus at 15 d of age at 7 d p.i. showed substantially reduced levels of reovirus antigen-positive cells (data not shown). Staining was restricted to small areas within the thalamus and surrounding the lateral ventricles. These areas of the brain also displayed low levels of activated caspase-3 staining (data not shown).

Apoptosis Is Unaltered in the Brains of Immune-Deficient Mice

To determine whether quantitative age- and immune-dependent differences exist in reovirus-induced apoptosis, protein lysates from the brains of three individual mice of each strain resected 7 d p.i. were resolved by SDS-PAGE and immunoblotted using an antibody specific for cleaved caspase-3 and an antiserum specific for actin as a loading control. The intensity of the cleaved caspase-3 signal was normalized to the intensity of the actin signal. The overall magnitude of apoptosis in the brains of IFNAR$^{-/-}$ and RAG2$^{-/-}$ mice inoculated at 4 d of age (Figure 6a,c) and at 15 d of age (Figure 6b,d) did not differ statistically.

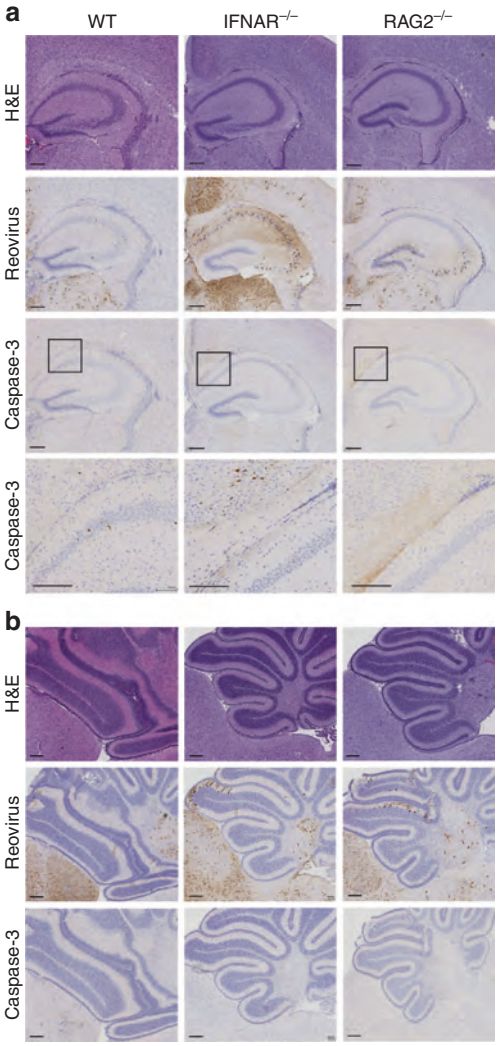

Figure 5. Reovirus tropism in the brains of WT, IFNAR$^{-/-}$, and RAG2$^{-/-}$ mice. WT, IFNAR$^{-/-}$, and RAG2$^{-/-}$ mice were inoculated intracranially with reovirus T3D at 100 PFU/g at 4 d of age. At 7 d p.i., mice were killed, brains were removed, the left hemispheres were homogenized for the determination of viral titer, and the right hemispheres were processed for immunohistochemistry. Consecutive coronal sections of the brain were stained with H&E, reovirus antiserum, or an anticleaved caspase-3 antibody. Representative sections of the brains are shown. (**a**) Hippocampal region stained with H&E or polyclonal reovirus antiserum and a higher-magnification image of the boxed inset stained for cleaved caspase-3 (scale bars, 200 μm). (**b**) Cerebellum and the hindbrain. Sections shown are from a WT, IFNAR$^{-/-}$, and a RAG2$^{-/-}$ mouse with a viral load of 3.9×10^8 PFU/brain, 3.8×10^9 PFU/brain, and 1.2×10^9 PFU/brain, respectively (scale bars, 200 μm). d p.i., day post inoculation; H&E, hematoxylin and eosin; IFNAR, interferon α/β receptor; PFU, plaque-forming unit; RAG, recombination-activating gene; T3D, type 3 Dearing.

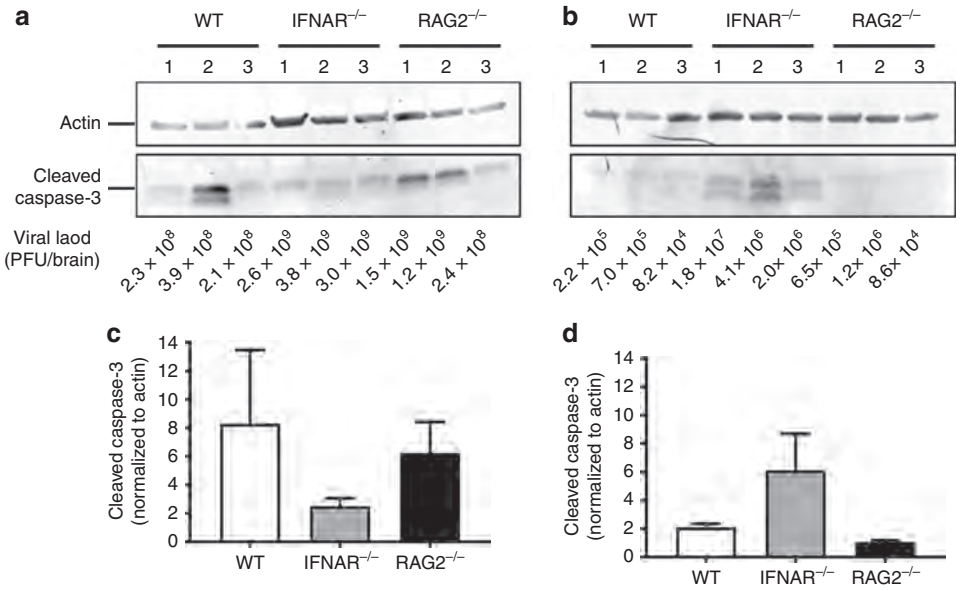

Figure 6. Quantification of apoptosis in the brains of WT, IFNAR$^{-/-}$, and RAG2$^{-/-}$ mice. Mice were inoculated intracranially with reovirus T3D at 100 PFU/g at either (**a**,**c**) 4 or (**b**,**d**) 15 d of age. Protein lysates from the brains of three T3D-infected WT, IFNAR$^{-/-}$, or RAG2$^{-/-}$ mice resected at 7 d p.i. were resolved by SDS-PAGE. (**a**,**b**) Lysates were immunoblotted using antisera specific for actin (top) and cleaved caspase-3 (bottom). Viral loads are listed for each sample. (**c**,**d**) Quantification of the band intensity of cleaved caspase-3 normalized to actin. d p.i., day post inoculation; IFNAR, interferon α/β receptor; PFU, plaque-forming unit; RAG, recombination-activating gene; T3D, type 3 Dearing.

DISCUSSION

In this study, we determined the precise timing of the age restriction to reovirus virulence in C57BL/6J mice based on mortality and determination of weight gain as a surrogate marker for reovirus-induced disease. We found that the age restriction for reovirus mortality and disease lies between 6 and 10 d of age. We were surprised to find that a lower proportion of mice inoculated at 4 d of age survived compared with mice inoculated at 2 d of age. This finding might be attributed to experimental variability caused by a suboptimal nurturing by the dam. Mice inoculated intracranially with serotype 3 reovirus strains likely succumb to encephalitis rather than to disease at other sites of infection, as a reovirus mutant incapable of disseminating systemically is as virulent as WT virus following intracranial inoculation (22). Interestingly, there was a significant increase in weight gain following inoculation with reovirus at 15 and 20 d of age relative to PBS-inoculated controls. It is possible that the virus-mediated increase in weight gain occurs as a consequence of virus-induced damage to the ventromedial hypothalamus, which is associated with increased appetite (23–25). Histological examination of brain tissue from mice infected at additional ages will provide more information about the age-dependent differences in reovirus neural tropism and pathology.

We thought it possible that age-related disease severity might track with virus titers in target tissues. Our results indicate that viral replication occurred even in mice that did not display overt neurological signs of infection. Brains of mice inoculated at 6 d of age harbored viral loads that were similar to those in the brains of mice inoculated at nonsusceptible ages; yet, survival rates and weight gain were comparable to mice inoculated at susceptible ages. Reovirus disseminated systemically in mice inoculated at susceptible ages, whereas systemic dissemination was limited in mice inoculated at nonsusceptible ages. Thus, we conclude that viral titers in the brain do not strictly correlate with susceptibility to reovirus-induced disease.

We used immune-deficient mice to investigate whether maturation of innate or adaptive immune responses contributes to the age restriction of reovirus disease. Our results indicate that IFN functions in controlling viral replication in mice of both susceptible and nonsusceptible ages, whereas adaptive immune responses are particularly important in controlling replication at later times post infection in mice of susceptible age. The increased susceptibility of older IFNAR$^{-/-}$ mice to reovirus infection suggests that age-dependent maturation of IFN responses contributes to the age-related virulence of reovirus. Some IFNAR$^{-/-}$ mice had signs of encephalitis, but others died quickly after the onset of illness. A previous study describes intestinal perforation, bacterial sepsis, and acute hepatitis as causes of death in IFNAR$^{-/-}$ mice inoculated with reovirus at 2 d of age (26).

Besides contributing to age-dependent susceptibility to reovirus infection, the type-I IFN response functions in the age-dependent susceptibility to infection with herpes simplex virus (HSV-1). Lower basal levels of IFNAR are expressed in the choroid plexus of uninfected newborn mice compared with adults. Concordantly, the adult choroid plexus is less susceptible to infection with HSV-1 relative to the

newborn brain. Similar to our findings with reovirus, HSV-1 susceptibility was restored in the brains of adult IFNAR$^{-/-}$ mice (27).

Cells of the innate immune system may also contribute directly to the age-dependent susceptibility to reovirus central nervous system disease. Microglia, the resident macrophage cells in the brain, modulate the immune response to brain infections by secreting inflammatory cytokines such as interleukin (IL)-1α, IL-6, and tumor necrosis factor-α (28). Microglia are virtually absent from the mouse hippocampus at birth, but the numbers of these cells increase markedly between 5 and 10 d of age and peak at 15 d of age (29). Microglial activation and proinflammatory cytokine production in the brain decrease with age under normal conditions and in response to stimulation with lipopolysaccharide (30,31), suggesting that the inflammatory response to viral infections of the brain is muted later in life. Consistent with this idea, the production of the proinflammatory cytokine IL-1α is increased in the brains of reovirus-infected newborn mice compared with adults and coincides with nervous tissue injury that precedes encephalitis (32). Our finding that the absence of RAG2 expression does not affect the timing of the age restriction to reovirus disease is consistent with the kinetics of adaptive immune effector maturation, which is initiated after the first month of life (33) and, thus, outside the interval during which reovirus susceptibility diminishes.

The results from this study define an age at which mice become refractory to reovirus disease and provide evidence that maturation of innate immune responses contributes to the mechanism of age restriction. These findings suggest that innate immune maturity influences diverse types of neural insults.

ACKNOWLEDGMENTS

We thank members of the Dermody lab for helpful discussions and Laurie Silva and Gwen Taylor for a critical review of the manuscript, the Vanderbilt Division of Animal Care for animal husbandry, and Kelli Boyd and colleagues from the Vanderbilt Translational Pathology Shared Resource for assistance.

STATEMENT OF FINANCIAL SUPPORT

This work was supported by Public Health Service awards T32 HD060554 (A.G.W.), F31 DK108562 (J.J.B.), and R01 AI38296 (T.S.D.). Additional support was provided by the Elizabeth B. Lamb Center for Pediatric Research.

Disclosure: The authors declare no competing financial interests.

REFERENCES

1. Griffin DE. Emergence and re-emergence of viral diseases of the central nervous system. Prog Neurobiol 2010;91:95–101.
2. Griffin DE. Viral encephalomyelitis. PLoS Pathog 2011;7:e1002004.
3. Tyler KL, McPhee DA, Fields BN. Distinct pathways of viral spread in the host determined by reovirus S1 gene segment. Science 1986;233:770–4.
4. Morrison LA, Sidman RL, Fields BN. Direct spread of reovirus from the intestinal lumen to the central nervous system through vagal autonomic nerve fibers. Proc Natl Acad Sci USA 1991;88:3852–6.
5. Antar AAR, Konopka JL, Campbell JA, et al. Junctional adhesion molecule-A is required for hematogenous dissemination of reovirus. Cell Host Microbe 2009;5:59–71.
6. Pruijssers AJ, Dermody TS Reovirus. In: Reiss CS, ed. Neurotropic Viral Infections. 2nd edn, New York, NY: Springer Nature; 2016:337-360.
7. Weiner HL, Powers ML, Fields BN. Absolute linkage of virulence and central nervous system cell tropism of reoviruses to viral hemagglutinin. J Infect Dis 1980;141:609–16.
8. Danthi P, Coffey CM, Parker JS, Abel TW, Dermody TS. Independent regulation of reovirus membrane penetration and apoptosis by the mu1 phi domain. PLoS Pathog 2008;4:e1000248.
9. Danthi P, Pruijssers AJ, Berger AK, Holm GH, Zinkel SS, Dermody TS. Bid regulates the pathogenesis of neurotropic reovirus. PLoS Pathog 2010;6:e1000980.
10. Margolis G, Kilham L, Gonatos N. Reovirus type III encephalitis: observations of virus-cell interactions in neural tissues. I. Light microscopy studies. Lab Invest 1971;24:91–109.
11. Raine CS, Fields BN. Ultrastructural features of reovirus type 3 encephalitis. J Neuropathol Exp Neurol 1973;32:19–33.
12. Tardieu M, Powers ML, Weiner HL. Age dependent susceptibility to Reovirus type 3 encephalitis: role of viral and host factors. Ann Neurol 1983;13:602–7.
13. Ivashkiv LB, Donlin LT. Regulation of type I interferon responses. Nat Rev Immunol 2014;14:36–49.
14. Goody RJ, Beckham JD, Rubtsova K, Tyler KL. JAK-STAT signaling pathways are activated in the brain following reovirus infection. J Neurovirol 2007;13:373–83.
15. Kobayashi T, Antar AA, Boehme KW, et al. A plasmid-based reverse genetics system for animal double-stranded RNA viruses. Cell Host Microbe 2007;1:147–57.
16. Furlong DB, Nibert ML, Fields BN. Sigma 1 protein of mammalian reoviruses extends from the surfaces of viral particles. J Virol 1988;62:246–56.
17. Virgin HW, Dermody TS, Tyler KT Cellular and humoral immunity to reovirus infection. In: Tyler KT, Oldstone MBA, eds. Curr Top Microbiol Immunol. Berlin: Springer; 1998:147–61.
18. Tyler KL, Bronson RT, Byers KB, Fields B. Molecular basis of viral neurotropism: experimental reovirus infection. Neurology 1985;35:88–92.
19. Pruijssers AJ, Hengel H, Abel TW, Dermody TS. Apoptosis induction influences reovirus replication and virulence in newborn mice. J Virol 2013;87:12980–9.
20. Tyler KL Pathogenesis of reovirus infections of the central nervous system. In: Tyler KL, Oldstone MA, eds. Reoviruses II Cytopathogenicity and Pathogenesis. Berlin, Heidelberg: Springer; 1998:93–124.
21. Richardson-Burns SM, Tyler KL. Regional differences in viral growth and central nervous system injury correlate with apoptosis. J Virol 2004;78:5466–75.
22. Boehme KW, Guglielmi KM, Dermody TS. Reovirus nonstructural protein sigma1s is required for establishment of viremia and systemic dissemination. Proc Natl Acad Sci USA 2009;106:19986–91.
23. Reyes-Vazquez C, Prieto-Gomez B, Dafny N. Interferon modulates central nervous system function. Brain Res 2012;1442:76–89.
24. Dafny N, Gillman MA, Lichtigfeld FJ. Cholecystokinin: induced suppression of feeding in fed, fasting and hypothalamic island rats. Brain Res Bull 1988;21:225–31.
25. King BM. The rise, fall, and resurrection of the ventromedial hypothalamus in the regulation of feeding behavior and body weight. Physiol Behav 2006;87:221–44.
26. Dionne KR, Galvin JM, Schittone SA, Clarke P, Tyler KL. Type I interferon signaling limits reoviral tropism within the brain and prevents lethal systemic infection. J Neurovirol 2011;17:314–26.
27. Wilcox DR, Folmsbee SS, Muller WJ, Longnecker R. The type I interferon response determines differences in choroid plexus susceptibility between newborns and adults in herpes simplex virus encephalitis. mBio 2016;7:e00437-16.
28. Rock RB, Gekker G, Hu S, et al. Role of microglia in central nervous system infections. Clin Microbiol Rev 2004;17:942–64.
29. Kim I, Mlsna LM, Yoon S, et al. A postnatal peak in microglial development in the mouse hippocampus is correlated with heightened sensitivity to seizure triggers. Brain Behav 2015;5:e00403.

30. Ferrazzano P, Chanana V, Uluc K, et al. Age-dependent microglial activation in immature brains after hypoxia- ischemia. CNS Neurol Disord Drug Targets 2013;12:338–49.
31. Inamizu T, Chang MP, Makinodan T. Influence of age on the production and regulation of interleukin-1 in mice. Immunology 1985;55:447–55.
32. Derrien M, Fields BN. Reovirus type 3 clone 9 increases interleukin-1 level in the brain of neonatal, but not adult, mice. Virology 1999;257: 35–44.
33. Landreth KS. Critical windows in development of the rodent immune system. Hum Exp Toxicol 2002;21:493–8.